# The Assessment and Response of Concrete Structures Subject to Fire

Angus H. Law

Doctor of Philosophy


The University of Edinburgh

2010

In memory of my grandfather, Harry Bernard Law

# Declaration

The writing of this thesis, and the research herein was conducted solely by Angus Law under the supervision of Dr Martin Gillie and Dr Stephen Welch. Where other sources are quoted, references are given in full.

Angus Law, 2010

# Abstract

Over the last 20 to 30 years, the field of structural fire design has shifted from relying on single element fire resistance testing to the consideration of the effects of full-frame behaviour. The change has been driven by the desire to build more advanced structures and reduce costs. It has been facilitated in part due to structural testing, and in part due to development of complex modelling techniques. This thesis considers the modelling of concrete structures, and presents new techniques and methodologies for analysing the performance of structures in fire.

The first part of this work traces modelling techniques from fundamental constitutive behaviour through to sectional capacity calculation. Load induced thermal strain and constitutive modelling approaches are investigated and their impact on structural behaviour is considered. A new, general, technique for conducting sectional analysis on concrete elements is also created. The method relies on analysis of the sectional tangent stiffness to efficiently calculate the biaxial bending capacity of a concrete section subject to any heating regime. This approach is more accurate and conservative than current methods and has the potential to be used as a design tool.

This work develops a series of new approaches for the design of large structures subject to fire. A rational and quantifiable methodology is developed for assessing the performance of a structure when subject to fire; this new approach addresses the mismatch in complexity between current

modelling techniques and measures of structural performance. It allows a more precise approach to be taken to the definition of failure; and can be easily used to compare the structure's response to different design fires.

Finally, a new technique for the definition of design fires founded on fundamental fire dynamics is presented. The approach challenges the assumptions typically made when applying temperature-time curves and is based around the observed phenomenon of travelling fires. A concrete framed structure is subject to a number of travelling fires and the response is assessed using both conventional techniques and the new, in depth analysis.

# Publications

## Journal Papers

A. Law, M. Gillie; Interaction Diagrams for Ambient and Heated Concrete Sections; Engineering Structures; Volume 32, Issue 6, June 2010, Pages 1641-1649

A. Law, M. Gillie; Concrete Structures Subject to Fire: Assessment for Design; Submitted for publication; currently under review.

A. Law, M. Gillie; The Inclusion of Load Induced Thermal Strain Finite-Element Models; currently under review.

A. Law, J. Stern-Gottfried, M. Gillie, G. Rein; The Effect of Different Design Fires on the Response of a Concrete Frame; currently under review.

## Conference Papers

A. Law, M. Gillie; Interaction Diagrams for Heated Concrete Sections using the Tangent Stiffness Matrix; Fourth International Conference on Structural Engineering, Mechanics and Computation, Cape Town, September 2010

A. Law, J. Stern-Gottfried, M. Gillie, G. Rein; The Influence of Travelling Fires on the Response of a Concrete Frame; Sixth International Conference on Structures in Fire, Lansing, Michigan, June 2010

J. Stern-Gottfried, A. Law, G. Rein, M. Gillie, J. L. Torero; A Performance Based Methodology Using Travelling Fires for Structural Analysis; Eighth International Conference on Performance-Based Codes and Fire Safety Design Methods, Lund, June 2010

A. Law, M. Gillie, P. Pankaj; Incorporation of Load Induced Thermal Strain in Finite Element Models; Applications of Structural Fire Engineering, Prague, February 2009

A. Law, M. Gillie; Load Induced Thermal Strain: Implications for Structural Behaviour; Fifth International Conference on Structures in Fire, Singapore, June 2008

# Acknowledgements

Particular thanks to Martin Gillie, my supervisor, for his support and guidance over the last three years. You have been spectacularly patient.

The support of my sponsors, the EPSRC and BRE trust is gratefully acknowledged, as is the help of my industrial colleagues, Danny, Tom, Julie, and Debbie.

I'd variously like to thank all my colleagues in John Muir; we've had a lot of fun, both at home and aboard. You've made the last three years a delight!

Over the course of my studies at Edinburgh, I've managed to bother most of the academic staff with one problem or another. I'd like to thank you all for being so generous with your time.

His sheer outrage is wondrous to behold: thanks to Jamie for all your help and input from a fire perspective.

Earl and Lady Grey have provided distraction, comfort, and inspiration throughout my studies, so thanks to them.

Lastly, thanks to Hannah. You've listened to my complaining, my enthusing, and my "interesting" stories; thank you for your support, your patience, and for helping me keep things in perspective.

# Table of Contents

# Table of Figures

# Table of Tables

# Nomenclature

Greek letters

| | |
|---|---|
| $\alpha$ | coefficient of thermal expansion |
| $\varepsilon$ | strain |
| $\sigma$ | stress |
| $\gamma$ | material strength safety factor |
| $\eta$ | stress block factor |
| $\kappa$ | curvature |

Subscripts

| | |
|---|---|
| *1* | 1st principal direction |
| *2* | 2nd principal direction |
| *3* | 3rd principal direction |
| *a* | Axial |
| *c* | Concrete |
| *cr* | creep |
| *cu2* | limiting strain in concrete |
| *el* | elastic |
| *em* | embedded |
| *k* | characteristic strength |
| *pl* | plastic |
| *s* | steel |
| *s1* | lower steel |
| *s2* | upper steel |
| *T* | temperature dependent |

| | |
|---|---|
| $th$ | thermal |
| $tr$ | transient |
| $u$ | at ultimate stress |
| $ult$ | ultimate |
| $x$ | about x-axis |
| $y$ | about y-axis |

Exceptions

| | |
|---|---|
| $E_T$ | Tangent modulus |
| $f_y$ | steel yield stress |
| $\bar{x}$ | Mean |
| $E^-$ | Gradient of linear descending branch of constitutive curve |

# 1

# Introduction

## 1.1. Background to the Project

The 1990s and the early 2000s, saw significant advances in the field of structural fire engineering. A series of full-scale fire tests and the subsequent modelling work revolutionized understanding of how structures perform when subject to fire. New techniques were created that allow engineers to design more efficient structures, exploit redundancy, and to understand the consequences of fire. Many of the most startling advances were made in relation to steel structures and composite slabs.

Our increasingly advanced understanding of structural behaviour in fire, coupled with the introduction of more flexible design standards has allowed

engineers to design structures based on performance objectives rather than by following prescribed rules. This approach is known as performance-based design and encompasses many different levels of complexity: from simple hand calculations, through to full structural modelling. As designs have become more efficient, techniques more advanced, and our technical awareness increased, it has become increasingly apparent that there remain serious limitations and blind-spots in our collective knowledge.

Although concrete's behaviour in fire has often been a topic for study, many of the recent developments have been made in relation to steel construction. Much of the research into structural behaviour in fire has also focused on the heating phase of a fire – that is, when the fire is growing. It is clear though, that building fires will always exhaust their supply of fuel, or be extinguished through intervention. The building's residual state, after a fire has occurred, is rarely considered.

As with any young discipline, there are a large number of gaps in our knowledge of structural fire safety. Research by institutions all over the world is gradually advancing our level of understanding, filling these gaps and building upon previous work. Continual refinement of existing techniques is symptomatic of a mature discipline with no major gaps in knowledge identified; structural fire engineering can still be considered relatively young. So, while some areas have been studied with very fine detail, there are other areas that have advanced very little or show wide internal discrepancies in understanding.

This work addresses a number of inconsistencies, and fills various gaps in our comprehension. The thesis is wide ranging, and approaches its subject from a number of different angles. Throughout though, the theme is to create a degree of consistency within the approaches used: where detailed attention is paid to material properties, the key behaviours of importance are identified and analysed; where highly complex finite-element element techniques are used, the methods of assessment are enhanced to provide a more consistent level of detail.

A significant area which this work does not address is spalling. Spalling is the sometimes explosive loss of concrete that can occur as a structural element is heated. The phenomenon is complex and though predictive models are under development by a number of researchers, an "engineering" approach is often taken for practical purposes. A predictive model is outwith the scope of this project, and it is the author's view that each area of work in this thesis would not benefit significantly from inclusion of spalling. Every principle presented and methodology discussed remains equally valid with or without the inclusion of spalling.

As the work progresses, the scale of the problems that are discussed gradually increases; after consideration of the micro level material properties, single element analyses are considered; this is followed by the development of a series of whole frame finite-element models and the introduction of different design fires. Finally, a number of the techniques developed are brought together into one, conceptually simple, methodology.

## 1.2. Aims of the Research

There are a number of additional, more specific, aims for this research.

- *To understand how concrete material behaviour and the way that it is modelled can affect structural behaviour.* In the past, compressive behaviour of concrete at high temperature has been studied extensively. However, the implementation of high temperature material models within finite-element analyses is a relatively unexplored area. This work will examine the phenomenon of load induced thermal strain and identify the key features which affect structural behaviour.
- *To develop a method for assessing structural capacity during and after a fire.* Current simplified techniques for sectional analyses are well understood at ambient temperature. As members are heated, though, the properties of the steel and concrete change and the simplified methods are no longer as effective. This thesis will closely examine the creation of interaction diagrams under both ambient and heated conditions, to allow structural capacity to be more rigorously defined.
- *To develop a methodology for assessing whole building behaviour aspects during and after a fire.* Existing methods used to assess the resilience of structures under fire conditions rely on basic structural measures. Large-scale finite-element modelling produces a significant amount of data from which only a small fraction is ever used to measure structural performance. This work develops a methodology for whole structural assessment which utilizes much of the available information and produces comprehensive output regarding the performance of the structure.

- *To understand whether, and how, different design fires can affect a concrete structure.* Current design approaches rely on simplified representations of temperature to represent fires which might occur in a building. These simplified scenarios have a number of assumptions which render them inappropriate for application to many modern buildings. This thesis explores a new approach to defining the fires that might occur and studies the affects of such fires on a concrete building.

## 1.3. Outline of Thesis Chapters and Appendices

**"Chapter One – Introduction"** A brief description of the background to the research, research aims, and thesis structure.

**"Chapter Two – Background"** A review chapter: a historical context for the current research is presented; the changes that temperature affects in concrete are discussed; and a review of current assessment techniques is conducted.

**"Chapter Three – Numerical Modelling of Concrete at High Temperature"** Different constitutive models for concrete are presented, compared, and discussed. The phenomenon known as load induced thermal strain is defined and methods for implementing it in numerical models are analysed. Its impact on a simplified structure is considered, and the three-dimensional effects are discussed.

**"Chapter Four – Sectional Analysis"** A new technique for creating bending moment/axial force interaction diagrams is presented. The properties of the tangent stiffness matrix are used to efficiently locate the failure surface of a concrete section. The technique is applied to heated concrete sections and compared to current methods.

**"Chapter Five – Whole Structures"** A finite-element model of a generic concrete structure is subjected to a series of design fires. The impacts are studied using a combination of techniques. The effect of partial column heating is analysed, and utilization rates for the entire structure are defined.

**"Chapter Six – Travelling Fires"** An existing travelling fire methodology is presented and applied to a finite-element model of a generic concrete structure. A number of fires of different area, shape, temperature distribution and duration are defined, and their effect on the structure is studied using conventional performance indicators.

**"Chapter Seven – Whole Structures and Travelling Fires"** The whole structure analysis techniques developed in chapter five are applied to analyse the difference between the various travelling fires presented in chapter six. Techniques for identifying the most vulnerable members and changing the structural design are discussed.

**"Chapter Eight – Conclusions and Further Work"** The final chapter rehearses and summarizes the main conclusions from the research conducted and discusses scope for further work.

**"Appendix I – Numerical Modelling of Materials"** Reviews the techniques for implementing a material model with a constitutive hardening curve in a finite-element code.

**"Appendix II – Concrete Structure"** Reviews the design and sensitivity analyses for the concrete structure that features in chapters five, six and seven.

**"Appendix III – Response of Structure"** Presents the response of the structure to the different applied fires in the form of loading capacity diagrams.

**"Appendix IV – Papers"** A selection of papers that were published from research completed for this thesis.

**"Appendix V – Selected Examples of Code"** Examples of some of the Fortran, MATLab and Python code that was written as part of this research.

# 2

# Background

The aim of this work is to characterize the behaviour of concrete structures during fire and develop techniques for assessing the capacity during and after a fire. Before it is possible to begin such a task, it is necessary to understand the background of the discipline: to identify trends and place the research within a historical context. Since all structural behaviour is rooted in material properties, it is also imperative to have a good understanding of how construction materials behave, both under ambient and heated conditions. This second chapter will review the background to the current state of structural fire engineering and discuss the changes that take place in concrete as it is heated.

## 2.1. Structural Behaviour

To create numerical models of structures, as this research will, not only do the material behaviours have to be characterized, but observations of the effects of fire on real structures must be made. Simple material descriptions can result in surprising, and complex, overall structural behaviour when real testing is conducted. It is the aim of numerical models to ensure that low level material behaviour can be successfully transferred into models that then predict and represent the global behaviour seen in larger scale structures. Though the focus of this thesis is the performance of concrete, the story of steel and concrete are so intertwined they are impossible to fully separate. As such, much of the information concerns structure made from both materials. This section will discuss developments in both testing and numerical modelling from a historical perspective.

### 2.1.1. Real Tests

The testing of structural assemblies in fire dates back to the late 1800s as reported by Babraskus [7]. As construction techniques became more advanced and multi-storey buildings became more common, designs moved away from traditional all masonry arches to more complex forms. The building's super-structure was increasingly made with a frame of iron members. Floors, meanwhile, began to be constructed from smaller masonry arches sprung from iron beams [7]. Initially, the aim of many fire tests was to establish, through experiment, the relative merits of the products created by competing patent holders of these new technologies. Many different organizations throughout Europe and the USA are documented as having conducted fire test on assemblies such as walls, floors, columns and doors [8].

#### 2.1.1.1. Standard Testing

In the UK, the first concerted efforts at fire resistance testing were published by Edwin Sachs [7] in 1899. Sachs is particularly worth mentioning, as his role in the field of fire testing is significant, but his role is also significant in the field of reinforced concrete design [35] and structural engineering in general. In 1897, he founded the British Fire Prevention Committee (BFPC) who undertook a series of tests on floor assemblies in purpose built masonry "huts". In 1906, concern about the quality and composition of aggregates led to the establishment by the BFPC of a Special Commission on Concrete Aggregates. One of the specific concerns was the use of materials that often contained un-burnt coal, as an aggregate. This was of special interest to Sachs, as he was the editor of "Concrete and Constructional Engineering". The close association between concrete and fire resistance has meant that unlike iron or steel members – which were often fitted with passive fire protection such as masonry boxes or tera cotta covers – fire resistance was considered from a very early stage. The first meeting of the Institute of Structural Engineers was held, with Sachs as its chair, in 1908 under its original name of "The Concrete Institute". In 1911, the initial primary driver for the specification of concrete cover was the need for fire resistance.

During this time, the procedure for fire resistance testing had become somewhat standardized. In 1903, the BFPC issued a standard on the classification of protection. This included minimum temperatures for the tests; required loading for some assemblies; and resistance duration requirements [8]. Though this standard became recognized in many countries, engineers in the USA opted to create their own standard.

After the death of Sachs in 1919 testing in the UK did not progress significantly; the BFPC ceased to function in 1924 [131]. Since 1906, the Fire Officers Committee (FOC) had been using a testing facility in Manchester. In 1929, The Royal Institute of British Architects (RIBA) moved this testing station to Borehamwood. In this intermediate period, most testing occurred at sponsors' premises or at fire stations. During this time, the progress of standardization was gathering pace in the United States.

The new the, American, National Fire Protection Association (NFPA) standard saw the introduction of the first temperature-time curve; it was based on the idealization of a number of other curves and was closest to a curve which had resulted from a number of wood stoked tests in New York in 1902. The initial rate of temperature increase was made higher to account for the recent introduction of gas or oil fired furnaces. A notable feature of this early standard was the provision that an assembly should be tested for 25% longer than the required period [8]. The first tests which systematically attempted to measure the temperatures in the furnace were conducted under the supervision of Simon Ingberg from the National Bureau of Standards [7] in 1922. It was recognized by Ingberg that the new standard curve had limitations. He understood that it did not represent a "real" fire situation. He also recognized though that to subject every assembly that required a fire rating to a whole series of more realistic curves would be prohibitively expensive. Ingberg, introduced the concept of fire severity whereby the different temperature-time curves could be compared using the equal area concept. Using this technique, Ingberg hypothesised that it was the integral of the fire curve that was important, not the shape of the temperature-time

curve. This concept lives on to the present day, and is used to give fire ratings to assemblies exposed to “natural” fires.

In the UK, meanwhile, the RIBA had recognized that variation in bylaws and lack of proper definitions was leading to misunderstandings and confusion in fire testing. It was proposed, therefore, to draft a suitable standard. After the consideration of a number of curves, it was eventually decided to adopt a curve similar the USA standard. The differences stem from the definition of temperature as a function of time rather than a graphical representation of temperature-time. This standard was published as BS-476 in 1932 and has since been incorporated into the Eurocodes and ISO standards [44,86].

The standard fire remained largely unchallenged until the 1970s when Pettersson developed the, so called, Swedish curves. These temperature-time curves used the heat release rate of the fire and balanced it with the heat losses from the compartment due to heat transfer through the walls and from the openings. Thus, the temperature in the compartment was dependent on the fuel load, the compartment ventilation and the geometry of the compartment. As the solutions were implicit, the curves were given in tabular or graphic form; a number of curves were given for different fire loads and opening factors. Pettersson’s temperature-time curves have subsequently been changed into an explicit form and are presented as the Eurocode parametric fires in Eurocode 1 [53,160]. Each of these fires has a simplified rate of cooling [161].

Since the inception of the first standard fires, fire testing on assemblies of elements has continued using a standard fire. Elements are given fire ratings of half hour intervals based on the amount of time that element is said to have survived a fire [27]. The failure criterion varies depending on the type of assembly that is being tested. Horizontal load bearing elements are normally defined as having failed when some deflection criteria has been met; vertical elements are said to have failed when they can no longer support the applied load. There are also integrity criteria which are designed to prevent the spread of smoke or fire. These criteria are equally applicable to both load bearing and non-load bearing elements. There is further discussion of different failure criteria later in this chapter and throughout the thesis.

In summary, standard testing is by definition conducted in an artificial environment. It is artificial in several senses:

- The assemblies are tested in isolation. Consequently, the interaction of the element with a larger structure is not represented or understood.
- The furnace and standard curve do not take into account the material that is being tests. For example, if the surface of the test assembly has a very high thermal inertia, then less gas (or oil) will be required to achieve the required temperature in the compartment at any given time. This results in a less severe test.
- The assembly can be tested any number of times until it achieves the require fire rating.
- Unlike the original standard, an assembly only needs to achieve the required time to obtain a rating. An assembly that failed after 1hr and

1s would achieve the same rating as an assembly that failed after 1hr 29min and 59s.

It should also be stated that there are some advantages of this testing method. For example, the standard is universally recognized and its meaning is therefore well understood by engineers around the world. Also, the long history of the test means that many products have been rated using the system: to change it would require the retesting of thousands of products.

#### 2.1.1.2. Moving Away From Standard Testing

In the UK from 1946, a fire grading system was introduced [61]. The aim of this was to safeguard life-safety and property. This system gave the required fire resistance ratings (according to BS 476) for different building occupancies and was generally regarded as being successful in its aim [107]. However, the economic rationality of fire protecting public and office buildings and the proportionality of the cost with respect to other aspects of safety was questioned [67].

During the 1970s, the desire to reduce or eliminate fire protection from steel structures led architects and engineers to find justifications for removing protection based on how the structure performed and the wider context of the building. Some of the earliest examples of this performance-based design include the Royal Exchange, Manchester, and the Pompidou centre, Paris [105]. These projects reasoned that fire protection could be omitted without additional danger to occupants or the fire-service and, in the case of the Pompidou centre, the main columns were filled and cooled with water to

allow the omission of external protection [105]. At this time, however, there was resistance to the introduction of fire safety engineering into structural fire design; this was both from structural engineers and regulators [108]. It was, though, recognized that the procedure of standard fire testing was both unreliable and expensive [126,163]. It was also thought that one of the limitations of the standard fire test was that it did not take into account the behaviour of the whole structure and that this could lead to failure of elements in real fires which passed the standard fire test [106]. As a consequence of these concerns, there was a move towards analytical structural fire engineering methods; alternative approaches to obtaining fire ratings were sought [36,59,87,95,160].

At this stage, most of the interest was in relation to steel members; the reason for this focus was due to the high cost of protecting steel members against fire [102]. Although some work was conducted on concrete members [77], as concrete's fire protection was seen as being inherent to the material, most of the work on concrete concentrated on cover [43]. However, there was a significant amount work on the material behaviour of concrete at high temperature [4,94,127]. It was also recognized that thermal expansion could play a significant role in the behaviour of members [39]. As computers became increasingly available and powerful, the focus shifted from analytical (hand calculation) approaches to numerical approaches [66,140]. The finite-element method and other numerical calculation methods were used to predict the behaviour of steel structures exposed to fire [30,128,141].

In summary, during this period of development there was a good deal of progress in the discipline of structural fire engineering. Shortcomings with traditional methods of design had been identified; pressure from consultants [107] and the innovation of new computer techniques were driving the development of the design guides [36,59] and model codes [33] that became the basis for the Structural Fire Eurocodes.

#### 2.1.1.3. Towards Whole Frame Behaviour

In the early hours of June 23rd 1990, a major fire occurred at 14 storey office building in Bishopsgate, London [149]. The building (Figure 2-1) was in the final stages of construction and although most of the partition walls and fire protection was fitted, sections of column protection were not present at the seat of the fire. The fire began in a sub-contractors hut on the 1st floor and caused extensive damage to the first and second floors. The fire was deemed to have burnt severely for two and a half hours with a total duration of four and a half hours. There were no casualties, but £25,000,000 of damage was caused; of this, only £2,000,000 was structural damage [45].

a) b)

Figure 2-1. Figures from official Broadgate report [149] a) Broadgate building prior to fire; b) part of burned section of the building.

The performance of the structure was considered to be satisfactory as there was no collapse, and adjoining property remained safe. Indeed, as the first fire of its kind [149], Broadgate revealed the degree to which whole structural frame could contribute to structural performance during a fire; it also showed that the single member approach to fire safety design was non-rational and over-conservative [102]. The relatively good performance of Broadgate, and the non-inclusion of the phenomena observed in design practices of the time led to a new phase in structural fire research.

In response to Broadgate and in an attempt to better understand how the structure had behaved, a series of large scale fire tests were conducted at BRE's testing facility at Cardington. Fire testing had been conducted at this

facility since 1970 [131], and by the early 1990's, there were 14 permanent rigs established. Three large scale structures were built at Cardington, the first was an eight storey composite steel structure completed in March 1993; the second was a timber frame test; and the third was a concrete frame.

In the steel test the design of the structure, and fires to which it was subject were heavily influenced by Broadgate [24]. In 1995 and 1996, a series of six tests were conducted on different parts of the structure. During the various tests, it was found that steel temperatures in some locations exceeded 1100 °C with no collapse occurring. Traditional design methods would have defined failure at approximately 680 °C; this emphasized the difference between the behaviour in a standard test and in a real structural assembly. A significant amount of computer modelling work was conducted on the Cardington steel frame tests.

Initial modelling attempts were generally successful; however, many simplifying assumptions were made [13]. As techniques became more advanced, the number of simplifying assumptions was reduced. Non-linear material and geometric effects were included in finite-element models developed by researchers at Sheffield, Edinburgh, and Imperial Universities [49,75,83].

The Cardington tests and the computer models definitively demonstrated that composite action of a whole structure could dramatically improve performance during a fire. As the beams were heated, the slab began to act

as a tensile membrane [121]. This change in behaviour caused the slab to perform better than it would have done if bending was the dominant mechanism: large deflections were achieved without loss of stability or compartmentation. Together, Broadgate and Cardington demonstrated that the single-element, standard testing approach was inadequate in terms of understanding ultimate performance, and overconservative. The experiments, in conjunction with some additional testing [18], resulted in the development of new design tools and guidance [10,11,121].

In 1998, a similar sized concrete frame was also constructed at Cardington. The frame was intended to analyse the performance of various aspects of construction and the performance of the structure. One aspect of the study was the response of the structure to fire [34]. However, due to the imminent closure of BRE's Cardington facility, the experimental setup and testing was conducted hastily in the late summer of 2001 [9,82]. Unfortunately during the test, spalling caused some of the fire protection material shielding the data collection equipment to become dislodged; as a result, the cabling for the data-logging equipment was destroyed and there is only a partial dataset. Though there have been general studies into the behaviour during the fire, in comparison with the steel tests at Cardington, little modelling work has been done, as the dataset was incomplete.

Though the full scale Cardington test represented a step change in the approach of researchers and engineers with regard to the behaviour of structures in fire, it also represents the zenith of large scale structural fire

testing to-date. Subsequently, there have been whole frame tests, but they have generally been much smaller experiments [16,109,110].

#### 2.1.1.4. Towards Performance Based Design

The net result of these developments is that design philosophies and engineering techniques in connection with fire have begun, and continue, to change. The conventional methods of prescriptive design had become an obstacle in the drive for more advanced and efficient structures. The mid-1990s saw the introduction of performance-based design in many countries around the world [29]. This allowed engineers to design structures to meet performance requirements rather than to follow a prescribed set of rules for each structural assembly. For example, design codes such as Eurocodes 0 to 4 [51,52,54,56,58] allow engineers a high degree of flexibility in the way they design structures. Prescriptive design remains acceptable, but if they wish, engineers may use more advanced approaches such as calculation methods or finite-element modelling to demonstrate that a structure is able to perform adequately in a fire.

## 2.2. Techniques For Design

Early modelling techniques were intended mainly as a substitute for the standard test. The aim was to calculate the critical temperature of a beam analytically rather than conduct an expensive and unreliable furnace test. Later, the focus shifted towards representing all aspects of structural behaviour that would occur in a real fire. There are a multitude of techniques that can be used for the design of structures in fire. They can be broadly divided into two approaches; “simplified” calculations, and “advanced” calculations. Many of the simplified approaches are described in a number of textbooks [29,42,129]; they will not, therefore, be described in full detail here.

Rather, special attention will be paid to the isotherm method which is specific to concrete design. The isotherm method is discussed further in chapter 4.

### 2.2.1. Isotherm Method

Hand calculations have the significant advantage that they are relatively basic; they can often be completed by hand, or in a simple spreadsheet. They do not require knowledge of advanced pieces of software, and can often be accomplished by following simple rules. It is not always necessary to resort to complex heat transfer models to estimate the temperature in the steel; there are a number of different estimation approaches which can be taken [29]. Temperatures in concrete, however, are more complex to predict due to the non-linear behaviour of the temperature properties.

To account for this, a number of pre-calculated temperature profiles for different concrete sections subject to the Standard Fire are available in codes [55]. These allow designers to perform calculations to predict the sectional capacity of the heated member. The simplest and most widespread [112] of these is the 500 $^{\circ}$C isotherm method. This technique is used to calculate the moment and axial interaction capacity of a concrete member under heating. As the high temperature behaviour of concrete is very complex, the behaviour is reduced to a simple "on or off" type analysis. Material that is found to be in excess of 500 $^{\circ}$C is ignored when calculating the resistance of the section. Likewise, material that is below the 500 $^{\circ}$C limit is assumed to be under ambient conditions.

The temperature of the steel reinforcement bars is assumed to be the same temperature as the surrounding concrete. The yield stress of the steel is assumed to be in line with realistic degradation rates. Other than these two modifications, the calculation of the axial/bending interaction diagram is much the same as is conducted under ambient conditions [119].

### 2.2.2. Finite-Element Modelling

The ability of computers to model structures subject to fire has advanced significantly since the mid-1990s. Early finite-element models were fairly limited in their range of applicability [150]. Typically, they were created to perform a specific task and performed this reasonably well. However, there was little consideration of anything more than single elements in isolation. As computers became more powerful and the events at Broadgate and Cardington drew attention towards the importance of full structural behaviour the finite-element tools became more advanced.

The software can be broadly split into two catagories: purpose built software aimed at structural fire engineering problems; and general purpose finite-element packages that are also able to model the effects of temperature. The two main purpose built software packages are Vulcan [137] and SAFIR [65]. These have been developed and validated [64,65] by researchers at the Universities of Sheffield and Liege. The general purpose software packages include Abaqus [1] and ANSYS [5] and have a huge range of functionality some parts of which are applicable to the field of structural fire engineering. The appropriateness of using such general packages in structural fire engineering has been demonstrated by a number of researchers who have successfully modelled structures subject to fire [75,81,101].

### 2.2.3. Defining Failure

One of the problems frequently encountered in both structural testing and numerical modelling is that of the definition of failure. If a slab collapses, then it can obviously be said to have failed. However, if a collapse occurs during a test this can cause considerable damage to the furnace [14]. Thus, definitions of failure for testing applications are conservative so that the test can be stopped before catastrophic failures occur [97]. Throughout this work a number of definitions of failure will be considered. Each of these definitions is made using a particular measure of structural behaviour. It is not clear that one definition is inherently superior to another. The measures stem from structural testing procedures or from material property definitions. They are frequently now applied not just to testing the performance of real structures, but also to the design of structures to resist fire. Finite-element models make it very easy to measure each of the indicators described below. Consequently, engineers can use one (or multiple) definitions to identify strengths and weaknesses in their designs.

#### 2.2.3.1. Deflection

Maximum deflection is frequently used as a failure criterion. Failure is typically defined as a ratio of deflection (e.g. span/20 [27]) or, where appropriate, can be defined as the deflection which would breach compartmentation. For the reasons described above, this definition is not strictly one of stability loss but rather a useful, if rather arbitrary, definition by which the performance of a structure can be measured.

It should also be noted that rate of deflection is also frequently used as an indication of the loss of stability and the start of runaway deflection. A limit

for rate of deflection is given in the British Standards [27] as $L^2/9000d$, where $d$ is the distance from the top of the section to the bottom of the design tension zone and $L$ is the span. This criteria is only used when the deflection has already exceeded $L/30$.

#### 2.2.3.2. Temperature

In steel structures the temperature of columns or beams is often used as a simple indication of failure. For concrete structures, this translates to the temperature of the tension reinforcement. The member is typically said to have failed when the yield stress of the steel reaches half its ambient capacity. This occurs at what is known as the "critical temperature"; for rebar this is usually taken as 593 °C [98].

#### 2.2.3.3. Excessive Steel Strain

In concrete structures, the rupture strain in steel reinforcement is often used as a basis for a failure criterion. Typically this measure is better suited to the numerical analysis of structures rather than fire tests because of the difficulties associated with instrumentation of rebar. The ultimate strain for steel at any temperature is usually taken as 0.2 [32,57].

## 2.3. Materials

All of the behaviours that structures exhibit as they are heated have their roots in the changing mechanical and thermal properties of construction materials. Many papers [79,90,94,144] and books [22,29,129] describe the properties of steel and concrete at ambient and high temperatures. This chapter does not intend to rehearse the full details of these studies. Rather, it aims to provide the reader with a summary of the main processes and trends that govern a material's behaviour at ambient and at high temperature.

Where a parameter or process is of particular relevance to this work, it will be explored in greater depth.

Since concrete is the primary focus for this thesis, it will be discussed in the most detail; steel will be treated more briefly. Recently, traditional concrete construction has been supplemented by the addition of Fibre Reinforced Polymers (FRP), and plastic or steel fibres. Both of these materials are outwith the scope of this study; the material properties and changes in concrete properties that these additions invoke will not be considered.

### 2.3.1. Concrete

The variation in different concretes due to exposure to high temperatures is extremely great [22]. It is possible to describe the qualitative processes that concrete undergoes as it is heated, but to predict exactly the quantitative behaviour for anything other than a precisely known mix of materials is very challenging. Instead, statistical averages of multiple tests on different concretes must be taken. These can be used as the basis for numerical models. This section briefly reviews the physical changes that concrete undergoes, and describes the main generally accepted phenomena that occur.

### 2.3.2. Physical Behaviour

Reinforced concrete consists of cement paste, aggregate and rebar [63]. Studies of concrete material properties at temperature have tended to focus mainly on plain concrete. It has been found that one of the main factors affecting compressive strength with temperature is aggregate type [22,144]. There are two main classes of aggregate type; Calcareous, and Silicous. Though the behaviours of these two types of concrete are different, the

processes that they undergo are similar in nature. Bazant [22] recognizes that due to the large number of factors affecting the compressive strength of concrete at high temperature, it is possible to draw only broad "qualitative" conclusions.

The behaviour of concrete in fire has been found to depend largely on the materials from which it is made. It has been noted that due to the varying compositions of different concretes, strength loss at 120 °C can range from 30% to 100%; by changing the concrete mix, it is possible to induce strength loss at a higher temperature [90]. However, cement type has been found to have little effect on the compressive strength and other researchers have stated that different water cement ratios do not affect the changes in the compressive strength [22,144].

As concrete is heated changes occur in its chemical composition, physical structure and water content. Most of these changes occur within the cement paste [22]. The first of these changes to initiate is evaporation of all the free water [79]. This process reaches its peak just above 100 °C. Below 105 °C it is generally accepted that the amount of chemically bound water does not change. However, high temperatures "drive out" the pore water present in the cement paste and above 105 °C the amount of chemically bound water reduces [22]. It has been found that from approximately 150 °C, the chemically bound water begins to be released from the hydrated calcium silicate. This causes shrinkage which, in conjunction with the thermal expansion of the aggregate, causes micro-cracking from approximately

300 ° C. The formation of these micro-cracks causes irreversible changes in the concrete's compressive strength and stiffness [79]. The development of these cracks can be limited as it has been found that compressive stress in the material during heating can have an impact on the compressive strength. This is because the compressive stress helps to keep cracks closed and is particularly the case where the loading ratio is greater than 20% [144].

Between 400 ° C and 600 ° C, cement crystals decompose causing weakening of the concrete [79]. It loses 80% of its compressive strength between 400 ° C and 800 ° C [164]. Indeed, when concrete has been heated to above 800 ° C it is reported that, on cooling, it can often be crumbled by hand [79]. Up to approximately 500 ° C, the weight loss of aggregates is minimal. The aggregates in most concrete remain stable up to this temperature particularly for lightweight aggregates [22]. Calcareous concretes begin to loose their strength at higher temperatures than concretes of silicious aggregates [144]. In siliceous aggregates, the quartz present experiences a crystalline structural change between 500 ° C and 650 ° C. This change is a non-recoverable endothermic reaction; in the case of calcareous aggregates decarbonation occurs, and carbon dioxide is expelled [22]. On cooling, the newly freed calcium oxide absorbs atmospheric water, and expands. This expansion causes the already formed cracks to expand further [79].

Above 1150 ° C all the minerals in the cement paste have either melted or turned to their glass phase [79]. A further phase change in siliceous aggregates between 1000 ° C and 1200 ° C results in the complete and

irreversible breakdown in the structure of the quartz. Further structural changes occur before melting commences at approximately 1700 ° C.

On cooling, depending on environmental conditions, and the composition of the concrete, further strength loss can be induced, or a slight recovery can be made [85,164,165]. Some researchers have found a further decrease in strength by 20% [144], while others have observed a recovery of 13% [85].

### 2.3.3. Parametric Description

The processes described above, and the composition of any concrete, have multiple and varied effects on the mechanical and thermal properties of concrete as it is heated and cooled. The exact rates of degradation in strength and stiffness etc. will depend on the exact mix of the concrete as well as the experimental setup. The results of innumerable experimental studies are not, therefore, presented; instead, the numerical models presented in Eurocode 2 are briefly described. These trends are generally accepted, and though quibbles may exist regarding precise values and exact rates of degradation, the behaviour is well documented in a number of well known sources [29,129]. The author feels, therefore, that to repeat these trends here would not add anything to this work and the reader is, therefore, referred to textbooks such as Buchanan's [29] and Purkiss' [129] for a discussion of the properties and to Eurocode 2 [55] for a detailed parameterized description of the phenomena. A very brief description is provided below to highlight the most important points of behaviour. Discussion of the various approaches to implementing these descriptions in finite-element codes is provided in chapter three.

#### 2.3.3.1. Thermal Properties

The most dramatic changes in the thermal properties of concrete are caused by the evaporation of water. Numerically, this is typically represented by a sudden increase in the specific heat capacity between 100 °C and 120 °C and then a return to the original value [101,162]. The size of this increase is dependent on the moisture content of the concrete being modelled. The other major change in the thermal properties of concrete is the reduction in conductivity due to cracking and degradation; there is also some minor reduction in the material's density.

#### 2.3.3.2. Mechanical Properties

The most important changes in the mechanical properties are the degradation of stiffness and strength, and the thermal expansion of the material.

Initially, there is little loss of ultimate strength, but above 500 °C the reduction in compressive strength is rapid [78,85]. It has been shown that prudent choice of aggregate can increase the temperature at which significant degradation occurs to 600 °C [89]. It is generally acknowledged that the material does not return to its original strength when it returns to ambient temperatures though the degree of recovery is uncertain [22,79,144,165], ranging from further degradation to some recovery.

The degradation of stiffness shows a broadly linear trend between 200 °C and 700 °C [143]. A number of researchers have presented models which attempt to replicate this behaviour. The methods are broadly similar and were summarised by Youseff [167].

The degree of thermal expansion is highly dependent on the types of aggregate used. Siliceous aggregates tend to expand the most, followed by calcareous, and light-weight aggregates which show almost no expansion [91]. The degree of expansion given in EC2 is broadly in line with other experimental data [22,143].

### 2.3.4. Steel

The behaviour of steel is significantly less complex than that of concrete. The main physical changes are the loss of strength and stiffness, and a crystalline phase change at 712 °C. As with concrete, the reader is referred to standard texts [29,129] for more information on the behaviour of steel at high temperatures.

## 2.4. Summary and Conclusions

This chapter has provided background for the remainder of the thesis: the history of structural fire engineering has been traced from the turn of the 1900s to the present day; the processes that concrete undergoes as it is heated are discussed; and some of the methods that can be used to assess structural performance have been described. This description is by no means a full account, but rather locates the current research in a broader context. There are a few conclusions that can be drawn from this chapter.

- Structural fire engineering is a relatively young discipline: the processes and techniques that are used are in a constant state of development.
- Despite its relative youth, many of the founding principles are based on work that was conducted up to 100 years ago. Many of the decisions that were made at that time appear rather arbitrary in

today's context. In spite of this, the work has had, and continues to have, a huge impact on the development of the field.

- An appreciation of the motivation and reasoning behind early decisions is necessary to understand the current techniques used in the field.
- Most of the more recent developments in structural fire engineering have occurred in relation to steel structures.
- The chemical processes and parametric changes that concrete undergoes as it is heated are well understood.
- An understanding of just one of the many phenomena that occur as a structure is heated is not sufficient to analyse the behaviour of concrete structures in fire.
- Definitions of structural failure are often arbitrary.

# 3

# Numerical Modelling of Concrete at High Temperature

The previous chapter discussed the degradation phenomena such as the reduction in strength and stiffness that occur as concrete is heated. However, to transfer these observable properties into codified modelling techniques, the parameters must be expressed mathematically. Some modelling techniques rely on the pre-definition of sectional moment/curvature and axial force/strain properties [73,97], but the most common approach is to define the material behaviour from predefined behaviours [55]. This allows the strain and corresponding stress to be calculated (or looked up) on an ad-hoc basis and used within a model as required. The definition of the relationship between strain and stress is known as a constitutive model. This chapter presents several constitutive models which were created specifically for

modelling concrete at high temperatures. This chapter also analyses the behaviour known as load induced thermal strain. New techniques for implementing this phenomena in constitutive curves are proposed and their influence on finite-element models are considered.

## 3.1. Constitutive Models

Once a set of material degradation parameters such as those discussed in the previous chapter have been described, it is necessary to link them together in a complete model. In the case of concrete in fire, a number of different researchers have created mathematical descriptions which attempt to represent the stress-strain behaviour of concrete as strain and temperature vary.

It is clear from the description of the processes which heated concrete undergoes that there are a large number of different strain constituents that influence the behaviour of concrete. There is differential expansion, cracking, shrinkage and creep; indeed, some researchers have studied with great depth the different strain processes which occur during concrete heating [92] and have identified many separate types of strain. The aim with most structural modelling, however, is not to create a model which captures all phenomena exactly, but rather capture the major trends which a material undergoes. As such, most stress-strain models for heated concrete simplify these down to the following equation [29,129]:

$$\varepsilon = \varepsilon_{th}(T) + \varepsilon_{\sigma}(\sigma,T) + \varepsilon_{cr}(\sigma,T,t) + \varepsilon_{tr}(\sigma,T) \tag{3.1}$$

Where, $\varepsilon$ is the total strain, $\varepsilon_{th}$ is the thermal strain, $\varepsilon_{\sigma}$ is the mechanical strain, $\varepsilon_{cr}$ is the creep strain, and $\varepsilon_{tr}$ is the transient strain. Though many

researchers have produced formulae for the estimation of specific properties, only a limited number [71,124,144,153,154] have produced complete constitutive models to describe the compressive stress strain behaviour of concrete. In recent years, several papers have summarized some of these models [113,167] – though there are differences in the way the models have been interpreted. Three of the most well known models are described in detail in this chapter: the Khoury-Terro model [153]; the Anderberg-Thelandersson model [4]; and the model adopted by Eurocode 2 [55].

Before these models are described, though, equation 3.1 will be examined more closely. The total strain to which a piece of concrete is subjected is composed of several parts:

*Thermal strain.* Thermal strain, also known as thermal expansion, is defined as the degree to which the material expands as it is heated. The thermal strain in concrete is caused by a combination of net expansion of the aggregate and the cement paste. Unrestrained thermal expansion does not induce any mechanical stresses in the concrete. Thermal strain is typically defined in terms of $\alpha$ (or strain per degree temperature change) and is a function of temperature.

*Mechanical strain.* Mechanical strain is the strain which directly induces stresses in the material. It is composed of elastic strain and plastic strain and is a function of temperature and stress.

*Creep strain.* Creep strain describes the strain which occurs with time and is a function of temperature, stress and time. In many situations, the creep strain is considered so small that it is negligible [113].

*Transient strain.* Transient strain is an additional plastic strain constituent that is dependent on temperature and stress. Often called load induced thermal strain (LITS), this constituent is considered in more detail below.

All of these constituents must be considered to accurately represent different types of structure. It is not, however, necessary to include the thermal strain in the constitutive model as this is not dependent on the stress in the material – only the temperature. Consequently, the following models describe the constitutive stress-stain curves excluding the influence of thermal expansion.

### 3.1.1. Khoury-Terro Model

Over the past three decades, a significant body of work has been completed at Imperial College [92,94] regarding the behaviour of concrete under different temperature and loading conditions. One of the focuses has been to advance the understanding of the phenomena known as load induced thermal strain. Based on the experimental data generated at Imperial, Terro [153] created a constitutive model for concrete that incorporated an empirically fitted equation for LITS.

The mechanical stress strain formulation was a simplified method of the model proposed by Schneider [144]. That is;

$$\varepsilon = \left[ 1 + \frac{1}{n-1} \cdot \left( \frac{\varepsilon}{\varepsilon_{uT}} \right)^n \right] \cdot \frac{\sigma}{E_T} \tag{3.2}$$

where;

$$E_T = \frac{2\sigma_{uT}}{\varepsilon_{uT}} \tag{3.3}$$

Where $\varepsilon_{uT}$ is the temperature dependent strain at peak stress, and $\sigma_{uT}$ is the temperature dependent ultimate stress. Schneider proposed that $n$ should be equal to 2.5 for lightweight concrete and 3.0 for normal concrete. Terro, however, adopted $n = 2$. The empirically fitted LITS equation took the form:

$$\varepsilon_{tr} = LITS \cdot \left( 0.032 + 3.226 \frac{\sigma}{\sigma_{uT}} \right) \tag{3.4}$$

where;

$$LITS = \left( 43.87 - 2.73T - 6.35 \cdot 10^{-2} T^2 + 2.19 \cdot 10^{-4} T^3 - 2.77 \cdot 10^{-7} T^4 \right) \cdot 10^{-6} \tag{3.5}$$

Equation 3.5 was fitted to the master LITS curve created by Khoury. However, Thames gravel concrete departed from the master curve above 400 °C and a fifth order polynomial was proposed for use in this case. A number of formulae were also presented for strain at maximum stress to account for different levels of pre-stress. Figure 3-1 shows the stress strain plot for Terro's equations at different temperatures.

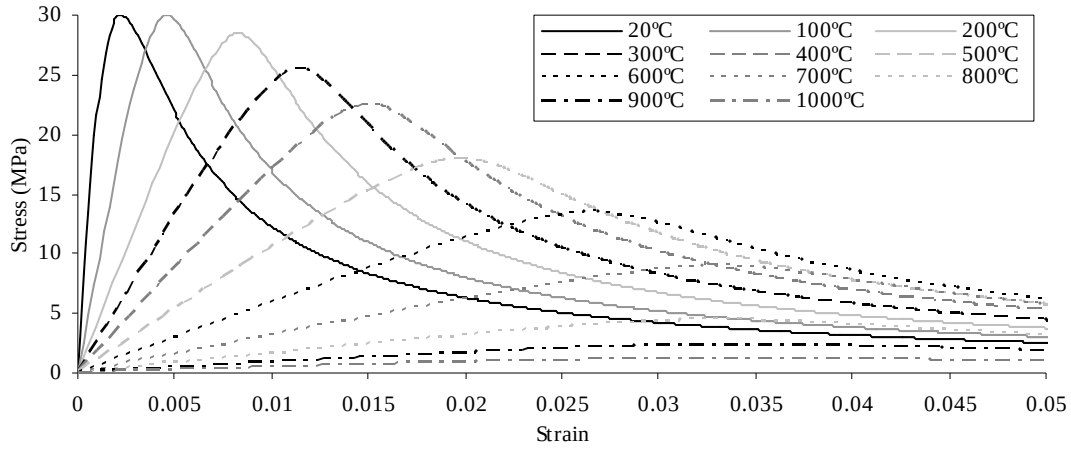


Figure 3-1. Constitutive curve for concrete at high temperature according to Terro's model.

There are several points that should be made about Terro's model:

- It does not explicitly state that the strain due to LITS is irreversible. Though this does not affect the ascending branch of the stress strain curve, it does influence the descending branch. It is assumed here that, given the irreversible nature of LITS, it is intended that the LITS be fully plastic.
- There is no allowance made for a time dependant creep component.
- In recent studies of constitutive models, there has been inconsistency in the application of the instantaneous stress-strain curve. The study by Li [113] regarded the relationship to be linear elastic, whereas, the study by Youssef [167] used the Schneider method above. This study will use the latter method since this allows for a descending branch, and provides a much closer match to available data.

- In the study by Youssef, where the Schneider method was adopted, it was concluded that the model achieved "good accuracy".

### 3.1.2. Anderberg Thelandersson Model

Anderberg's method [26,113,167], published in 1976, is based on results from experimental data from the Lund Institute of Technology. As with Terro's model, Anderberg's approach subdivides the strains in accordance with equation 3.1 and explicitly considers the presence of transient strain components.

The instantaneous stress-strain component is given in two parts. A parabolic ascending branch, and a mostly linear descending branch. The parabolic curve continues beyond the strain at ultimate stress in order to provide a smooth transition between the ascending and descending branches. These equations take the form:

For $0 \leq \varepsilon \leq \varepsilon_1$

$$\sigma = E_T\left(\varepsilon - \frac{\varepsilon^2}{2\varepsilon_{uT}}\right) \tag{3.6}$$

For $\varepsilon_1 \leq \varepsilon \leq \varepsilon_{ult}$

$$\sigma = \sigma_1 + E^{-}\left(\varepsilon - \varepsilon_1\right) \tag{3.7}$$

In which

$$\sigma_1 = E\left(\varepsilon_1 - \frac{\varepsilon_1^2}{2\varepsilon_{uT}}\right) \tag{3.8}$$

$$\varepsilon_1 = \varepsilon_{uT}\left(1 - \frac{E^-}{E}\right) \tag{3.9}$$

$$\varepsilon_{uT} = \frac{2\sigma_{uT}}{E} \tag{3.10}$$

Anderberg defines transient strain as:

For $T \leq 550\,^{\circ}\mathrm{C}$

$$\varepsilon_{tr} = -k_{tr}\left(\frac{\sigma}{\sigma_{u0}}\right)\varepsilon_{th} \tag{3.11}$$

For $T \geq 550\,^{\circ}\mathrm{C}$

$$\frac{\partial \varepsilon_{tr}}{\partial T} = -0.0001\left(\frac{\sigma}{\sigma_{u0}}\right) \tag{3.12}$$

Where $\sigma_{u0}$ ultimate stress at ambient, and $k_{tr}$ is given as 2.35.

The transient strain part of Anderberg's formulation has been the subject of much discussion. Work by Khoury [93] has demonstrated that there is no link directly between thermal expansion and transient strain. Discussion has primarily focused on whether or not it is valid to use a numerical relationship despite there being no physical basis for it. Despite the issues from which the model suffers, recently further research has obtained "$k_{tr}$" values for different types of concrete [155]. However, the scope for such work has been shown to be limited since there are some concretes for which thermal expansion is zero, yet LITS still occurs; this could not be represented by this model.

In an attempt to address the problem of linking the transient strain to thermal expansion, Nielsen [122] proposed a modification to Anderberg's equation which removes the link to thermal expansion giving:

$$\varepsilon_{tr} = -0.00038 \cdot \left( \frac{\sigma_{cT}}{f_c} \right) \cdot T \tag{3.13}$$

Unlike Anderberg's transient strain component, this can be used for all values of temperature and stress. Nielsen's formula has been shown to provide a good match to both experimental data and the model proposed by Terro. Anderberg's model also includes a creep strain component. However, it was noted that practically it may be neglected in short term transient conditions [113] – such as exposure to fire. For other applications, for example in nuclear reactor design, it would be necessary to consider creep due to the longer term exposure to elevated temperatures.

Figure 3-2 shows the final constitutive curves for various temperatures for Anderberg's equations including Nielsen's modification.

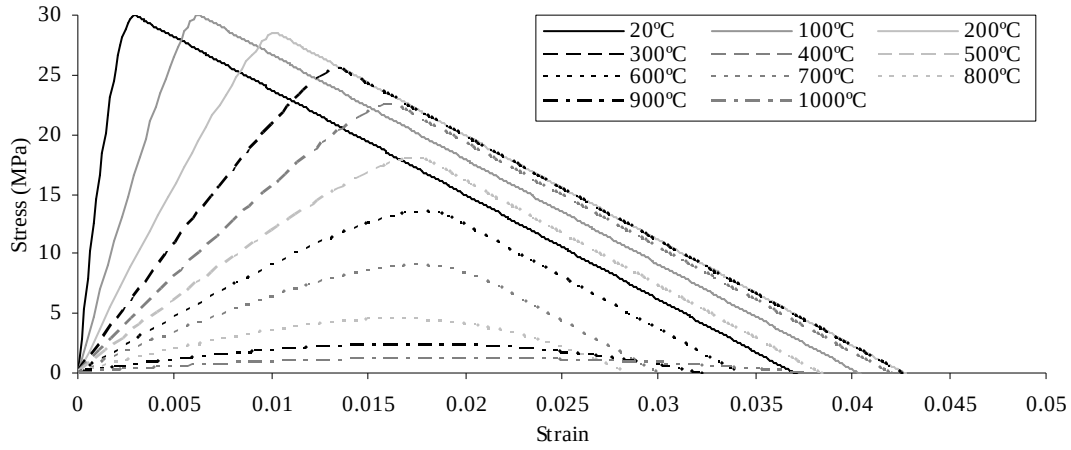


Figure 3-2. Constitutive curves for Anderberg's model corresponding to various different temperatures.

Several points can be made about Anderberg's model:

- Though a formula for creep strain is included, it can be omitted under certain conditions. This is convenient numerically since its inclusion would require the introduction of time into any simulation; without it, this is not necessary.
- The issues relating to the link between transient strain and thermal expansion can be resolved satisfactorily by the use of Nielsen's formula.
- It has been demonstrated to compare well with experimental data.
- It is highly sensitive to the variation of Young's modulus.

### 3.1.3. Eurocode 2 Model

Chapter two referred to Eurocode 2 [55] in relation to quantification of the degradation rates of various material properties. Also presented in this Eurocode is a formulation for a full constitutive model that defines the

material's stress strain relationship using a single equation. The ascending branch of the stress-strain curve uses the equation:

$$\sigma = \frac{3\varepsilon\sigma_{cT}}{\varepsilon_{uT}\left(2+\left(\frac{\varepsilon}{\varepsilon_{uT}}\right)^{3}\right)} \tag{3.15}$$

The definition of the descending branch is left as a matter of discretion for the user. It can be either linear or non-linear according to equation 3.15; the maximum allowable strain is, however, defined. Figure 3-3 shows the stress strain diagram for Eurocode 2 with a linear descending branch.

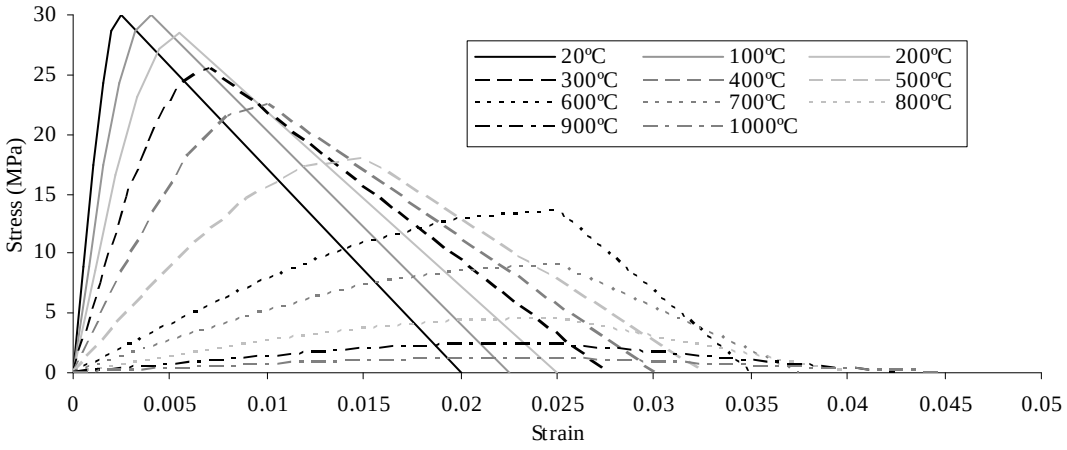


Figure 3-3. Definition of constitutive stress-strain curves according to Eurocode 2-2.

Though it is explicitly acknowledged in the Eurocode document that the total strain is composed of the constituents of equation 3.1, no guidance is offered specifically regarding the inclusion of LITS. It must be assumed, therefore, that transient strain components are implicitly included in the formulation. This assumption is confirmed by the similarities that can be found when comparing the various methods.

## 3.2. Comparison of Methods

Chapter two described the changes in the material parameters that are used to inform the constitutive models above. Since the different models above were calibrated using different types and mixes of concrete, a direct comparison of the models with their "as is" values would be misleading. A useful comparison between the models can only be made where there is a degree of uniformity in input parameters such as ultimate strength, and strain at peak stress. To allow comparison, parameters from different sources have been used. This method of comparison has been used before – though with different selection of parameters [113].

The same parameters have been used as inputs for the Terro and the Anderberg models; the reference ambient ultimate stress was taken as 30MPa; the strains at ultimate stress which Terro recommended [153] have been used for both models. Since both of these methods calculate the elastic modulus directly from this value, the elastic moduli are also the same. To allow these models to be compared with the Eurocode, the degradation of ultimate compressive strength recommended in the Eurocode was used as the ultimate compressive strength. Since the Eurocode is a free-standing document, it has been left "as is"; to change any of the input parameters would be distorting it from its intended form. Figure 3-4(a-d) shows the comparisons at different temperatures.

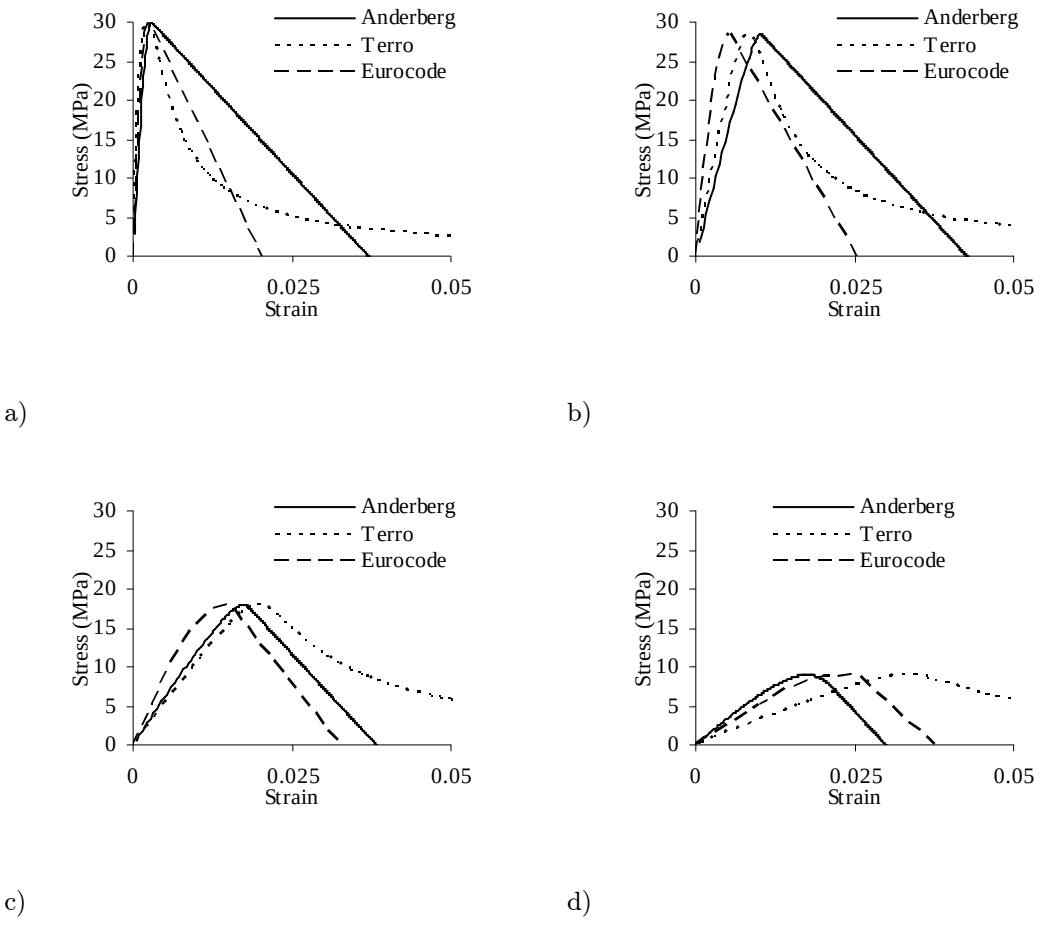


Figure 3-4. Comparison of three constitutive models at; a) ambient; b) 200 ˚; c) 500 ˚C; and d) 700 ˚C.

The ascending branches for the models are fairly consistent; though similarities between them start to reduce above 500 ˚C. The strains at peak stress are also broadly similar – with the exception of the 700 ˚C model. The main difference between the models is their descending branches. This is unsurprising, as the Anderberg and Eurocode models define a linear descending branch, while the Terro model shows a non-linear curve. It should be noted that there is provision within the Eurocode to use a non-linear descending branch as will be adopted in chapter four.

It is notable that one model is not consistently steeper, or has the lowest strain at ultimate stress. This demonstrates that in terms of stiffness and strain at peak stress, it is difficult to highlight one model as being particularly better – or worse – than another. It can be concluded, therefore, that, like the degradation parameters, though the work of different researchers may be different in the specifics, the overall effects are roughly equivalent. It should be noted though that the Eurocode model is steeper at 200 °C and 500 °C. The effects of this can be seen in the higher stresses that are generated during heated that are described later in this chapter.

Figure 3.4 shows the net results of all the contributions of the strains in equation 3.1. It does not, however, give any indication of the development of plastic or elastic strains. As with any material the development of plastic strains has a significant impact the behaviour of a concrete structure. Of the different strain constituents, the two plastic contributions are the plastic part of the conventional elasto-plastic response, and the transient stain component. As transient strain – sometimes called load induced thermal strain – is particularly important in concrete structures, particular attention will be given to it here.

## 3.3. Load Induced Thermal Strain

Load induced thermal strain in concrete has been studied for many years from a materials science perspective. The influence of LITS on the micro behaviour of concrete has been well understood, particularly in one dimension. The influence of LITS on overall structural behaviour, however, has been less well considered. Also neglected have been techniques for

including LITS in material models. This section will present the basic principles of LITS in significant detail: terminologies used to describe it are defined and explained; the impact of modelling techniques is also analysed with respect to the response of a structure during the cooling phase of a fire.

### 3.3.1. Previous Work

As presented in equation 3.1, the total strain developed in heated concrete is composed of a number of different constituents. Load induced thermal strain is an umbrella term used to refer to a number of these strain constituents [92]. The presence of LITS constituents alters the strain behaviour of concrete if the material is heated under applied stress. In fact, concrete heated under high compressive stresses can be observed to shrink – rather than expand due to thermal expansion. The most significant constituents of LITS (but not all) are non-recoverable; hence, the effects of LITS are only evident on first heating.

There has been a great deal of work concerning LITS over the past four decades [22,94,144,154]. Modern development of LITS started in the 1960s with the realisation that LITS existed [94]. The following decade saw a great deal of work which identified numerous LITS components and isolated them – demonstrating that the main component was distinct and had its own properties.

During the 1980s a large amount of work was carried out – particularly at Imperial College [93] – which suggested the existence of a "master" LITS

curve whose properties were independent from other concrete properties such as strength, age, moisture content, and aggregate type. As previously discussed with reference to Anderberg's model, Khoury *et al.* also showed that LITS was physically independent from free thermal expansion.

Despite the volume of work on the material property aspects of LITS, the implications for structural behaviour are yet to be fully understood. The presence of LITS causes additional strains. These could cause structures to respond differently than previously expected if LITS was not included. Since the strains involved are largely irrecoverable, LITS has an active influence during heating, but is not active during cooling. As the development of larger, whole frame, structural models becomes more commonplace, the understanding of how a structural member behaves and interacts with the rest of a building under heating *and* cooling becomes more important; the influence of preloading and the development of locked-in strains becomes more pertinent.

Although there are a large number of constituents involved in LITS it is not necessary to build phenomenological models which include every phenomenon separately. The models reviewed in the previous section include LITS either explicitly or implicitly by modelling the net outcome rather than the processes involved. Although modellers have also begun to include these LITS models in their simulations [26,120] no one of these models has been found to represent structural behaviour more satisfactorily than others. The process that is used to include LITS constituents in a material model is worth

analysing more closely so that the full implications of inclusion in finite-element models can be understood. To do this, it is necessary to also fully understand what is meant by LITS.

### 3.3.2. Explanation of LITS

LITS is defined as the difference in strain between the free thermal expansion ($\varepsilon_{th}$) of concrete, and the thermal expansion when the same concrete is heated under a level of pre-stress. Figure 3-5 shows the difference between a typical unstressed sample and a pre-stressed sample. It can be observed that under higher levels of pre-stress the material shrinks.

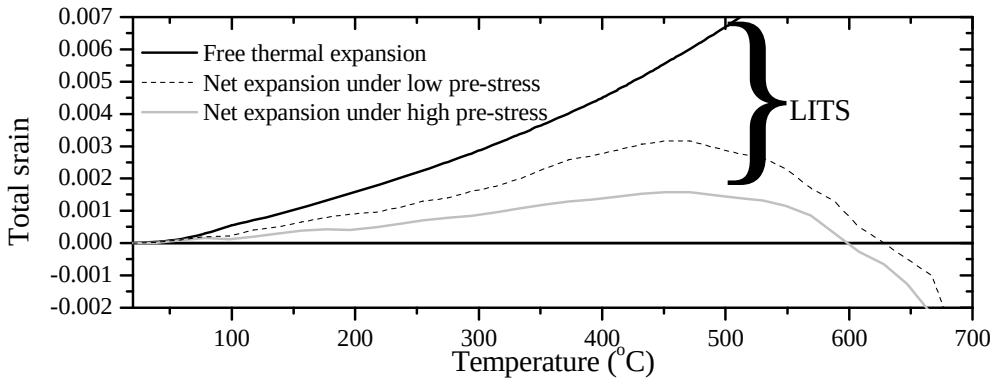


Figure 3-5. Difference between strain when heated with different levels of applied stress

The existence of a large number of distinct phenomena contributing to LITS has led to a number of different terms being used to describe them. This has caused some confusion regarding what different terms mean. The more commonly used terms are:

*Basic creep*. Basic creep is used to describe the strain of thermally stabilized concrete when under constant load at constant temperature. In conditions

where the temperature is not constant, by definition, the term basic creep cannot be used. Instead, Khoury [92] adopts the term of a "time dependent" strain which develops under transient heating conditions.

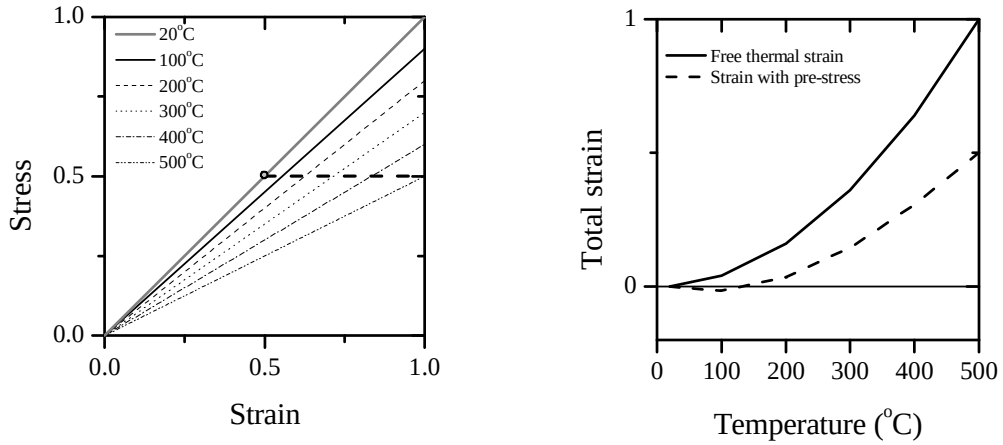


a) b)

Figure 3-6. Modelling LITS as part of the constitutive curve; a) elastic modulus at different temperatures; b) effect of different elastic moduli on total strain, corrected for initial strain.

*Elastic strain*. Though LITS appears to manifest itself as a change in the thermal expansion under different pre-stresses and temperatures, it can instead be thought of as being part of the stress-strain definition of the material. The elastic constituent of LITS is caused by the change in elastic modulus as temperature increases, as illustrated in Figure 3-6a. The horizontal constant stress line shows how the strain increases with increase in temperature. The influence of this change is demonstrated in Figure 3-6b where the total strain experienced by the material does not follow free thermal expansion. Instead, the strain at each temperature is reduced by the

reduction in elastic modulus. It should be noted that the total strain for the pre-stressed sample is corrected for initial strain.

Of course, the LITS developed in Figure 3-6b will be fully elastic, and were the material to be cooled back to the starting temperature the strains would be fully recovered. If, however, plastic strains were introduced they would not recover on cooling; the combination of these different types of strain is what is meant by the multiple components of LITS. Defining LITS in this way allows it to be included in the material's constitutive model for the concrete.

*Transitional thermal creep* (*ttc*). Transitional thermal creep develops plastically during first-time heating of sealed concrete under load [94]. It has been suggested that *ttc* is by far the largest component of LITS [153] and it should be emphasized that *ttc* is distinct from basic creep or time dependent strain. It is thought that the origins of transitional thermal creep are in the cement paste and that the addition of aggregate restrains it.

*Drying creep* is the shrinkage experienced by the material due to the evaporation of water. This can only occur where the specimen is unsealed and, therefore, able to dry out.

*Transient creep* and *transient strain* describe the same phenomenon and refer to the sum of *ttc* and drying creep. Though both these terms are technically time dependant it is thought, that for practical purposes, they can be

regarded as quasi-instantaneous. Since drying creep is regularly omitted from the transient strain calculation, and because *ttc* is such a large component of LITS, the three terms; *ttc*, transient strain, and LITS have been incorrectly regarded as synonymous. Henceforth, for clarity, transient creep/strain will be referred to as transient strain.

The effect of these plastic strain constituents is to modify the stress/total-strain relationship. Instead of tracing the path of the elastic modulus, strain will be offset by the additional strain constituents. It should also be noted relaxation will occur along the elastic modulus as shown in Figure 3-7. Since the strains are non-recoverable, they will be modelled here using plastic theory.

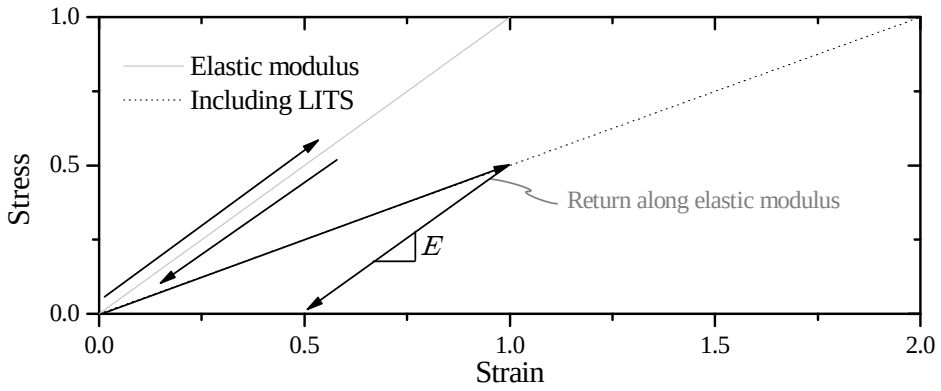


Figure 3-7. Elastic modulus and path followed after modification by plastic components; return is along the original elastic modulus.

### 3.3.3. Apparent Elastic Modulus

The constitutive curves described in the previous section have key features in common: they both present a constitutive stress strain curve which varies with temperature; the curves are based on the way that material strength

and elastic modulus degrade with increased temperature; the curves are then modified by the transient strain component (or the LITS component in the Terro model). This three step method of obtaining a final constitutive curve is demonstrated in Figure 3-8a.

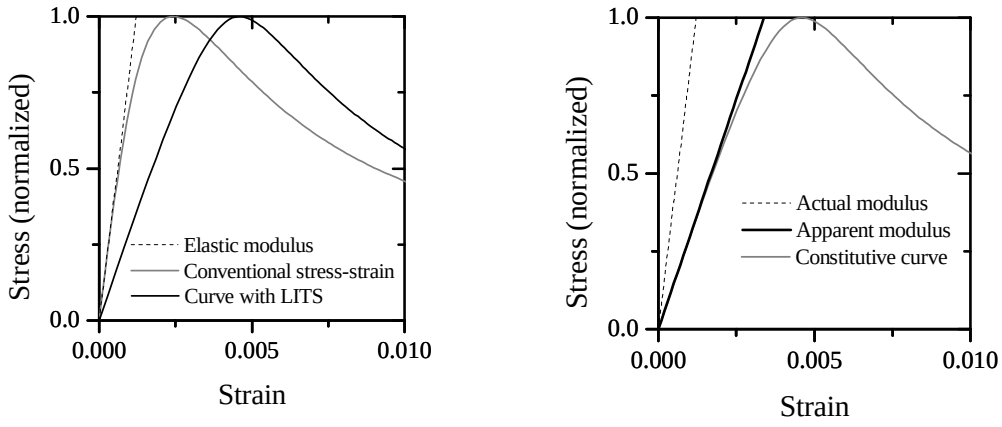


a) b)

Figure 3-8. Construction of the final constitutive curve: a) three step formulation of constitutive curve at a given temperature; b) apparent and actual elastic moduli.

For most stress-strain curves, there is an elastic region before the onset of plastic strain. It is reasonable, therefore, to assume that the initial tangent modulus is equal to the elastic modulus. Put another way, the first section of the stress-strain curve is within the elastic region of the material. The situation becomes less clear with the inclusion of LITS. The modification of the original stress-strain curve by the LITS components causes plastic strains to develop as soon as the material is stressed. The implication of this is that the tangent modulus of the constitutive stress-strain curve is never equal to elastic modulus of the material – even at zero strain, or where the ascending branch is straight.

It is, therefore, impossible to identify the elastic modulus of the material from simple inspection of the constitutive curve. If this is attempted, a value of elastic modulus will be obtained which is not the actual modulus, but the "apparent" modulus of the material. This will result in significant underestimation of the true plastic strains which would develop if the actual modulus was in use. Figure 3-8b illustrates the difference between the apparent elastic modulus of a material and the actual modulus as defined by the constitutive equations.

In finite-element applications the difference between the actual and apparent material moduli must be carefully considered. There are circumstances under which the differences between the moduli will not affect the response of a structural model. For example, under increasing strain or heating the solution will simply follow the defined curves in the appropriate way. However, if the applied strain is reduced, there are multiple heating phases, or there are more complex loading patterns to be considered, the mal-definition of the plastic strains becomes significant. This has not been a major issue for most models as the emphasis has predominantly been on the heating phase of the fire. However, as attention turns to cooling it is necessary to consider these components more carefully.

The mechanical properties of concrete described in Eurocode 2 [55] have the potential to suffer from these problems. The model is defined by the specification of peak stress, peak strain, and strain-at-peak-stress – not elastic modulus. Thus, the user has to define an elastic modulus to associate with

the model. A reasonable assumption might be to assume that the elastic modulus should be equal to the initial gradient of the constitutive curve. However, as discussed above, this may not be a useful or accurate assumption.

### 3.3.4. Simple Example

The influence of the definition of elastic modulus is demonstrated using a series of simple constitutive models. As with all the finite-element modelling conducted as part of this thesis, the code that was used was the commercially available software package Abaqus [1]. A plain concrete column pinned at both ends and idealised as a single element was considered. The temperature was raised uniformly to 500 °C and then cooled back down to ambient temperature. Five different constitutive models were applied: the Anderberg model; the Anderberg model with use of the apparent elastic modulus; the Terro model; the Terro model with the use of the apparent elastic modulus; and the Eurocode model. The constitutive curves for ambient and 500 °C are shown in Figure 3-9. The resulting stress from the heating and cooling regimes was then plotted against the temperature (Figure 3-10b.).

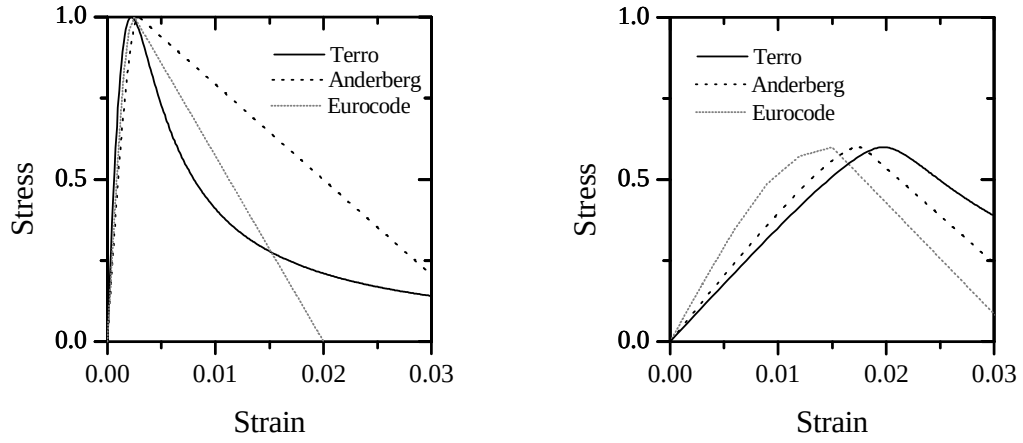


Figure 3-9. Constitutive curves at two different temperatures: a) at ambient; b) at 500 °C.

Thermal expansion caused compressive stresses to build up as the column was heated due to the fixed ends of the column. Though the associated material models followed the same path through heating, the strains that built up in the models with the apparent moduli were predominantly elastic, whereas, in the models with the actual moduli, most of the strain was plastic. This only becomes evident on cooling, where the apparent models slowly released the stresses and were only pulled into tension when the temperature was close to returning to ambient. The models which used the actual moduli, on the other hand, were unable to recover the strains developed and rapidly progressed into tension.

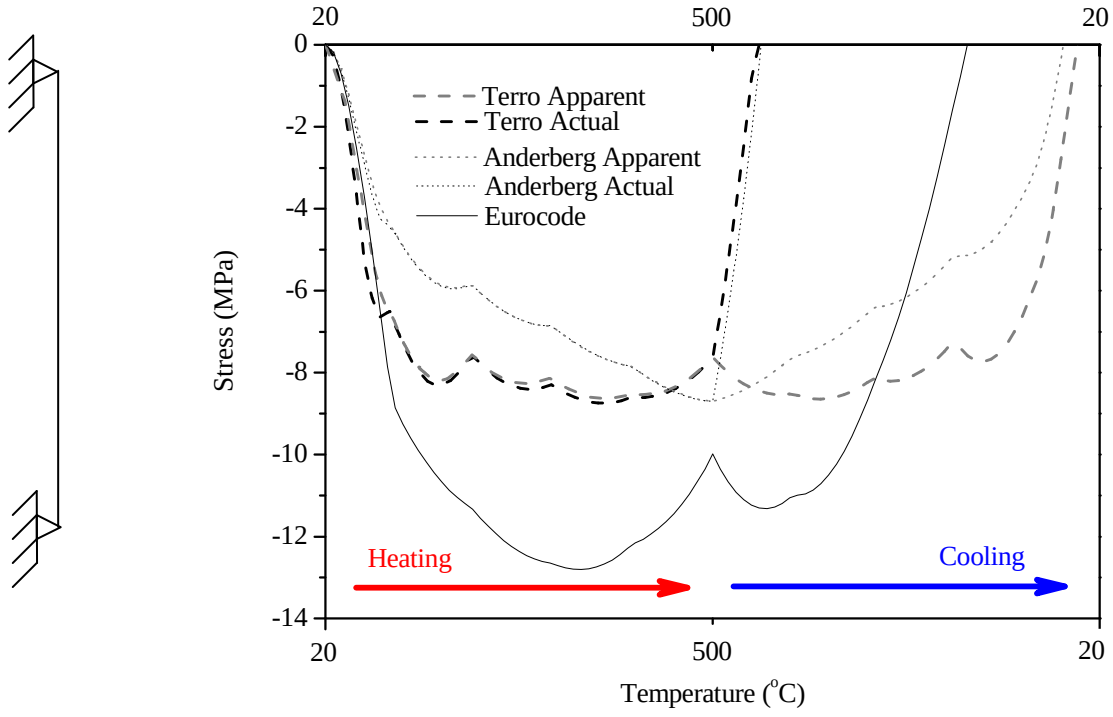


a) b)

Figure 3-10. a) The simplified beam/column setup; b) Stress response to heating and cooling regime.

Also presented in Figure 3-10 is the stress path that the Eurocode 2 model takes under the same heating regime. The first notable difference between this model and the two research models is that the stresses generated were significantly higher. This was due to the steeper gradient of the constitutive curve in the ascending branch between the temperatures of 200 °C and 500 °C as previously observed. Though this could be considered as an important difference between the models, it is of no specific relevance to this study which is primarily concerned with the development of elastic and plastic strains.

Analysis of the cooling stress path demonstrated that though the Eurocode model does not exhibit either strain type – mostly plastic or mostly elastic – in the extreme, it is much more similar to the apparent models. This is expected since the elastic modulus was derived from the gradient of the constitutive curve. The plastic strains are more significant than the other apparent models because the curvature of the ascending branch in the Eurocode is greater than that of the other models. Once the material becomes subject to tension, the stress/temperature relationship is dependent on the tensile properties of the material. In this model these were not considered; however, it should be noted that were the tension/compression properties similar, the actual moduli models would experience much larger tensile stresses.

Though this is a very simplified model, it demonstrates that it is necessary to consider the difference between the apparent and the actual elastic modulus

of a model. It shows that a difference of definition can have significant impact on the structural response during cooling or unloading.

### 3.3.5. More than One Dimension

This method works well in one dimension; in more than one dimension, however, inclusion of LITS using this method has other impacts. These need to be thoroughly considered in order to effectively model the phenomenon and understand its impact. When in the elastic region, stress and strain are related by:

$$\underset{\sim}{\sigma} = \underset{\sim}{\underset{\sim}{D}}\,\underset{\sim}{\varepsilon} \tag{3.16}$$

In the post-elastic regime the plastic strains are governed by the flow rule. Consider a single element, subject to a displacement-controlled loading in principal direction 2, but free to move in the transverse directions with a Drucker-Prager (see appendix I for further details) yield surface and a perfectly plastic material behaviour, as shown in

Figure 3-11. The associative isotropic flow rule dictates that once the yield surface is reached, plastic strain must occur in a direction orthogonal to the yield surface in stress space. This means that plastic strains are induced in directions other than the one in which the load is applied. If a non-associative flow rule were used, this would change. The principle, however, would be the same so for the purposes of this chapter an associative flow rule will be used.

The implications of this for the implementation of LITS via a constitutive curve are significant. The inclusion of LITS in the constitutive curve whether

implicitly (with an “apparent” elastic modulus) or explicitly (with an “actual” elastic modulus) will result in a proportion of that LITS becoming active in the transverse directions. The magnitude of the extra strain would depend on the stress state of the material, and on the degree of plasticity developed in the principal direction. For example: should the element described above be at a stress state at point A, no plastic strains would be induced in the 1-direction.

In the case of the apparent modulus a large proportion of the extra incremental transverse strain may be elastic; while in the case of the actual modulus, the major constituent of the incremental strain would plastic.

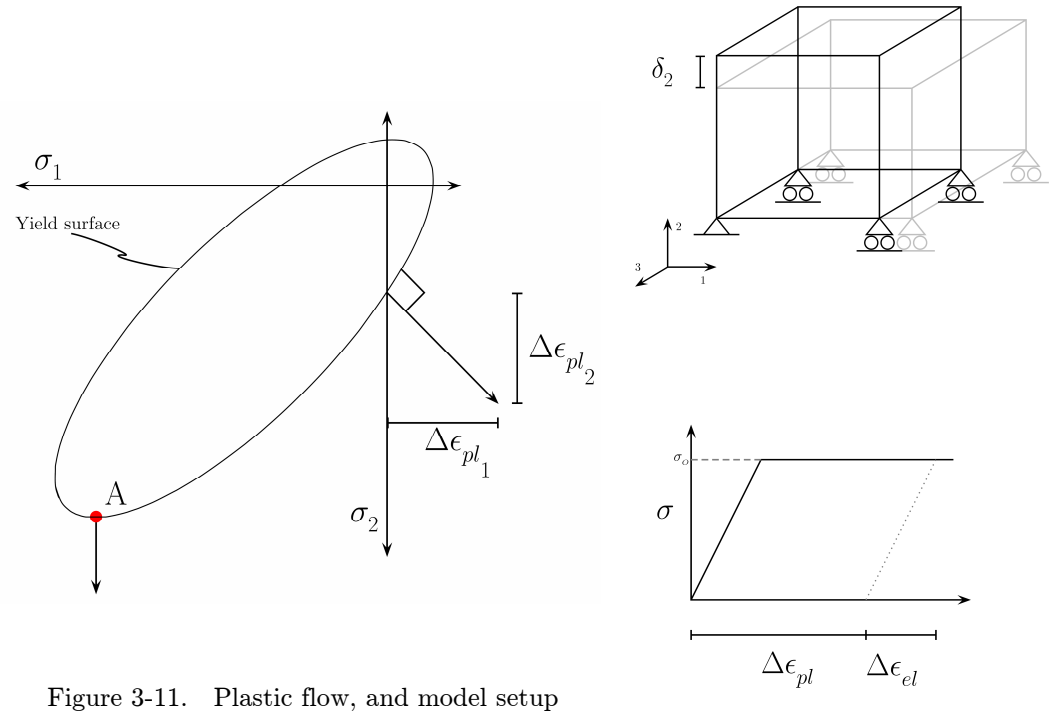


Figure 3-11. Plastic flow, and model setup

The impact of this difference is demonstrated below using the Drucker-Prager yield criterion with a constitutive curve corresponding to that of the 200 ° C

Terro LITS curve. This temperature was used as there is a significant difference between the actual and apparent moduli, but the temperature is not too extreme. Two different models were created each with a different elastic modulus – apparent or actual – but with the same constitutive curve. The models consisted of a single cubic element, restrained at the base in the 2-direction (but free to displace in the 1- and 3-directions) and were strained in the 2-direction. The corresponding deformations and plastic strains were recorded.

Figure 3-12a shows the total deformation in each of the principal directions. The deformations in the 2-direction (i.e. the direction of strain control) are the same for both of the models. In the unrestricted directions, however, there are significant differences in the total deformations, particularly in the inelastic phase of the constitutive model. The origin of these differences can be clearly seen from Figure 3-12b. In the "apparent" model the plastic strains do not develop until much later in the deformation process. The "actual" model on the other hand – because of the difference between the elastic modulus and the shape of the constitutive curve – activates the plastic strain components immediately. This difference in plastic strain is entirely due to the activation of the flow rule at a much lower stress. Consequently, though the plastic strain in the loading direction is what would be expected from using the "actual" modulus in the constitutive curve, the impact of this approach can be clearly seen in the non-loading directions.

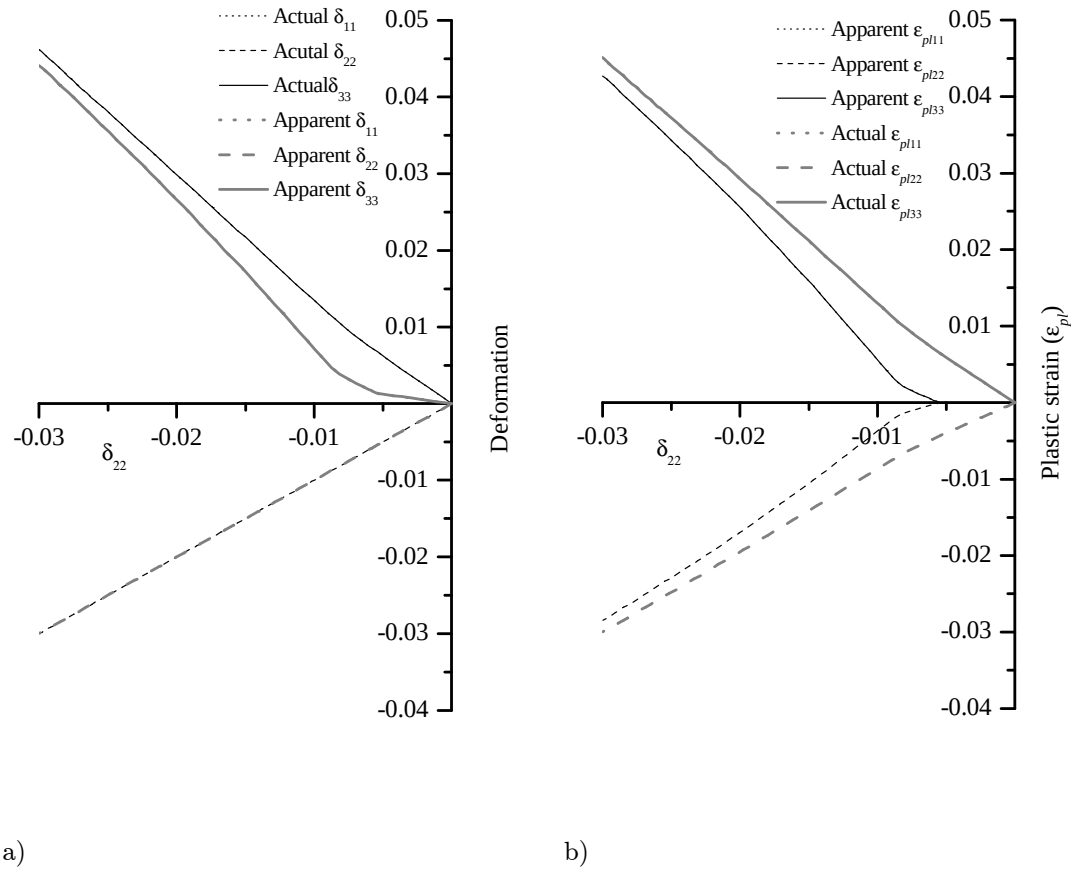


a) b)

Figure 3-12. Strain tests: a) total deformations; b) plastic strains.

### 3.3.6. The Embedded Modulus

To allow the modelling of LITS to be representative, a new method for the inclusions of LITS in the constitutive model, while avoiding this transverse strain issue, is proposed. The Drucker-Prager yield criterion and plasticity equations are solved in a two step method: first, the elastic strains and corresponding plastic strains are calculated using the apparent modulus and the normal solution methods (Figure 3-13); then, the elastic and plastic strains are recalculated using the actual modulus (Figure 3-14). As such, the actual modulus is *embedded* within the solution procedure. This second stage can expressed simply as:

$$\varepsilon_{el1} = \frac{\sigma}{E_{em}} \tag{3.17}$$

where $E_{em}$ is the embedded actual modulus, and $\sigma$ is the stress calculated from the previous solution. Since:

$$\varepsilon_{el0} + \varepsilon_{pl0} = \varepsilon_{total} \tag{8}$$

The new plastic strain can be directly calculated from:

$$\varepsilon_{pl1} = \varepsilon_{total} - \varepsilon_{el1} \tag{9}$$

The new plastic and elastic strains are then used in the subsequent analysis. The equivalent plastic strain is not, however, changed. Consequently, the strains developed in the transverse directions are in line with those that would occur when using an apparent modulus, but the plastic strains developed in the principal direction are as would be expected from using the actual modulus. It should also be noted that where plastic strain has occurred, but the yield function is found to be negative (i.e. the total strain is reduced), the corresponding elastic stresses must be recalculated using the embedded modulus. Otherwise, the redistributed strains would be reabsorbed into the elastic region on return to zero stress.

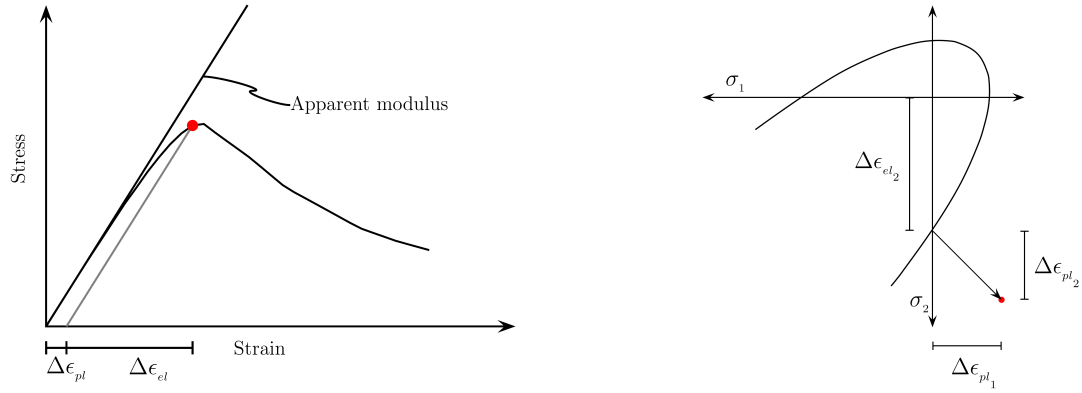


a) b)

Figure 3-13. Calculation of plastic and elastic strains: a) hardening with apparent modulus; b) the corresponding strains

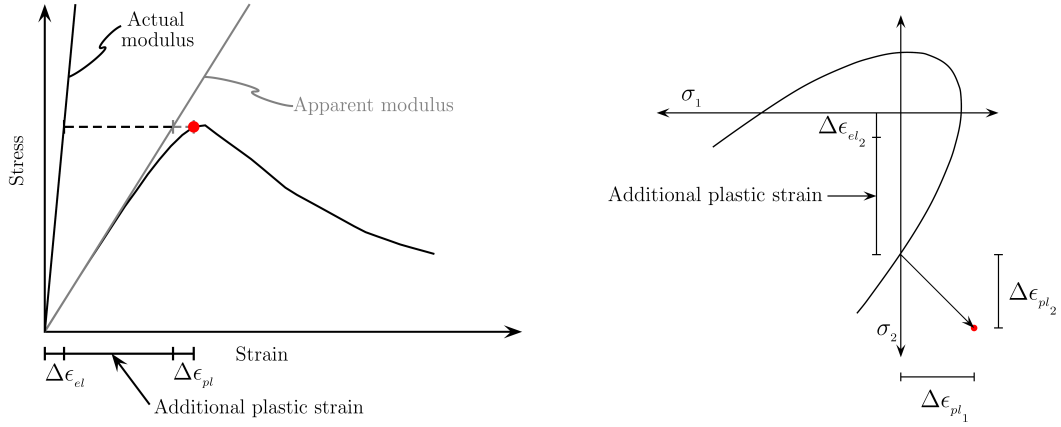


a) b)

Figure 3-14. Redistribution of strains due to the difference between actual modulus and apparent modulus: a) redistribution with respect to the constitutive curve; b) additional plastic strain component in strain space.

A Drucker-Prager [31,38,40,41,80,125,169] model was created which incorporated this method of modification by the embedded modulus. The implementation of a failure surface in a finite-element model is discussed in

some detail in appendix I. A model with an apparent elastic modulus and an embedded actual modulus was subjected to a test as described above. The results were compared with the previous tests (Figure 3-15).

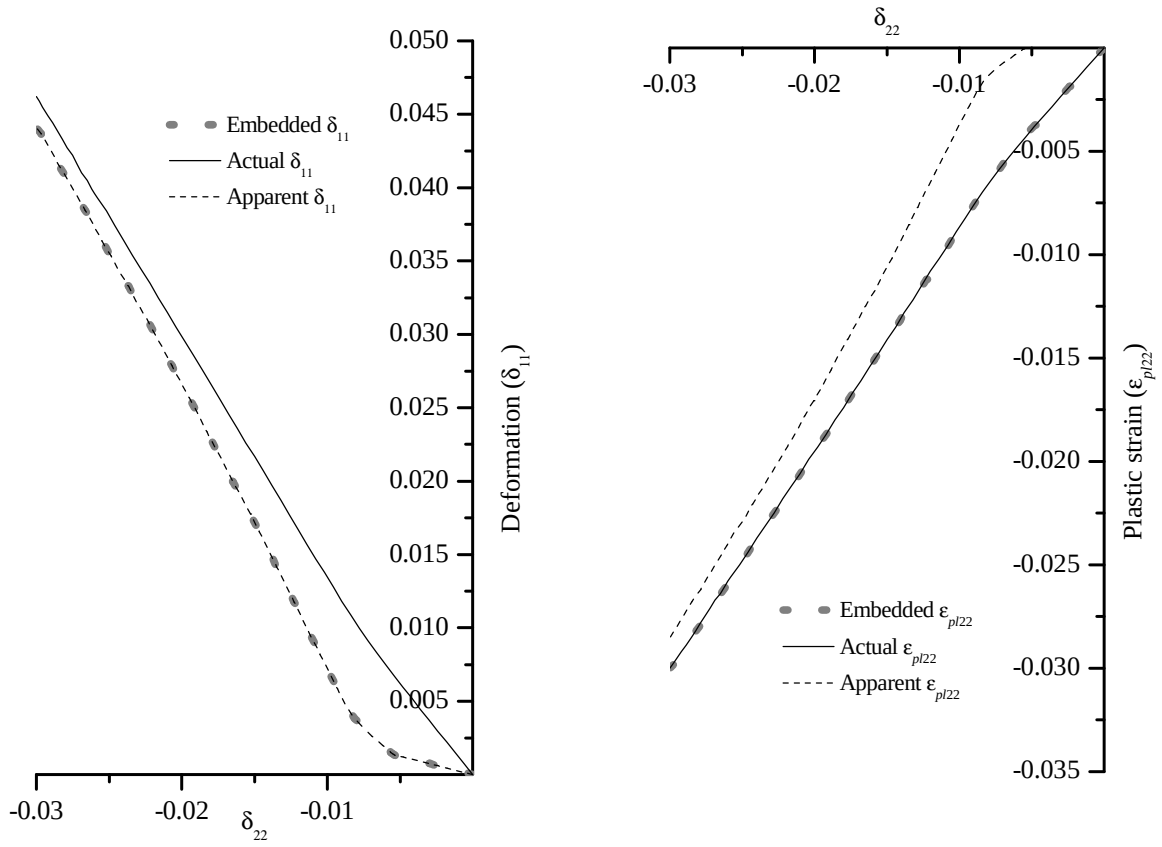


a) b)

Figure 3-15. Comparison of the embedded method against the other methods: a) total deformation; b) plastic strain.

The total lateral deflections experienced by the "embedded" material are the same as those experienced by the "apparent" material. Equally, the total plastic strain experienced in the loading direction is the same as those experienced by the "actual" material. Thus, it can be said that a fully plastic

transient strain component has been included in the model without affecting the deformations in the non-loading directions. This allows the plastic LITS effects to be successfully modelled uni-axially and in proportion to the applied stress in the way stated in the governing LITS equations.

## 3.4. Discussion and Conclusions

This chapter has summarised the main aspects of constitutive modelling for concrete at high temperature. Special attention has been paid to the phenomenon know as LITS. It has been shown that though there are a number of different models for predicting the development of LITS, the differences between them are relatively small. The most important aspect of including LITS in numerical models has been identified as the presence of an elastic modulus that is distinct from the tangent of the constitutive curve. It has been demonstrated that this simple modification can be made to existing finite-element codes to allow the key characteristics of load induced thermal strain to be represented in a more realistic fashion.

There are several conclusions which can be drawn from this chapter:

- The different constitutive models studied produce similar final curves.
- The explicit consideration of plastic LITS in the two research models allows plastic strains to be more realistically considered.
- The consideration of an embedded modulus allows the true LITS plastic strains to develop in an implicit model such as that in the Eurocode.
- The development of realistic plastic strains is particularly important on cooling where significant strain reversal occurs.

- The three dimensional implications of the development of plastic LITS can be analysed and redistributed simply using an embedded modulus technique.

# 4

# Sectional Analysis

The previous chapter presented various constitutive models that can be used to represent concrete in numerical modelling. Before this work moves on to consider the application of these types of models to larger scale finite-element simulations, assessment and design techniques used for concrete will be discussed in more detail. Chapter two reviewed the various metrics that are used to assess structures during testing and modelling. Another design tool that is frequently used is that of sectional analysis; the 500 $^{\circ}$C isotherm method was briefly discussed, this will be analysed in more detail here. However, this chapter presents more than the codified methods of sectional assessment: bending moment axial force interaction diagrams are a commonly used tool in any design office. When designing for fire conditions, the large axial forces which develop place an additional importance on the

consideration of the interplay between axial forces and moments. This chapter brings the process of sectional analysis back to first principles. The Eurocode 2 constitutive model that was discussed in the previous chapter is implemented to create a new method of deriving interaction surfaces from the sectional tangent stiffness matrix.

## 4.1. Background

The design of reinforced concrete sections requires the specification of a number of parameters such as the section breadth and depth; the area of steel; and the strengths of the concrete and steel. Where a section is subject to both an axial force and bending moments about one or both axes, interaction diagrams are commonly used to determine the area of steel required to resist the moments and forces to which the section is subjected. Design guides [37] which support structural design codes (e.g. Eurocode 2 [54]) often provide interaction diagrams for use with typical concrete sections at ambient temperature that allow the user to circumvent the cumbersome calculations necessary to determine suitable section parameters directly. However, there are many situations, such as fire loading, where structural engineers may need interaction diagrams for sections which are not covered by the standard cases. In these circumstances it is necessary to produce interaction diagrams from first principles.

This chapter considers the creation, use and reliability of interaction diagrams for concrete sections; in particular those subject to fire loading. One of the problems frequently encountered in structural fire engineering is that of the definition of failure. The motivation for creating interaction diagrams for sections at high temperature lies in the difficulty of defining failure for a

single element. Often failure of heated sections is loosely defined as the beginning of run-away deflections, or the time at which steel reinforcement reaches a pre-determined temperature, but such definitions are too vague to lead to efficient design. The use of carefully prepared interaction diagrams allows for a much tighter definition of section failure. Although a full understanding of the failure *process* requires global structural modelling, the use of an interaction diagram in conjunction with knowledge of the loading state of a section allows an engineer to determine how close a single member is to failure.

The first part of this chapter reviews the available methods for constructing interaction diagrams for use in the design and also the assessment of concrete sections. It highlights the difficulties associated with obtaining interaction diagrams for determining ultimate capacity using existing methods. A new method of creating two- or three-dimensional interaction diagrams of sections under any temperature field based on the tangent stiffness matrix of a section is then presented. It is anticipated that this technique will allow design engineers to make rapid assessments of the capacity of any concrete section when subject to arbitrary fire loading. This is important as it allows fires other than the standard or parametric fires to be considered and the techniques will be applied extensively in later chapters. The method can be implemented easily in any of the programming languages or mathematical analysis packages commonly available in design offices. Finally this chapter makes comparisons between using interaction diagrams constructed using this method to design heated concrete sections, and existing Eurocode design

methods as described in chapter two. It is concluded that current methods are not conservative.

## 4.2. Creating Interaction Diagrams – Existing Methods

### 4.2.1. Interaction Diagrams for Ambient Temperature Design

Interaction diagrams used for design are based on the assumption that there is a maximum allowable concrete compressive strain which prevents concrete crushing [119] (Figure 4-1). It is also frequently assumed that plane sections remain plane, that the tensile strength of concrete is negligible [48,134,166] and that the concrete stress distribution can be represented by a rectangular stress-block [117,119]. From these assumptions, the derivation of an interaction diagram is relatively simple. By holding extreme fibre strains at the maximum permissible value while curvature is varied, moment and axial force (M-N) pairs that lie on the interaction diagram for the section can be obtained by appropriate integrations of the resulting stresses over the section. Where the stress block is used, the integration is very simple and can be conducted by hand or using a spreadsheet.

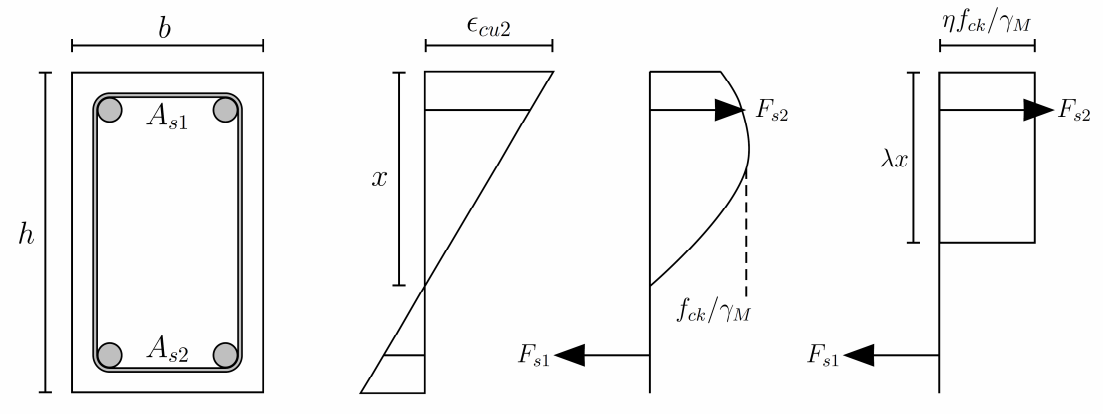


Figure 4-1. The development of a stress block from first principles.

This method enables the creation of interaction curves in uniaxial bending, and also interaction surfaces when biaxial bending is considered. The method is efficient because each M-N pair calculated is known to lie on the design interaction curve due to the assumption of a maximum permissible concrete strain. Diagrams produced this way can either be used directly or be normalized appropriately to allow the engineer to specify the section properties. However, because the assumptions made regarding maximum strain and the size of the associated stress block are design assumptions (which may include safety factors), the interaction diagrams obtained are not indications of failure strength, but rather show an appropriate conservative design capacity.

### 4.2.2. Interaction Diagrams for Assessment

Assessment of the ultimate, rather than design, capacity of a section may be required in a number of situations, including that of assessing the strength of a section under fire loading. Assessing ultimate capacity requires a different approach to that used for assessing design capacity. The assumption of a maximum fixed permissible concrete strain cannot be made because, for heated sections, the strain at ultimate stress is temperature dependent and, consequently, the maximum moment capacity may occur at curvature that induces a strain greater than, or less than, the strain required to crush the concrete in different parts of the section. Similarly, a realistic concrete stress-strain relationship should be used, rather than a simplified stress block. Since the appropriate compressive strain is not known, it is no longer straightforward to find strain-curvature pairs that lie on the interaction curve for a section.

Several methods for obtaining interaction diagrams when maximum compressive strains are not specified have been presented. The simplest rely on variations of a "brute force" approach in which a section is analysed for many combinations of $\varepsilon_a$ and $\kappa$ (axial strain and curvature); appropriate integrations of the section stresses are then used to plot a point in M-N space for each combination. Assembly of all these points gives a "cloud" of points which are all inside or on the interaction curve [21,74,136]. By connecting the outer-most points in this cloud, the interaction curve can be drawn. Figure 4-2c demonstrates the generation of a number points which would contribute to the cloud of data. A significant problem with this method is that there is no clear way of determining which points lie on the interaction curve and which points lie just inside it, so determining the interaction curve from a cloud of points is awkward. These problems are magnified if biaxial bending is considered and an interaction surface required. The method is also computationally expensive as many integrations of the stresses over the section are required.

An alternative approach to integrating stresses over an entire section is to use the "rapid exact" inelastic biaxial bending analysis technique [60,139] which allows very efficient analytical integration of the stresses. This method relies on Green's Theorem [100] to convert the costly double integration of stresses over a section to a highly efficient line integral around the section boundary. Implementation of the method requires the stress-strain relationships of the materials to be analytically integrable but can be applied to any cross-section. Although computationally much more efficient than

simple brute-force methods, the problem of identifying points that lie on the interaction diagram remains.

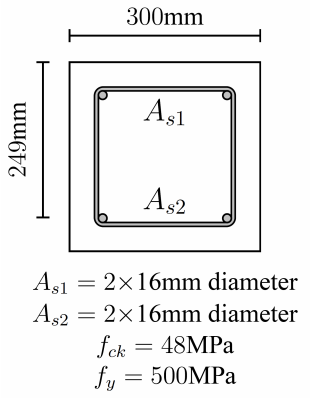


a)

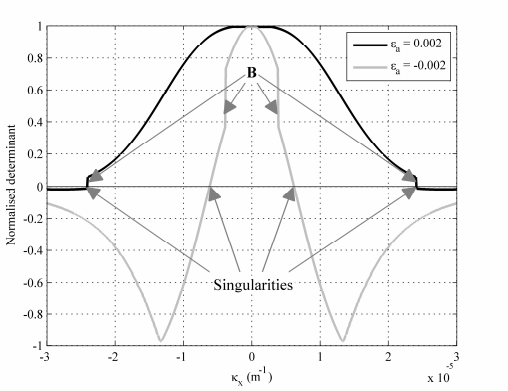


b)

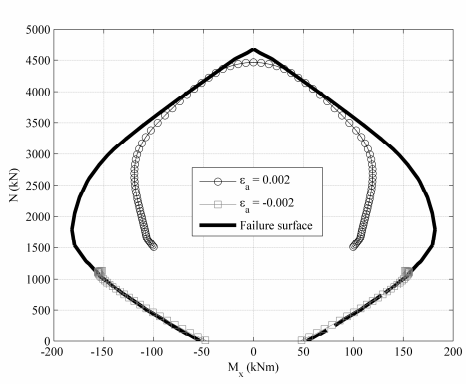


c)

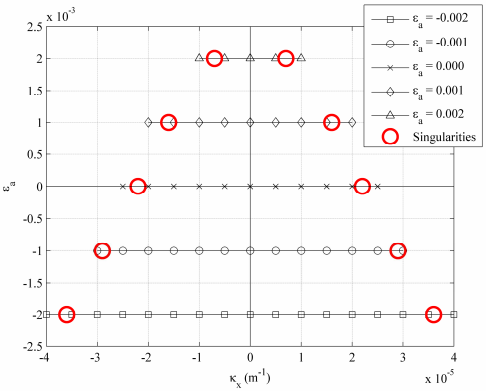


d)

Figure 4-2. a) Arrangement of the section, and material properties; b) Change of the determinant of the stiffness matrix with respect to curvature for two values of axial strain; c) Interaction plot for two different values of axial strain with varying curvature; d) Conceptual illustration of the search algorithm used for identifying strain-curvature points on the interaction diagram. Points where the stiffness matrix determinant is singular (circles) lie between curvatures that cause the determinant to change sign. The precise location of singularities between such curvatures is found using the secant method.

### 4.2.3. Sectional Analysis at High Temperatures

Exposure of a concrete section to a fire, and the resulting temperature increase cause the capacity to reduce and the shape of the failure surface to change. In design, several methods are available for assessment of a heated member's capacity [53]. The most commonly used and simplest is the 500 °C isotherm method [55,112]. As described in chapter two, this method allows the design bending capacity of a heated section to be calculated based on the assumption that concrete retains its full strength below 500 °C and has negligible strength above 500 °C. Reinforcement material properties are calculated based on centre-line temperatures. The design capacity is assessed using the stress block method based on accidental limit-state (fire) partial safety factors. This approach avoids the need to calculate an interaction diagram altogether but is very crude and can be unconservative, as will be demonstrated later in this study.

Several authors have created M-N interaction diagrams for sections at high temperatures [19,69,74], and others have created moment-curvature relationships based on similar assumptions [47,48,135]. These studies have predominantly focused on uniaxial bending; chapter 5 indicates that biaxial bending is often the most critical case. In order to create interaction diagrams for heated sections, it is necessary to correctly represent the degradation of material properties caused by temperature and also to represent the strains due to thermal expansion. The effects of concrete spalling on section capacity can be included by the adjustment of the geometry of the section. Once these effects have been taken into account, it is then possible in principle to create an interaction diagram using any of the (non-design) methods outlined above.

However, in practice each method has practical difficulties when used at high temperature.

"Brute-force" methods are relatively simple to implement for heated sections but the problems associated with these for ambient temperature analyses are amplified for high temperature analyses as a new diagram must be generated for every cross-sectional temperature distribution. The rapid exact method becomes unwieldy at high temperatures for two reasons. First, the stress-strain relationship of concrete becomes more complex and this makes it difficult to integrate with respect to strain. Second, as the integration is over a region of both non-uniform strain and temperature, the stress-strain curve must be integrated with respect to the both change in strain and change in temperature over the region.

## 4.3. An Alternative – The Tangent Modulus Method

In this section an alternative method is proposed to create interaction diagrams for sections both at ambient temperature and when heated by exploiting tangent stiffness matrices. The method has the key benefit of bypassing the difficulties in determining M-N pairs that lie exactly on an interaction curve or surface.

### 4.3.1. Theory

Although typically used in structural stability calculations as part of Shandley's tangent modulus equation [21], tangent stiffness matrices can also be used to locate failure surfaces. A section's tangent stiffness matrix relates small changes in generalized strains (typically an axial strain and two curvatures are needed for the analysis of biaxial bending of concrete sections)

to small changes in the corresponding stress-resultants (an axial force and two bending moments). When a section's response is non-linear, the tangent stiffness matrix is distinct from the elastic stiffness matrix. For the set of stress-resultants mentioned, the relationship between incremental stress-resultants, tangent stiffness matrix, and incremental generalized strains of a section can be written in the standard form:

$$\begin{bmatrix} \delta P \\ \delta M_x \\ \delta M_y \end{bmatrix} = \begin{bmatrix} K_{11} & K_{12} & K_{13} \\ K_{21} & K_{22} & K_{23} \\ K_{31} & K_{32} & K_{33} \end{bmatrix} \begin{bmatrix} \delta \varepsilon_a \\ \delta \kappa_x \\ \delta \kappa_y \end{bmatrix} \tag{1}$$

or,

$$\delta \mathbf{F} = \mathbf{K} \delta \boldsymbol{\varepsilon}, \tag{2}$$

where Rotter [139] gives:

$$\begin{aligned} K_{11} &= \int\int E_T dA \\ K_{12} &= K_{21} = \int\int E_T y dA \\ K_{13} &= K_{31} = \int\int E_T x dA \\ K_{22} &= \int\int E_T y^2 dA \\ K_{23} &= K_{32} = \int\int E_T xy dA \\ K_{33} &= \int\int E_T x^2 dA \end{aligned} \tag{3}$$

The set of stress-resultants that lie on the failure surface of a section are those that arise when an incremental change in the generalized strain vector result in $\boldsymbol{\delta}\mathbf{F}=0$. That is, stress-resultants on the failure surface are those that occur when $\mathbf{K}$ is singular, or

$$\det(\mathbf{K})=0 \tag{4}$$

This fact can be used to determine stress-resultant vectors, **F**, for a section that are located on the interaction surface if incremental strain vectors which correspond to the above condition can be determined.

### 4.3.2. Implementation

It should be noted that, as with all non-finite-element calculations in this thesis, the following calculations were conducted using commercially available software, MATLab [116].

#### 4.3.2.1. Ambient temperature

Implementation of the tangent stiffness method for constructing interaction diagrams will be discussed with reference to a simple section at ambient temperature. The section dimensions and properties are shown in Figure 4-2a. Assumptions made in this implementation are: plane sections remain plane; the concrete compressive stress-strain behaviour is as given in Eurocode 2 [55]; the tensile strength of concrete is zero; the stress-strain relationship of steel is elasto-plastic; and there is no bond slip between steel and concrete. Each of these assumptions has been made in various combinations by other authors [25,136,166]. They result in a marginally conservative estimate of strength (with the exception of bond slip).

To produce the interaction curve for the section subject to uniaxial bending ($\kappa_y$=0), values of curvature for which det(**K**)=0 were found for discrete values of axial strain. These curvatures were identified using the Secant method, in conjunction with a simple search function to identify the neighbourhoods where det(**K**)=0 approached zero. For example, variation of det(**K**)=0 against curvature for axial strain values of $\varepsilon_a$ = -0.002 and 0.002 is shown in

Figure 4-2b. Points where det(**K**)=0 are marked as singularities on the figure; each of these represents a point on the interaction curve in terms of strain and curvature. Step changes in the value of det(**K**)=0, caused by yielding of the reinforcement in either compression or tension, are marked by B on the figure. The corresponding curves in terms of moment and axial force are plotted in Figure 4-2c. Figure 4-2d illustrates conceptually an effective search algorithm for finding points where det(**K**)=0. For incremental values of axial strain the determinant is evaluated at a number of curvatures. A change in the sign of the determinant between curvature values indicates that a region where a singularity occurs has been reached. Once the singularity region is located, the secant method can be invoked to locate the precise location of the highlighted singularities. A number of techniques for finding the final location of the singularity region were attempted. It was found that the most efficient involved the process illustrated Figure 4-2d whereby the singularity region was found by a series of coarse iterations in one direction, and then when the sign of the determinant changed, the direction of search was reversed and the search step was reduced. This method, though not strictly the most efficient for each individual point, was the most robust algorithm. This was because it could be used to locate every point whether it was at a rebar yield location, or a gradually changing value of determinant. It allowed the algorithm to operate without the need for a series of logical steps to determine what type of point it would be and where the region of singularity would be.

Once strain vectors that lay on the interaction surface had been determined, numerical integration was used to compute **K** and the corresponding **F**. The final interaction curve in terms of force and moment is shown in Figure 4-4b.

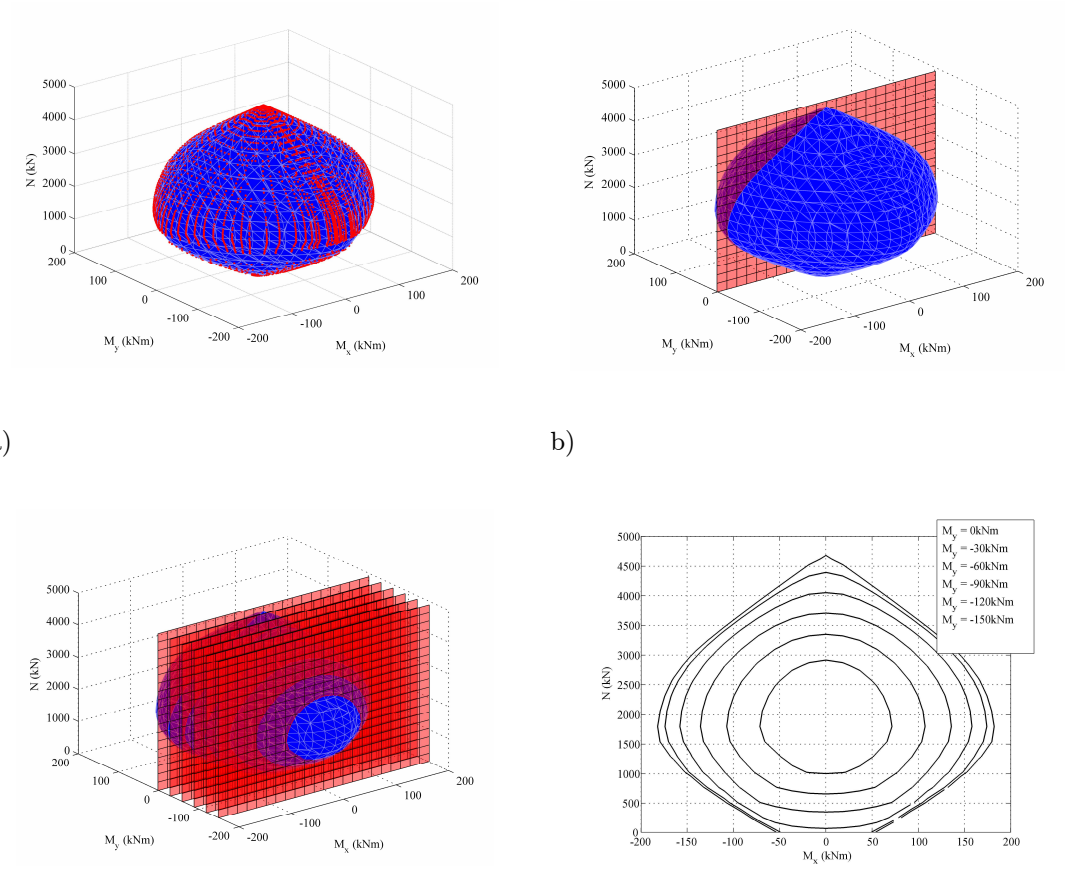


a) b)

c) d)

Figure 4-3. a) Surface plotted through all points; b) Slice taken through uniaxial bending plane; c) Multiple slices taken at different values of $M_y$; d) Surface removed, plot rotated and viewed from one side, and the different values of $M_x$ and N displaced for each value of $M_y$.

The procedure was easily extended to produce interaction surfaces corresponding to biaxial bending by introducing variations to $\kappa_y$. This was achieved by the use of a parameter which defined $\kappa_y$ as a ratio of $\kappa_x$.

Variation of this parameter from a large negative ratio to a large positive ratio by means of the tangent of an angle gave the full range of the biaxial failure surface, where a value of zero gave uniaxial bending about the *x*-axis. This full surface is shown in Figure 4-3a and discussed in more detail below.

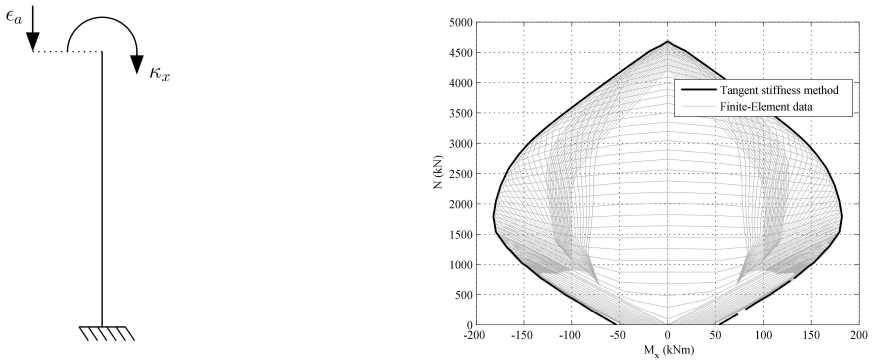


a) b)

Figure 4-4. a) Geometry, boundary conditions, and loading of the finite-element model; b) Interaction diagram from tangent modulus method (bold) and the full field of data generated by the finite-element model.

Presentation of interaction curves for uniaxial bending is well established and straightforward (e.g. Figure 4-2b). Presentation of interaction surfaces for biaxial bending in a form readily accessible to the design engineer is less easy. The presentation of a surface plot (Figure 4-3a) is not terribly useful in this respect. Visualisation choices are often dependent on the purpose for which the plot to be used. For generality, the plots in this study are presented as $M_x$, $N$ interaction diagrams with multiple curves representing different values of $M_y$ (Figure 4-3b and c). Thus, a large amount of information can be summarised on one diagram (Figure 4-3d). The process employed to create these diagrams is shown sequentially in Figure 4-3. A single plot is sufficient for a member with a minimum of one axis of symmetry. However, where a

section is entirely asymmetric, two diagrams may be required to encompass all of the information. Alternatively, the section could be viewed along its biaxial bending plane. In design, the tensile capacity of concrete sections is not normally considered. As such, just the compressive capacities are presented in this chapter.

#### 4.3.2.2. Verification

Verification of the above implementation was undertaken by comparing the results with finite-element analyses of the same problem. A stocky cross-section of the section was subject to a series of strain/curvature analyses using the parametric study feature in Abaqus [1] (effectively a brute-force type of analysis). The analyses were conducted on a single beam element, and the effects of non-linear geometry were neglected (to ensure a purely sectional analysis). The arrangement of the model is shown in Figure 4-4a. The full "cloud" of data resulting from the finite-element analyses and the failure curve resulting from employing the tangent modulus method are shown in Figure 4-4b. The outer points in the data from the finite-element analyses are in good agreement with the interaction curve predicted by the tangent stiffness method so the implementation is considered verified.

#### 4.3.2.3. Thermal Strains

Applying a tangent stiffness analysis to a heated section is very similar to applying it to a section at ambient temperature. However, the assumption of plane sections remaining plane must be examined more closely.

In unloaded axially and flexurally restrained members, the mechanical strain in any fibre is equal to the thermal strain. Thermal strains, therefore, directly

induce stresses within the member (Figure 4-5). In unrestrained members, this is not the case; thermal strains induce changes in curvature and length, but no net moment or force [152]. Instead, they produce a deflection and internal self equilibrating internal stresses. The forces in the section balance as some regions are in compression, and some are in tension. In an unrestrained member, this leads to an initial mechanical strain state which is not zero. Thus, it has been recognised that to obtain valid load-axial strain or moment-curvature relationships, adjustments must be made to the initial state of the strain field to compensate for the thermal strain. In symmetrically heated sections, this can be done by the application of an axial strain to cancel out the axial force. The axial strain is calculated iteratively, such that the forces due to the combination of axial strain and thermal strain are in equilibrium [48].

Where a section is non-symmetrically heated, and thermal curvature is induced, the procedure is more complicated, but similar. Instead of the application of axial strain to equilibrate the axial force, a curvature and an axial strain must be applied until both the internal moment and axial force are in equilibrium. Where biaxial moments are introduced, equilibrium must be obtained by the adjustment of biaxial curvatures and axial strains.

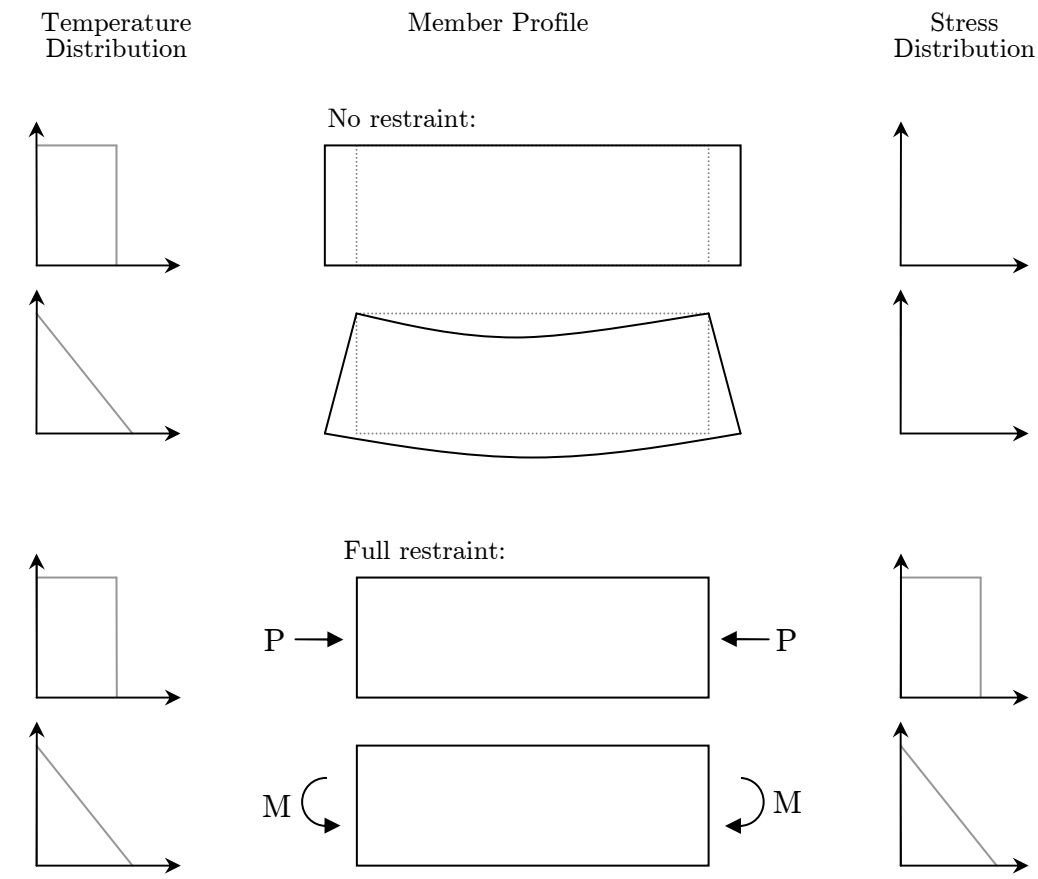


Figure 4-5. Illustration of thermally induced stain in an unrestrained section and thermally induced stress in a restrained section.

Application of the initial strain state and subsequent calculation of the sectional yield surface allows the surface to be drawn for a cross section without reference to the member boundary conditions. In the case where an axial member remains unrestrained, no axial force will develop, and the loading state can be plotted from the applied bending moments. On the other hand, where a member is fully restrained the axial loading the member undergoes can be derived from simple calculations, or a finite-element model. In this situation, the axial load would be equal and opposite to the axial load due to the initial strain state [156]. Likewise, in a flexurally unrestrained

member no net bending moment would be induced by the thermal curvature. In the case where a member is at least partially restrained in rotation at both ends, bending moments would develop due to the thermal strains.

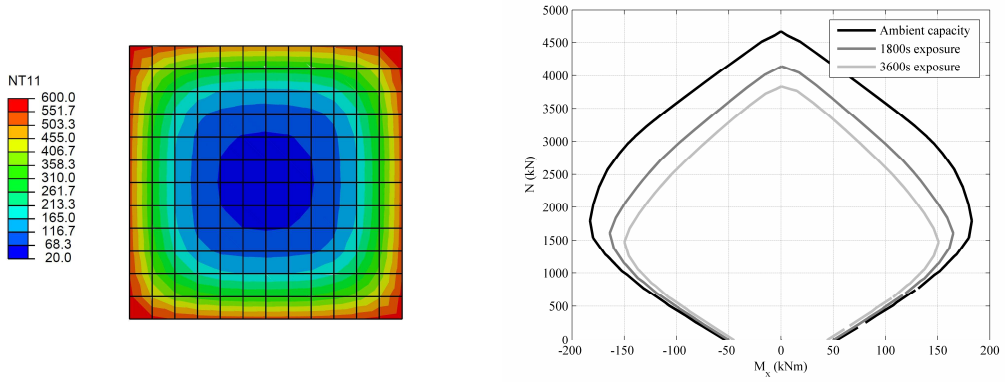


a) b)

Figure 4-6. a) Temperature distribution in the column at one hour (°C); b) Uniaxial interaction diagram at ambient, t = 1800s and t = 3600s.

The section described and analysed above was now assumed to be uniformly exposed to a gas temperature of 600 ° C for one hour. A heat-transfer analysis was conducted using material properties from Eurocode 2 for calcareous concrete as inputs to the finite-element model. The temperature distribution in the column at one hour is shown in Figure 4-6a. Subsequently, mechanical analysis using the tangent stiffness method was undertaken to determine the interaction curve after one hour of heating. The steel stiffness and strength degradation rates given in Eurocode 2 were approximated to those of a perfectly elasto-plastic material and used in this analysis. A direct comparison between the uniaixal capacities of the ambient and heated sections can be made; Figure 4-6b shows the progressive change in the extent of the failure surface for the value of $M_y = 0$ and demonstrates the use of the

tangent-stiffness method for determining interaction curves of heated sections.

## 4.4. Application of the Method

### 4.4.1. Analysis of a Heated Section

To show the versatility of the tangent modulus method and to compare its predictions with existing methods, a beam similar to that of Dwaikat [47] was analysed (Figure 4-7a). The section was assumed to be subject to a Standard Fire [53] from three sides for a duration of two hours, and a heat transfer analysis of the section was conducted in the same manner as described above. The beam cross-section was then analysed using the tangent stiffness method for the predicted temperature fields at several intervals during the heating for a range of biaxial bending conditions. A bending capacity analysis of the beam was also conducted using the Eurocode 500 °C isotherm method. The same heat transfer data was used for this analysis, and values of $\eta = 1.0$, $\gamma_{M,fi} = 1.0$ and $\lambda = 0.8$ (Figure 4-1) were used in accordance with EC2. The results of all these analyses are also shown in Figure 4-7 and a direct comparison between failure surfaces at different temperatures with $M_y = 0$ is shown in Figure 4-8. Unlike a uniformly heated section [19,151], an asymmetrically heated section's interaction surface distorts as well as shrinking during heating [69]. The asymmetry in the failure diagram results from the reference axis remaining at a constant location while the plastic neutral axis moves through the section. For further examples of the application of this method, see chapter six and appendix II.

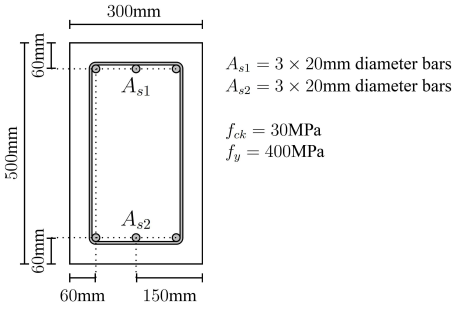


a)

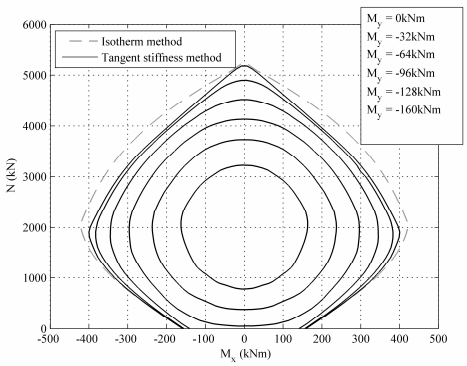


b)

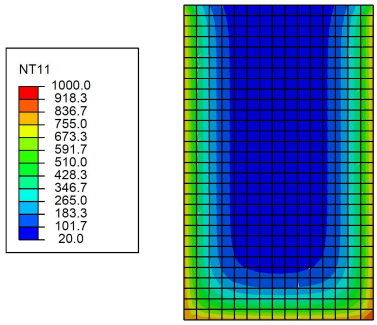


c)

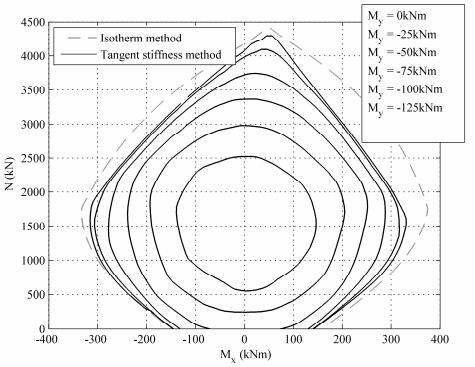


d)

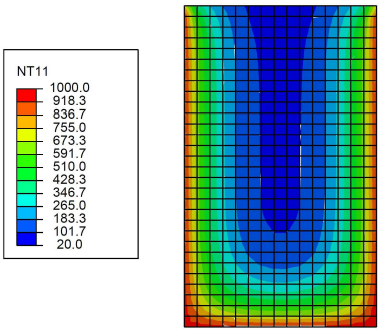


e)

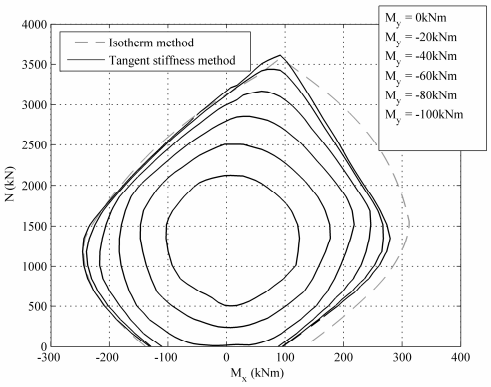


f)

Figure 4-7. a) Arrangement of the section; b) Ambient interaction diagram for the section using both tangent method and isotherm method; c) Section temperature profile after one hour ( $^\circ$C); d) Interaction diagram for the section at one hour using both tangent method and isotherm method; e) Section temperature profile after two hours ( $^\circ$C); f) Interaction diagram for the section at two hours using both tangent method and isotherm method.

### 4.4.2. Discussion

Comparison of the results highlights significant differences between the predictions of the two methods. For uniaxial bending, Figure 4-7 shows:

- The methods predict maximum axial capacity to within 2% of each other at all temperatures.
- At ambient temperature (Figure 4-2b), the pure bending capacities given by the two methods are negligibly different. There is less than 1% difference between the calculations.
- At ambient temperature (Figure 4-2b), the isotherm method overestimates the capacity of the beam under combinations of moment and axial force by a maximum of 5%.
- As the temperature of the section increases, the pure bending capacities given by the isotherm method are significantly above those given by the tangent stiffness method. This is particularly the case in sagging, where up to a 35% overestimation is obtained. Pure hogging produces a moment overestimation of 5%.
- The isotherm method almost universally over-estimates the capacity of the section under combinations of sagging moment and axial force. In the high axial load region, this overestimation grows from 5% to 15% as the section is heated.
- In contrast, overestimation of the hogging moment decreases as the section is heated. In fact, when the section is at its hottest, the agreement between the two results is very good with an error of less than 3% throughout.

These observations of the uniaxial bending results for both methods show that the 500 $^{\circ}$C isotherm method cannot be assumed to be a conservative

design approach. It consistently overestimates the capacity of the section, particularly in sagging. Other researchers have found the isotherm method to be unconservative in pure uniaxial bending [76]. This study shows that the unconservatism extends to bending with different levels of axial force.

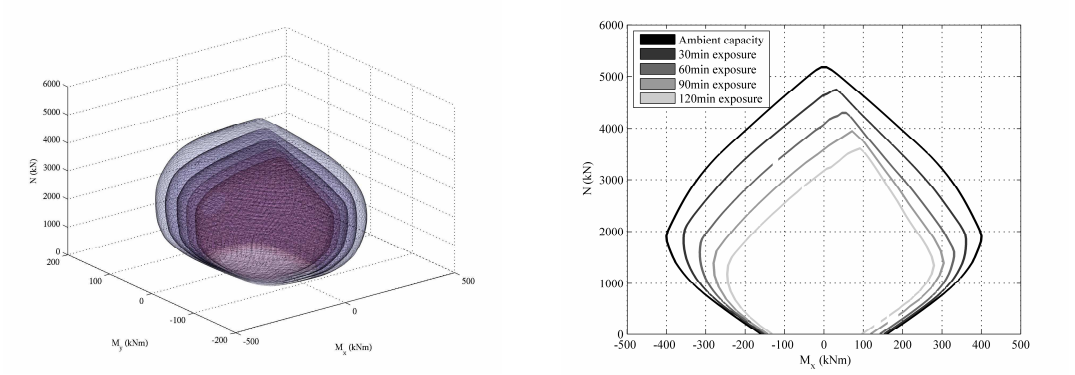


a) b)

Figure 4-8. a) Multiple failure surfaces; b) Comparison of uniaxial interaction diagram.

Although it is unsurprising that a crude assessment such as the isotherm method does not give accurate results, it is of concern that the results are unconservative. The causes of this unconservatism are twofold: the specific differences between the prediction of sagging and hogging capacity at higher temperatures are largely attributable to the assumptions inherent in the isotherm method. However, it is possible to attribute some of the error directly to the use of a stress block technique.

Heated concrete reaches its maximum compressive strength at a higher strain than cold concrete. Thus, in order for a section to develop a given axial load when subject to sagging bending, the neutral axis will be lower in a heated section than a cold section. Consequently, the internal lever arm and hence

the moment capacity will be reduced. These effects are fully captured by the tangent stiffness method but ignored in the isotherm method, which is unconservative as a result. In hogging, however, the effect described is largely cancelled out by the fact that the heated section soffit has been effectively removed in the isotherm method due to its high temperature. The removal of this area and its corresponding contribution to the total bending moment largely cancels out the overestimation caused by the inappropriate maximum strain assumptions. The above considerations highlight how the isotherm method has certain assumptions that inevitably will lead to unconservative predictions for some strain-curvature combinations, as demonstrated above. However, there are aspects of the underlying stress-block method that produce further inaccuracies.

The dimensions of the stress block used in this method are determined by the parameters $\lambda$ and $\eta$ as shown in Figure 4-1. These in turn are specified to ensure that under pure bending at ambient temperature the stress-block applies a force of the same magnitude and with the same lever-arm about the neutral axis as would occur if a full material stress-strain curve were used in an analysis. For a concrete strength of 50MPa or less, values of $\lambda$ and $\eta$ are given as 0.8, and 1.0 respectively in Eurocode 2. Under accidental loading (fire) conditions, the value of $\gamma_M$ for concrete in Eurocode 2 is modified from 1.5 to 1.0 thus meaning any section analysis undertaken using the isotherm method has effectively no material safety factor and relies only on the values of $\lambda$ and $\eta$. These simplified terms cannot accurately represent both the correct stresses and the appropriate lever arms which result from the true concrete stress-strain curve under any but the simplest load cases. This is

particularly the case when the neutral axis is not in the section, and the stress block acts over the whole section. Although an accurate prediction of the pure axial capacity can be obtained (because $\eta = 1$, and the value of $\lambda$ is irrelevant) this study shows that this method produces inaccurate and unconservative results when bending moments are present.

Given the interdependence of these safety factors for obtaining a conservative design at high temperature, it is of interest to examine the effect of arbitrary modifications of the stress-block. Modification of either $\eta$ to 0.8, or $\gamma_c$ to 1.2, allow a conservative result to be obtained for the ambient case (Figure 4-9a). However, this is an inefficient approach as in both of these cases the maximum axial capacity is significantly underestimated. Furthermore, neither of these modifications is sufficient to ensure that the entire interaction envelope of the isotherm method was within the failure surface given by the tangent stiffness method for the heated (120min) case. Further modification of the material partial safety factors to the ambient temperature design values (1.15 and 1.5 for steel and concrete respectively) in the heated case reveals that the predictions of moment capacity remain unconservative (Figure 4-9b). The overestimation caused by the stress block technique can be further analysed by applying the isotherm technique with a full concrete stress-strain relationship Figure 4-9b. This modification, however, is not sufficient to allow for a fully conservative capacity assessment.

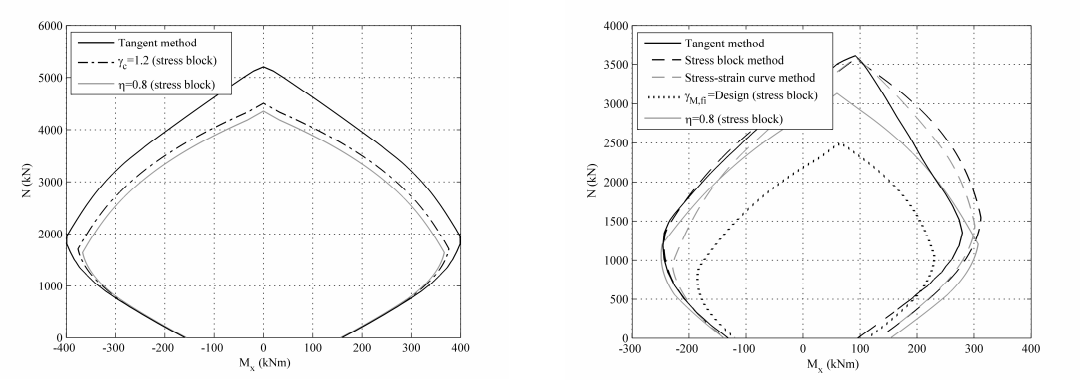


a) b)

Figure 4-9. a) Different individual safety factors; b) Equivalent capacities for the tangent method, stress block method, full stress-strain curve method, design safety factors, and with a reduced stress block.

The variation of parameters and techniques in the manner described above allows the source of the unconservatism in the heated sections to be more closely analysed. It is possible to obtain a more conservative result by modification of the stress block. However, despite modification of the partial safety factors, the permissible sagging moment in the heated section (as predicted by the isotherm method) remained significantly unconservative. The sagging overestimation is specifically caused by the difference in the location of the neutral axis between the two methods. The lower neutral axis in the heated section causes a lower moment to be generated than in the ambient, reduced area, section. The adoption of a more realistic stress-strain curve for the ambient concrete, does not give a conservative result. It is therefore concluded that the unconservatism in the predicted capacities is caused more by the assumption of ambient concrete behaviour inherent in the isotherm method, rather than because of the use of the stress block technique. Another cut-off value such as 400 °C or 300 °C would, inevitably,

give a more conservative answer. However, this would not solve the underlying problem with the cool concrete assumption.

## 4.5. CONCLUSIONS

Several conclusions can be drawn from this chapter:

- The failure surfaces of ambient and heated reinforced concrete sections can be found rapidly and accurately by locating singularities in the sectional tangent modulus matrix.
- The $500\,^{\circ}\mathrm{C}$ isotherm method is unconservative in predicting the failure surface of a heated section due to the stress block method (see above) and the assumption of uniform temperature in the concrete.
- Biaxial failure surfaces for ambient and heated reinforced concrete sections can be clearly represented on a single diagram.
- When all the partial safety factors are removed, the stress block method is unconservative in predicting the failure surface of a section at ambient temperature.

# 5

# Whole Structure

The previous chapters have focused on the localized behaviour of concrete; either the constitutive behaviour or elemental sectional analysis. It is clear, however, that an understanding of a structure's behaviour during a fire is only possible if the whole structural frame is considered. The design of structures in fire relies on knowledge of the loads applied to a structure and the capacity of the structure to resist them. Current methods of fire design often use simple measures – such as those described in chapter two – to define structural performance. Though useful, these measures do not allow the designer to fully comprehend the state of a structure; rather, they offer localized snapshots of particular phenomena. This chapter presents a methodology for combining temperature dependent sectional assessment with finite-element structural analysis techniques. The approach allows the

identification of vulnerable structural elements; the quantification of member utilization throughout the structure; and comparison of structural performance between different fires. The technique is demonstrated on a concrete frame subject to three design fires, and the impact of vertically differential column heating is investigated. It is concluded that the methodology presented offers an effective approach for analysing structures subject to different fires that is much more rational than existing techniques. The sectional analysis technique presented in the previous chapter is used, and a simplified approach to shear assessment is adopted.

## 5.1. Introduction

In recent years there has been a large amount of research on the behaviour of concrete structures in fire. This work has ranged from examining single members [99] or slabs [114] to large frames or assemblies [9,12]. Modelling techniques have been developed and validated [50,75,84,142] to allow researchers to gain insight into structural phenomena that experimental techniques alone would not provide. These techniques have also allowed design engineers to begin to predict the behaviour of structures in fire. As computer processing power has grown, it has become possible to model larger assemblies of elements [15,118]. However, as modelling has become more advanced, and structures more complex, the measures used to gauge structural performance have remained unchanged [27,32]. The result is that very complex numerical models with hundreds of thousands of degrees of freedom are used to represent a structure, but assessments of the structure and definitions of structural failure in fire remain based on criteria developed for very simple structural systems, such as single elements tested in furnaces.

As discussed in chapter two, the problem of the definition of failure is not a new one [8]. When a structural element is no longer able to resist the applied force and collapses, it can clearly be said to have failed. However, the failure of one element within a redundant structure does not imply failure of the entire structure at the fire limit state. Despite this, standard definitions of failure are element based, and include limits on deflections, rates of deflection [27], mechanical strain [57] and temperature [98]. Each of these is a reasonable definition for failure of an individual, statically-determinate structural element but it is not clear that they are suitable for an entire structure in fire, which will typically be highly redundant. Moreover, if these traditional measures are used, it is difficult to quantify the degree to which an entire structure is at risk of collapse. Comparisons between the different failure definitions is also problematic; it is hard to know for example whether a structure that exceeds a strain-based failure criterion is more at risk of collapse than one which exceeds a runaway deflection-based criterion.

Where numerical structural modelling takes place, much more detailed information is available that can give a fuller picture of structural behaviour. This chapter demonstrates how it is possible to use the huge amount of information available from advanced finite-element analyses in conjunction with cross-sectional analyses of every part of the heated and unheated structure to give a quantitative assessment of how highly utilized is a whole structure, or any part of it, throughout a design fire. The chapter focuses specifically on the assessment of the columns in a concrete frame, although the techniques presented could be used in the assessment of many types of structure.

This chapter is split into several sections: firstly, current assessment techniques are reviewed and a new methodology is outlined. Next, the method is demonstrated on a single column within a structure before being applied to a full structural model. Finally, the method is used to compare the effect of different fires and heating regimes on the structure and it is shown that the changes in structural behaviour that result are much more apparent than when traditional methods of assessing structural distress under fire are used. The techniques developed in this chapter are applied extensively in chapter seven.

## 5.2. Assessment Methods

Assessment of fire-affected structures is needed both during real fire tests on structural elements, and on models which have been developed to predict structural behaviour for design.

### 5.2.1. Single Parameter Assessment

The single parameter assessments that are typically used are: rebar temperature; deflection; rate of deflection; and strain in the tension rebar [27,32,57,98]. It was recognized in chapter two that though these measures can be used for comparative assessment, it is impossible to obtain a quantification of how heavily utilised, or how close it is to failure the structure is. Another technique must be sought.

### 5.2.2. Sectional Assessment

Another tool for assessing structural members is sectional analysis. This was discussed in detail in chapter 4, so will not be described again here. Chapter 4 dealt with the capacity calculation of a single section. This makes it possible for the designer to check that a heated section – with reduced

capacity – is able to resist the axial forces and moments which are applied during a fire scenario. However, as the history of structural fire engineering has shown, the calculation of the applied loading during a fire can be highly complex; it is not as simple as applying a reduction factor to the ambient design loading [53]. As a structure is heated, the thermal expansions can induce higher moments and axial forces throughout the structure. These additional forces can be calculated analytically [130,156], or can be calculated using finite-element analysis [17,118,151,157]. Chapter four developed a method for efficiently assessing the ultimate sectional capacity of a heated member [103]. However, the technique was presented in isolation without reference to loading; in this chapter, sectional analysis is used throughout to assess the degree of member utilization and characterise the utilization of the whole structure.

### 5.2.3. Combined Approach

The methodology presented in this chapter combines the use of sectional analysis with finite-element analysis. Previous work has used interaction diagrams and structural analysis to calculate a member's load ratio at any time during a fire [69,70], but the technique has not been fully explored with work generally focusing on the assessment of a single member [46]. However, there is no limit on the number of sections that can be assessed. This chapter applies load ratio analysis to the full structural frame.

The structure's loading through time is calculated from a finite-element analysis and each section's capacity (as affected by temperature and loading) is calculated using sectional analysis. Every part of the structure is

considered and the load ratio for each section is assessed. A similar but simplified process is conducted for the shear loads in the structure. By presenting the results in various ways, it is possible to identify how close to failure each section is, how seriously affected a structure is by fire in an overall sense; and to compare how the structural response varies between fires. The combination of the finite-element method with capacity analysis allows this approach to make use of the phenomenal amount of data that can be generated by finite-element analysis. It is also a useful tool for comparing differences between different design fires and different designs, and is considerably more thorough than the single measures described above.

## 5.3. Application of the Method

### 5.3.1. Example Structure

To enable the methodology outlined above to be demonstrated, the technique was applied to a typical concrete structure. A nine storey, flat-slab concrete frame was designed in accordance with the Eurocodes [53-55]. A plan and elevation for the structure are shown in Figure 5-1. The floor slabs were 200mm thick; the interior columns were 400x400mm; and the exterior columns were 300x300mm. The design strength of the concrete in the columns was 48MPa, and that in the slabs 40MPa.

For the purposes of this thesis, the fires were restricted to fourth floor burning. As such, it was possible to create a finite-element model of the central floors of the structure. The finite-element model used throughout the remainder of this thesis extended from the base of the columns at the third-storey level, to the top of the columns at the fifth-storey level. The slab was

modelled using shell elements, and the columns were modelled using three-dimensional solid elements. The rebar were modelled using truss elements.

Two finite-element models were created using the commercially available software, Abaqus [1]. A heat transfer model was created to predict the concrete temperatures. The thermal properties were in accordance with those of a 1.5% moisture content concrete, as defined in Eurocode 2 [55]. The gas temperatures defined for the fire were applied to the structure by radiation and convection to the surface of the concrete. An emissivity of 0.7 and a convective coefficient of 25W/m$^2$K were assumed.

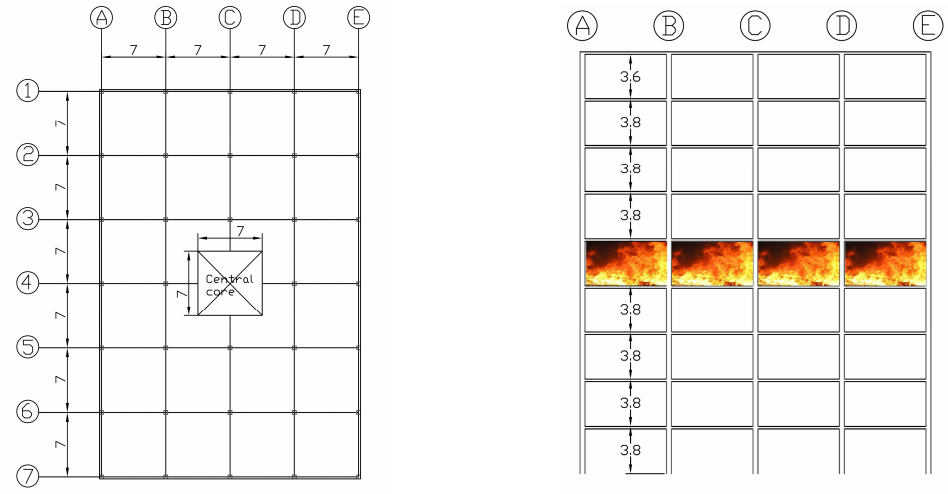


Figure 5-1. Plan and elevation of concrete structure, dimensions in metres.

For the mechanical analysis, all of the material properties used in the model were temperature dependent and in accordance with EC2. The degradation of stiffness and strength as defined in the Eurocode are given in Figure 5-2. It should be noted that there was no recovery of concrete strength on cooling. This functionality was not available as part of the Abaqus software and was

achieved through the creation of a user defined subroutine (appendix V). The yield criterion used for the concrete was the "damaged plasticity" model, based on the work of Lubliner [115]. This approach uses fracture energy to model the tension behaviour in the concrete. A sensitivity study was conducted to analyse the impact of using different fracture energies on the global behaviour of the structure. It was found that the use of an artificially high fracture energy made the numerical modelling more stable. The effect of this on the global trends and deflections in the model was minimal: 3.9% in the case of the columns, and less than 2% in the case of the slabs. It was decided, therefore, that the use of fracture energy of 1085N/m in the slab, and ductile tensile behaviour in the columns were acceptable in this study as they did not have a significant impact on the behaviour. A series of mesh sensitivity studies were also conducted to find the optimum mesh density. The final mesh density used was 8×8×18 elements per floor per column, and an average element size of 0.4735m in the slab. Figure 5-3 shows the final model that was used in the finite-element study under ambient loading conditions. Full details of the sensitivity studies are presented in appendix II. It should be noted that the interface of the shell element in the slab and solid elements in the column, though unconventional, was effective at transferring bending into the column. This was achieved by refining the shell mesh such that rotation was transferred through the combined action of multiple translational degrees of freedom. The effectiveness of this system can be seen from both the analysis of longitudinal column stress (Figure 5-3), and analysis of the column bending moments.

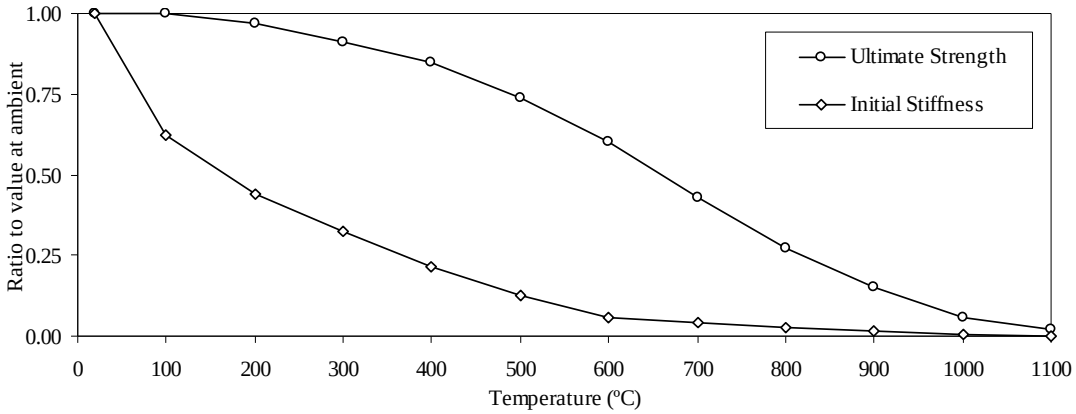


Figure 5-2. Degredation of strength and stiffness as temperature increases [55].

The base of each column was assumed to be fixed in translation and rotation, and the top of each of the columns was fixed in all directions other than the vertical. As the higher storeys of the structure were not modelled, the equivalent loads that would have been transferred into the column heads were calculated using a full-frame elastic model and applied to the remaining structure during the loading phase of the analysis. The central core of the building was not modelled discretely but was assumed to provide rigid support to the adjoining structure.

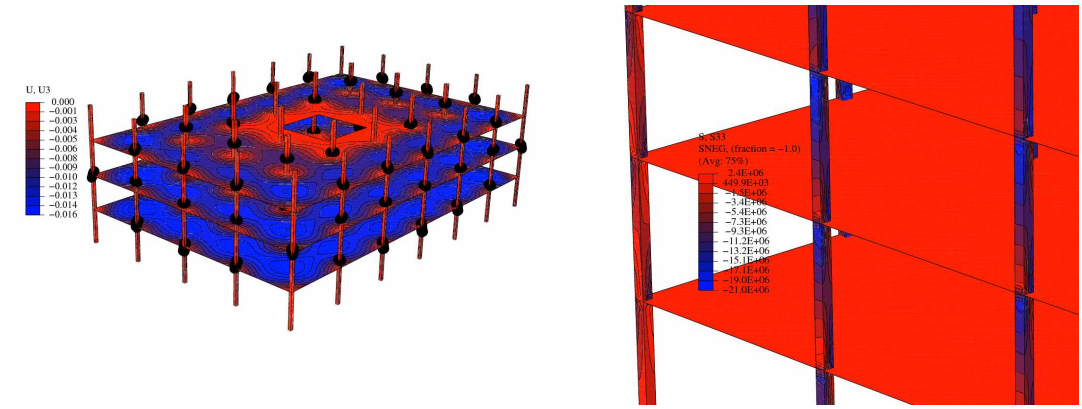


a) b)

Figure 5-3. The complete finite-element model: a) whole assembly deflection under ambient loading; b) principle stress detail of the slab/column interface.

#### 5.3.1.1. Assessment of M-N capacity of a Single Column

Initially the structure was analysed when subject to a Standard Fire. Using the results from the finite-element analyses, nodal coordinates and corresponding stresses were reported for every node of interest. From this it was possible to calculate the bending moments and in turn, derive the shear forces. This process was conducted throughout the height of every column for each time-step of the analysis. All of the data processing, sectional analysis, and subsequent calculations to do this were performed using the commercially available software, MATLab [116].

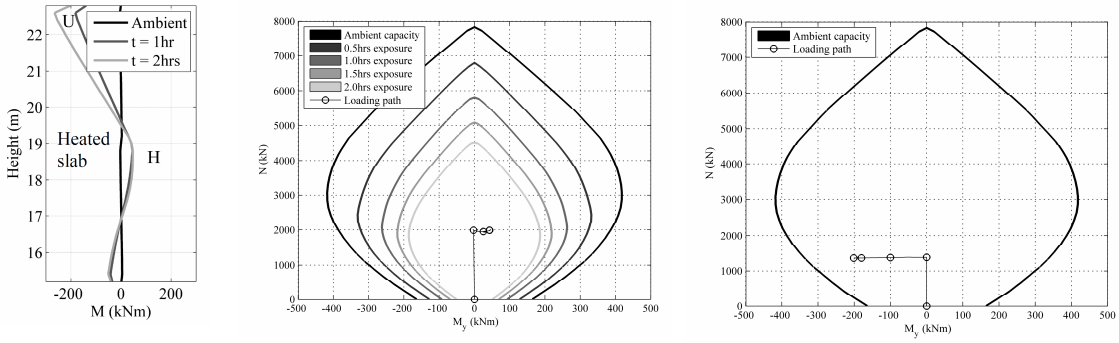


a) b) c)

Figure 5-4. a) the moment distribution in column C2 due to the Standard Fire; b) the changing capacity of the heated column with the loading path associated with height=19.0m; c) the ambient capacity of the upper column, with the loading path associated with height=22.8m.

The results of the above process are presented for column C2 first because the forces that developed were significant, but also because the column loading was symmetrical in one direction, this meant all moments and shear forces developed about one axis and are therefore simple to display on a single graph. Figure 5-4a shows the moment in column C2 after one and two

hours of exposure to the Standard Fire. From this distribution, it is possible to plot the load path of different parts of the column with respect to local capacity of the column. The change in axial/moment capacity of the heated part of the column due to material degradation was calculated using sectional analysis [103] and is shown in Figure 5-4b. Also plotted is the loading path at the top of the heated column (marked H on the bending moment diagram) as calculated from the full-frame finite-element model. Figure 5-4c presents the axial/moment capacity and corresponding loading path at the top of the unheated column (marked U on the bending moment diagram) as the fire progresses.

From these results, it is possible to create a utilization rating for each part of the column. In this context, a utilization factor is defined as the inverse of a safety factor; if a column is carrying half of its maximum axial load, the safety factor would be two, and the utilization factor 0.5. A completely unloaded column would have a utilization rating of 0.0, and a column which was on the brink of failure would have a rating of 1.0. For the case of Figure 5-4b, after two hours the section utilization rating is 0.48. The loading path and associated capacity shown in Figure 5-4c give a utilization factor of 0.53 after two hours.

#### 5.3.1.2. Assessment of All Columns

Although both of the sections analysed above remained well below their maximum utilization, it is possible to extend the analysis to include all columns in the building. The maximum utilization factor in each column can be identified, and its height and time of occurrence can be noted. By following this process, it is possible to analyse the whole structure to show

the total degree of utilization. Over the duration of the fire exposure, the loading and the capacities of the columns constantly change. The change in moments over the course of the 2 hour standard fire is shown in figure Figure 5-5. Appendix II shows similar plots for axial force, shear force, shear magnitude, and biaxial bending.

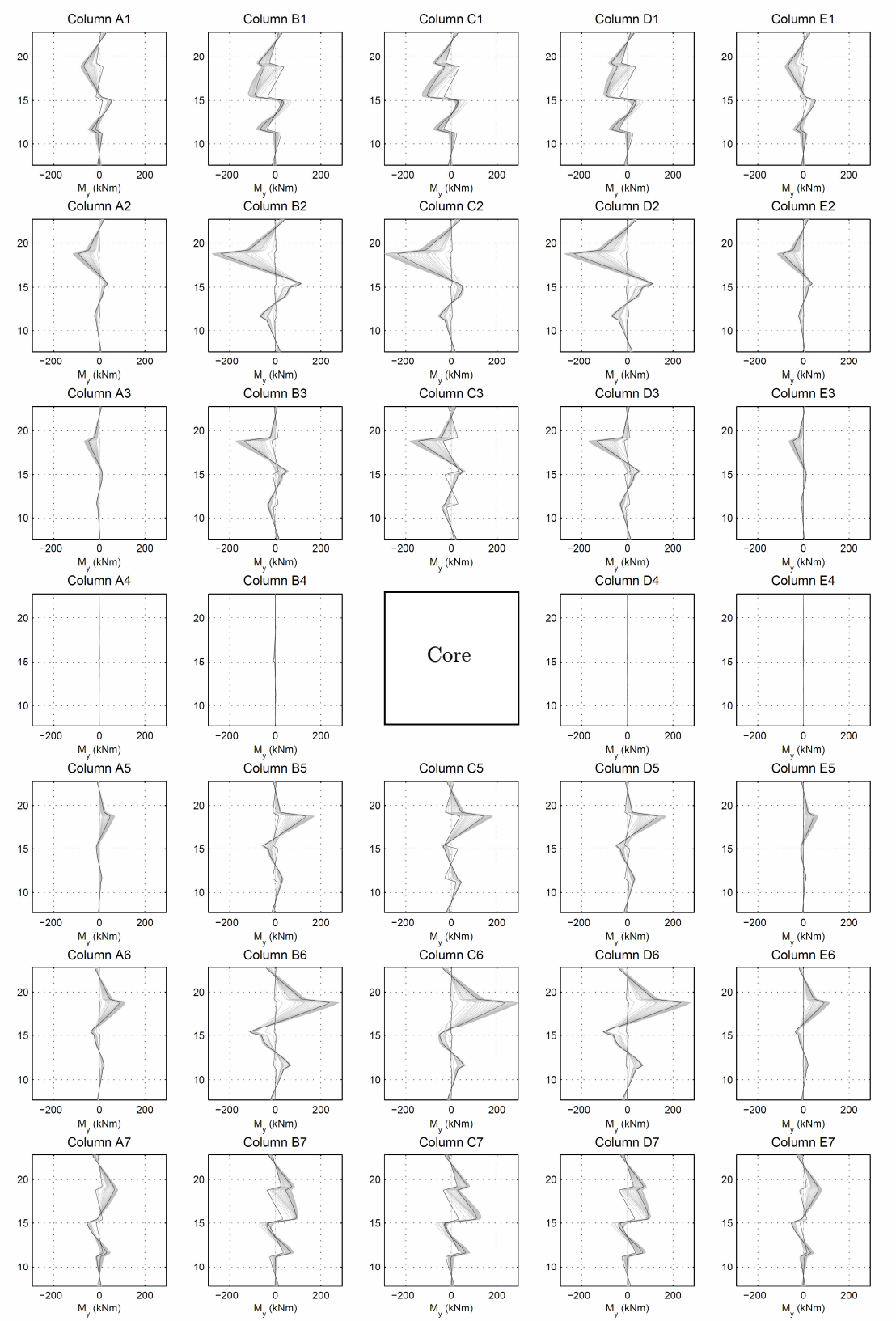


Figure 5-5. Bending moment distribution in each column as the analysis progresses.

zFrom calculating the loading factors from the data presented in Figure 5-5 and appendix II each column can be characterized. Figure 5-6a shows the percentage of columns that are at, or below, a certain utilization factor for different times during the fire. It shows that at ambient temperature 50% of columns are below 30% utilization; in contrast, after 2hrs, only 6% of columns are below 50% utilized. Lines on the far left of this figure represent a structure and loading arrangement that is at low utilization. As the line moves further to the right, utilization of the structure increases.

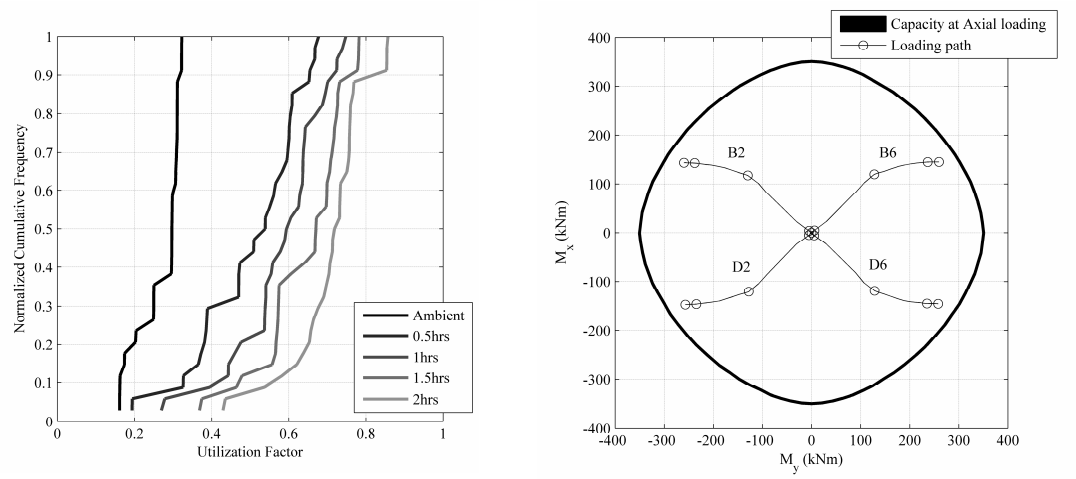


a) b)

Figure 5-6. a) The overall utilization of the columns when the structure is subject to a Standard Fire; b) The loading paths of the most utilized columns in terms of biaxial moment compared to the capacity at the relevant axial force.

Figure 5-6b shows the loading paths – in terms of biaxial moment – of the four most heavily utilized columns during the development of the fire. After two hours these columns were 85% utilized. It should be noted that, as with column C2, these maximum moments occurred in the upper (unheated) section of column. In 79% of the columns, the most utilized section was in the

upper (unheated) column; only in some of the edge columns did the highest section utilization occur in the heated region of the column.

#### 5.3.1.3. Shear Capacity

Shear failure is often the cause of failure in concrete columns. For the above method to be representative of the true utilization of the columns, therefore, there must be some consideration of the shear capacity. For this work, a simplified approach is adopted based on the "truss analogy" shear capacity of a concrete beam given in Eurocode 2 [54]. The shear capacity is given as:

$$V = \frac{A_s z f_y \cot\theta}{s}$$

where $A_s$ is the area of shear reinforcement, $z$ is the lever arm, $f_y$ is the steel strength, and $s$ is the spacing of the shear links. The angle $\theta$ represents the angle of inclination of the concrete strut; a conservative value is $45^\circ$. By taking the maximum steel temperature at any point in the shear link, it is possible to provide a conservative estimate of the section's shear capacity using this approach. Though this method lacks the subtlety of the bending capacity calculations above, it is a useful starting point for considering shear utilization

Figure 5-7a shows the distribution of shear force in column C2 as a two hour Standard Fire progresses. The capacities of the columns were calculated using the above formula and the appropriate ultimate steel stress based on temperature. It can be seen that at ambient temperature 50% of the columns were below 26% utilization. As with the moment/axial utilization factor, a line further to the right represents a more highly utilized section. After two

hours, the introduction of high temperatures led to a significant increase in the utilization such that only 5% of columns were less than 50% utilized. Unlike the moment/axial analysis, the utilization of some of the columns is greater than one. If the capacity analysis from the Eurocode is taken to represent the actual capacity then this would imply that the column would have failed. The finite-element model, however, did not display any evidence of failure by this mode.

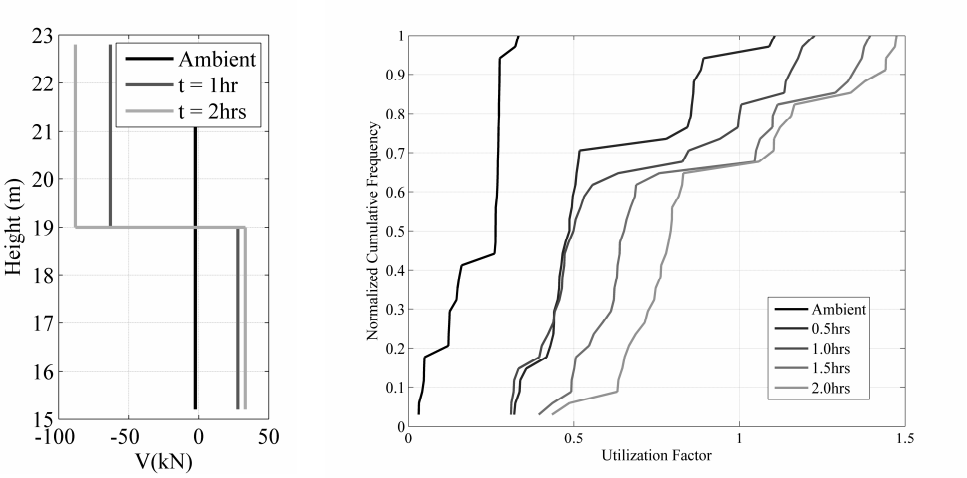


a) b)

Figure 5-7. a) Column shear force induced by Standard Fire; b) Normalized cumulative utilization frequency of whole structure.

A loading larger than that of the sectional shear capacity is a manifestation of the inherent conservatisms built into the assumptions in the Eurocode method. Adjustment of the compression strut angle, $\theta$, increases the sectional capacity sufficiently to support all the measured forces. The presence of such large shear forces in the model is not, therefore, inconsistent with the theoretical capacity of the section; rather, they represent the finite-element model's ability to exploit the full shear capacity of the section. The sections

which experienced the highest utilization would experience the highest utilization irrespective of the assumptions made regarding strut angle. In contrast to the calculations for moment and axial force capacity, where 1.0 represented the actual limit of the structural capacity, the shear calculation represented degree of structural distress relative to a conservative capacity estimate.

As with the moment/axial utilization, it was also found that most of the columns which recorded the highest shear utilization did so by the largest amount in the upper (unheated) portion of the column.

### 5.3.2. Different Scenarios

The previous section presented a robust method of analysing heated structures that has the advantage of assessing the entire structure, rather than focussing on the effect of a single measurement such as strain or deflection. A further strength of the assessment technique presented above is that they can be used to assess the relative impact of different fires on the structure and to identify how the mechanics of a structure varies in response to different fires.

#### 5.3.2.1. Three Different Fires

The concrete frame was re-analysed when subject to three fires; a two hour Standard Fire (as above), a "short hot" parametric fire, and a "long cool" parametric fire. The "short hot" fire had a peak temperature of 989 °C and a total duration of 37 minutes; the "long cool" fire had a peak of 915 °C and a duration of 145 minutes. The degree of column utilisation for each case is shown in Figure 5-8. It is clear that the "short hot" fire can be considered the

least severe as the utilization of the columns is less for both shear and axial/moment. In terms of axial/moment, the Standard Fire is most severe, while both the "long cool" fire and the Standard fire show a similar level of utilization in terms of shear. It should be noted that, to avoid confusion, the shear utilization results were normalized with respect to the maximum value obtained for all the analyses in this chapter.

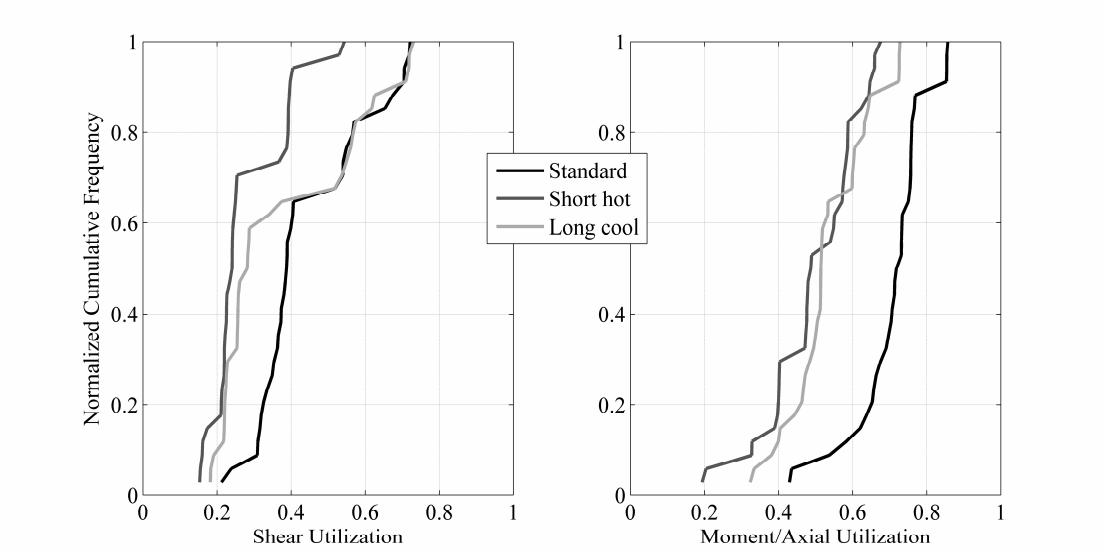


Figure 5-8. a) Maximum shear utilization under the three fire cases; b) Maximum moment/axial utilization under the three fire cases.

The similarities and differences between the fires are also notable: Table 5-1 presents information about column utilization for the different fire cases. For the Standard Fire, D2 and D6 were the most utilized columns; 79% of the columns were most utilized in their upper (unheated) lengths; the mean maximum utilization factor ( $\overline{x}$ ) was 0.73; 75% of the columns were less than 76% utilized; and 95% of the columns were less than 85% utilized. The same breakdown of data is given for the shear force analyses. It should be noted that though the model is symmetrical, minor differences in the mesh, and

rounding errors caused slight differences to the utilization factors for different, but symmetric, columns. This effect can be observed in the most utilized columns for the Standard Fire: columns D2 and D6 are rated highest for moment/axial and B2 and B6 are rated highest for shear. In both these cases, the differences between the two columns' rating is less than 0.3%. The next most utilized columns in both cases are the symmetric pair; Figure 5-9 illustrates the degree of symmetry between different columns on opposing sides of the structure.

Table 5-1 Summary of data from the different fires – see text for detail of the various columns.

| | Moment/Axial | | | | | | Shear | | | | | |
|---|---|---|---|---|---|---|---|---|---|---|---|---|
| | 1st | 2nd | Up | $\bar{x}$ | 75th | 95th | 1st | 2nd | Up | $\bar{x}$ | 75th | 95th |
| Standard | D2 | D6 | 79% | 0.73 | 0.76 | 0.85 | B2 | B6 | 82% | 0.45 | 0.54 | 0.71 |
| Short Hot | A2 | A6 | 91% | 0.49 | 0.58 | 0.66 | B4 | D4 | 88% | 0.28 | 0.38 | 0.45 |
| Long Cool | D2 | B6 | 59% | 0.52 | 0.60 | 0.73 | B2 | B6 | 88% | 0.38 | 0.56 | 0.72 |

For the three fires above, the longer two fires both gave the same four most critical columns. These were the highest axially loaded columns, and also experienced the highest moment development as illustrated in Figure 5-9a. In both cases the highest utilization occurred in the upper, cool, column. The most utilized columns during the "short hot" fire were different for the moment/axial and the shear rating. It was found that the moment rating was highest in the unheated part of edge column A2 and its symmetric pairs. This was not because the column was loaded significantly more than for the other fires, but rather because the other columns were loaded less due to the reduced thermal expansion caused by the shorter fire. This is illustrated in

Figure 5-9 as a comparison between the loading paths for different fires and columns.

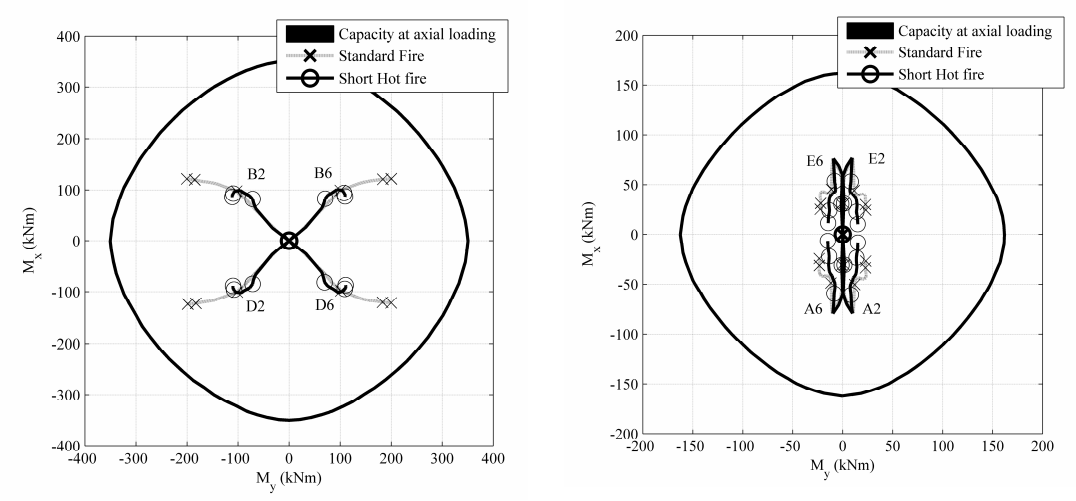


a) b)

Figure 5-9. a) The ambient capacity and loading paths of a symmetric set of internal columns for two different fires; b) The ambient capacity and loading paths for a symmetric set of edge columns.

The mean utilization and the 75$^{th}$ and 95$^{th}$ percentiles given in Table 5-1 are useful measures for quantifying how the different fires affect the structure. For example, the mean gives a broad indication of how well utilized the structure is (the "short hot" was the least and the Standard Fire was the most). However, it hides the detail of the most heavily loaded members; the ninety-fifth percentile gives a good indication of how heavily loaded the most critical members are.

#### 5.3.2.2. Partial Column Heating

The analyses above have consistently shown that the maximum utilizations tended to occur in the upper (unheated) part of the column. The cause of

this was that the heated, lower, columns had much lower stiffnesses than the unheated, upper, columns. This induced a load shedding mechanism whereby more of the load was borne by the upper columns. The physicality of the shedding mechanism was verified using a simplified analytical column.

A simple two degree of freedom stiffness matrix was created to analyse the behaviour of two columns with different stiffness (Figure 5-10a). From the column temperature data it was calculated that the unloaded bending stiffness of the heated column, C2, after two hours of Standard Fire exposure was 12% of its original bending stiffness. The horizontal load transferred into the column due to the slab's expansion was calculated from the shear data in the finite-element model, and was applied to the arrangement shown in Figure 5-10a. The bending moment and shear distribution were calculated and are shown in Figure 5-10b and c. The results show that the finite-element model is in good agreement with the analytical solution in terms of the distribution of moments along the length of the column. The values obtained are also similar with the maximum moment 15% larger in the finite-element analysis and very good agreement over the heated length of the column.

The identification of this load shedding mechanism leads directly to the question of how changes in the lower column stiffness affect the distribution of loads. Traditional furnace tests and standard fires typically assume a uniform heat distribution both horizontally and vertically throughout the compartment. Recently, the assumption of horizontal uniformity has been

questioned [147], and some authors have investigated the effect of non-uniform fires on structures [20]. However, in the context of the effect of column stiffness it is also worth considering the impact of vertical non-uniformity.

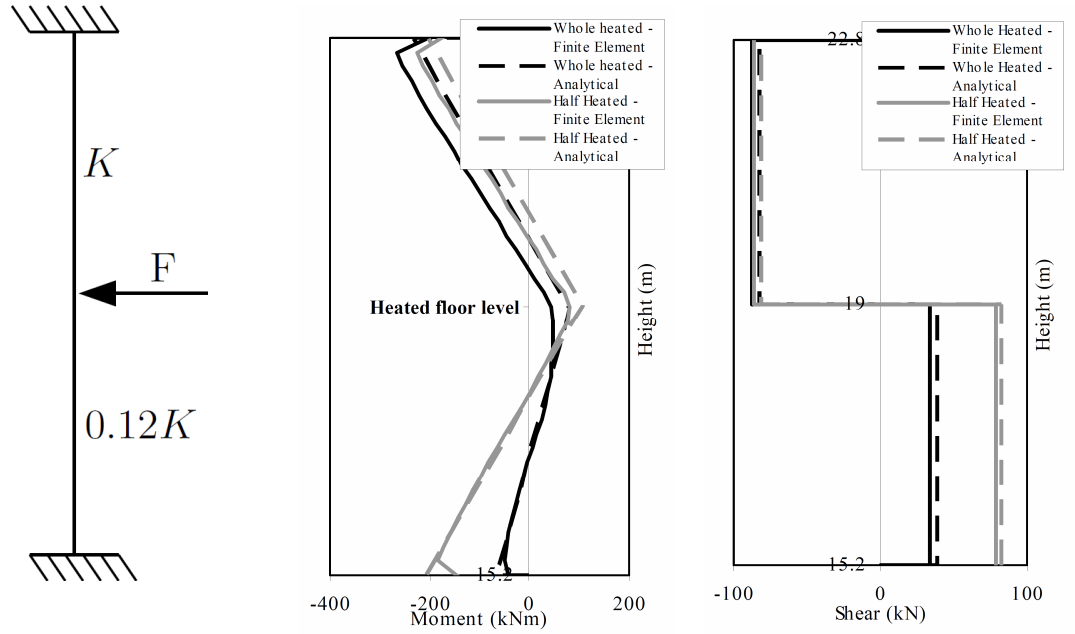


a) b) c)

Figure 5-10. a) Analytical model setup; b) Bending moment diagrams from analytical and finite-element model; c) Shear force diagrams for analytical and finite-element models.

In a fire scenario, a structure is mostly heated by the hot smoke layer. This layer is in the top region of a fire compartment [44]; experiments have shown that the lower regions of a compartment are relatively unaffected by a fire. Since the overall stiffness of a column is determined by the sectional stiffness and the length over which it is present, a partially heated column would have a different net stiffness and, therefore, a different distribution of shear and moment.

To investigate the impact of partial column heating on the load shedding mechanism identified in the previous section, another simple analytical analysis was conducted. A four degree of freedom stiffness matrix was created in the same arrangement as Figure 5-10a. The lower column, however, was allocated two stiffnesses: the ambient stiffness in the lower half; and the reduced, heated, stiffness in the upper half. The results and their comparison with ambient and whole column heating distributions are also shown in Figure 5-10a and b. It can be clearly seen that the shear force is much more evenly distributed between the two columns when only the upper half of the column is heated. The maximum moment achieved in both upper and lower columns is also similar. Also shown in Figure 5-10 are the moments and shear forces calculated from the finite-element analysis of the concrete frame when only the top half of the lower column was heated. It can be seen that the analytical results and the finite-element results are in good agreement in terms of the maximum shears (a 4% and 6% difference in the lower and upper column respectively). The trend shown in the moment distribution is also very similar; however, the difference between the results is slightly larger in the upper column with a 10% difference in maximum moments.

The influence of the change of heating distribution had a big impact on the amount of load shedding that occurred. Larger moments and shears were induced in the lower column (Fig 7). The overall impact of the differential heating can be studied further by the application of the assessment method described above. The finite-element model was rerun with the three fires described in the previous section; however, now only the upper halves of the

columns in the fire compartment were exposed to the elevated temperatures. Table 5-2 presents a summary of these results.

Table 5-2. Summary of data from the partial column heating

| | Moment/Axial | | | | | | Shear | | | | | |
|---|---|---|---|---|---|---|---|---|---|---|---|---|
| | 1st | 2nd | Up | $\bar{x}$ | 75th | 95th | 1st | 2nd | Up | $\bar{x}$ | 75th | 95th |
| Standard (half) | E6 | A2 | 41% | 0.75 | 0.81 | 0.86 | D2 | B2 | 29% | 0.63 | 0.69 | 0.99 |
| Short Hot (half) | A2 | E6 | 38% | 0.55 | 0.59 | 0.62 | B4 | D4 | 88% | 0.29 | 0.35 | 0.50 |
| Long Cool (half) | E6 | A2 | 41% | 0.72 | 0.78 | 0.81 | D2 | B2 | 68% | 0.46 | 0.59 | 0.75 |

In the case of the Standard Fire, although there was not a significant impact on mean degree of structural utilization (75% as opposed to 73% with the whole column heated), there was a significant shift in the location of failure. When the whole column was heated, 79% and 82% of the most critical ratings occurred in the upper column for moment/axial and shear respectively; when only the upper half of the column was heated, only 41% and 44% of the most critical ratings occurred in the upper column for moment/axial and shear respectively.

The trends that were observed during the half column heating cases were similar to those observed during the whole column heating cases. However, there were significant differences. These were particularly evident when the structure was subject to the Standard Fire. For example, mean shear utilization was 40% higher during the half-column heating scenario, and the axial/moment utilization was also increased though to a lesser degree (3%).

Another significant change between the two Standard Fire cases was the most common location of failure. For both moment/axial utilization and the shear utilization, the most common location of failure changed from the upper to the lower column. This change was caused by the reduction in the amount of load shedding when only half of the column was heated.

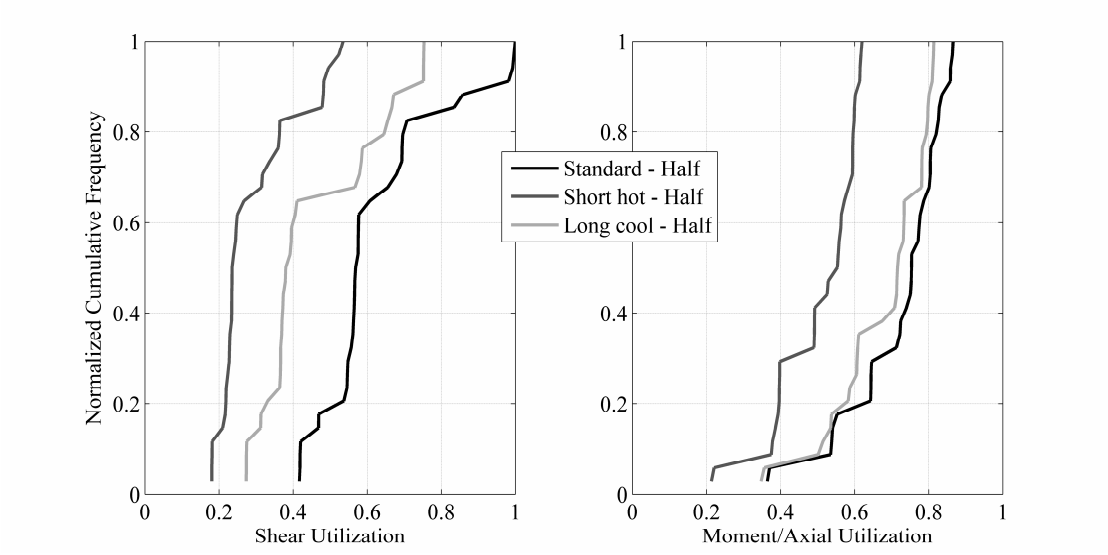


Figure 5-11. Utilization rates due to partial column heating

Both the parametric fires showed similar trends in the moment/axial utilization. There was also a shift in the location of maximum utilization as most highly utilized sections were in the lower column rather than the upper column. The mean utilization rates were also higher in both cases. It should be noted that in contrast to the axial/moment behaviour, the changes in the patterns of shear utilization were not significant. The main reason for this was that these fires were not long enough to cause a significant change in the in temperature of the steel and the associated effect on the shear capacity. However, there was still a small degree of load shedding due to the very hot peripheral concrete. By the time the steel had begun to heat up significantly,

the large shear forces had already begun to decrease as the fire was over. This caused slightly higher shears to occur in the upper columns, without degradation in the shear capacity. Thus, the regions of highest utilization were largely in the upper column.

## 5.4. Discussion and Conclusions

The previous sections have presented a thorough method of assessing a structure during a fire. Though the technique is presented with reference to the columns in a concrete frame, the principles of sectional utilization can be applied to many types of construction.

The main conclusion from this work is that the results of finite-element analyses can be used to extract far more detailed and useful information about the state of a fire-loaded structure than is often done when traditional "failure" measures are adopted. Specific information regarding the most critical members in a structure subject to fire loading is available. It is also possible to obtain more general information about the effect on a structure of a fire by combining information about the utilization of many cross-sections through time as fire loading progresses.

A second key conclusion is that the method presented allows comparison of the effects of different design fires to be made. Conventional methods of assessing structures in fire, as described in the introduction, do not readily lend themselves to meaningful comparisons between the effects of different design fires because it is difficult to separate the effect of the section's loading, from the section's capacity, from the fire's duration, and to make a

direct comparison. The method presented here allows a meaningful comparison to be made as the effects of changing load and capacity with time are fully accounted for. The fact that the areas in which the structure is highly utilized are clearly identified is a further benefit that in turn allows an understanding of how the structural behaviour changes with various design fires. For example, this work has demonstrated that significant variations in column utilization occur due to different fires and to localized heating of columns. The increased stiffness of the heated columns due to the half-heating scenario caused the locations of the most utilized sections to migrate from being predominantly in the upper (unheated) column, to the heated part of the lower column. Changes in structural behaviour such as this would not be apparent using traditional failure measures for heated structures and it would thus not be possible to determine effects of changing a design fire.

The information about the degree of structural utilization is flexible and could be used in many different ways. Different percentiles could be used to indicate the utilization of the whole structure, or to quantify specifically the distress in the most heavily loaded members. The facility of this method to compare the degree of column utilization between different scenarios is particularly useful.

In conclusion, methods of structural fire analysis are frequently highly complex, while the techniques currently used to measure structural performance are often arbitrary and basic. This chapter presents a methodology that attempts to redress the mismatch between the complexities of these two design elements.

# 6

# Travelling Fires

The previous chapter demonstrated how the mismatch between the complex finite-element tools and the measures used to assess them can be addressed. This chapter addresses another mismatch: that of the difference between the definition of a fire in a building and the techniques used to model the structure's response. When fires occur in real buildings, they rarely burn uniformly across the entire floorplate of the structure. They tend to travel, igniting fuel in their path and exhausting it before they move away. Current structural design approaches do not reflect this. This chapter presents a new methodology for defining a design fire and creates a number of different "travelling fires". The finite-element model of a generic concrete structure from the previous chapter is used to study the impact of each fire; both relative to one another, and when compared with the conventional codified

temperature-time curves. To avoid confusion the simpler, more conventional, methods of assessing the structure are used as the structural metrics. The use of the more advanced analyses presented in chapter five to assess these different fires is explored in chapter seven.

This chapter demonstrates that, in terms of the structural metrics used, travelling fires have a significant impact on the performance of structures and that the current approaches cannot be assumed to be conservative. Further, it is found that fires of a medium duration which burn approximately 25% of the floorplate at any one time are the most severe. It is concluded that the new approach is simple to implement; provides realistic fire scenarios; and is more conservative than current methods.

## 6.1. Introduction

Chapter two recognised that since the early 20$^{th}$ century, standard testing has been used all over the world to give fire ratings to different structural assemblies [8]. The standard fire temperature-time curve [6,27] was created in an attempt to regulate testing between different laboratories thereby ensuring a uniform standard of safety. However, almost as soon as it was conceived, a number of problems were identified with it. Though these problems have remained, standard testing has proved a useful and universal tool for assembly classification. Since the inception of the Standard Fire, a number of other temperature-time curves have been proposed and introduced. Initially based on work by Pettersson, these curves have been modified and are typically referred to as the parametric fires [44]. They allow a range of possible curves to be calculated from the fuel load and ventilation conditions in a compartment [53]. The parametric fires represent a more realistic fire

scenario than the standard fire, as they assume burn-out of the available fuel and can be roughly replicated by wooden cribs in a small fire compartment. This approach has been used for a number of "natural fire" tests on different structural assemblies and the concept of "fire severity" has been applied to find an equivalent rating under the standard fire [111].

An assumption that has remained unquestioned with each of these temperature-time curves has been that of uniform compartment temperature. It is assumed that every part of a structural element or compartment is uniformly subject to the same temperature – as defined by the temperature-time curve. Although it may be possible to replicate these conditions in a furnace, recent major fires at the Windsor Tower [62], World Trade Centers [68,123] and TU-delft [168] have clearly demonstrated that building fires typically burn non-uniformly. They have shown that fires tend to move around buildings in a manner determined by the available fuel, ventilation and building geometry. In addition, tests have shown that there is a high degree of temperature variation even within small compartments [2,146,159].

Chapter two demonstrates that as our understanding of how structures respond to fire has developed, it has been increasingly acknowledged that structural elements cannot be treated in isolation; to understand how a structure behaves in a fire, whole frame effects must be considered. This approach has led to the development of rational design tools which have allowed designers to exploit more of the redundancies available in structural assemblies. Complex finite-element modelling techniques are also available

which allow designers to model full structural frames and their response to high temperature; this performance-based approach allows engineers to identify the most vulnerable regions of the structure and modify the design accordingly.

When the fire design of a structure was based on the furnace testing of a single element, both the structural member and the temperature-time curve were gross simplifications of reality. In recent years the representation of structure, though not perfect, has become much more realistic; design fires, however, have remained unchanged. Without a more realistic representation of the fire to which a structure is subject, engineers will never be able to understand how a structure would respond to a real fire. It is difficult to justify continuing to develop more realistic structural models when one of the dominating input parameters – temperature – remains very crude. Without some development of the available design fires, it will be impossible to obtain the "consistent level of crudeness" which has been identified as a need within the discipline [28].

This chapter presents and implements a new methodology for defining design fires. The new approach is based on fire dynamics, and allows for the development of different temperatures in different parts of fire compartment – the key phenomenon missing from existing models. Fundamental to the new approach is the idea of the travelling fire that has been observed in recent case studies. The approach has been developed by researchers at the University of Edinburgh [147,148] and its influence on structures has begun

to be studied [88,133]. This chapter applies the new methodology to the previously developed large scale finite-element model and the effects of different fires are analysed using a variety of structural measures.

## 6.2. Limitations of Current Design Fires

The current parametric and standard fires are based on the extrapolation of existing fire test data, which stems from tests performed in small compartments that are almost cubic in nature. This test geometry allows for good mixing of the fire gases and thus for a uniform temperature distribution throughout the compartment. While both of these methods have great merits and represented breakthroughs in the discipline at their times of adoption, they have inherent limitations with regards to their range of applicability [132,147,148].

For example, Eurocode 1 states that the design equations are only valid for compartments with floor areas up to $500m^2$ and heights up to 4m, the enclosure must have no openings through the ceiling, and the compartment linings are also restricted to a thermal inertia between 1000 and 2200 $J/m^2s^{½}K$, which means that highly conductive linings such as glass facades and highly insulating materials cannot be taken into account. As a result, common features in modern construction like large enclosures, high ceilings, atria, large open spaces, multiple floors connected by voids, and glass facades are excluded from the range of applicability of the current methodologies. These limitations, which are largely associated with the physical size and geometric features of the experimental compartments on which the methods are based, ought to be carefully considered when the methods are applied to

an engineering design. This is particularly relevant given the large floor plates and complicated architecture of modern buildings.

A recent survey of buildings in Edinburgh, UK [88] underlines the narrow design fire specifications in the Eurocodes. For buildings built over a long period of time starting in the early 20th century, 66% of their total volume falls within the limitations. However, in a newly constructed, modern building that has open spaces and glass facades, only 8% of the total volume is within the limitations. This suggests that modern building trends are moving out of the limits of current design practice.

## 6.3. Travelling Fires

In light of the various limitations outlined above, a new methodology based on the fundamental fire dynamics of the compartment has been proposed [104,146,147]. The new approach uses two different temperatures to represent the gas temperature in a compartment: a very high temperature in the region of the seat of the fire; and a cooler temperature for the rest of the compartment. The approach provides a flexible technique whereby the full range of possible fires can be represented. For example, a fire which engulfs the entire floorplate simultaneously can be represented. Likewise, a fire that travels slowly from one end of the compartment to the other can also be defined [96]. Rather than basing the type of fire on predicted factors such as glazing breakage, the burn area of the fire is directly specified by the design engineer. As such, different fires can be created without artificially manipulating the physical input parameters.

### 6.3.1. Temperature Definition

The new approach represents the temperature distribution on the ceiling of a fire compartment by means of "near-field" and the "far-field" regions (Figure 6-1). The near-field is the region directly above the seat of the fire; here it is typical for structural elements to be exposed to temperatures of approximately 1200 °C due to direct flame impingement [44]. The far-field represents the temperature of the hot gases as they move away from the seat of the fire; far-field temperatures are defined using Alpert's ceiling jet correlation [3].

$$T_{\max} - T_{\infty} = \frac{5.38\left(\dot{Q}/r\right)^{2/3}}{H} \tag{1}$$

where $T_{\max}$ is the maximum temperature within the ceiling jet (K); $T_{\infty}$ is the ambient temperature (K); $\dot{Q}$ is the total heat release rate (kW); $r$ is the distance from the centre of the fire (m); and $H$ is the floor to ceiling height (m).

As the fire consumes the available fuel and ignites new material in its path, it moves around the floorplate. Consequently, the temperature for any one location is constantly changing according to Alpert's distribution. To make the amount of information passed to the structural analysis managable, the monotonically decreasing far-field temperature distribution is reduced to a single, characteristic, temperature. This is calculated as the fourth-power average of the temperature as it changes over the distance between the end of the near-field and the end of the far-field, thereby weighting the temperature

towards radiative heat transfer and giving worse case conditions. The total heat release rate required for Alpert's formula is calculated directly from the heat release rate per unit area. Figure 6-1 demonstrates the concept of a near-field and a far-field for a travelling fire. Any single location is exposed to a pre-heating far-field temperature for a duration before the arrival of the flaming region. After the fuel has been consumed and the fire moves away, the region is then subject to the far-field temperature until all the fuel in the compartment has been consumed.

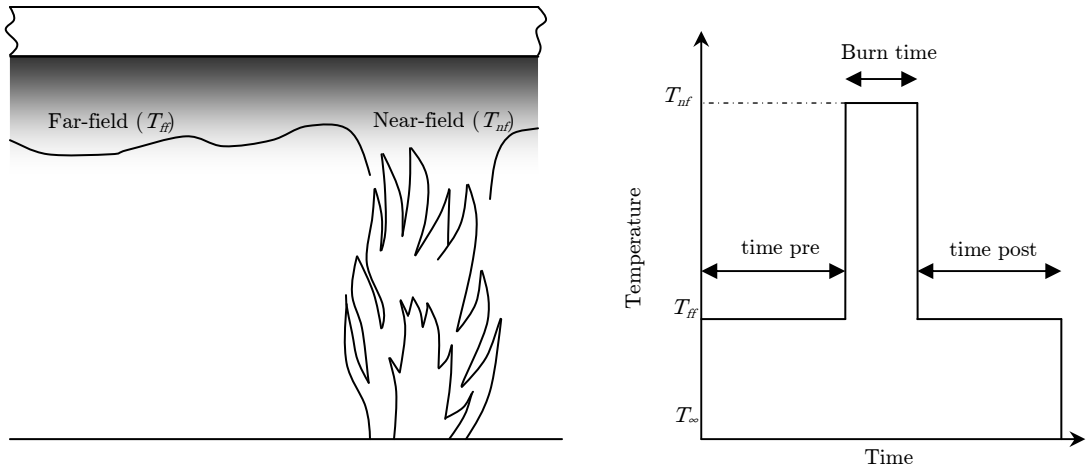


a) b)

Figure 6-1. a) Near-field and far-field temperatures induced by localized travelling fire; b) far-field and near-field exposure durations.

### 6.3.2. Burn Area

The flexibility of the method stems from the ability to directly define the size, shape, and path of the burn area. It is assumed that, once alight, any area of the floorplate will continue to burn at the same rate until all the fuel is consumed. The burn duration of any area can, therefore, be simply calculated from the total fuel load and the heat release rate. Once the fuel is

exhausted, the fire will move to a new area. The size of the burn area can range from 1% to 100% of the compartment.

## 6.4. Structural Assessment

The methodology presented above can be used to study the impact of different travelling fires on the response of a structure. However, without a means to compare the structural response, it is impossible to drawn any conclusions. As discussed in previous chapters, there are many different methods of assessment available for fire-affected structures of varying degrees of complexity.

The previous chapter developed a new methodology to assess structures when subject to fire. The author feels that to introduce this new analysis techniques at the same time as studying the effect of fires would over complicate and already difficult scenario. The response of the structure to the different travelling fires will, therefore, be split into two sections: the flexural assessment of the slab; and the more complex analysis of the columns. This chapter will deal with the conventional assessment techniques outlined in previous chapters. Temperature, strain and deflection will all be used as measures that can be used to compare the response of the structure to the different fires. The following chapter will apply the more advanced analysis techniques to study the column behaviour.

## 6.5. Case Study

The remainder of this thesis is a case study that demonstrates how the methodology above can be applied to a structural model. Initially, a number of “base case” scenarios are considered and the differences between the

structural response compared; a parametric study is then conducted to assess the validity and effect of the various assumptions made by the new approach. The impact of the shape and path of the fire is also considered. Chapter seven focuses on applying the more advanced analysis techniques to the same set of fires.

### 6.5.1. Structural Arrangement

The finite-element model that was used is identical to that described in chapter five. For further discussion of this model, and the sensitivity studies, see also appendix II.

### 6.5.2. Base Case Fires

The "base case" set, or family, of fires were defined as a simple fire type that moved linearly from one side of the structure to the other. Their burn areas had a range of sizes: 1%, 2.5%, 5%, 10%, 25%, 50% and 100% of the floor area. It was assumed that the fuel load ($q_f$) was 570MJ/m$^2$; the heat release rate ($\dot{Q}''$) was 500kW/m$^2$; and the radius for Alpert's equation was measured from the centre of the burn area. This resulted in a burn duration of 19 minutes for any single area. The 25% burn area fire, therefore, lasted for a total time of 76 minutes, and had a far-field temperature of 805 $^\circ$C. The 2.5% burn area fire, meanwhile, had a duration of 760 minutes and a far-field temperature of 325 $^\circ$C. Figure 6-2 shows the duration and far-field temperatures for each of the base case fires. It should be noted for the 100% area fire, the far-field temperature is the same as the near-field temperature.

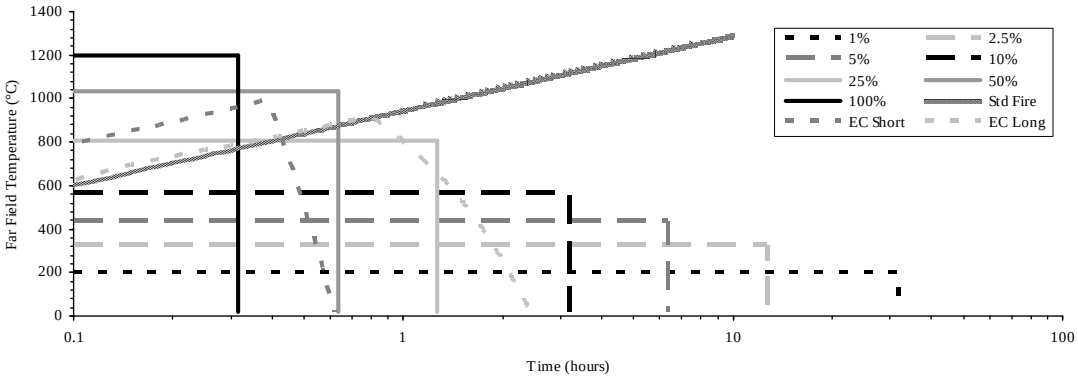


Figure 6-2. Far-field temperatures and durations for different burn area fires. Standard and Parametric fire curves are also shown for reference.

#### 6.5.2.1. Structural and Thermal Analysis

A thermal and structural analysis were conducted using the finite-element model described above. Figure 6-3 shows the slab soffit temperature part way through the 2.5% and 25% burn area fires. To allow meaningful conclusions to be drawn from the modelling, it should be noted that the analyses were comparative, not absolute. The initial aim of these analyses was to compare the response of the structure to the different fires rather than to obtain a detailed description of the structural behaviour in each scenario. Therefore, for the remainder of this chapter, the metrics that will be used to quantify the response of the structure will be the three simple measures discussed above – temperature, strain in the tension steel, and central deflection of each bay.

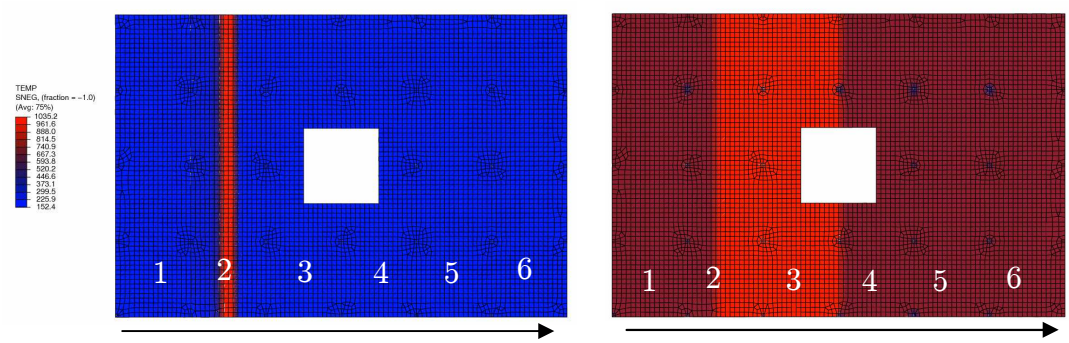


a) b)

Figure 6-3. a) The progression of the 2.5% fire across the floorplate; b) The progression of the 25% fire across the floorplate. Bay numbers are indicated in both figures.

The heat transfer analyses allowed the temperature in the slab soffit rebar to be monitored. Figure 6-4 shows the temperature profiles for the tension rebar in bays 1-6 for the 5% burn area fire. It can be clearly seen that the final bay to be subjected to the near-field experienced the highest temperature; the long pre-heat induced a higher maximum temperature in this bay, which causes it to be most critical. This trend was the same with each of the base case fires.

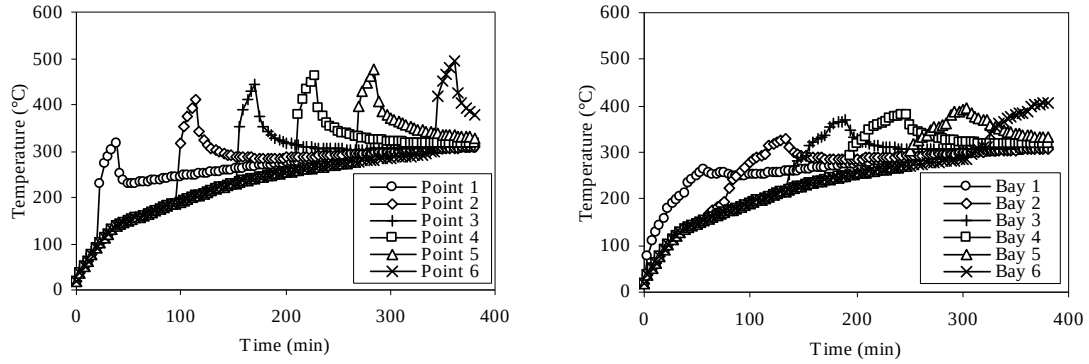


a) b)

Figure 6-4. a) Single point rebar temperature at the centre of bays 1-6 during the 5% base case fire; b) Average rebar temperatures for the whole of bays 1-6 for the 5% base case fire.

Figure 6-4 also shows the average temperature in the soffit rebar for each bay. It is notable that the average bay temperatures are lower than the single point temperatures. This is because the near-field of the 5% burn area fire does not cover the whole area of any bay simultaneously; thus, the average rebar temperatures are lower. The bay average lower rebar temperatures are a more representative measure of structural vulnerability as they will not be distorted by localized heating effects. For example, were a localised fire to heat only a tiny area of the bay, it would have minimal impact on the overall structural behaviour, but would induce high rebar temperatures. Thus, the bay average lower rebar temperatures will be used as the measure of rebar temperature for the remainder of this chapter.

A comparison of the rebar temperatures induced in the final bay by the different base case fires (Figure 6-5) shows clearly that the highest temperatures are caused by the medium duration fires: 10% and 25% burn areas.

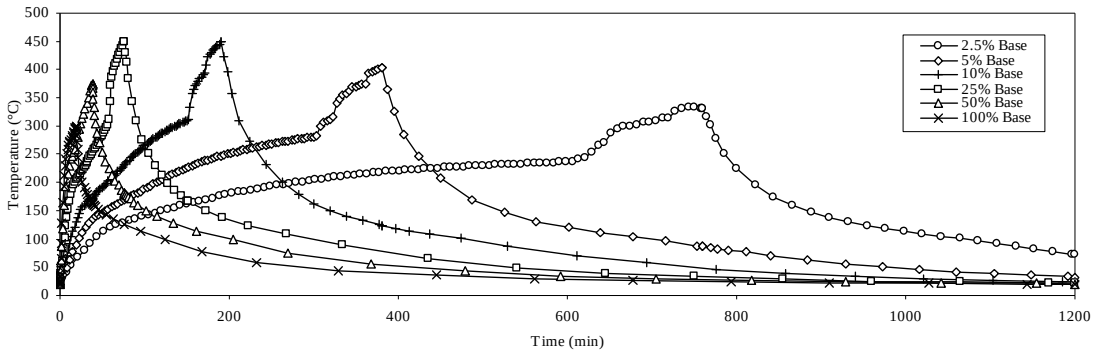


Figure 6-5. Temperature profiles for the rebar during the base case fires.

The rebar strains show a similar trend; however, rather than the peak occurring during the heating phase, the maximum rebar strains occurred during the cooling phase. Figure 6-6 shows the trace of the maximum hogging and sagging strain and their corresponding locations on the floorplate. It should be noted that the majority of the slab is pulled into tension on cooling. This is consistent with experimental observations that perimeter columns experience significant residual lateral deflection even after cooling [9].

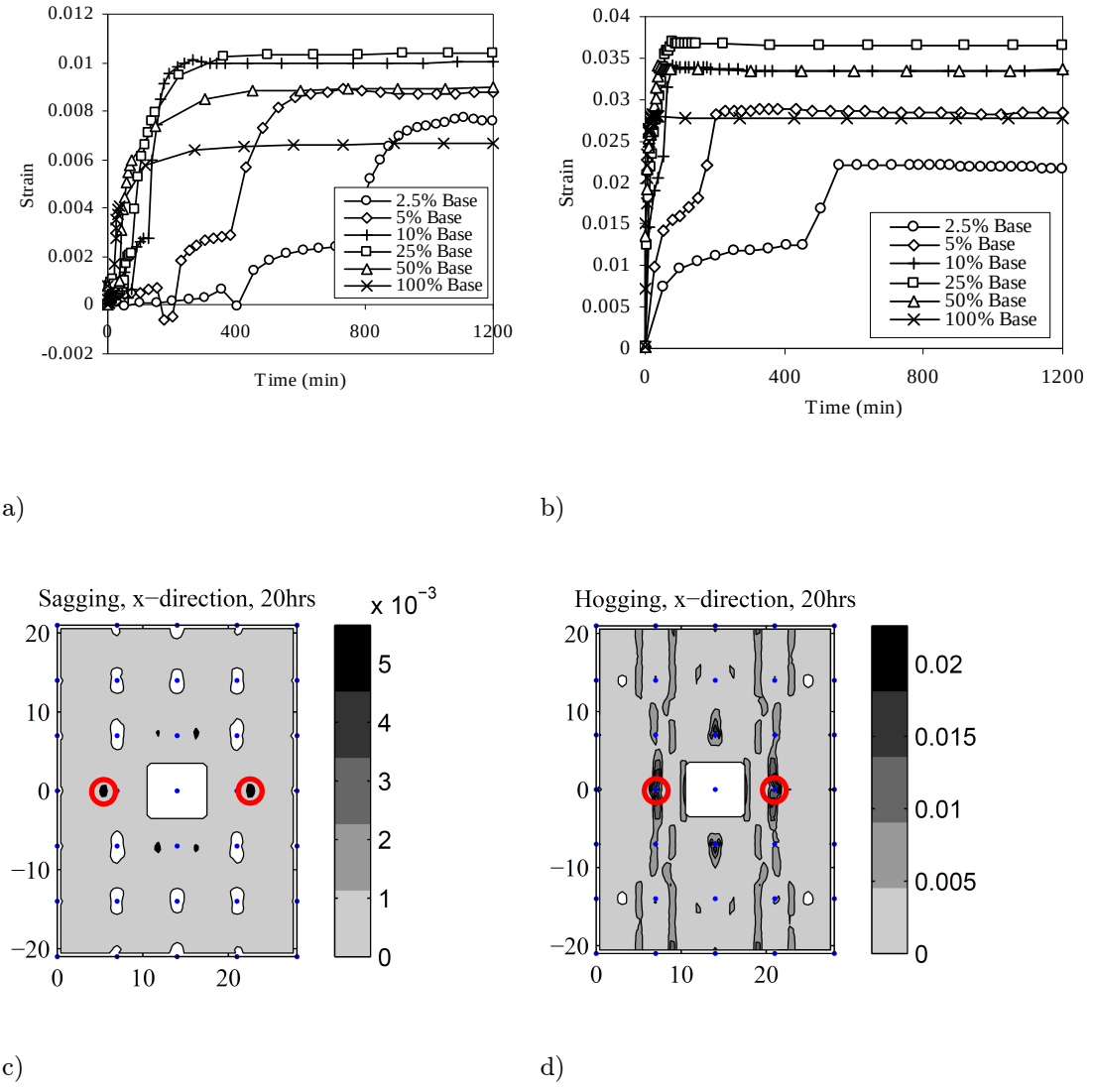


Figure 6-6. Strain behaviour during each of the base case fires

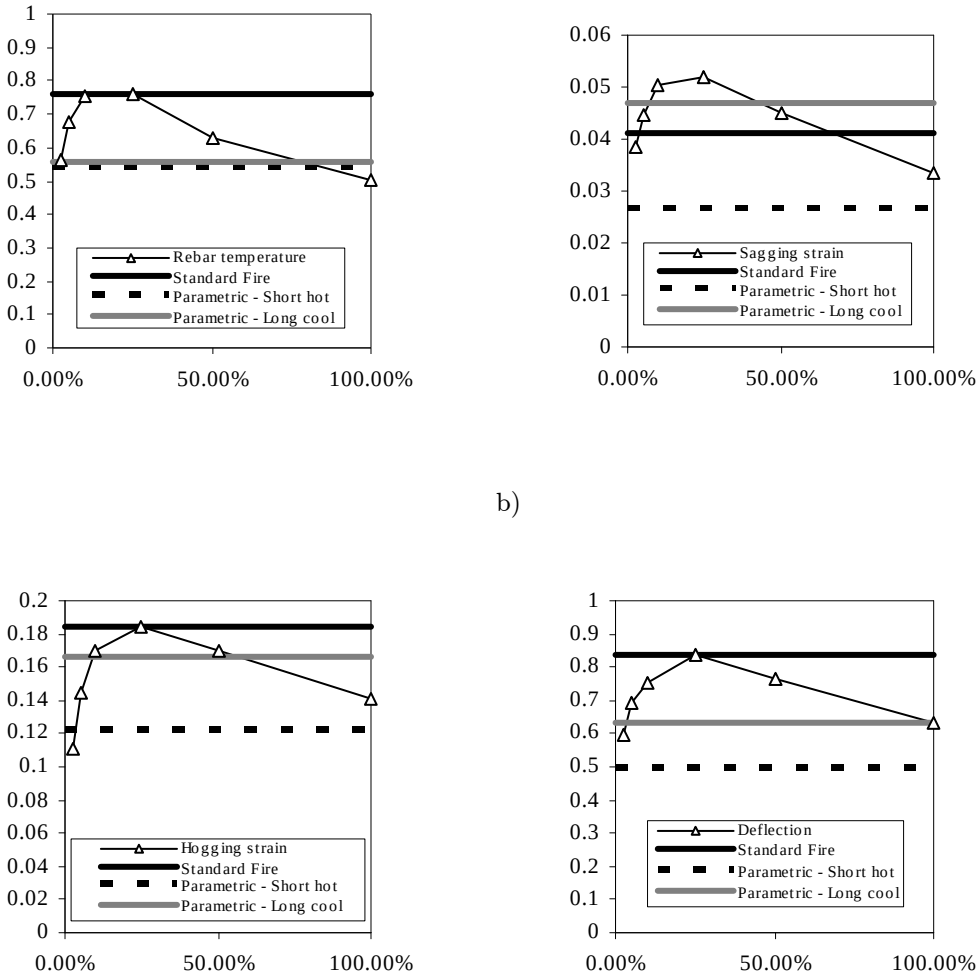


Figure 6-7. Change in structural distress with burn area: a) rebar temperature, Standard Fire equivalent is 1hr 37min; b) sagging strain, value for Standard Fire given after 3 hours; c) hogging strain, Standard Fire equivalent is 1hr 18min; and d) deflection, Standard Fire equivalent is 1hr 54 min.

Each measurement technique can be normalized with respect to the appropriate failure definition: 593 ° C for rebar, span/20 for deflection, and 0.2 for rebar strain. It is possible therefore to observe how the level of

structural distress changes as the percentage burn area is increased. A comparison can also be made with the behaviour of the structure subject to the various codified fires. The structure was subjected to a three hour standard fire, a "short hot" parametric fire and a "long cool" parametric fire. The "short hot" fire had a peak temperature of 989 °C and a total duration of 37 minutes, and the "long cool" fire had a peak temperature of 915 °C and a duration of 145 minutes. The response of the building to these fires in terms of the structural measures monitored was also analysed. The most severe response generated by the travelling fire was compared to the time it took for the Standard Fire to induce the same degree of distress. For the rebar temperature, the equivalent time was 1 hour 37 minutes; for the deflection, the equivalent time was 1 hour and 54 minutes; for the hoggig strain, the equivalent time was 1 hour and 18 minutes; and for the hogging strain, the maximum strain obtained during the travelling fires was not obtained even after three hours. Figure 6-7 shows the trends for each of the measures as the burn area changes.

It is clear that the 25% burn area fire induced the highest degree of structural distress in each of the "failure" metrics. The trend in every metric is the same: the lower burn area fires caused a lower degree of structural distress; the medium length fires (5%, 10% and 25%) caused a higher degree of structural distress; the high burn area, shorter duration, fires caused a lower degree of structural distress. It is also notable, that the temperature and deflection measures show the structure as much closer to "failure" than the strain measures. The comparison between the results from the base case fires, and the codified fires shows a mixture of results. The lack of consistency

in the time taken for the Standard Fire to induce the same degree of severity as the most severe travelling fire is worth noting. It indicates that the when compared to a more realistic fire, the Standard Fire produces a very non-uniform degree of safety between the different measures. After three hours of exposure to the Standard Fire, the sagging strain obtained was lower than that obtained during many of the travelling fires, and the "long cool" parametric fire. This was because there was no cooling phase during the standard fire so the structure was not pulled into tension. It can be seen that the parametric fires universally induced less extreme structural conditions than the medium burn area base case fires.

The response of the concrete frame to the base case and codified fires demonstrated three points.

- It cannot be assumed that the range of parametric fires are able to induce the most extreme structural conditions realistically possible; a travelling fire based on fundamental fire dynamics can induce a worse structural scenario.
- The lack of a cooling phase in the Standard Fire does not allow all the forces that are likely to develop over the course of a real fire to develop; it cannot, therefore be considered conservative.
- The medium duration (and burn area) fires induce the most extreme structural response; the very short fires with a large burn area, and the very long fires with a small burn area are less severe for the structure.

## 6.6. SENSITIVITY STUDY

In light of these points, a sensitivity study was conducted to establish the validity and conservatism of the various assumptions made in the travelling fire methodology. As the 25% fire was found to be the most severe by every metric, this burn area was used throughout the sensitivity study. The method used to define the far-field temperature was varied, and the response of the structure was monitored using the same metrics that were used in the previous section. The far-field temperature cases studied are described below and illustrated in Figure 6-8.

*Alpert's temperature profile*. Rather than averaging Alpert's temperature profile as above, the monotonically decreasing temperature profile defined by Alpert's equation was directly applied to the structure. The movement of the fire was also varied: the previous analyses assumed that the fire would suddenly "jump" between burn areas after the exhaustion of the fuel. The effect of this was studied by allowing the fire to move slowly along the floorplate of the structure.

*Single far field.* As with the previous analyses, Alpert's far-field temperature profile was reduced to a single value by fourth power averaging.

*Two far fields.* Rather than reducing the far-field to a single value either side of the burn area, the two far-field area's temperatures were defined independently averaged. This gave two far fields as the fire progressed through the structure.

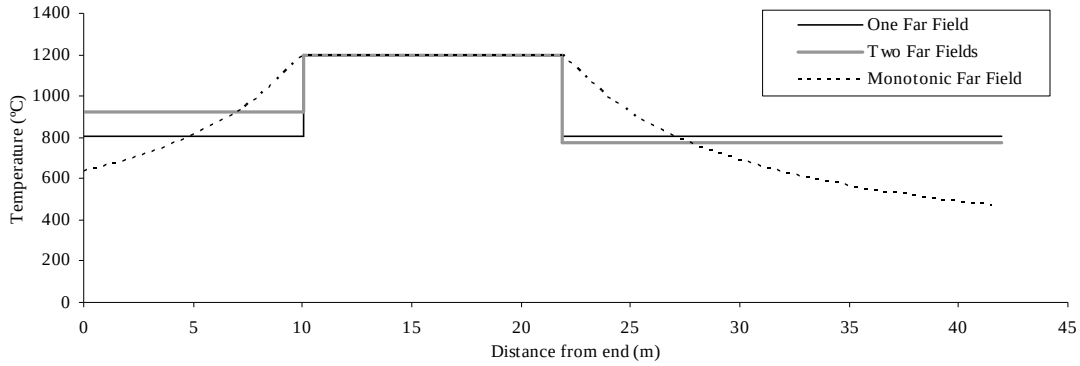


Figure 6-8. Temperature profiles for parametric study

The results from the parametric study (Figure 6-9) show that there is little variation in the performance metrics between the different fires. It is therefore reasonable to use the simple, averaged, temperature profile as for the whole of the far-field temperature region. This makes the temperature definitions in the heat transfer model significantly easier to apply: a key consideration for the use of such an approach in design.

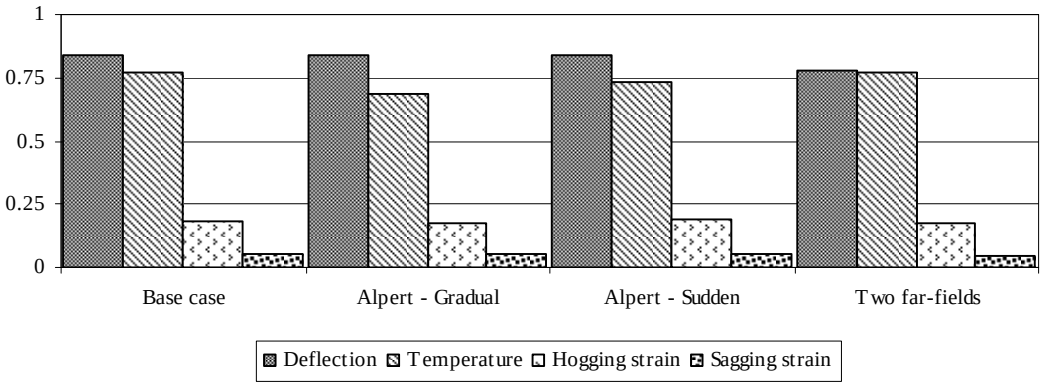


Figure 6-9. Effect of far-field definition on each metric

## 6.7. Different Shapes of Fire

The above analyses have focused on fires which start at one end of the structure and the progress across the floorplate. In reality a fire could follow any number if paths; it has long been recognised that to recreate every possible fire scenario would be unfeasible [8]. However, since the advent of modelling techniques such as the finite-element method it has become possible to evaluate a number of different structural scenarios quickly. This chapter has developed a number of fires and applied them to the same structures: however, it would still be unfeasible to attempt to model every possible fire. In an attempt to quantify the impact that different fire paths and shapes have on the structure, this study analyses the effect of three other possible fire patterns. The different fire shapes are illustrated in Figure 6-10 and are described below:

*Corner fire.* The fire initiated in one corner of the structure and spread clockwise around the building's core until all the fuel was consumed.

*Ring fire, Outwards.* The fire was initiated in a ring around the core, and spread concentrically outwards.

*Ring fire, Inwards.* The fire was initiated in a peripheral ring around the edge of the structure, and spread concentrically inwards towards the core.

It should be noted that in each of these cases, the burn area is 25%. This figure was chosen as it induced the highest degree of structural distress in the initial base case study.

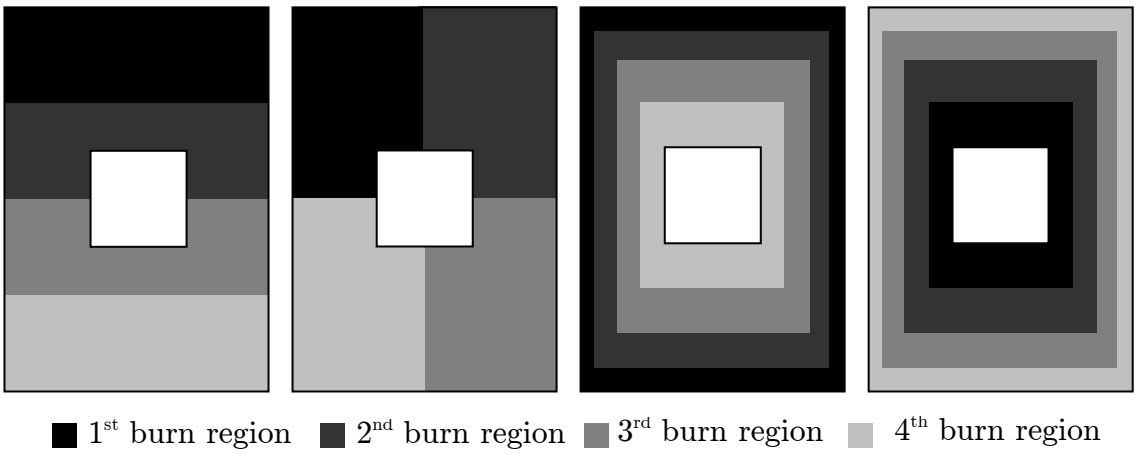


Figure 6-10. Different fire shapes and paths.

The analysis of the different failure metrics reveals that there is some variation between the different fires paths for all of the different paths. The results were broadly similar with some metrics showing an increase and some showing a decrease. Between all of the different fires the maximum relative increase in comparison with the base case model was: 8% for deflection; 5% and 10% for hogging and sagging strain respectively; and 0% for the rebar temperature. Figure 6-11 shows the difference between the four fire shapes analysed.

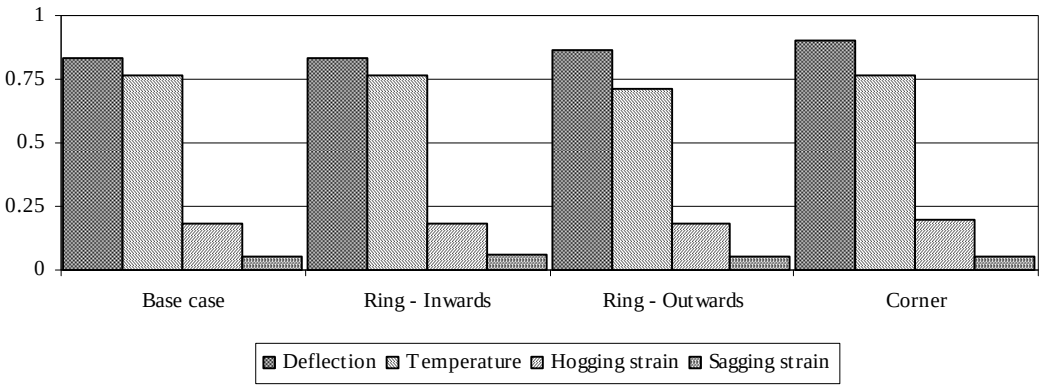


Figure 6-11. Influence of path on failure metrics.

## 6.8. DISCUSSION

A comparative analysis of the impact of a number of different design fires on a concrete frame has been conducted. A new approach to defining temperature-time curves for design has been presented. The relative impact of the conventional codified curves and the new "travelling fire" methodology has been studied. There are a number of points that should be emphasised.

The "travelling fire" approach is based on observations from real large-building fires, and founded on the fundamental fire dynamics of a large open plan floorplate. It allows a range of fires to be considered and, thus, allows structural engineers to better understand how different fires might affect the behaviour of a building. Though based on complex temperature distribution data, a simplified approach allows a single value far-field temperature distribution. It has been demonstrated that this simplification is a good approximation to more complex temperature defined by fire dynamics and a gradually progressing fire. The simplified far-field approach is easily implemented in finite-element codes.

The generic concrete frame which was subjected to the various fires was the same in each of the analyses. Though a number of simplifications were made to allow the series of stable finite-element analyses to take place, the strength of this study is in the comparison between identical models. It is know that a small degree (~6%) of accuracy was lost due to tension behaviour simplifications. However, the aim of this study was not to give an absolute value for deflection or strain after a certain fire: rather, the aim was to

compare the how different fires affect the same structure. It has been possible to draw strong comparative conclusions, particularly given the variety of measures used to assess the structure.

## 6.9. Conclusions

There are a number of conclusions which can be drawn from this study:

- Complex temperature profiles can be applied to finite-element modles in a relatively simple manner.
- Travelling fires have a more severe impact on the performance of a structure than the Eurocode parametic fires. These fires cannot, therefore, be considered conservative.
- The fires of medium duration and burn area are the most severe in terms of their impact on the structure.
- The 25% burn area fire was conclusively found to be the most severe by every measure used.
- The assumption of a simplified far-field temperature was valid: more complex and realistic temperature profiles had little impact on the overall structural behaviour.

# 7

# Travelling Fires and Whole Structure Assessment

This chapter draws together the techniques that have been developed throughout this thesis and applies them to the generic concrete structure that has featured in chapters five and six. Chapters four and five developed and applied techniques for assessing the capacity and loading of a structure. The previous chapter focused primarily on the slab. This allowed the various assessment methods to be applied simply and appropriately to the shell model of the concrete slab. In this chapter, the attention will shift to the columns. Initially, the columns will be analysed using the most appropriate simple measure, namely rebar temperature. Then, the effect of the different fires on the capacity and the loading of the structure will be examined more closely than in previous chapters. Finally, the new utilization assessment

techniques will be applied to the all of the columns in the structure and the fires will be compared quantitatively and methodically. The general trends which a structure undergoes are analysed and the potential for design modifications is made clear. The chapter will first focus on the "base case" fires and then move onto the various parametric studies.

## 7.1. Rebar Temperature Assessment

Many of the metrics that were used to assess the slab in the previous chapter are not appropriate for the assessment of columns. For example, the tension strain in the steel is not a particularly useful measure as the column is likely to be mostly or entirely in compression. The usefulness of deflection as a metric is also questionable: should it be the lateral deflection of the top of the column relative to the base, or the vertical displacement of the top of the column. A more appropriate measure, perhaps, is steel temperature, as this give some indication of both the axial and flexural resistance of the column. Of course, depending on the degree of steel reinforcement, the bulk of the column's resistance may be given by the concrete. Nevertheless, steel reinforcement temperature offers a simple measure for structural resistance.

The maximum temperature of the longitudinal rebar was monitored for the duration of each fire. As with the slabs it was found that the final member to be heated achieved the maximum rebar temperature; in each case this was the final column in each row. Figure 7-1 shows the temperature profile for the hottest rebar in columns E1-E7 over the duration of the 25% burn area fire.

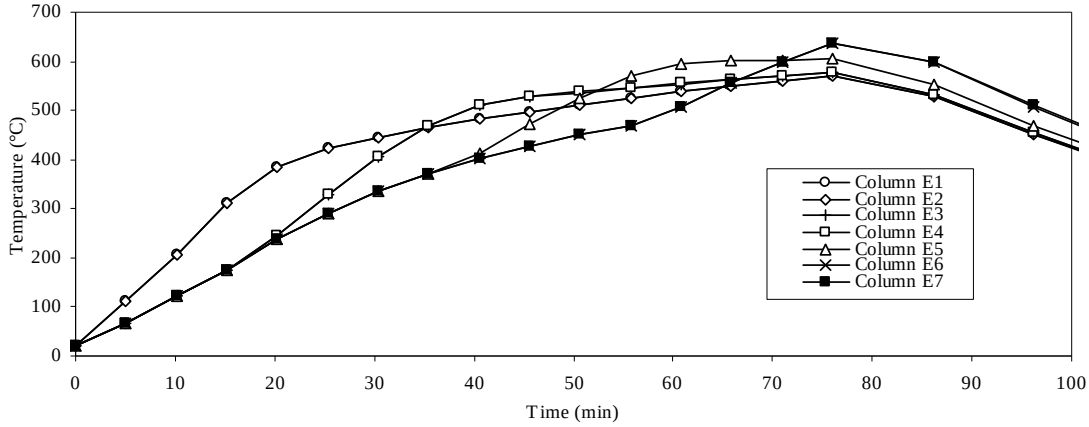


Figure 7-1. Temperature profile in column steel due to 25% fire.

It is clear that the final column to be exposed to the near-field temperature was heated to the highest temperature. This was the case with each of the base case analyses. Figure 7-2a shows the temperature profiles of the rebar which obtained the maximum temperatures. It can be seen that as with the slab analysis in the previous chapter, the peak rebar temperatures were induced by fires of medium duration fires and medium burn area. The maximum temperature obtained can be plotted as a function of burn area as shown in Figure 7-2b.

From these plots, it is clear that the medium duration and medium burn area fires are the most severe in terms of this measure of distress. This is a similar finding to the conclusions of chapter six where the medium fires were consistently found to induce the most severe structural response.

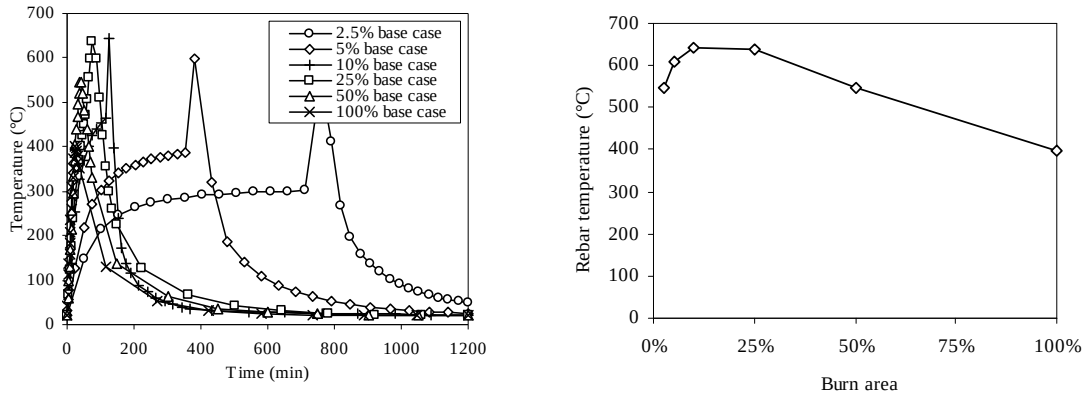


a) b)

Figure 7-2. Maximum temperature profiles for each of the base case fires; a) in profile for the hottest column in each base case; b) maximum temperature in terms of burn area.

### 7.1.1. Sectional Analysis

To allow the utilization rate of the columns to be analysed, a series of sectional analyses were conducted. Figure 7-3 shows the sectional analysis for column B4 at different stages during the fire. At 11400s, the shape of the interaction clearly becomes asymmetrical as was seen in chapter 4. This time is halfway through the burn period of the fire and consequently, at this time column B4 has been exposed to the near-field on one side, but not on the other. This is the cause of the asymmetric interaction diagram. On further times steps, after the near-field passed and the whole column had been exposed to the highest temperatures for a duration of 19 minutes, the symmetry of the diagram is restored, though it is clear that exposure to the near-field has reduced the overall sectional capacity significantly. Much of this reduction is present even after cooling as the ultimate concrete strength was assumed to be irrecoverable. Appendix IV presents a series of similar diagrams for each of the columns for the 5% base case fire. Figure 7-3 also

shows the current loading at the top of the heated column. It can be seen that throughout the analysis, the loading remained well within the limits of the section's capacity.

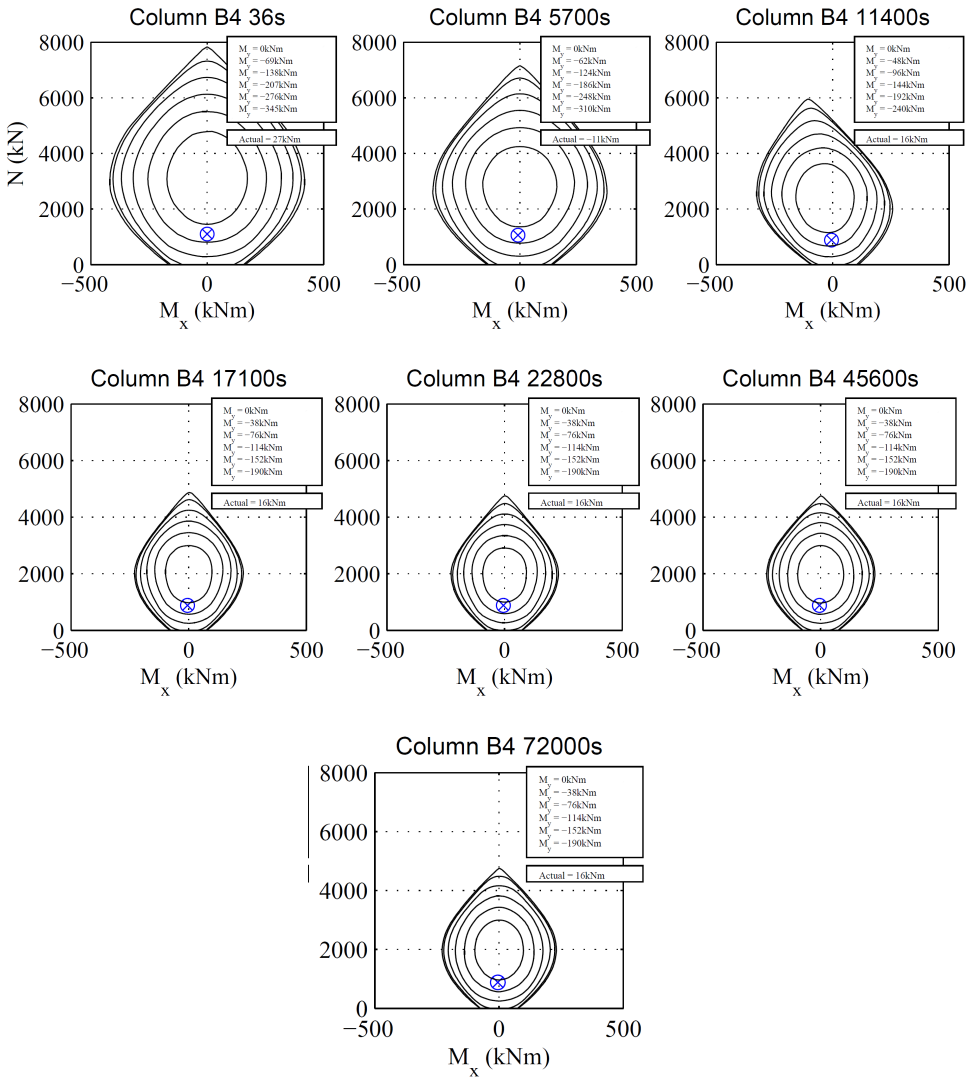


Figure 7-3. Plots of how the sectional analysis develops during the 5% fire.

Though these plots are useful in that they provide information about the changes in sectional capacity with time, they must be analysed further using the methodology presented in chapter five to allow a deeper insight into how the fires affect the columns.

## 7.2. Utilization Analysis

### 7.2.1. Base case fires

Each of the base case fires which were presented in chapter six were applied to the structure. The columns were also analysed using the methodology presented in chapter six. Figure 7-4 shows the utilization rates for the columns and Table 7-1 highlights the key statistics for each fire. From this it is clear that the maximum burn area, shortest duration fires (100% and 50% burn areas) have the lowest impact on the columns.

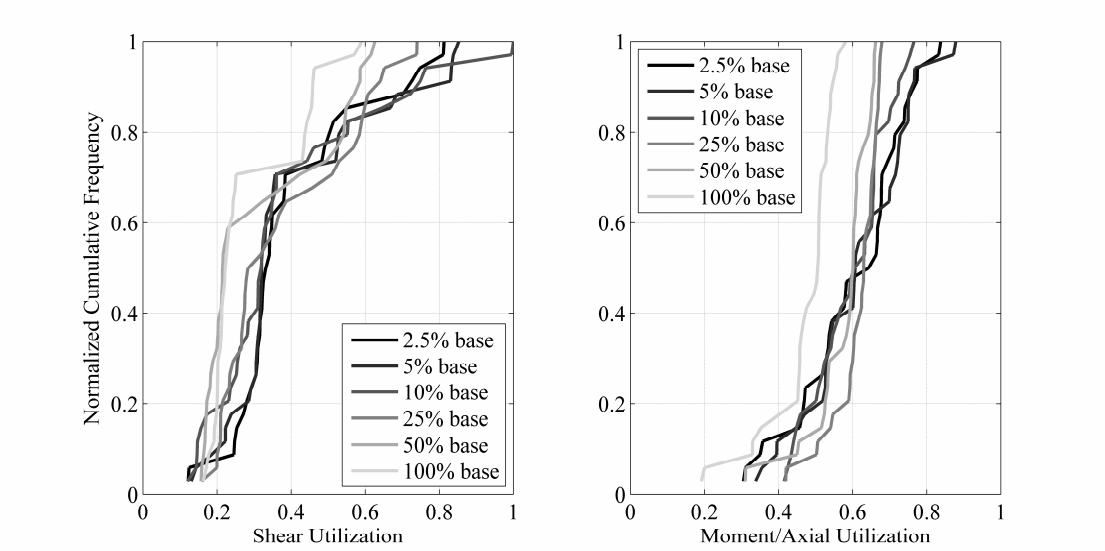


Figure 7-4. Utilization rates of columns subject to the base case fires.

What is particularly striking about the statistics is that the mean utilization for the 2.5% through to the 25% burn area fires are very similar. This is the case for both the moment/axial utilization and the shear utilization. The higher percentile measures show that the 5% and 10% burn area fires cause the highest utilization. This is visualized in Figure 7-5a and b, where it can be seen that in contrast to the more conventional metrics of structural

performance, the column utilization approach identifies the lower percentage area fires as being the most critical for structural performance.

Table 7-1. Key statistics from each of the base case fires.

| | Moment/Axial | | | | | | Shear | | | | | |
|---|---|---|---|---|---|---|---|---|---|---|---|---|
| | 1st | 2nd | Up | $\bar{x}$ | 75th | 95th | 1st | 2nd | Up | $\bar{x}$ | 75th | 95th |
| 2.5% Base | E7 | A7 | 38% | 0.60 | 0.70 | 0.79 | D6 | B6 | 85% | 0.40 | 0.49 | 0.77 |
| 5% Base | A7 | E7 | 53% | 0.61 | 0.72 | 0.80 | B2 | D2 | 88% | 0.40 | 0.52 | 0.83 |
| 10% Base | A6 | E6 | 38% | 0.60 | 0.66 | 0.75 | B6 | D6 | 82% | 0.39 | 0.45 | 0.84 |
| 25% Base | E6 | A7 | 41% | 0.61 | 0.66 | 0.67 | D2 | B2 | 85% | 0.38 | 0.55 | 0.68 |
| 50% Base | E6 | D7 | 41% | 0.58 | 0.62 | 0.66 | B4 | D4 | 88% | 0.32 | 0.51 | 0.60 |
| 100% Base | E5 | A2 | 74% | 0.47 | 0.53 | 0.56 | B4 | D4 | 88% | 0.29 | 0.43 | 0.50 |

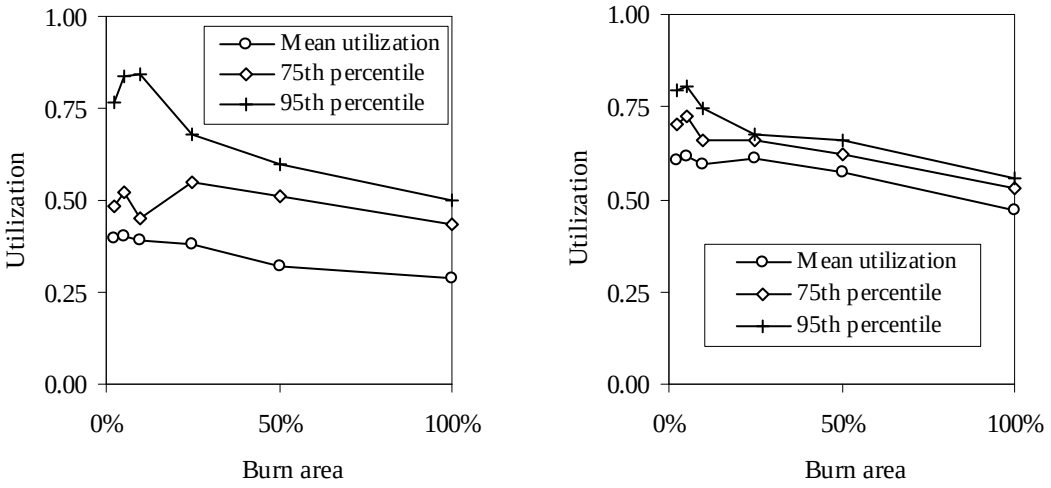


a) b)

Figure 7-5. Utilization rates as a function of burn area; a) shear utilization; b) moment/axial utilization.

There are several other trends that can be picked out from this data. The most critical columns in terms of moment/axial force are the perimeter columns in every case. In contrast, the most critical columns in terms of shear force are the internal columns. Another contrast between the bending and shear utilization measures is the location of the most critical section in each column. The most critical shear utilization consistently occurs in the upper section of the column, while more critical utilizations occur in the lower section of the column when moment/axial force are considered.

### 7.2.2. Parametric Study

As discussed in chapter six, the base case fires make a number of assumptions regarding the definition of the far-field. The sensitivity of the model to these assumptions was studied using the single parameter measures in chapter six. Here, the same models are analysed using the whole structure utilization approach. Figure 7-6 shows the cumulative percentage utilization for the most critical step during each fire. It can be seen that the four options for far-field temperature definition give very similar results. These can be directly compared in Table 7-2. The largest differences between the models occur in the shear utilization at the 95$^{th}$ percentile. It can be seen that in this case, the one far-field approach to temperature definition is conservative. This is not the case with the moment/axial force where there is a maximum difference of five percentage points between single temperature far-field and the gradual Alpert distribution.

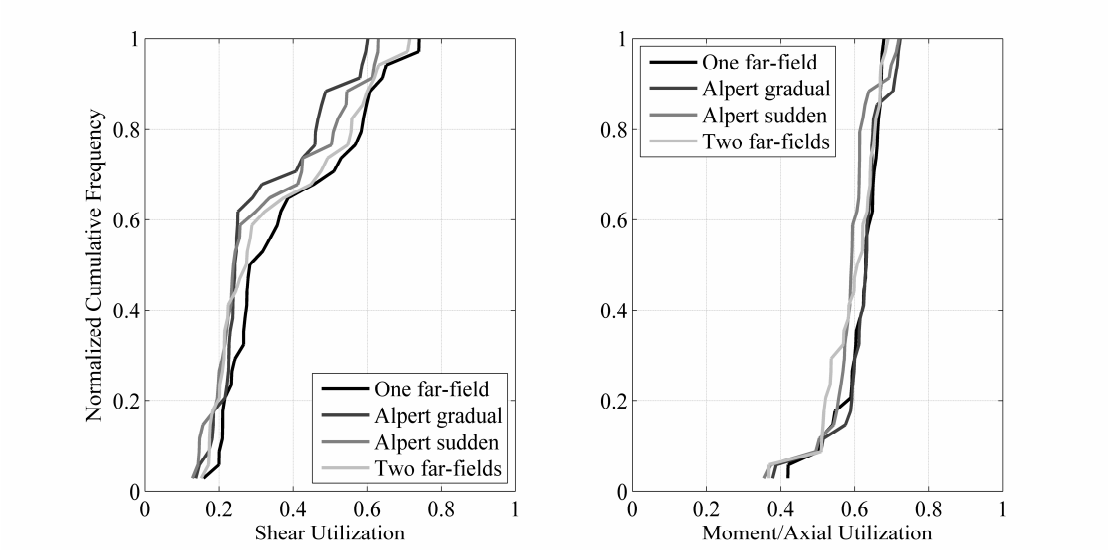


Figure 7-6. Utilization rates due to different methods of far-field temperature definition as described in section 6.6.

Table 7-2. Key statistics from fires of different far-field temperature definition

| | Moment/Axial | | | | | | Shear | | | | | |
|---|---|---|---|---|---|---|---|---|---|---|---|---|
| | 1st | 2nd | Up | $\bar{x}$ | 75th | 95th | 1st | 2nd | Up | $\bar{x}$ | 75th | 95th |
| One far-field | E6 | A7 | 41% | 0.61 | 0.66 | 0.67 | D2 | B2 | 85% | 0.38 | 0.55 | 0.68 |
| Alpert gradual | B6 | B3 | 53% | 0.62 | 0.65 | 0.72 | B2 | D2 | 94% | 0.31 | 0.44 | 0.59 |
| Alpert sudden | B6 | D6 | 53% | 0.59 | 0.61 | 0.70 | B6 | D6 | 94% | 0.33 | 0.47 | 0.62 |
| Two far-fields | E6 | B6 | 53% | 0.59 | 0.65 | 0.68 | B2 | D2 | 88% | 0.35 | 0.52 | 0.66 |

### 7.2.3. Different Paths

The final variation that was studied was the effect of different fire shapes and paths. Four different options as described in chapter six were trialled and the results are presented in Figure 7-7 and Table 7-3. It can be seen that in terms of the overall maximum moment/axial utilization, there is very little difference between the different fire types. The 95th percentile shows a

difference in utilization between the different fires of five percentage points. Though the overall shear utilization is similar, the percentile differences are slightly bigger with eight percentage points at the 95$^{th}$ percentile.

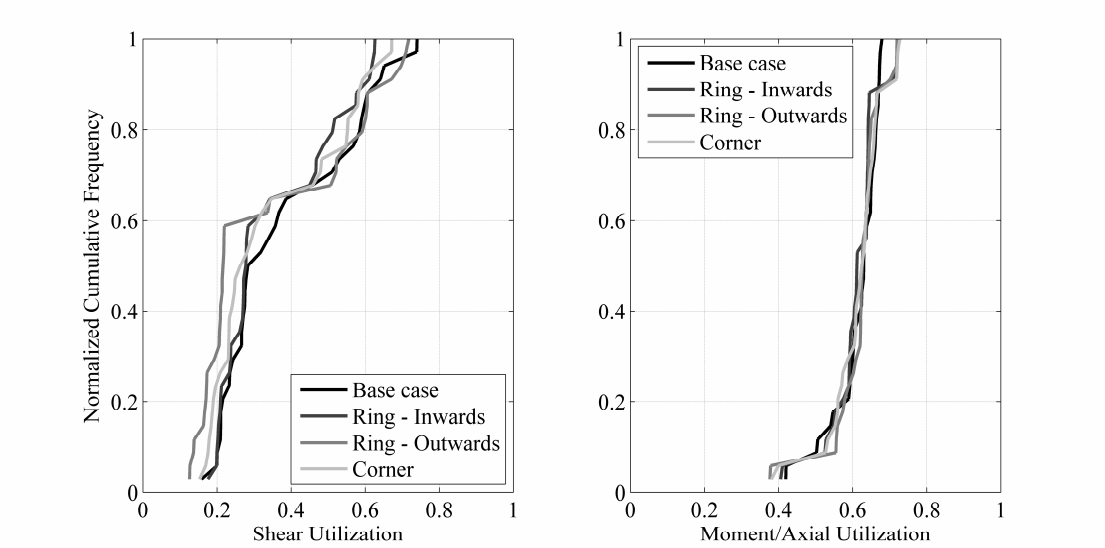


Figure 7-7. Rate of utilization for fires of different shape and path.

Table 7-3. Key statistics from fires of different shape and path

| | Moment/Axial | | | | | | Shear | | | | | |
|---|---|---|---|---|---|---|---|---|---|---|---|---|
| | 1$^{st}$ | 2$^{nd}$ | Up | $\bar{x}$ | 75$^{th}$ | 95$^{th}$ | 1$^{st}$ | 2$^{nd}$ | Up | $\bar{x}$ | 75$^{th}$ | 95$^{th}$ |
| Base case | E6 | A7 | 41% | 0.61 | 0.66 | 0.67 | D2 | B2 | 85% | 0.38 | 0.55 | 0.68 |
| Ring, inwards | B6 | B2 | 53% | 0.61 | 0.64 | 0.72 | B6 | D6 | 88% | 0.35 | 0.48 | 0.62 |
| Ring, outwards | B6 | B2 | 53% | 0.62 | 0.64 | 0.72 | B6 | D2 | 88% | 0.34 | 0.54 | 0.70 |
| Corner | D6 | D2 | 53% | 0.61 | 0.66 | 0.72 | B2 | D2 | 85% | 0.35 | 0.52 | 0.64 |

A clear difference between the different fires is the location of the most critical column. The moment/axial utilization data show a clear shift from

the external columns during the base case, to the most heavily axially loaded internal columns during the non-base case fires.

## 7.3. Discussion

The above analysis has studied the impact of travelling fires on the response of a generic concrete frame through the use a relatively simple single measure (rebar temperature) and through the use of the methodology developed in chapter five. Since the structure and the fires (indeed the models) are the same, the results from this analysis are comparable with the results from chapter six. The overall results from this chapter are less clear than from the previous chapter, in which every metric of structural behaviour indicated that the medium duration, 25% burn area fire had the most significant impact on structural performance.

However, the approach of column assessment is much more useful in terms of analysing the most highly utilized parts of the structure. If the data from all of the fires and the mean, maximum and minimum utilizations for each column are plotted (Figure 7-8) it is possible to draw more general conclusions about the impact of each of the fires. Figure 7-8 shows the different rates of utilization in both moment and shear; from this information, it is possible to make informed design decisions about what parts of the structure perform best and worst in a fire.

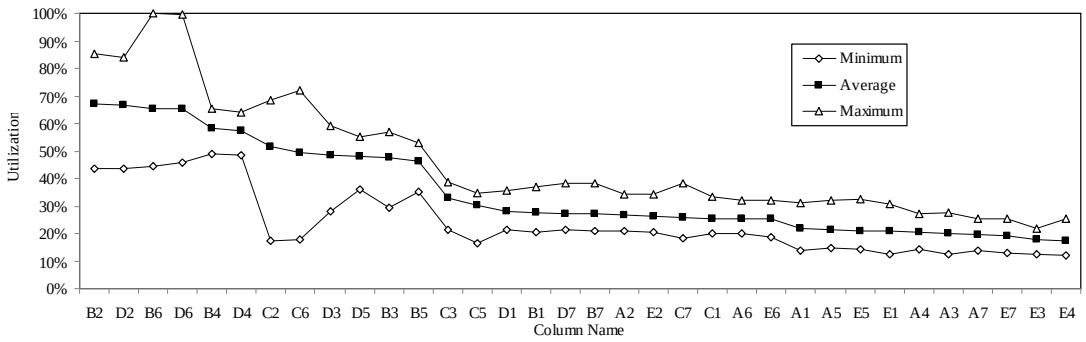


a)

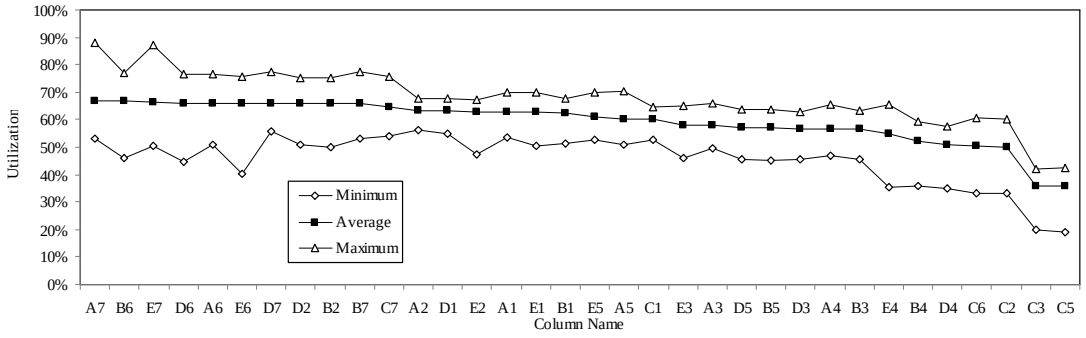


b)

Figure 7-8. Average, maximum and minimum utilization rates for each column; a) shear utilization; axial/moment utilization.

The shear data clearly shows that there are a large number of columns that are consistently utilized at a fairly low degree (<40% of the maximum utilization). From the location visualization, it is clear that these are predominantly the perimeter columns. It can also be seen that irrespective of the non-uniform nature of the fire that columns B2, B6, D2, and D6 are consistently the most heavily utilized. Based on this information, it would be possible to change the design to strengthen these columns. For example, it would be possible to increase the amount of shear reinforcement, and then reanalyse the structure.

It is also useful to identify the maximum utilizations as well as the average utilizations. This would allow designers to be aware of any extreme reactions to a particular fire that are not represented in the average figures.

Unlike the shear utilization trends which clearly show a difference in utilization between the internal and the perimeter columns, the moment/axial utilization rates are more constant over all of the columns (between 55% and 70% utilization). This implies that the safety factor between all of the columns is fairly uniform for this measure. The most notable exceptions to this are the columns C3 and C5 that show significantly less utilization than the others. In light of this information, the designer could reduce the sizes of these concrete sections as they are overdesigned from a fire perspective.

Another trend that can be seen in the axial/moment behaviour that is not evident in the shear utilization is that the column numbers 6 and 7 in each row tend to be more highly utilized then columns 1 and 2. This is an effect of the direction of travel of most of the fires to which the structure was subjected.

The method of combining utilization information from all of the different fires is analogous to the approach taken when designing structures against imposed load at ambient temperatures. The shears and moments that are induced by different combinations of imposed loads (for example, on alternate spans) are calculated, and the structure is designed to resist the entire envelope of fire. In the case of the structure above, a number of realistic

design fires were applied and the response of the frame to each one was analysed individually. This is a more thorough approach than just applying one Standard Fire curve to the structure which is, perhaps, equivalent to applying full imposed and dead load and simply designing the structure accordingly.

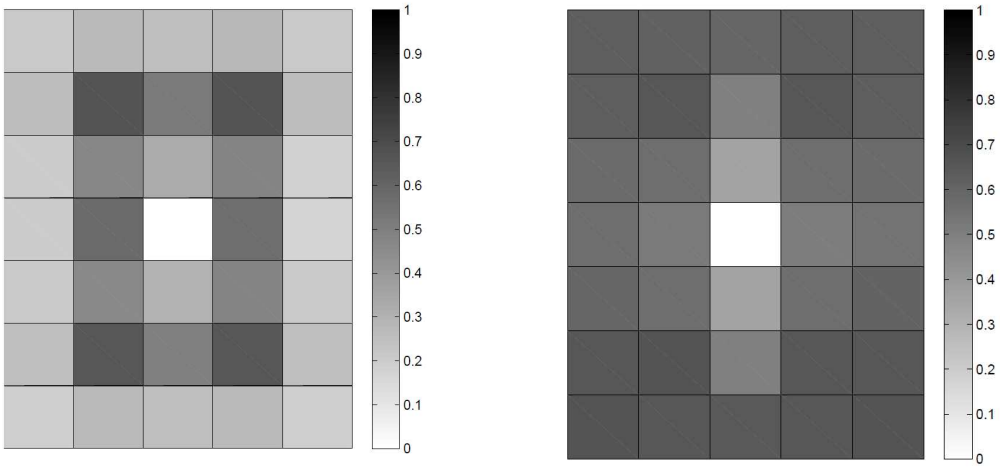


a) b)

Figure 7-9. Mean utilization rates plotted for each column; a) shear utilization; b) bending/axial utilization.

## 7.4. Conclusions

This chapter has combined the structural assessment methodology presented in chapter five with the travelling fires presented and analysed in chapter six. Both of these techniques are novel, and together they form a potentially powerful tool for the fire design of large structures. There are a number of specific conclusions that can be drawn from this chapter:

- Different measures of structural performance can give different results in terms of structural performance.

- Temperature analysis of the column rebar indicates that the medium duration, medium burn area fires are the most severe.
- Detailed utilization analysis of every column shows that the lower burn area fires (5% and 10% burn areas) are more severe for the structure.
- Changes in the far-field temperature definition cause the utilization of the columns to change by a maximum of 9%.
- Fires of different path and shape have very little (<1%) overall impact on the global structural utilization.
- Data from a number of fires can be averaged to draw general conclusions about the overall performance of each column. Vulnerable as well as over-designed columns can be identified.

# 8

# Conclusions and Further Work

This thesis has discussed a number of different aspects of the assessment and behaviour of concrete structures during fire. The broader context of structural fire engineering has been presented and the role of this research has been placed within the discipline. The work has touched on a number of the key points that concern structural fire engineering today: the intricacies of constitutive numerical modelling, load induced thermal strain (LITS), and how they can be implemented have been discussed; a new technique for single element assessment has been developed and applied; a new methodology for assessing the performance of structural models in fires has been presented; and the effect of different design fires on a structure has been analysed using a combination of techniques. This final chapter will review the specific conclusions from each of the areas studied, and discuss more general conclusions from the work as a whole.

## 8.1. Constitutive Models

Constitutive models are the root from which the behaviour of finite-element models are governed. Subtle changes to the constitutive modelling can induce significant differences in the results of a finite-element model. Several conclusions can be drawn from the work on constitutive modelling of concrete:

- The constitutive models reviewed are broadly similar in their trends and implementation.
- The Eurocode 2 model implicitly includes LITS behaviour; by not defining the elastic modulus of concrete, it is left to the user to make an appropriate assumption.
- Users of EC2 can represent plastic LITS strains more correctly by using an elastic modulus which is distinct from the initial tangent of the constitutive curve.
- More realistic representation of plastic strains causes more significant strain reversal to occur on cooling.
- It is possible to manipulate the LITS contributions to the non-loading directions by redistributing the plastic strains when calculating the different plastic stresses and strains in the material model.

## 8.2. Element Assessment

A new technique for creating biaxial interaction diagrams for concrete sections was created. The method is appropriate for ambient and heated sections and is significantly more efficient than a conventional "brute force" approach. Several conclusions can be drawn from this research:

- It is possible to efficiently create biaxial interaction diagrams by exploiting the properties of the sectional tangent stiffness matrix.
- A simple algorithm can be used to find the stationary points of the tangent stiffness matrix.
- Biaxial bending moment diagrams can be represented easily in two-dimensions by using concentric rings to represent values of out-of-plane moment.
- The method is general and can be used for a section of any dimensions and rebar of any arrangement. It is also not limited to conventional heating patterns.
- The 500 °C isotherm method is inherently unconservative due to the assumption of an ambient concrete core.

## 8.3. Methodology of Structural Assessment

A new methodology was created for analysing structures subject to fire. This approach brought together a number of different analysis techniques and thereby allowed a broader understanding of how a fire might affect a structure to be developed. There are several conclusions that can be drawn from this research:

- It is possible to monitor the applied column loading even where elemental output of section forces/moments is not possible.
- Sectional analysis can be used to analyse the impact of fire upon the capacity of every column in a building.
- Utilization factors (loading ratios) can be given to every part of every column to quantify how heavily the structure is used.

- Comparison can be made between different analyses to quantify and compare the impact of different fires.
- Heating of the column in the fire compartment causes a load shedding mechanism which causes most of the critical behaviour to occur in the unheated, upper, column.
- More realistic heating of the column in the fire compartment causes more of the critical behaviour to occur in the heated section.

## 8.4. Travelling Fires

The impacts of a series of travelling fires on a concrete structure were studied. The travelling fire methodology was presented, and applied to a structural model. The response of the structure was monitored using a number of different metrics. There were several conclusions that were drawn from this study.

- Non-uniform, travelling, fires can have a more significant impact on a structure than conventional codified fires.
- The medium duration, medium burn area fires were clearly found to have the most severe impact on the slab's performance. The 25% burn area fire was found to be the most severe for the slab.
- It was appropriate to make simplifying assumptions regarding the degradation of far-field temperature.
- The path of the fire had some impact (~10%) on the response of the fire and cannot therefore be considered negligible.
- Conventional assessment methods found that the medium duration fires had the most severe impact on the columns.

- The advanced utilization techniques showed that the columns were most heavily utilized during the longer fires.

## 8.5. General Discussion and Conclusions

The direct conclusions of this research project are presented above and throughout this thesis. However, there are also a number of more general conclusions that can be drawn from the process and outcomes of the research conducted for this thesis.

Throughout the course of this work, care has been taken to identify gaps in existing knowledge and inconsistencies in the way that physical understanding is applied to current problems. The work on load induced thermal strain has shown that there is a mismatch between the way LITS is understood by those who study it closely, and those who wish to represent its effects in finite-element models. The findings of this research allow this gap to be bridged in a way that both represents the key phenomena, and allows simple implementation.

Likewise, the work on sectional analysis applied a detailed physical understanding to identify the key assumptions that render current design techniques unconservative. The new approach to creating interaction diagrams also provides a leap in complexity and rigor that lets this technique be used more flexibly for design.

The finite-element analyses of the generic concrete structure have been used to address a number of inconsistencies that exist in design process. There are two main mismatches in the complexity that have been identified and addressed: the design fires; and the assessment techniques. In each of these areas, the complexity of the finite-element tools used to model the structure were significantly in excess of the design techniques used to apply the fire and measure the structural response.

Within each finite-element analysis, there are also a number of factors to consider. Numerically, concrete is a difficult material to work with. There are many different parameters that can be defined and chosen by modellers: rate of strength and stiffness degradation; shape of constitutive curve; ultimate tensile strength; and yield surface to name just a few. In changing each of these parameters, the modeller will alter the results of the analysis and each one can be critical in determining the accuracy and appropriateness of any simulation. Equally, in some circumstances precise and careful definition of some parameters may be almost irrelevant to the overall outcome of the model. This analogy can be extended to all aspects of finite-element modelling; geometry, connections, element type, etc. This is demonstrated quite comprehensively in appendix II where a series of sensitivity studies are conducted to analyse the impact of mesh sensitivity and tensions property assumptions. Though there were variations in the overall behaviour due to changes in these parameters, it was demonstrated in chapter 6, that the largest variations were caused by the way the fire was defined.

This illustrates that a finite-element modeller must understand what they are attempting to model and the relative importance of different factors in order to create an appropriate model. It is difficult to see the benefit of developing very complex and precise definition of some material properties when their overall impact on global behaviour is negligible in comparison to the impact of small changes in the fire. For example, the different constitutive models create marginally different results but the apparently subtle changes in the elastic modulus caused huge differences in the overall output.

An area of concrete behaviour that was not considered or quantified in this thesis was the effect of spalling. There were two main reasons for this: firstly, it was not within the scope of this work to develop a model for predicting spalling; secondly, it was felt that the inclusion of spalling would over-complicate each of the techniques that were being presented without providing insight into the cause. Were it necessary to include spalling, the sectional analysis techniques could be adapted to include loss of concrete cover by simply removing material. Each of the finite-element analyses could also be modified to account for lost material [82]. Despite the omission of spalling, it is worth noting that in the finite-element analyses in chapters five, six and seven, the concrete did not recover any of its strength as it cooled.

This research has described and applied a number of different measures of structural performance to quantify the behaviour of the structure during a fire. These have ranged in complexity from single structural measures, to a basic measure of shear capacity, to a well defined approach for assessing axial/bending capacity. The work in this thesis has shown that different

assessment techniques can produce different results. The section utilization assessment methodology that has been developed is a robust and much more detailed way of assessing a structures performance than any of the single measures that were used. Though the assessment technique was complex to develop during the course of this project, the underlying principle is very simple.

In ambient design, a series of partial safety factors are applied so that a generally agreed level of safety is obtained throughout the structure. When specifying member dimensions or rebar arrangement, the aim of the engineer is to design the most efficient section possible. The resistance of the member must be greater than the applied loading, but this is the only control. If the designer can specify a section with a factor of safety of 1.01, this is preferable to a factor of safety of, say, 1.2. Therefore, within certain constraints (section availability, regular numbers for rebar spacing) sections will have a relatively uniform degree of safety relative to the predicted loading throughout the structure. The safety in the structure is derived from the pre-defined partial safety factors rather than from the designer – whose aim is to build as close to the limit as possible.

In fire design, there is very little consideration of the factors of safety in elements. Methods such as the isotherm technique allow designers to check the resistance of sections, but the question for most fire design is typically whether or not a member fails and how long it takes to do so. The single measure approaches described previously are often used for this purpose. The

methodology developed in this thesis allows the factor of safety (or utilization factor) for any section in the structure to be calculated with respect to its fire induced loading. Engineers can then make decisions based on the calculated factors or safety to increase the robustness of some members, and decrease the protection or size of other members. It allows a much better understanding of the degree of safety in a structure during a fire.

As stated above, the development and implementation of the approach in this work was a complex process. However, it should be noted that once the framework for assessment had been created and implemented, the process of assessing the structure and creating reports such as those in chapter five and seven was entirely automatable. Once a finite-element model has been created, much of the work of analysing the structural performance can be completed automatically. Since much of the time that is spent on finite-element modelling is in the creation of the model and analysis of the results, it is not prohibitively time consuming to run a small number of possible fire scenarios, if the analysis process is automatic.

The latter chapters of this thesis present, implement, and analyse the effects of a travelling fires on the response of a structure. A number of specific conclusions have been made above. However, there are other points that can be discussed that relate to two main issues: the appropriateness of using travelling fires; and how travelling fires relate to the rest of this work.

Chapter six details the limitations of current temperature-time curves; however, there are a number of more general points in favour of such an approach that can be made. The use of a family of travelling fires in the design of a building allows an approach that is analogous to techniques currently used for ambient design to resist loading. Travelling fires allow an envelope of likely behaviour to be developed in the same way that different arrangements of live load are used to find the required section sizes in ambient design. An argument against the use of travelling fires (or even parametric fires) is that they do not encompass all of the possible fires to which a building is may be subjected. There are several counter arguments to this position which are worth outlining:

- Experience from real fires and results from fire dynamics have shown fires can grow much more rapidly and be much hotter than a Standard Fire.
- A Standard Fire does not include a cooling phases which are often the most critical time for some structures.
- *If* the Standard Fire curve represented the most extreme set of fires to which a structure was subjected then the equivalent in ambient design would be designing a structure to resist all the different loading combinations at the same time and would result in an unacceptably conservative structure. Further to this point, it would also be equivalent to designing a planned residential space to resist the loading that would be imposed by a plant room; this degree of future proofing would also be unacceptably inefficient for the initial structural design.

- *If* the aim of design is to create the most efficient structure, then the use of a family of fires allows optimization in the same way as structures are optimized for different loadings at ambient design.

Though useful in its own right, the travelling fire methodology dovetails with the structural assessment approaches presented in chapter five. Together, they provide a powerful technique to allow the quantification of the degree of safety present in a building that is subject to fire. All of the principles that were discussed above in relation to the assessment methodology are applicable to the travelling fires. A "family" of different fires is the logical progression once it is possible to quantitatively assess the response of the whole structure.

This work has explored and presented a number of new techniques and methodologies for modelling, designing and assessing the response of concrete structures to fires. There are a number of specific and technical outcomes as well as more general approaches for understanding the response of structures to fire and addressing mismatches in complexity. It has provided a number of outcomes that are potentially useful both in academia and industry.

## 8.6. Suggestions for Further Work

Of course, there is a huge amount more work that can be conducted on the response of concrete structures to fire. There are two types of further work that can be suggested: further research; and implementation of the findings of the thesis.

Further areas of research include the development of the sectional analysis techniques to include more complex sections such as concrete filled steel tubes; this would require some quantification of the degree of de-bonding between the steel and the concrete, but the analysis techniques could be based around the tangent-stiffness techniques introduced above.

The consideration of shear effects in this work has been basic. It is clear that shear plays an important role in the behaviour and, indeed, failure of concrete structures in fire. An experimental project linked to detailed structural modelling would provide useful insights into the shear behaviour of concrete at high temperatures.

There are a number of outcomes from this project that could be implemented with positive effect:

- The findings in relation to load induced thermal strains show that it is relatively easy to include plastic LITS effects in finite-element models. The developers of such codes could, with only slight modifications, implement a more realistic LITS model in their software. This would allow LITS effects to be explicitly considered within finite-element models without the need for researchers or designers to write their own material models. It should be noted that since the work herein first developed, these techniques have been implemented in the finite-element code "SAFIR" [72].

- The sectional analysis technique developed could be written into a simple program to allow engineers to assess the capacity of their sections more conservatively and accurately.
- The assessment methodologies though complex to create are very easy to apply and use. These could be implemented as an additional package or as an add-on to existing codes to allow designers to generate reports on how structures have performed during an analysis.
- The travelling fire methodology could easily be applied to the design of large structures. This would provide a more rational, and arguably safer, approach to designing large open spaces.

# References


[1] Abaqus: *Abaqus Analysis User's Manual*. Providence, Dassault Systemes Simulia Corp, 2008

[2] Abecassis-Empis C, Reszka P, Steinhaus T, et al.: *Characterisation of Dalmarnock Fire Test One*. Experimental Thermal and Fluid Science 2008, 32:1334-43

[3] Alpert RL: *Calculation of Response Time of Ceiling-Mounted Fire Detectors*. Fire Technology 1972, 8:181-95

[4] Anderberg Y, Thelandersson S: *Stress and Deformation Characteristics of Concrete, 2 - Experimental Investigation and Material Behaviour Model*. Sweden, University of Lund, 1976

[5] *Ansys*, http://www.ansys.com/, 2010

[6] *Astm E 119 - 00a Standard Test Methods for Fire Tests of Buildings Construction and Materials*, 2000

[7] Babrauskas V, Williamson RB: *The Historical Basis of Fire Resistance Testing — Part I*. Fire Technology 1978, 14:184-94

[8] Babrauskas V, Williamson RB: *The Historical Basis of Fire Resistance Testing — Part II*. Fire Technology 1978, 14:304-16

[9] Bailey C: *Holistic Behaviour of Concrete Buildings in Fire*. Structures and Buildings 2002, 152:199-212

[10] Bailey C, Moore D: *The Structural Behaviour of Steel Frames with Composite Floorslabs Subject to Fire: Part 1: Theory*. The Structural Engineer 2000, 78:19-27

[11] Bailey C, Moore D: *The Structural Behaviour of Steel Frames with Composite Floorslabs Subject to Fire: Part 2: Design*. The Structural Engineer 2000, 78:28-33

[12] Bailey CG: *Full-Scale Fires Tests on Hollowcore Floors*. The Structural Engineer, 2008, pp 33-9

[13] Bailey CG, Burgess IW, Plank RJ: *Computer Simulation of a Full-Scale Structural Fire Test*. The Structural Engineer 1995, 74:93-100

[14] Bailey CG, Ellobody E: *Fire Tests on Unbonded Post-Tensioned One-Way Concrete Slabs*. Magazine of Concrete Research 2009, 61:67-76

[15] Bailey CG, Ellobody E: *Whole-Building Behaviour of Bonded Post-Tensioned Concrete Floor Plates Exposed to Fire*. Engineering Structures 2009, 31:1800-10

[16] Bailey CG, Lennon T: *Full-Scale Fire Tests on Hollowcore Floors*. The Structural Engineer 2008, 86:33-9

[17] Bailey CG, Moore DB, Lennon T: *The Structural Behaviour of Steel Columns During a Compartment Fire in a Multi-Storey Braced Steel-Frame*. Journal of Constructional Steel Research 1999, 52:137-57

[18] Bailey CG, White DS, Moore DB: *The Tensile Membrane Action of Unrestrained Composite Slabs Simulated under Fire Conditions*. Engineering Structures 2000, 22:1583-95

[19] Bamonte P: *On the Role of Second-Order Effects in Hsc Columns Exposed to Fire*. Presented at the Fifth International Conference of Structures in Fire, Singapore, 2008

[20] Bamonte P, Felicetti R: *Fire Scenario and Structural Behaviour of Underground Parking Lots Exposed to Fire*. Presented at the Application of Structural Fire Engineering, Prague, 2009

[21] Bazant ZP, Cedolin L: *Stability of Structures: Elastic, Inelastic, Fracture, and Damage Theories*. New York, Oxford University Press, 1991
[22] Bazant ZP, Kaplan MF: *Concrete at High Temperatures: Material Properties and Mathematical Models*. Harlow, Longman Group Limited, 1996
[23] Bazant ZP, Prat PC: *Effect of Temperature and Humidity on Fracture Energy of Concrete*. ACI Materials Journal 1988, 85:232-71
[24] *The Behaviour of Multi-Storey Steel Framed Buildings in Fire*. Rotherham, British Steel plc, 1999
[25] Bonet JL, Miguel PF, Fernandez MA, et al.: *Analytical Approach to Failure Surfaces in Reinforced Concrete Sections Subjected to Axial Loads and Biaxial Bending*. Journal of Structural Engineering 2004, 130:2006-15
[26] Bratina S, Saje M, Planinc I: *The Effects of Different Strain Contributions on the Response of Rc Beams in Fire*. Engineering Strucutres 2007, 29:418-30
[27] BS476-20:1987: *Fire Tests on Buildings Materials and Structures - Part 20: Method for Determination of the Fire Resistance of Elements of Construction*, BSI, 1987
[28] Buchanan A: *The Challenges of Predicting Structural Performance in Fires*. Presented at the Ninth International Symposium for Fire Safey Science, Karlsruhe, 2008
[29] Buchanan AH: *Structural Design for Fire Safety*. Chichester, WILEY, 2006
[30] Burgess IW, El-Rimawi JA, Plank RJ: *Analysis of Beams with Non-Uniform Temperature Profile Due to Fire Exposure*. Journal of Construction Steel Research 1990, 16:169-92
[31] Calladine CR: *Plasticity for Engineers: Theory and Applications*. Chichester, Horwood Publishing, 2000
[32] CEB-FIB: *Fire Design of Concrete Structures: Structural Behaviour and Assessment*. Lausanne, FiB, 2008
[33] CEB-FIP: *Model Code 1990*, Thomas Telford, 1993
[34] Chana P: *The European Concrete Building Project*. The Structural Engineer 2000, 78:12-3
[35] Chrimes M, Sutherland J, Humm D (editors): *Historic Concrete: The Background to Appraisal*. London, Thomas Telford, 2001
[36] CIB-W14: *Design Guide Structural Fire Safety*. Fire Safety Journal 1986, 10:75-147
[37] Cobb F: *Structural Engineering Pocket Book*. Amsterdam, Elsevier, 2004
[38] Cook RD, Malkus DS, Plesha ME, et al.: *Concepts and Applications of Finite Element Analysis*. Chichester, Wiley, 2002
[39] Cooke GME: *Thermal Bowing in Fire and How It Affects Building Design*. Borehamwood, Fire Research Station, 1988
[40] Crisfield MA: *Non-Linear Finite Element Analysis of Solids and Structures*. Chichester, Wiley, 1991
[41] Crisfield MA: *Non-Linear Finite Element Analysis of Solids and Structures: Advanced Topics*. Chichester, Wiley, 1997
[42] Custer RLP, Meacham BJ: *Introduction to Performance-Based Fire Safety*. Quincy, National Fire Protection Association, 1997
[43] *Design and Detailing of Concrete Structures for Fire Resistance; Interim Guidance by a Joint Committee of the Institution of*

*Structural Engineers and the Concrete Socitey*. London, Institution of Structural Engineers, 1978

[44] Drysdale D: *An Introduction to Fire Dynamics*. Chichester, Wiley, 1998

[45] Drysdale DD: *Special Issue on Response of Composite Steel Framed Structures to Fire*. Fire Safety Journal 2001, 36:719-20

[46] Dwaikat M, Kodur V: *A Simplified Approach for Evaluating Plastic Axial and Moment Capacity Curves for Beam-Columns with Non-Uniform Thermal Gradients*. Engineering Structures 2010, 32:1423-36

[47] Dwaikat MB, Kodur VKR: *A Numerical Approach for Modeling the Fire Induced Restraint Effects in Reinforced Concrete Beams*. Fire Safety Journal 2008, 43:291-307

[48] El-Fitiany SF, Youssef MA: *Assessing the Flexural and Axial Behaviour of Reinforced Concrete Members at Elevated Temperatures Using Sectional Analysis*. Fire Safety Journal 2009, 44:691-703

[49] Elghazouli AY, Izzuddin BA: *Analytical Assessment of the Structural Performance of Composite Floors Subject to Compartment Fires*. Fire Safety Journal 2001, 36:769-93

[50] Ellobody E, Bailey CG: *Testing and Modelling of Bonded and Unbonded Post-Tensioned Concrete Slabs in Fire*. Fith International Conference on Structures in Fire. Singapore, 2008

[51] EN1990: *Eurocode 0: Basis of Structural Design*, 2004

[52] EN1991-1-1: *Eurocode 1: Actions on Structures - Part 1-1: General Actions - Densities, Self-Weight and Imposed Loads*, 2009

[53] EN1991-1-2: *Eurocode 1: Actions of Structures - Part 1-2: General Actions - Actions on Structures Exposed to Fire*, 1999

[54] EN1992-1-1: *Eurocode 2: Design of Concrete Structures - Part 1-1: General Rules and Rules for Buildings*, 1999

[55] EN1992-1-2: *Eurocode 2: Design of Concrete Structures - Part 1-2: General Rules - Structural Fire Design*, 2004

[56] EN1993-1-1: *Eurocode 3: Design of Steel Structures - Part 1-1: General Rules and Rules for Buildings*, 2010

[57] EN1993-1-2: *Eurocode 3: Design of Steel Structures - Part 1-2: General Rules - Structural Fire Design*, 2005

[58] EN1994-1-1: *Eurocode 4: Design of Composite Steel and Structures - Part 1-1:General - Structural Fire Design*, 2008

[59] *European Recommendations for the Fires Safety of Steel Structures*, ECCS - Technical Committee 3, 1983

[60] Fafitis A: *Interaction Surfaces of Reinforced-Concrete Sections in Biaxial Bending*. Journal of Structural Engineering 2001, 127:840-6

[61] *Fire Grading of Buildings, Part I*, H M Stationary Office, 1946

[62] Fletcher I, Welch S, Capote JA, et al.: *Model-Based Analysis of a Concrete Building Subjected to Fire*. Presented at the Advanced Research Workshop on Fire Computer Modelling, Santander, Spain, October 2007

[63] Fletcher IA, Welch S, Torero JL, et al.: *Behaviour of Concrete Structures in Fire*. Thermal Science 2007, 11:37-52

[64] Foster S, Chladná M, Hsieh C, et al.: *Thermal and Structural Behaviour of a Full-Scale Composite Building Subject to a Severe Compartment Fire*. Fire Safety Journal 2007, 42:183-99

[65] Franssen JM: *Safir. A Thermal/Strucutral Program Modelling Structures under Fire*. AISC Engineering Journal 2005, 42:143-58

[66] Franssen JM, Dotreppe JC: *Fire Resistance of Columns in Steel Frames*. Fire Safety Journal 1992, 19:159-75

[67] *Future Fire Policy, a Consultative Document*. London, H M Stationary Office, 1980
[68] Gann RG: *Reconstruction of the Fires in the World Trade Center Towers*, NIST NCSTAR 1-5, 2005
[69] Garlock MEM, Quiel SE: *Plastic Axial Load and Moment Interaction Curves for Fire-Exposed Steel Sections with Thermal Gradients*. Journal of Structural Engineering 2008, 134:874-80
[70] Garlock MM, Quiel SE: *The Behavior of Steel Perimeter Columns in a High-Rise Building under Fire*. AISC Engineering Journal 2007, 44:359-72
[71] Gawin D, Pesavento F, Schrefler BA: *Modelling of Deformations of High Strength Concrete at Elevated Temperatures*. Materials and Structures 2004, 37:218-36
[72] Gernay T, Franssen JM: *Consideration of Transient Creep in the Eurocode Constitutive Model for Concrete in the Fire Situation*. Presented at the Sixth International Conference on Structures in Fire, Lansing, USA, 2010
[73] Gillie M: *The Behaviour of Steel-Framed Composite Structures in Fire*. Edinburgh, Edinburgh, 2000
[74] Gillie M, Usmani A, Rotter M: *Bending and Membrane Action in Concrete Slabs*. Fire and Materials 2004, 28:139-57
[75] Gillie M, Usmani A, Rotter M, et al.: *Modelling of Heated Composite Floor Slabs with Reference to the Cardington Experiments*. Fire Safety Journal 2001:745-67
[76] Goncalves MC, Rodrigues JPC: *Ultimate Bending Moment Capacity of Reinforced Concrete Beam Sections at High Temperatures*. Presented at the International Workshop of Fire Design of Concrete Structures, Coimbra, Portugal, 2007
[77] Haksever A, Anderberg Y: *Comparison between Measured and Computed Structural Response of Some Reinforced Concrete Columns in Fire*. Fire Safety Journal 1981, 4:293-7
[78] Handoo SK, Agarwal S, Agarwal SK: *Physicochemical, Mineralogical, and Morphological Characteristics of Concrete Exposed to Elevated Temperatures*. Cement and Concrete Research 2002, 32:1009-18
[79] Hertz KD: *Concrete Strength for Fire Safety Design*. Magazine of Concrete Research 2005, 57:445-53
[80] Hill R: *The Mathematical Theory of Plasticity*. Oxford, Oxford University Press, 1950
[81] Hu Y, Burgess I, Davison B, et al.: *Modelling of Flexible End Plate Connections in Fire Using Cohesive Elements*. Presented at the Fith international conference of Structures in Fire, Singapore, 2008
[82] Huang Z: *The Behaviour of Reinforced Concrete Slabs in Fire*. Fire Safety Journal, In Press, Corrected Proof
[83] Huang Z, Burgess IW, Plank RJ: *Non-Linear Structural Modelling of a Fire Test Subject to High Restraint*. Fire Safety Journal 2001, 36:795-814
[84] Huang Z, Burgess IW, Plank RJ: *Fire Resistance of Composite Floors Subject to Compartment Fires*. Journal of Construction Steel Research 2004, 60:339-60
[85] Husem M: *The Effects of High Temperature on Compressive and Flexural Strengths of Ordinary and High-Performance Concrete*. Fire Safety Journal 2006, 41:155-63

[86] *ISO 834-1 Fire-Resistance Tests - Elements of Building Construction - Part 1 General Requirements*, International Organization for Standardization, 1999
[87] Janss J, Minne R: *Buckling of Steel Columns in Fire Conditions*. Fire Safety Journal 1981, 4:227-35
[88] Jonsdottir A, Rein G: *Out of Range*. Fire Risk Management, 2009, pp 14-7
[89] Khoury G: *Compressive Strength of Concrete at High Temperatures: A Reassessment*. Magazine of Concrete Research 1992, 44:291-309
[90] Khoury GA: *Effect of Fire on Concrete and Concrete Structures*. Progress in Structural Engineering and Materials 2000, 2:429-47
[91] Khoury GA: *Strain of Heated Concrete During Two Thermal Cycles. Part 1: Strain over Two Cycles, During First Heating and at Subsequent Constant Temperature*. Magazine of Concrete Research 2006, 58:369-85
[92] Khoury GA: *Strain of Heated Concrete During Two Thermal Cycles. Part 3: Isolation of Strain Components and Strain Model Development*. Magazine of Concrete Research 2006, 58:421-32
[93] Khoury GA, Grainger BN, Sullivan PJE: *Strain of Concrete During First Heating to 600c under Load*. Magazine of Concrete Research 1985, 37:195-215
[94] Khoury GA, Grainger BN, Sullivan PJE: *Transient Thermal Strain of Concrete: Literature Review, Conditions within Specimen and Behaviour of Individual Constituents*. Magazine of Concrete Research 1985, 37:131-44
[95] Kirby BR: *Recent Developments and Applications in Structural Fire Engineering Design--a Review*. Fire Safety Journal 1986, 11:141-79
[96] Kirby BR, Wainman DE, Tomlinson LN, et al.: *Natural Fires in Large-Scale Compartments - a British Steel Technical Fire Research Station Collaborative Project*. Rotherham, British Steel Laboritories, 1994
[97] Kodur V, Dwaikat M, Raut N: *Macroscopic Fe Model for Tracing the Fire Response of Reinforced Concrete Structures*. Engineering Structures 2009, 31:2368-79
[98] Kodur VKR, Harmathy TZ: *Properties of Building Materials*. Sfpe Handbook of Fire Protection Engineering. Quincy, MA, 2008
[99] Kodur VKR, Wang TC, Cheng FP: *Predicting the Fire Resistance Behaviour of High Strength Concrete Columns*. Cement and Concrete Composites 2004, 26:141-53
[100] Kreyszig E: *Advance Engineering Mathematics*. New York, Wiley, 1999
[101] Lamont S, Usmani AS, Drysdale DD: *Heat Transfer Analysis of the Composite Slab in the Cardington Frame Fire Tests*. Fire Safety Journal 2001, 36:815-39
[102] Lane B: *The Response of Steel Framed Structures under Fire Conditions*, The University of Edinburgh, 1997
[103] Law A, Gillie M: *Interaction Diagrams for Ambient and Heated Concrete Sections*. Engineering Structures 2010, 32:1641-9
[104] Law A, Stern-Gottfried J, Gillie M, et al.: *The Influence of Travelling Fires on the Response of a Concrete Frame*. Presented at the International Conference of Structures in Fire, Lansing, Michigan, 2010
[105] Law M: *Designing Fire Safety for Steel - Recent Work*. Presented at the ASCE Spring Convention, New York, USA, 1981

[106] Law M: *Development of Calculation Methods for the Design of Structural Fire Protection*. Structural Survey 1985, 3:103-9
[107] Law M: *Translation of Research into Practice: Building Design*. Presented at the International Symposium of Fire Safety Science, Maryland, 1985
[108] Law M: *Some Selected Papers by Margaret Law*. London, ARUP, 2002
[109] Lennon T: *Whole Building Behaviour - Results from a Series of Large Scale Tests*. Presented at the CIB-CTBUH International Conference on Tall Buildings, Malaysia, 2003
[110] Lennon T, Hopkin D, El-Rimawi J, et al.: *Large Scale Natural Fire Tests on Protected Engineered Timber Floor Systems*. Fire Safety Journal, In Press, Corrected Proof
[111] Lennon T, Hopkin D, El-Rimawi J, et al.: *Large Scale Natural Fire Tests on Protected Engineered Timber Floor Systems*. Fire Safety Journal 2010, In Press, Corrected Proof
[112] Lennon T, Rupasinghe R, Canisius G, et al.: *Concrete Structures in Fire: Performance, Design and Analysis*. Watford, BRE press, 2007
[113] Li L-Y, Prukiss J: *Stress-Strain Constitutive Equations of Concrete Material at Elevated Temperatures*. Fire Safety Journal 2005, 40:669-86
[114] Lim L, Buchanan A, Moss P, et al.: *Numerical Modelling of Two-Way Reinforced Concrete Slabs in Fire*. Engineering Structures 2004, 26:1081-91
[115] Lubliner J, Oliver J, Oller S, et al.: *A Plastic-Damage Model for Concrete*. International Journal of Solids and Structures 1989, 25:299-326
[116] *Matlab*. Natick, The MathWorks Inc, 2008
[117] Mosley B, Bungey J, Hulse R: *Reinforced Concrete Design to Eurocode 2*. New York, Palgrave MacMillan, 2007
[118] Moss PJ, Dhakal RP, Wang G, et al.: *The Fire Behaviour of Multi-Bay, Two-Way Reinforced Concrete Slabs*. Engineering Structures 2008, 30:3566-73
[119] Nawy EG: *Reinforced Concrete; a Fundamental Approach*. London, Pearson, 2009
[120] Nechnech W, Meftah F, Reynouard JM: *An Elasto-Plastic Damage Model for Plain Concrete Subjected to High Temperatures*. Engineering Structures 2002, 24:597-611
[121] Newman GM, Robinson JT, Bailey CG: *Fire Safe Design: A New Approach to Multi-Storey Steel Framed Buildings*. Ascot, Berkshire, Steel Construction Institute, 2000
[122] Nielsen CV, Pearce CJ, Bicanic N: *Theoretical Model of High Temperature Effects on Uniaxial Concrete Member under Elastic Restraint*. Magazine of Concrete Research 2002, 54:239-49
[123] NIST: *Structural Fire Response and Probable Collapse Sequence of World Trade Centre Building 7 Volume 1*, National Institute of Standards and Technology, 2008
[124] Ortiz M: *A Constitutive Theory for the Inelastic Behaviour of Concrete*. Mechanics of Materials 1985, 4:49-93
[125] Pankaj: *Finite Element Analysis in Strain Softening and Localisation Problems*. Department of Civil Engineering. Swansea, University College of Swansea, 1990
[126] Pettersson O, Witteveen J: *On the Fire Resistance of Structural Steel Elements Derived from Standard Fire Tests or by Calculation*. Fire Safety Journal 1980, 2:73-87

[127] Purkiss JA: *High Temperature Effects*. Presented at the Design of Sturctures against Fire, Aston, Birmingham, 1986
[128] Purkiss JA: *Developments in the Fire Safety Design of Structural Steelwork*. Journal of Constructional Steel Research 1988, 11:149-73
[129] Purkiss JA: *Fire Safety Engineering Design of Structures*. Oxford, Butterworth-Heinemann, 2007
[130] Quiel SE, Garlock MEM: *A Closed-Form Analysis of Perimeter Member Behaviour in a Steel Building Frame Subject to Fire*. Engineering Structures 2008, 30:3276-84
[131] Read RHH: *A Short History of the Fire Research Station, Borehamwood*. Garston, BRE, 1994
[132] Rein G, Zhang X, Williams P, et al.: *Multi-Story Fire Analysis for High-Rise Buildings*. Presented at the Proceedings of the 11th International Interflam Conference; http://hdl.handle.net/1842/1980 (accessed on July 2010), London, September 2007
[133] Roben C: *The Effect of Cooling and Non-Uniform Fires on Structural Behaviour*. School of Engineering. Edinburgh, The University of Edinburgh, 2009
[134] Rocca S, Galati N, Nanni A: *Interaction Diagram Methodology for Design of Frp-Confined Reinforced Concrete Columns*. Construction and Building Materials 2009, 23:1508-20
[135] Rodriguez-Gutierrez JA, Aristizabal-Ochoa JD: *Reinforced, Partially, and Fully Prestressed Slender Concrete Columns under Biaxial Bending and Axial Load*. Journal of Structural Engineering 2001, 127:774-83
[136] Rodriguez JA, Aristizabal-Ochoa JD: *Biaxial Interaction Diagrams for Short Rc Columns of Any Cross Section*. Journal of Structural Engineering 1999, 125:672-83
[137] Rose PS, Bailey CG, Burgess IW, et al.: *The Influence of Floor Slabs on the Structural Performance of the Cardington Frame in Fire*. Journal of Constructional Steel Research 1998, 46:310-1
[138] Rots JG, Kusters GMA, Blaauwendraad J: *The Need for Fracture Mechanics Options in Finite Elements Models for Concrete Strucutres*. Presented at the The International Conference on Computer Aided Analysis and Design of Concrete Sturctures, 1984
[139] Rotter M: *Rapid Exact Inelastic Biaxial Bending Analysis*. Journal of Structural Engineering 1985, 111:2659-74
[140] Rubert A, Schaumann P: *Structural Steel and Plane Frame Assemblies under Fire Action*. Fire Safety Journal 1986, 10:173-84
[141] Saab HA, Nethercot DA: *Modelling Steel Frame Behaviour under Fire Conditions*. Engineering Structures 1991, 13:371-82
[142] Sanad AM, Rotter JM, Usmani AS, et al.: *Composite Beams in Large Buildings under Fire -- Numerical Modelling and Structural Behaviour*. Fire Safety Journal 2000, 35:165-88
[143] Schneider U: *Modelling of Concrete Behaviour at High Temperatures*. Presented at the Design of Structures against Fire, Aston, Birmingham, 1986
[144] Schneider U: *Concrete at High Temperatures - a General Review*. Fire Safety Journal 1988, 13:55-68
[145] Shah SP, Swartz SE, Ouyang C: *Fracture Mechanics of Concrete: Application of Fracture Mechanics to Concrete, Rock, and Other Quasi-Brittle Materials*. New York, Wiley, 1995
[146] Stern-Gottfried J, Law A, Rein G, et al.: *A Performance Based Methodology Using Travelling Fires for Structural Analysis*. Presented

at the 8th International Conference on Performance-Based Codes and Fire Safety Design Methods, Lund, June 2010

[147] Stern-Gottfried J, Rein G, Lane B, et al.: *An Innovative Approach to Design Fires for Structural Analysis of Non-Conventional Buildings*. Presented at the Applications of Structural Fire Engineering, Prague, 2009

[148] Stern-Gottfried J, Rein G, Torero JL: *Travel Guide*. Fire Risk Management, 2009, pp 12-6

[149] *Structural Fire Engineering Investigation of Broadgate Phase 8 Fire*. Ascot, Berkshire, The Steel Construction Institute, 1991

[150] Sullivan PJE, Terro MJ, Morris WA: *Critical Review of Fire-Dedicated Thermal and Structural Computer Programs*. Journal of Applied Fire Science 1994, 3:113-5

[151] Taerwe L: *From Member Design to Global Structural Behaviour*. Presented at the International Workshop of Fire Design of Concrete Structures, Coimbra, Portugal, 2007

[152] Tassios TP, Chronopoulos MP: *Structural Response of Rc Elements under Fire*. The Structural Engineer 1991, 69:227-81

[153] Terro MJ: *Numerical Modeling of the Behaviour of Concrete Structures in Fire*. ACI Structural Journal 1998, 95:183-93

[154] Thelandersson S: *Modeling of Combined Thermal and Mechanical Action in Concrete*. Journal of Engineering Mechanics 1987, 113:893-906

[155] Tokoyoda M, Yamashita H, Toyoda K, et al.: *An Experimental Study of Transent Strain for a Concrete with Limestone Aggregate*. Presented at the Fire design of concrete structures, University of Coimbra, Portugal, 8th 9th November 2007 2007

[156] Usmani AS, Rotter JM, Lamont A, et al.: *Fundamental Principles of Structural Behaviour under Thermal Effects*. Fire Safety Journal 2001, 36:721-44

[157] Wang YC, Lennon T, Moore DB: *The Behaviour of Steel Frames Subject to Fire*. Journal of Constructional Steel Research 1995, 35:291-322

[158] Webster R: *Reinforced Concrete Framed Structure: Comparative Design to Ec2 and Bs 8110*. Watford, BRE Bookshop, 2003

[159] Welch S, Jowsey A, Deeny S, et al.: *Bre Large Compartment Fire Tests--Characterising Post-Flashover Fires for Model Validation*. Fire Safety Journal 2007, 42:548-67

[160] Wickstrom U: *Temperature Calculation of Insulated Steel Columns Exposed to Natural Fire*. Fire Safety Journal 1981, 4:219-25

[161] Wickström U: *Temperature Calculation of Insulated Steel Columns Exposed to Natural Fire*. Fire Safety Journal 1981, 4:219-25

[162] Wickstrom U, Palsson J: *A Scheme for Verification of Computer Codes for Calculating Temperature in Fire Exposed Structures*. Boras, SP Swedish National Testing and Research Institute, 1999

[163] Witteveen J, Twilt L: *A Critical View on the Results of Standard Fire Resistance Tests on Steel Columns*. Fire Safety Journal 1981, 4:259-70

[164] Xiao J, Konig G: *Study on Concrete at Hight Temperature in China - an Overview*. Fire Safety Journal 2004, 39:89-103

[165] Yang H, Lin Y, Hsiao C, et al.: *Evaluating Residual Compressive Strength of Concrete at Elevated Temperatures Using Ultrasonic Pulse Velocity*. Fire Safety Journal 2009, 44:121-30

[166] Yen JYR: *Quasi-Newton Method for Reinforced-Concrete Column Analysis and Design*. Journal of Structural Engineering 1991, 117:657-66

[167] Youssef MA, Moftah M: *General Stress-Strain Relationship for Concrete at Elevated Temperatures*. Engineering Structures 2007, 29:2618-34

[168] Zannoni M: *Brand Bij Bouwkunde*, COT Instituut voor Veilingheids – en Crisismanagement, 2008

[169] Zienkiewicz OC: *The Finite Element Method*. London, McGraw-Hill, 1977

# Appendix I

## Numerical Modelling of Materials

# 1. Numerical Modelling of Materials

This section describes how to implement a material model in a finite-element code. The first section describes the general theory; while sections 2 and 3 focus on hardening and the specific parameters required to implement a Drucker-Prager model respectively; section 4 briefly describes and illustrates the modifications necessary for a two surface yield criteria. This appendix compliments the development of the embedded modulus technique described in chapter 3 and represents the combination of the description of finite-element theory from a number of sources which were all drawn upon to create this summary [38,40,41,80,125,169] all of which were used to create this summary.

## *1.1 General Rules*

The starting point for any material model is with the simple relation,

$$\sigma_{new} = \sigma_{old} + D\dot{\varepsilon}$$

Where $D$ is the elastic tangent modulus,

$$D = \frac{E}{(1+\nu)(1-2\nu)}\begin{bmatrix} 1-\nu & \nu & \nu & & & \\ \nu & 1-\nu & \nu & & & \\ \nu & \nu & 1-\nu & & & \\ & & & \frac{1-2\nu}{2} & & \\ & & & & \frac{1-2\nu}{2} & \\ & & & & & \frac{1-2\nu}{2} \end{bmatrix}$$

The yield function $F$ is analysed. If $F$ is found to be greater than 0, a flow rule must be employed to relax the stresses such that $F$=0. This is called the

return to the yield surface. See below for specific yield functions and flow rules.

In order to return to the yield surface, the plastic deformation must be allocated both a direction and a magnitude. In associated flow, the direction is determined by the flow vector *a*, and the magnitude is governed by the "plastic multiplier" $d\lambda$. As such, plastic strain is calculated by,

$$\varepsilon_{pl} = \frac{\partial f}{\partial \sigma} d\lambda$$

Where,

$$d\lambda = \frac{a^T D d\varepsilon}{A + a^T D a}$$

This relationship only holds true while the strains are infinitesimal. Consequently, if an attempt is made to solve this explicitly, the solution will not be exact. F will not equal zero. Where this solution method is used, the phenomena known as "drift" occurs. This is when the calculated solution gradually diverges from the correct solution. Reducing the size of each increment can significantly improve results from this method.

The other approach is to use an implicit method where the solution is found iteratively. Only the fully implicit approach will be examined here. The fully implicit approach – the backward Euler method – allows an initial estimate of *a* and $\Delta\lambda$ to be based on the fully elastic stress. This is known as the trial

stress. A new value of $\Delta\varepsilon$ is calculated and, thus, a new stress can be obtained. This stress is then used to calculate a new value of $F$. If $F$=0 is not satisfied, then the new stress is then adopted as the trial stress, and the process is repeated. This process is shown below:

$$\Delta\lambda = \frac{F_{(n+1)T}}{a^T_{(n+1)T} D a_{(n+1)} + A_n}$$

$$\sigma_{n+1} = \sigma_{(n+1)T} - \Delta\lambda D a_{(n+1)T}$$

$$Y_{n+1} = Y_n + \Delta\lambda h_n$$

$$F\left(\sigma_{n+1}, \kappa\left(Y_{n+1}\right)\right) = 0$$

Where $A_n$, $k_{n+1}$ and $h_n$ are hardening parameters which will be dealt with below. This process is shown diagrammatically in figure 1.

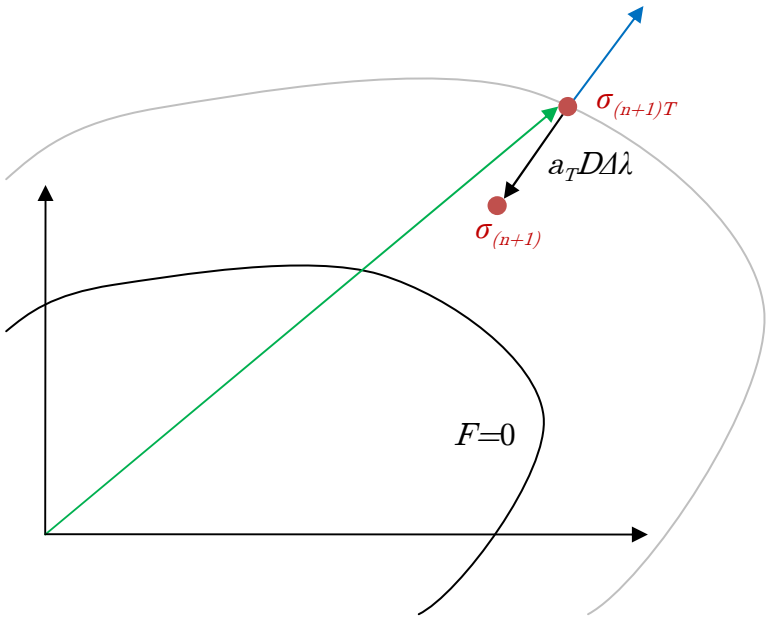


Figure 1. Illustration of the return to the yield surface.

Once the new values of stress and strain are calculated, they can be updated ready for use in the next increment. Abaqus also requires the tangent modulus to be updated. There are several ways of deriving the tangent modulus, but the method described here finds what is commonly termed the consistent tangent modulus. The "consistency" is derived from the fact that it is derived using the results of the backward Euler method described above. Consequently, it recognises that the strains are not infinitesimal. This method of calculating the tangent modulus requires the double differential $\partial a/\partial\sigma$ to be found. The consistent tangent modulus is found using the following equation:

$$D_n^{ep} = D_n^* - \frac{D_n^* a_n a_n^T D_n^*}{A_n + a_n^T D_n^* a_n}$$

Where,

$$D_n^* = \left(I + \Delta\lambda D B_n\right)^{-1} D$$

and I is a 6×6 identity matrix, $\Delta\lambda$ is the sum of the plastic multipliers found using the backward Euler method, $D$ is the elastic tangent modulus, and $B_n$ is:

$$B_n = \left.\frac{\partial b}{\partial\sigma}\right|_n$$

The subscript $n$ denotes that evaluation is conducted at the final stress found by the backward Euler method.

### *1.2 Hardening*

The hardening of a material allows the yield surface to expand or displace, as well as for plastic flow to occur. Isotropic hardening allows the yield surface to expand, while kinematic hardening allows displacement to occur. This section will only consider the isotropic condition. The isotropic expansion of the yield surface is allowed by the modification of the parameter $\sigma_o$. To allow this to be correctly updated, the hardening modulus $H$ must be found. From this, the parameter $A$ can be derived.

$$H = \frac{dY}{d\varepsilon_y^p}$$

where $dY$ denotes change in stress, and $d\varepsilon_y^p$ change in plastic strain.

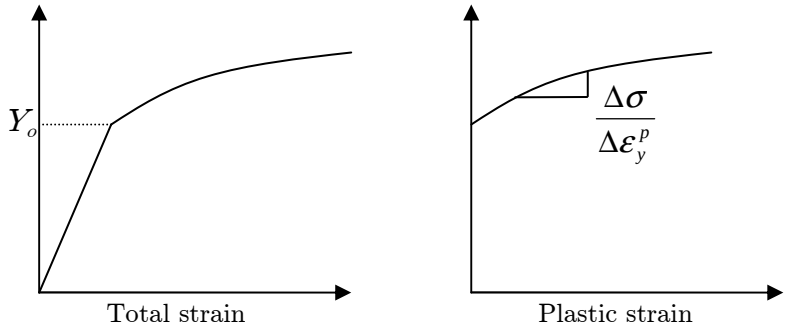


Figure 2. Hardening curves; a) total strain; and b) plastic strain

Two approaches can be used to derive these parameters; the work hardening hypothesis, or the strain hardening hypothesis. These allow the multidimensional plastic strain to be related to a uniaxial hardening diagram as shown in Figure 2. The plastic strain shown here is known as the equivalent plastic strain $d\varepsilon_y^p$. It can be shown for strain hardening that:

$$d\varepsilon_y^p = d\lambda\sqrt{\frac{2}{3}\left(\frac{\partial f}{\partial \sigma}\right)^T\left(\frac{\partial f}{\partial \sigma}\right)}$$

and,

$$A = H\left(\frac{\partial f_2}{\partial Y} - \frac{\partial f}{\partial Y}\right)\sqrt{\frac{2}{3}\left(\frac{\partial f}{\partial \sigma}\right)^T\left(\frac{\partial f}{\partial \sigma}\right)}$$

For work hardening:

$$d\varepsilon_y^p = -d\lambda\frac{\partial F}{\partial Y}$$

and,

$$A = H\left(\frac{\partial F}{\partial Y}\right)^2$$

During the iteration process involved in the backward Euler method, these values are updated incrementally. Note that the lower case $h$ is the incremental form of $H$. However, unlike $a$ and $F$, the hardening parameters are not estimated from the trial stresses but from the previous increment. Consequently, in the first iteration,

$$H_{inital} = \left.\frac{dY}{d\varepsilon_y^p}\right|_o \quad H_{inital} = \left.\frac{dY}{d\varepsilon_y^p}\right|_o$$

$$Y_{inital} = Y_o$$

### *1.3 Drucker-Prager Surface*

The equations shown in *section 1.1.* are in a general form; as such, they can be applied to any yield surface defined by the equation $F(\sigma, Y(\kappa)) = 0$. The

model implemented here is a simple Drucker-Prager model. The derivations for the different parameters $a$ and $\partial a/\partial\sigma$ can be found in literature [41] and are presented, but not derived, here.

### *1.3.1 Yield Surface*

The yield surface in a Drucker-Prager model takes the form of a cone and can be written as:

$$f = \left(\alpha I_1 + \sqrt{J_2}\right) - \kappa_o$$

Where,

$$\alpha = \frac{2\sin\phi}{\sqrt{3}(3 \pm \sin\phi)}$$

$$\kappa_o = \frac{6c\cos\phi}{\sqrt{3}(3 \pm \sin\phi)}$$

$$I_1 = \sigma_1 + \sigma_2 + \sigma_3$$

$$J_2 = \frac{1}{6}\left[(\sigma_1 - \sigma_2)^2 + (\sigma_3 - \sigma_2)^2 + (\sigma_3 - \sigma_1)^2\right] + \sigma_{12}^2 + \sigma_{23}^2 + \sigma_{31}^2$$

The angle $\varphi$ is the angle of friction of the material, and $c$ is the cohesion of the material. This can be related to the uniaxial tensile yield by:

$$f_t = Y = \frac{6c\cos\phi}{3 + \sin\phi}$$

and uniaxial compression by;

$$f_c = Y = \frac{2c\cos\phi}{1 - \sin\phi}$$

giving;

$$f_t = \frac{3+\sin\phi}{3(1-\sin\phi)} f_c$$

Hence, if the hardening curve is defined as compression, then;

$$c = \frac{(1-\sin\phi)}{2\cos\phi} \cdot Y$$

And tension, then;

$$c = \frac{(3+\sin\phi)}{6\cos\phi} \cdot Y$$

### *1.3.2 The Flow Rule*

The flow rule can be found by differentiating the yield function. The general form of this is shown in section 1.1.1, the different parameters change depending on the yield function being used. For Drucker-Prager:

$$\frac{\partial f}{\partial \sigma} = a = \alpha a_1 + C_2 a_2$$

Where,

$$C_2 = \frac{1}{2\sqrt{J_2}}$$

$$a_1 = \begin{bmatrix} 1 \\ 1 \\ 1 \\ 0 \\ 0 \\ 0 \end{bmatrix} \qquad a_2 = \begin{bmatrix} \sigma_x \\ \sigma_y \\ \sigma_z \\ 2\tau_{xy} \\ 2\tau_{yz} \\ 2\tau_{zx} \end{bmatrix}$$

and,

$$\sigma_x = \sigma_1 - \frac{I_1}{3} \qquad \sigma_y = \sigma_2 - \frac{I_1}{3} \qquad \sigma_z = \sigma_3 - \frac{I_1}{3}$$

### *1.3.3 Hardening Parameters*

The hardening parameters which are unique to the Drucker-Prager yield surface can be derived for strain hardening and for work hardening. For strain hardening, they are defined by;

$$d\varepsilon_y^p = d\lambda\left(\frac{8\sin^2\phi}{3(3-\sin\phi)^2} + \frac{1}{3}\right)^{1/2}$$

and the parameter $A$ is related to $H$ by,

$$A = H\frac{3+\sin\phi}{3-\sin\phi}\frac{1}{\sqrt{3}}\left(\frac{3+\sin\phi}{\sqrt{3}(3-\sin\phi)}\right)^{1/2}$$

For work hardening, the equivalent plastic strain is defined by:

$$d\varepsilon_y^p = d\lambda\left(\frac{3+\sin\phi}{\sqrt{3}(3-\sin\phi)}\right)$$

and the parameter $A$ by;

$$A = H\left(\frac{3+\sin\phi}{\sqrt{3}(3-\sin\phi)}\right)^2$$

If hardening is defined as a uniaxial compressive curve then, for work hardening:

$$d\varepsilon_y^p = d\lambda\left(\frac{\sqrt{3}(1-\sin\phi)}{3-\sin\phi}\right)$$

and,

$$A = H\left(\frac{\sqrt{3}(1-\sin\phi)}{3-\sin\phi}\right)^2$$

### *1.3.4 Consistent Tangent Modulus*

The final step in the calculations required is to form the consistent tangent modulus. This requires knowledge of the double differential of the yield function:

$$B = \frac{\partial a}{\partial \sigma} = C_2 \frac{\partial a_2}{\partial \sigma} + C_{22} a_2 a_2^T$$

Where

$$C_{22} = -\frac{1}{4J_2^{3/2}}$$

$$\frac{\partial a_2}{\partial \sigma} = \frac{1}{3}\begin{bmatrix} 2 & -1 & -1 & & & \\ -1 & 2 & -1 & & & \\ -1 & -1 & 2 & & & \\ & & & 6 & & \\ & & & & 6 & \\ & & & & & 6 \end{bmatrix}$$

and $C_2$ and $a_2$ are the same as for the single differential.

### *1.4 Multi-surface yield criteria: Drucker-Prager*

The Drucker-Prager model described above is sufficient for many applications in concrete modelling. It has been used many times in the past with reasonable results. For this study, however, it is felt a slightly more complex model would be appropriate. There are several different ways that the Drucker-Prager model can be made more representative of real concrete. The yield surface can be made dependent on the third stress invariant. This allows the triaxial/biaxial compression to be more accurately modelled. Another modification can be made by modelling the compression/tension yield surfaces with different equations. This allows a more accurate representation of the relative tensile and compressive yield stresses. It also enables the hardening rules to be changed for compression and tension. Since the main aim for this model is to accurately model the compressive behaviour at high temperature, it is felt that separating these rules would be more beneficial to the model than using the third stress invariant to vary the shape of the yield surface. There is also significantly more scientific justification in terms of evidence. A large amount of work has investigated the tensile and compressive behaviour of high temperature concrete, while there is relatively little work about the tri-axial behaviour. Thus, this paper will focus on the development of a two yield surface criteria. It should be noted that this approach is not new, and has been attempted before and has also been implemented in commercial finite-element curves such as Abaqus.

### *1.4.1 Conceptual Illustration*

The model is composed of two intersecting Drucker-Prager yield criteria (figure 3). Return to the yield surface is achieved in exactly the same way as with a single criterion yield surface. The only exception is in the singularity regions. A singularity region is generated from the point of intersection of the

two yield surfaces. Any stress which lies in this region will be retuned to the intersection point of the surfaces.

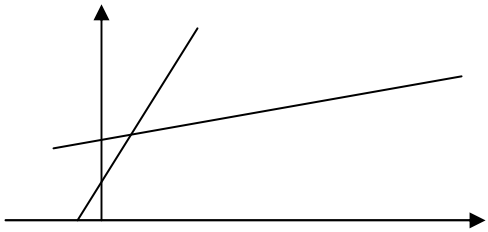

a)

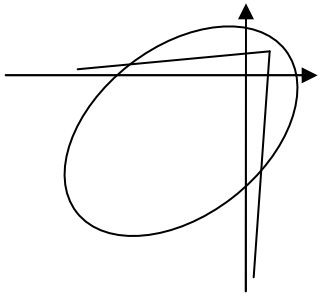

b)

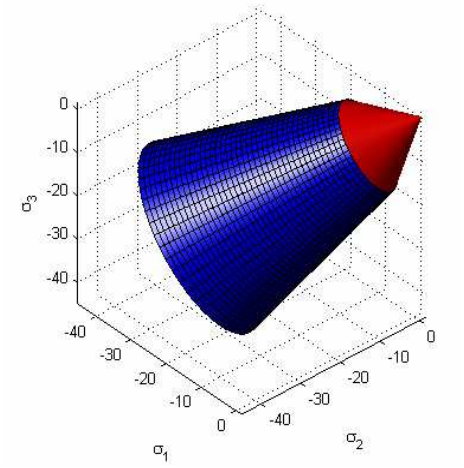


c)

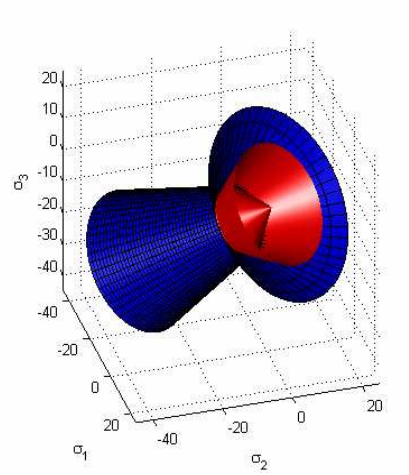


d)

Figure 3. Multi-surface Drucker-Prager yield criterion; a) along the hydrostatic axis; b) in biaxial plane; c) in three dimensions; d) the borders of the singularity region.

# Appendix II

## Concrete Structure

# 1. Design of Generic Concrete Structure

Chapters four to seven present the results from a series of analyses on a generic concrete structure. Unfortunately, there were no pre-existing plans for a sufficiently simple structure available to the author. Thus, the structure was designed from scratch in accordance with Eurocodes 0, 1 and 2 [53-55,57]. This appendix presents the final design specifications which were implemented in the finite-element model. To ensure that the structure was representative of a generic office building, the design was informed by existing designs and plans [9,158].

## *1.1 Layout and global geometry*

- The plan (Figure 1) is intended to be regular so that the causes of different structural effects can be better understood.
- The proposed building is 42x28m and has nine stories.
- There are 24 7x7m bays.
- Inter-story height is 3.8m.
- The bays of the building surround a central core.
- Material properties and loading
- The concrete design strength used in the columns is 48MPa.
- The concrete design strength used in the slab is 40MPa.
- Steel rebar strength is assumed to be 500MPa throughout the structure.
- Imposed loading of 5kN/m$^2$ was assumed for all the office space.
- Imposed loading of 1.5kN/m$^2$ was assumed for the roof.
- Partial safety factors were assumed to be 1.5 and 1.15 for the imposed and permanent loads respectively.

- Reduction factors were applied to imposed loads from multiple stories in accordance with NA 2.6.
- The building was designed for 1 hour of fire resistance.

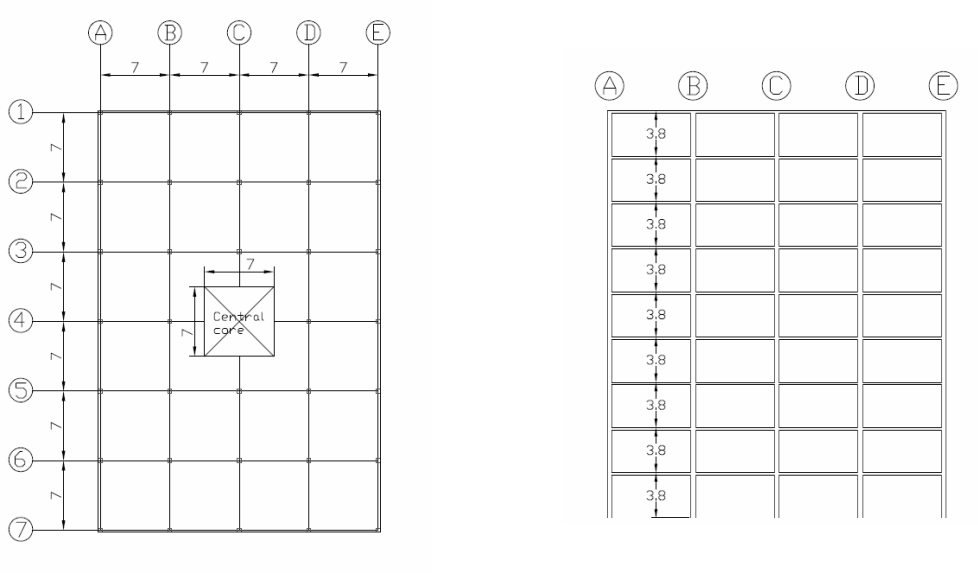


Figure 1. Plan and elevation

## *1.2 Structural design*

- The proposed form of construction is flat slab.
- The slab is 200mm thick throughout.
- A finite-element model of the proposed geometry was created, and the corresponding bending moments, shear forces and axial forces in the slabs and columns calculated. These can be found in appendix A and B. Once sections were sized, this analysis was re-run to check values were still within design allowances.
- Based on the required capacities, each member was designed in accordance with Eurocode 2 [54].

- Edge columns were designed with 300x300mm sections.
- Internal column were designed with 400x400mm sections.
- Full details of the specification of the rebar for the columns are given below. The specifications for slabs are displayed on the same graphs as the bending moment calculations.

### *1.3 Rebar Provision in Slabs and Columns*

The following pages show the various loadings and rebar provisions for the sections of the flat slab and the columns.

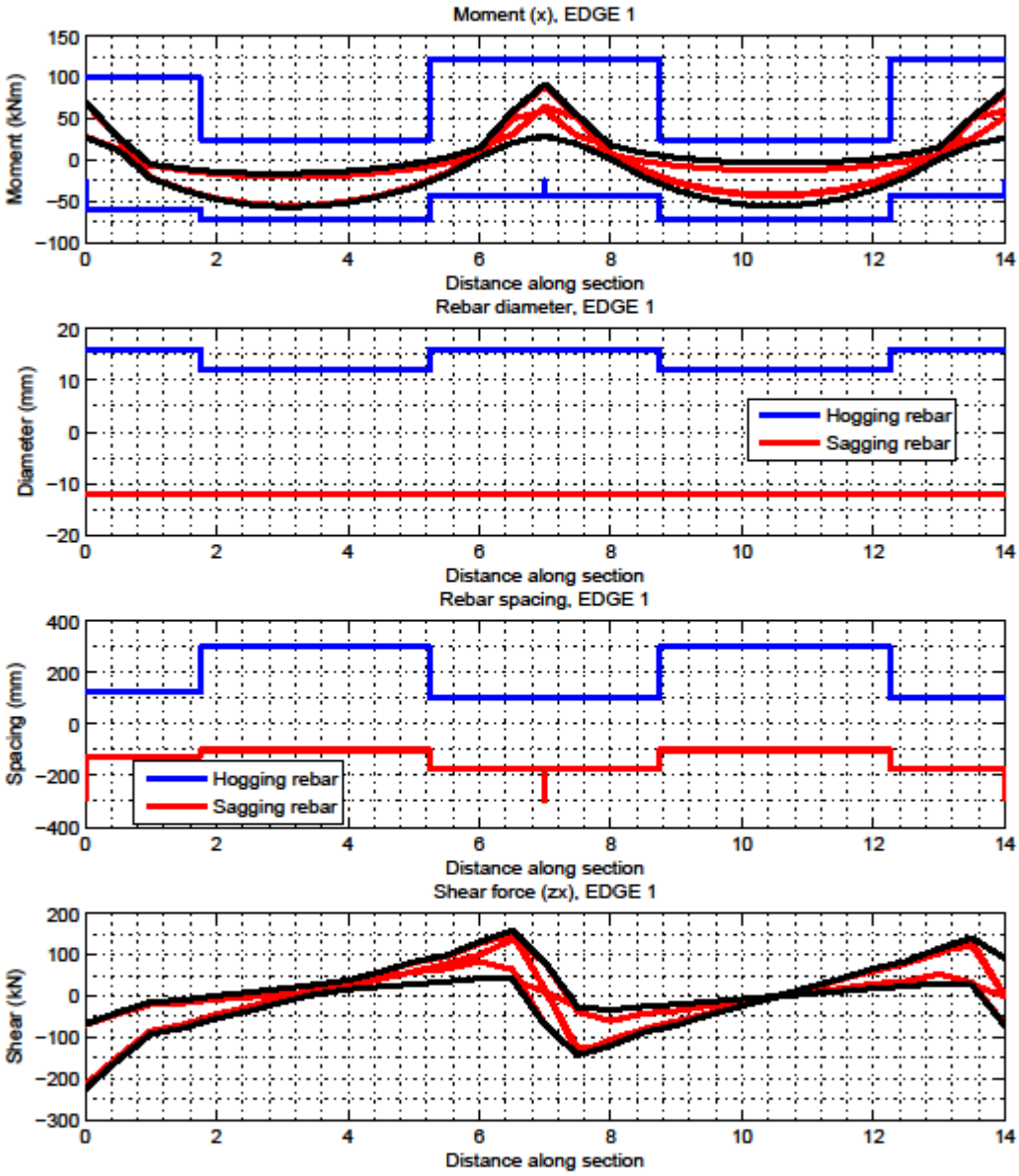
Moment (x), EDGE 1
Moment (kNm)
Distance along section
Rebar diameter, EDGE 1
Diameter (mm)
Hogging rebar
Sagging rebar
Distance along section
Rebar spacing, EDGE 1
Spacing (mm)
Hogging rebar
Sagging rebar
Distance along section
Shear force (zx), EDGE 1
Shear (kN)
Distance along section

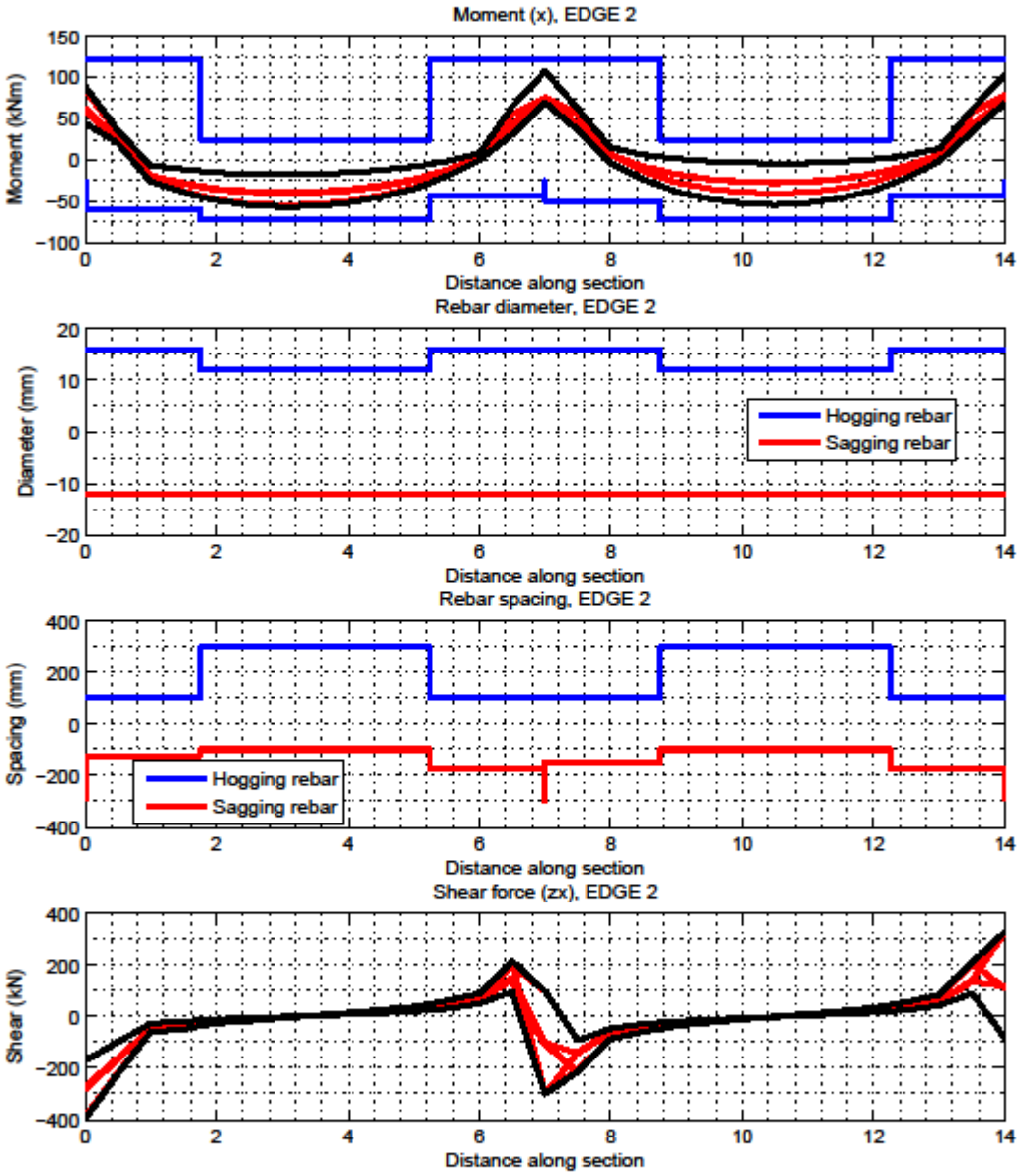
Moment (x), EDGE 2
Moment (kNm)
Distance along section
Rebar diameter, EDGE 2
Diameter (mm)
Hogging rebar
Sagging rebar
Distance along section
Rebar spacing, EDGE 2
Spacing (mm)
Hogging rebar
Sagging rebar
Distance along section
Shear force (zx), EDGE 2
Shear (kN)
Distance along section

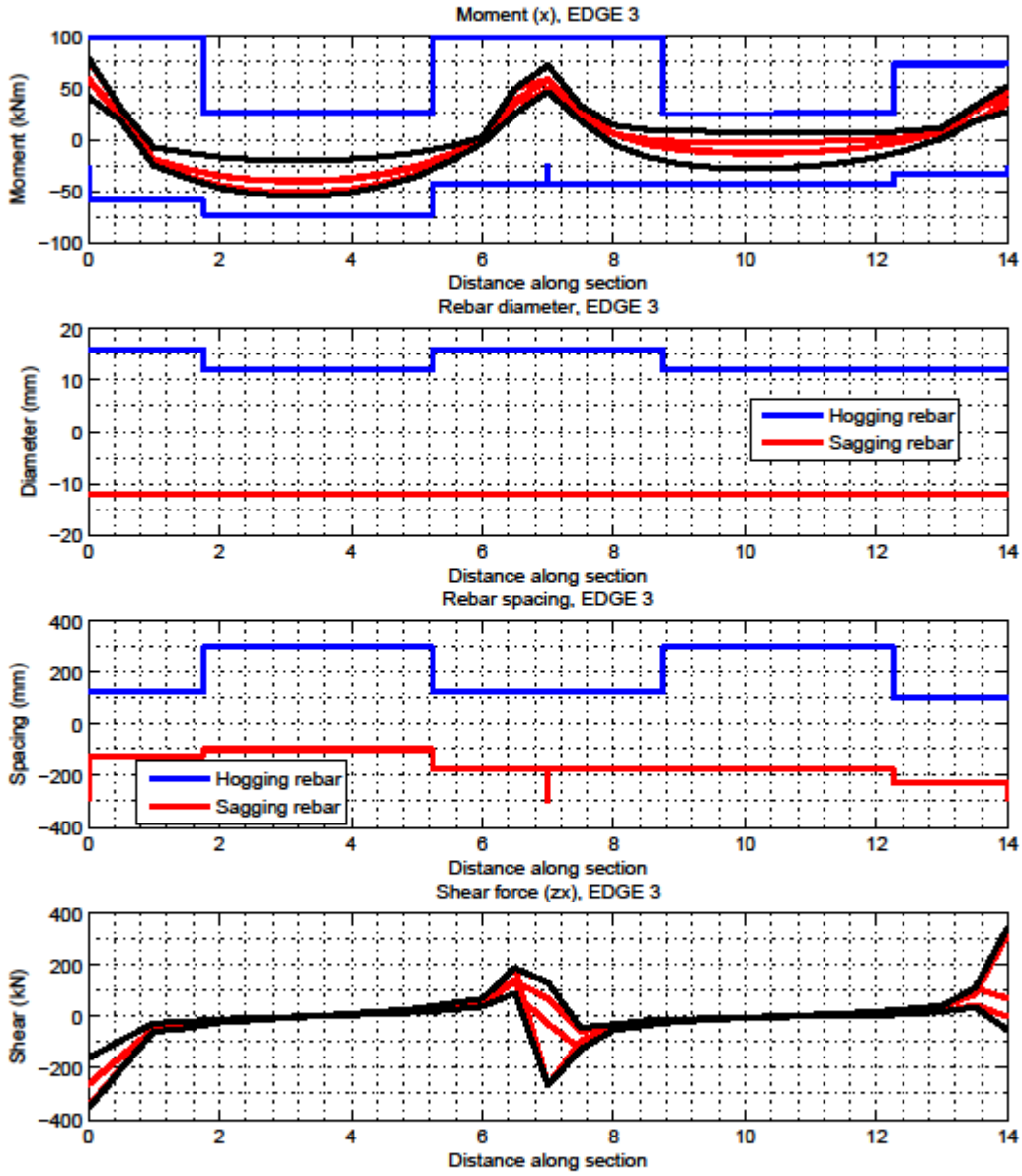
Moment (x), EDGE 3
Moment (kNm)
Distance along section
Rebar diameter, EDGE 3
Diameter (mm)
Hogging rebar
Sagging rebar
Distance along section
Rebar spacing, EDGE 3
Spacing (mm)
Hogging rebar
Sagging rebar
Distance along section
Shear force (zx), EDGE 3
Shear (kN)
Distance along section

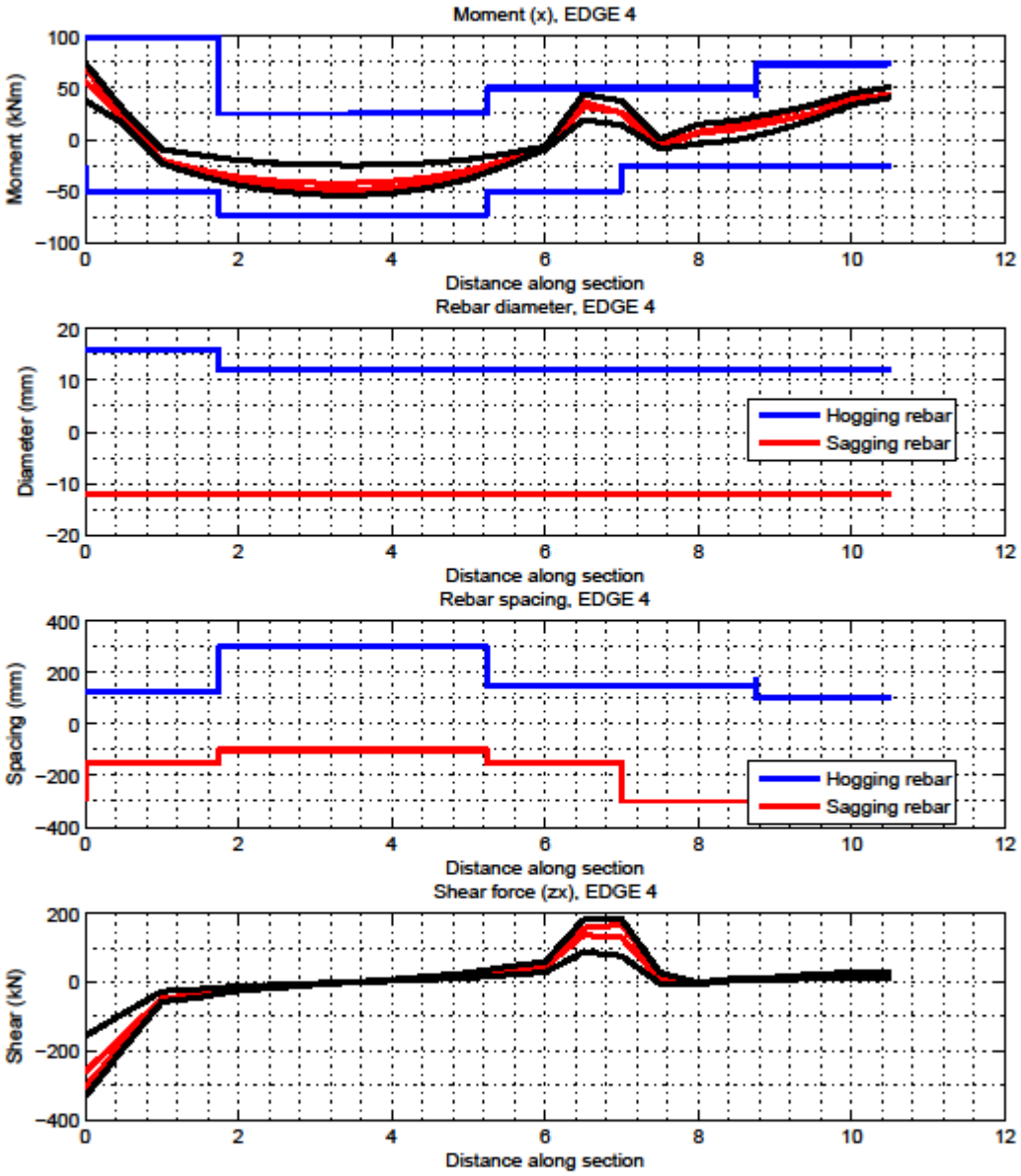
Moment (x), EDGE 4
Moment (kNm)
Distance along section
Rebar diameter, EDGE 4
Diameter (mm)
Hogging rebar
Sagging rebar
Distance along section
Rebar spacing, EDGE 4
Spacing (mm)
Hogging rebar
Sagging rebar
Distance along section
Shear force (zx), EDGE 4
Shear (kN)
Distance along section

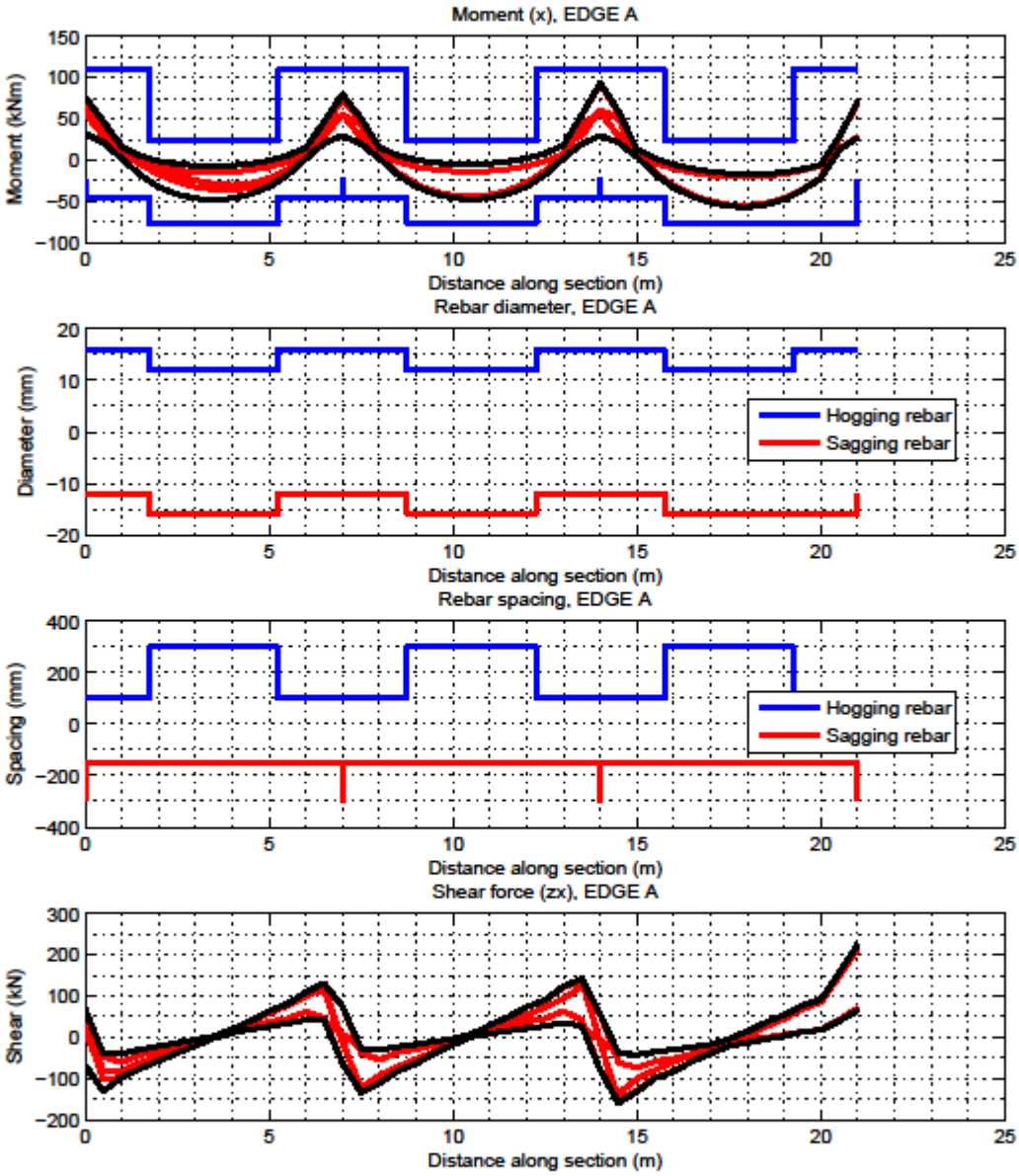
Moment (x), EDGE A
Moment (kNm)
150
100
50
0
−50
−100
0
5
10
15
20
25
Distance along section (m)
Rebar diameter, EDGE A
Diameter (mm)
20
10
0
−10
−20
Hogging rebar
Sagging rebar
Distance along section (m)
Rebar spacing, EDGE A
Spacing (mm)
400
200
0
−200
−400
Hogging rebar
Sagging rebar
Distance along section (m)
Shear force (zx), EDGE A
Shear (kN)
300
200
100
0
−100
−200
Distance along section (m)

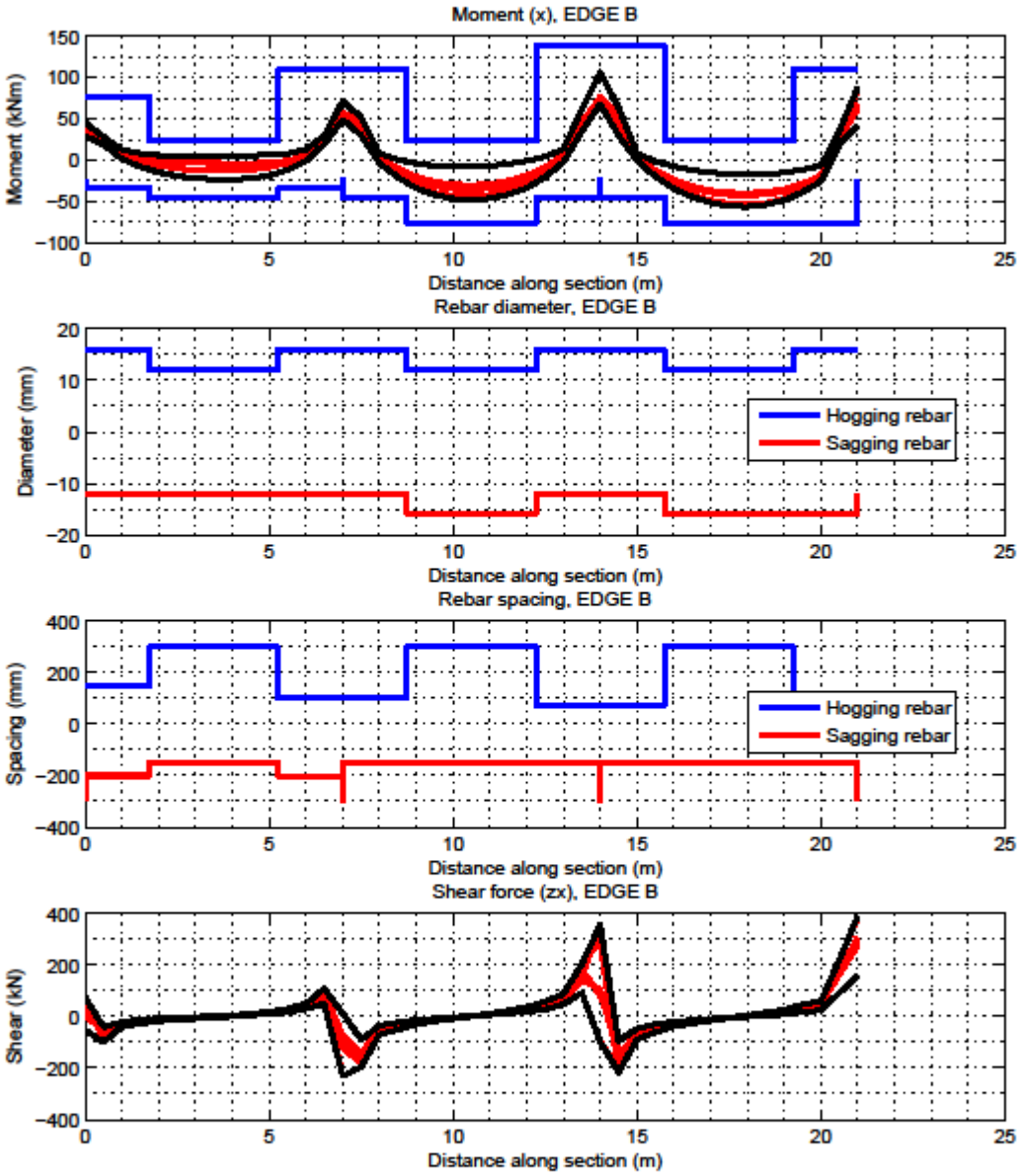
Moment (x), EDGE B
Moment (kNm)
Distance along section (m)
Rebar diameter, EDGE B
Diameter (mm)
Hogging rebar
Sagging rebar
Distance along section (m)
Rebar spacing, EDGE B
Spacing (mm)
Hogging rebar
Sagging rebar
Distance along section (m)
Shear force (zx), EDGE B
Shear (kN)
Distance along section (m)

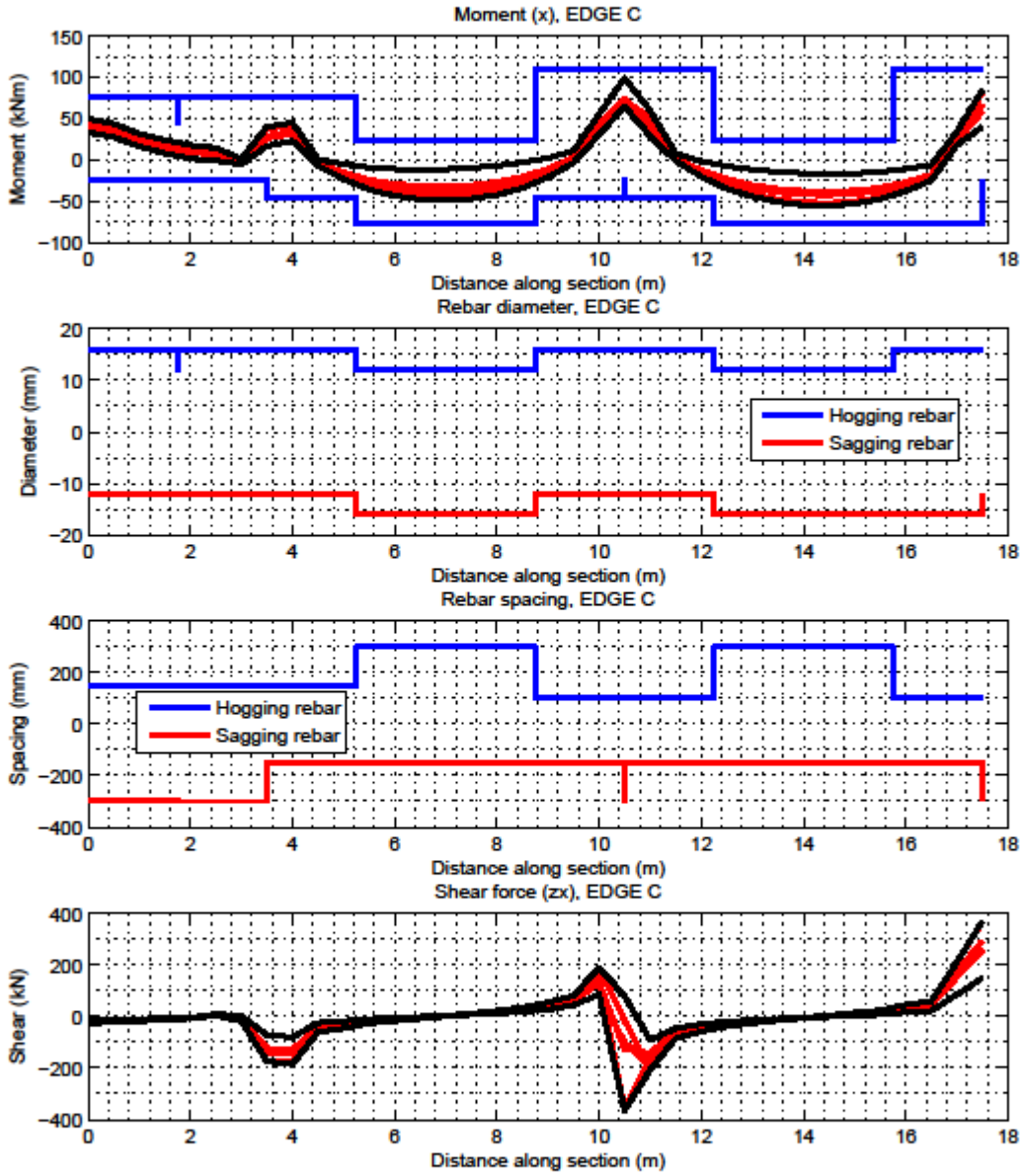
Moment (x), EDGE C
Moment (kNm)
Distance along section (m)
Rebar diameter, EDGE C
Diameter (mm)
Hogging rebar
Sagging rebar
Distance along section (m)
Rebar spacing, EDGE C
Spacing (mm)
Hogging rebar
Sagging rebar
Distance along section (m)
Shear force (zx), EDGE C
Shear (kN)
Distance along section (m)

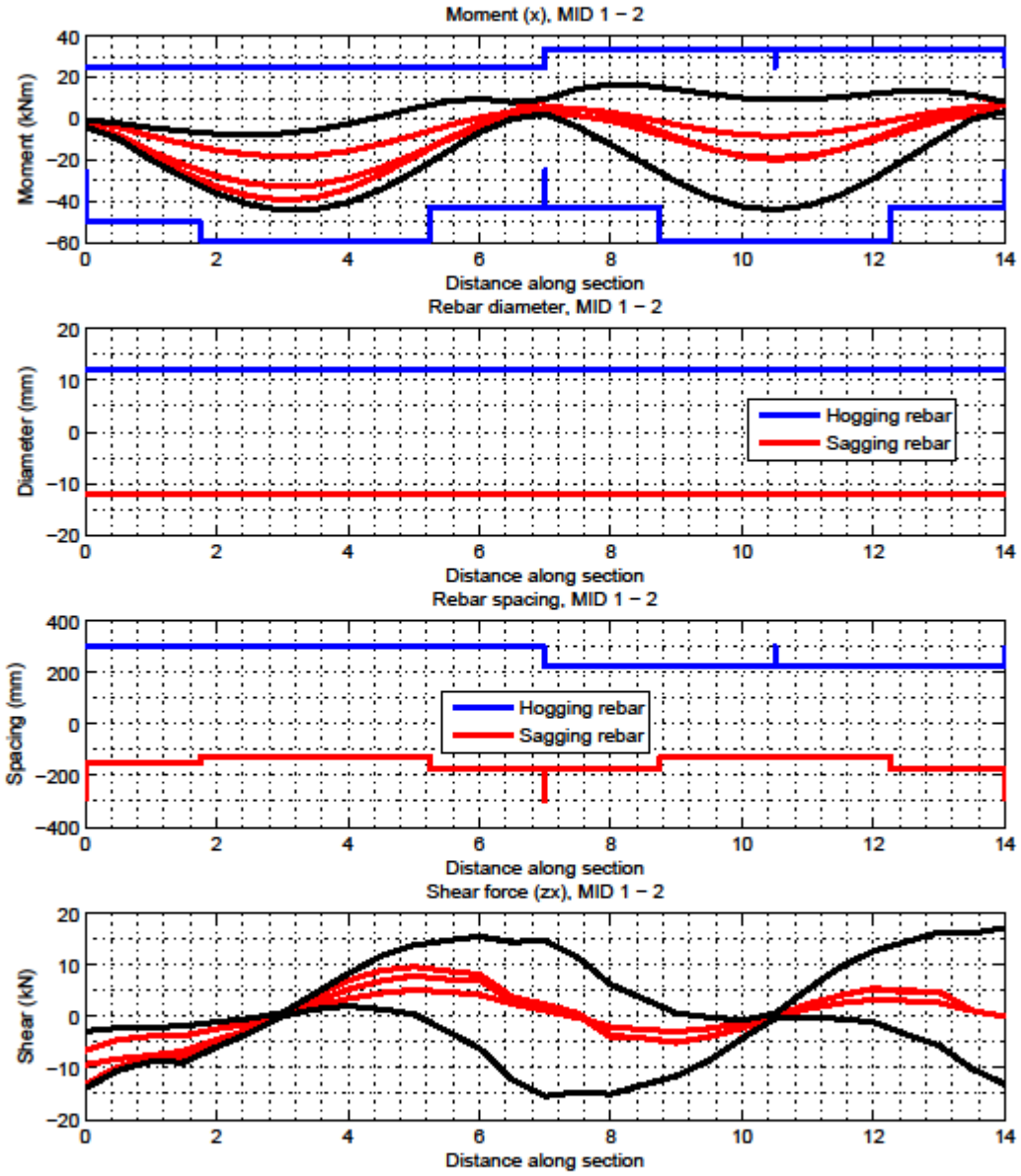
Moment (x), MID 1 – 2
Moment (kNm)
Distance along section
Rebar diameter, MID 1 – 2
Diameter (mm)
Hogging rebar
Sagging rebar
Distance along section
Rebar spacing, MID 1 – 2
Spacing (mm)
Hogging rebar
Sagging rebar
Distance along section
Shear force (zx), MID 1 – 2
Shear (kN)
Distance along section

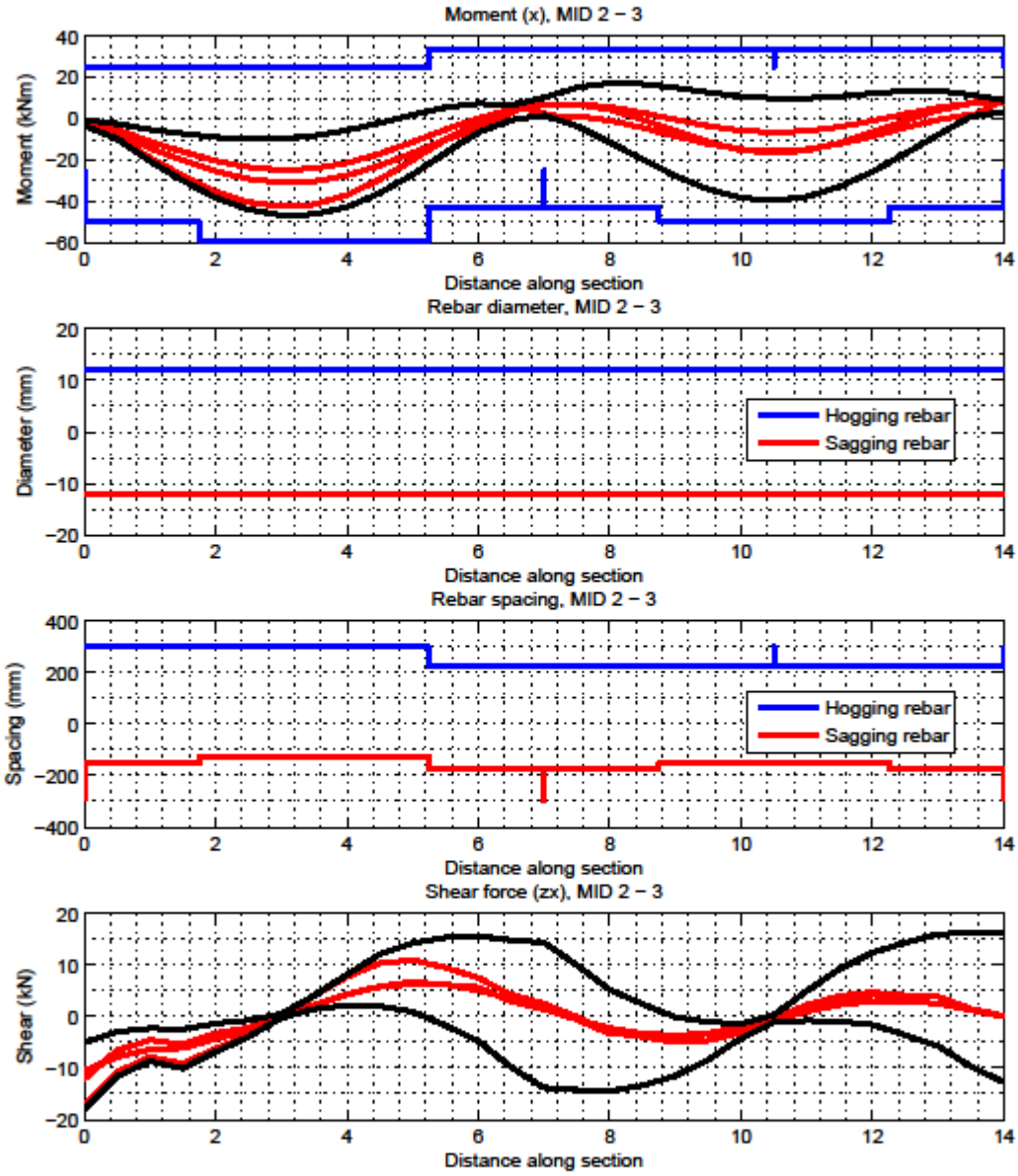
Moment (x), MID 2 – 3
Moment (kNm)
Distance along section
Rebar diameter, MID 2 – 3
Diameter (mm)
Hogging rebar
Sagging rebar
Distance along section
Rebar spacing, MID 2 – 3
Spacing (mm)
Hogging rebar
Sagging rebar
Distance along section
Shear force (zx), MID 2 – 3
Shear (kN)
Distance along section

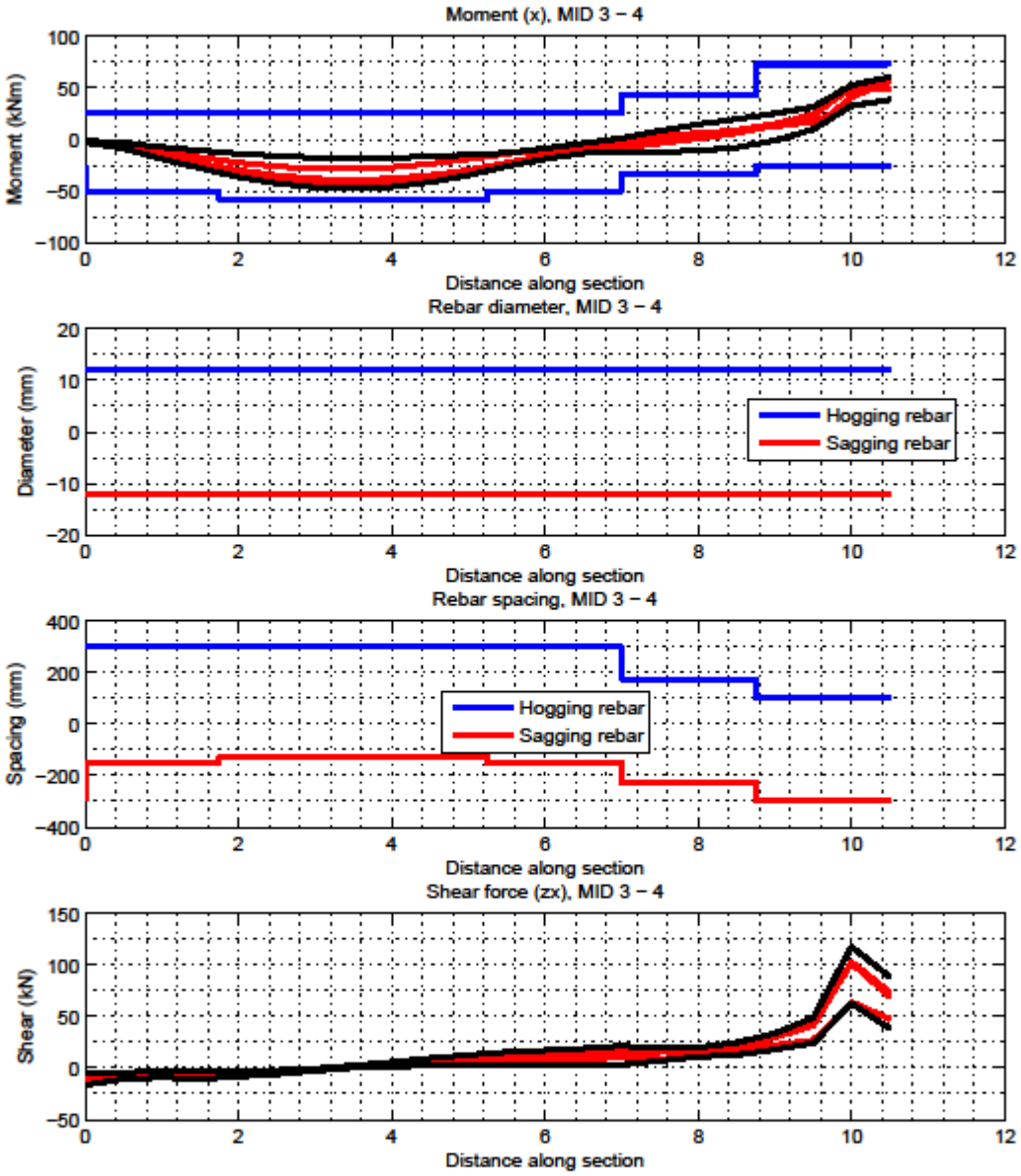
Moment (x), MID 3 – 4
Moment (kNm)
Distance along section
Rebar diameter, MID 3 – 4
Diameter (mm)
Hogging rebar
Sagging rebar
Distance along section
Rebar spacing, MID 3 – 4
Spacing (mm)
Hogging rebar
Sagging rebar
Distance along section
Shear force (zx), MID 3 – 4
Shear (kN)
Distance along section

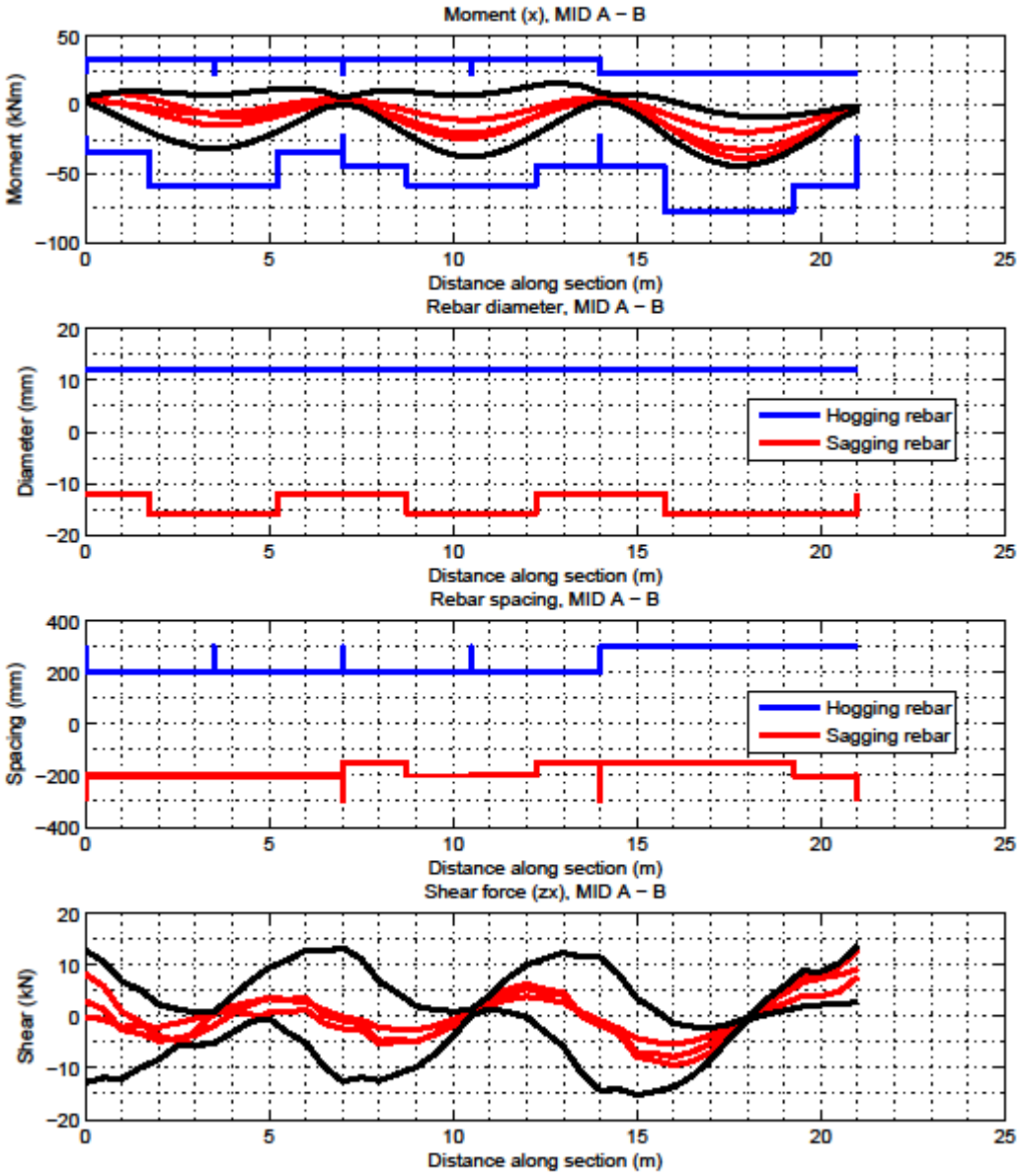
Moment (x), MID A – B
Moment (kNm)
50
0
−50
−100
0
5
10
15
20
25
Distance along section (m)
Rebar diameter, MID A – B
Diameter (mm)
20
10
0
−10
−20
Hogging rebar
Sagging rebar
Distance along section (m)
Rebar spacing, MID A – B
Spacing (mm)
400
200
0
−200
−400
Hogging rebar
Sagging rebar
Distance along section (m)
Shear force (zx), MID A – B
Shear (kN)
20
10
0
−10
−20
Distance along section (m)

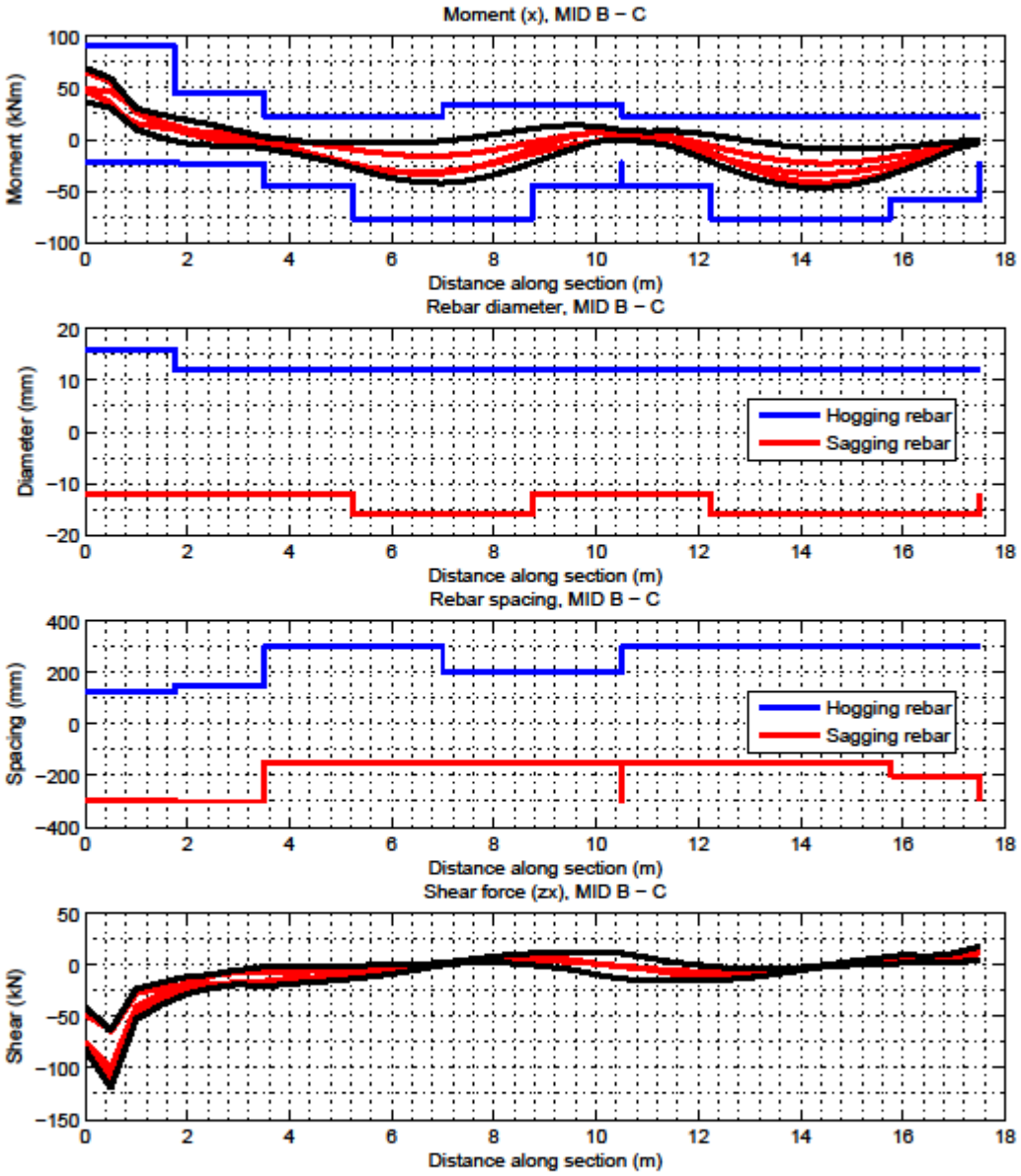
Moment (x), MID B – C
Moment (kNm)
Distance along section (m)
Rebar diameter, MID B – C
Diameter (mm)
Hogging rebar
Sagging rebar
Distance along section (m)
Rebar spacing, MID B – C
Spacing (mm)
Hogging rebar
Sagging rebar
Distance along section (m)
Shear force (zx), MID B – C
Shear (kN)
Distance along section (m)

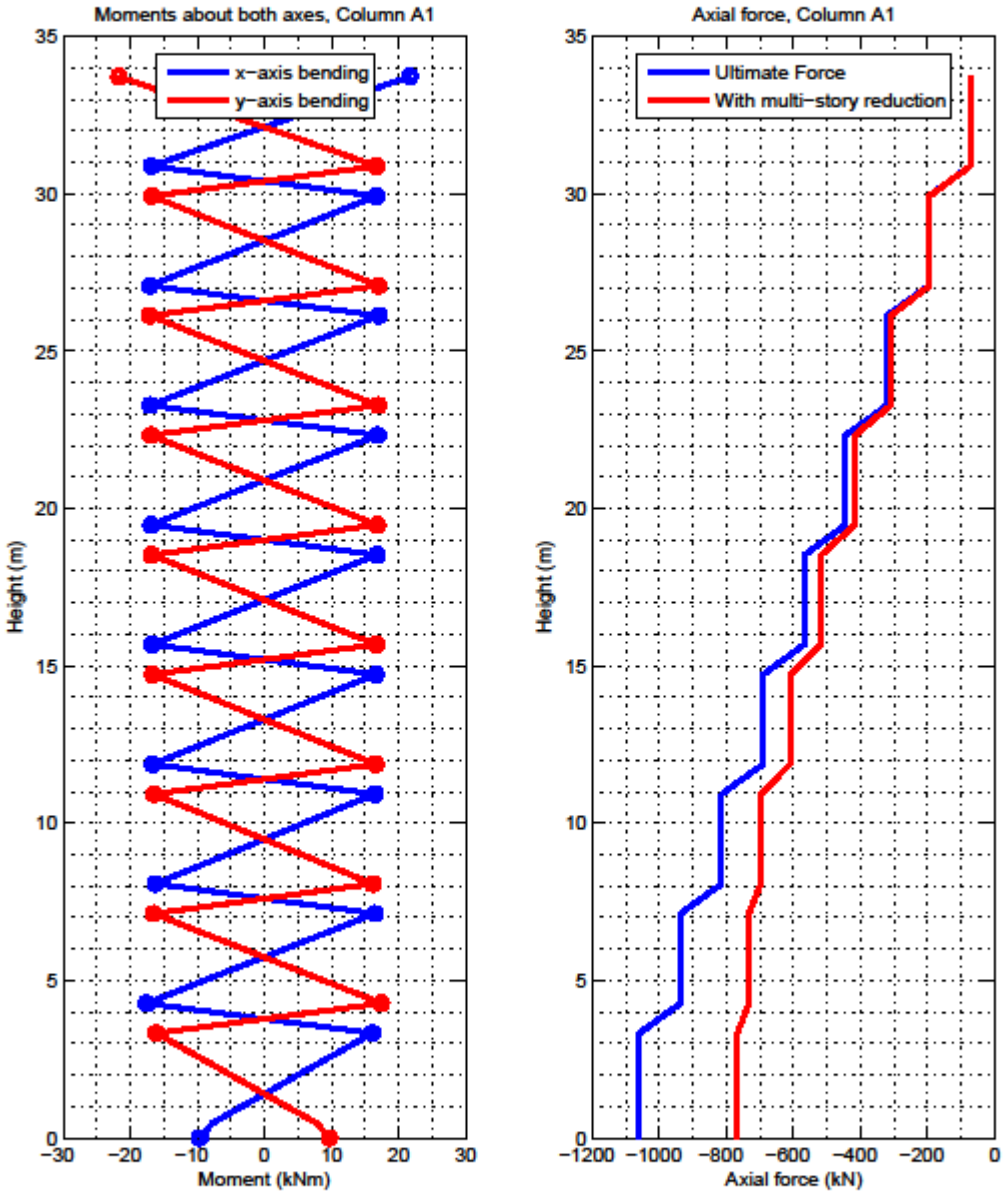
Moments about both axes, Column A1
x−axis bending
y−axis bending
Height (m)
Moment (kNm)
Axial force, Column A1
Ultimate Force
With multi−story reduction
Height (m)
Axial force (kN)

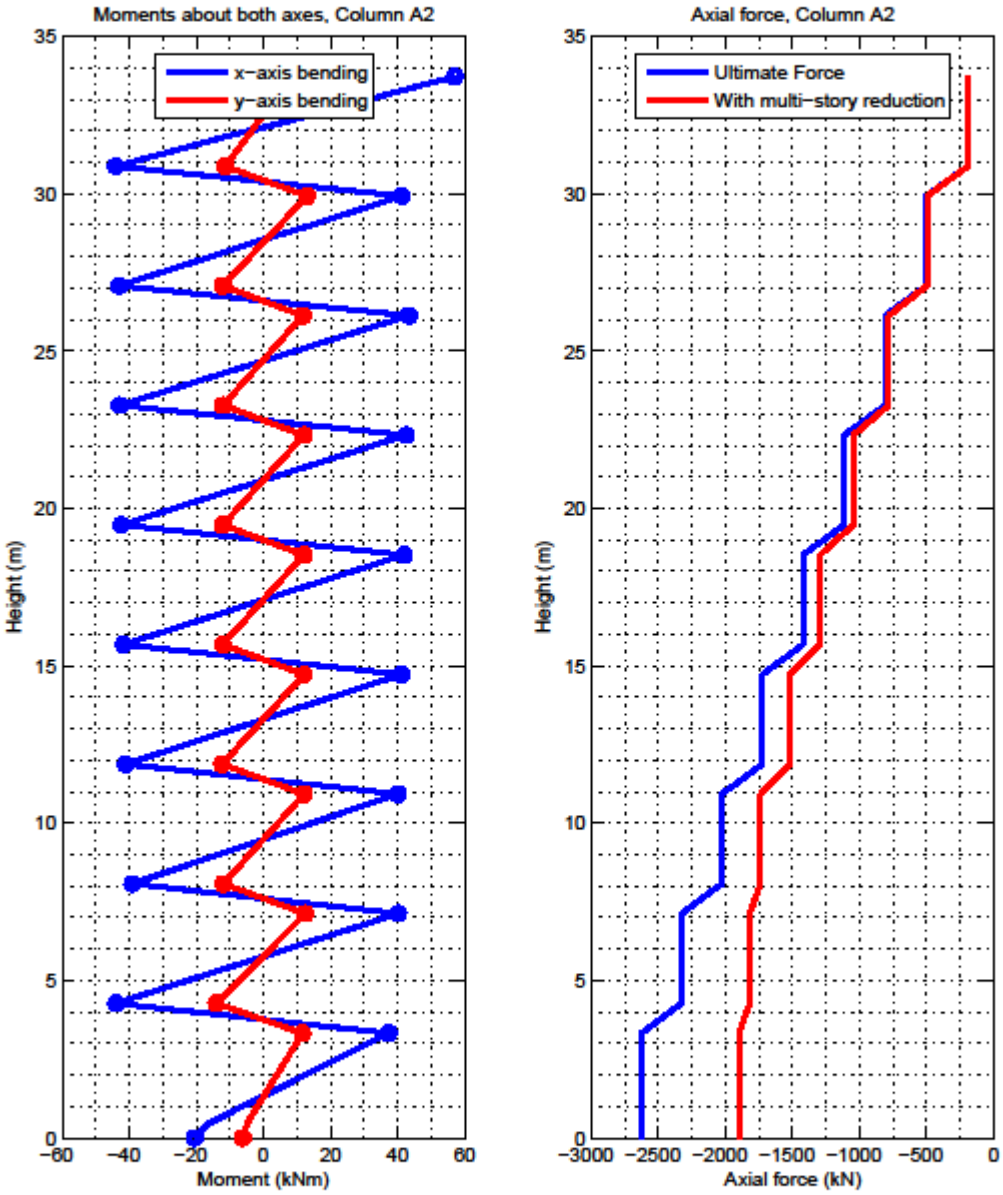
Moments about both axes, Column A2
x−axis bending
y−axis bending
Height (m)
Moment (kNm)
Axial force, Column A2
Ultimate Force
With multi−story reduction
Height (m)
Axial force (kN)

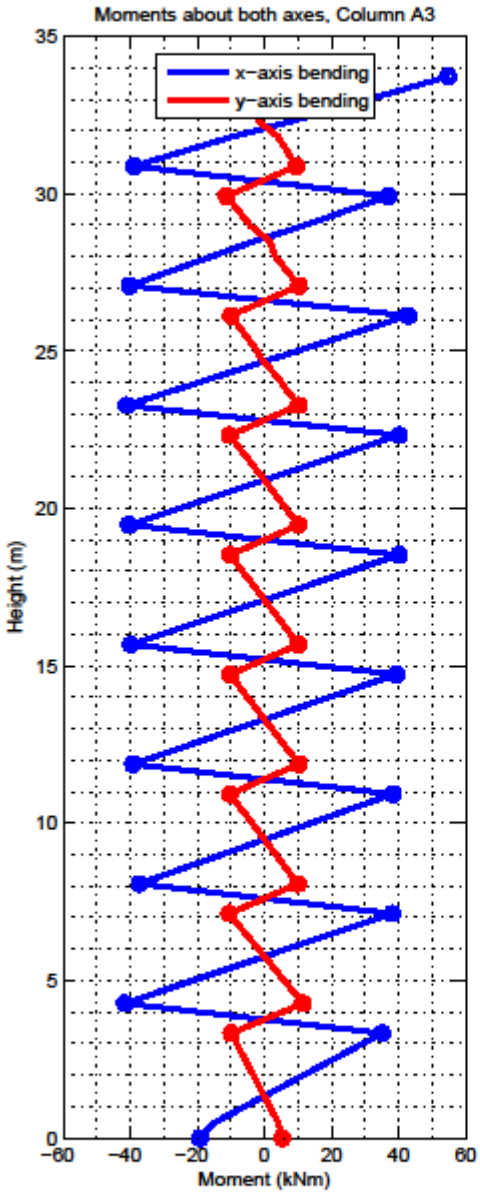
Moments about both axes, Column A3
x−axis bending
y−axis bending
Height (m)
Moment (kNm)
0
5
10
15
20
25
30
35
−60
−40
−20
0
20
40
60

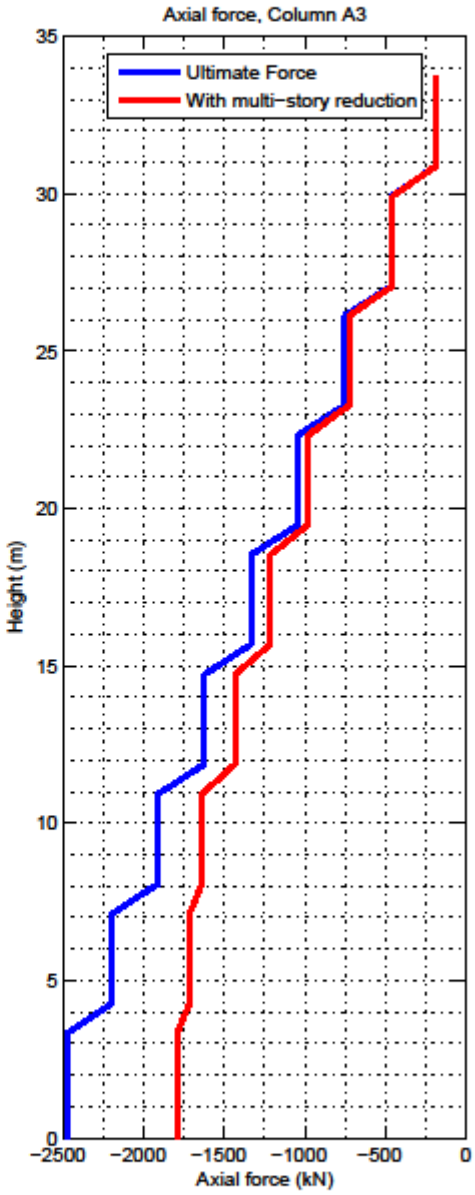
Axial force, Column A3
Ultimate Force
With multi−story reduction
Height (m)
Axial force (kN)
0
5
10
15
20
25
30
35
−2500
−2000
−1500
−1000
−500
0

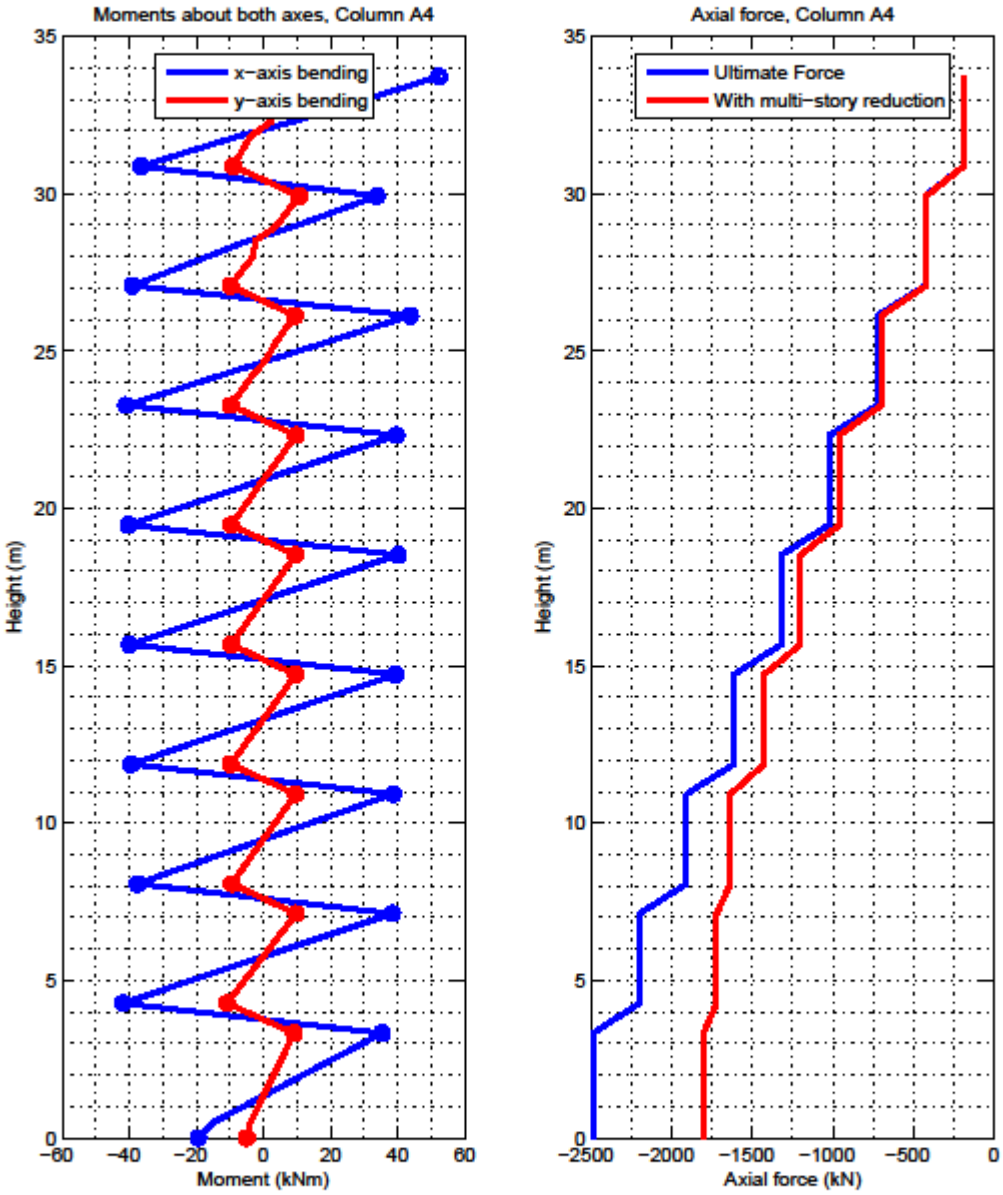
Moments about both axes, Column A4
x−axis bending
y−axis bending
Height (m)
Moment (kNm)
0
5
10
15
20
25
30
35
−60
−40
−20
0
20
40
60
Axial force, Column A4
Ultimate Force
With multi−story reduction
Height (m)
Axial force (kN)
−2500
−2000
−1500
−1000
−500
0

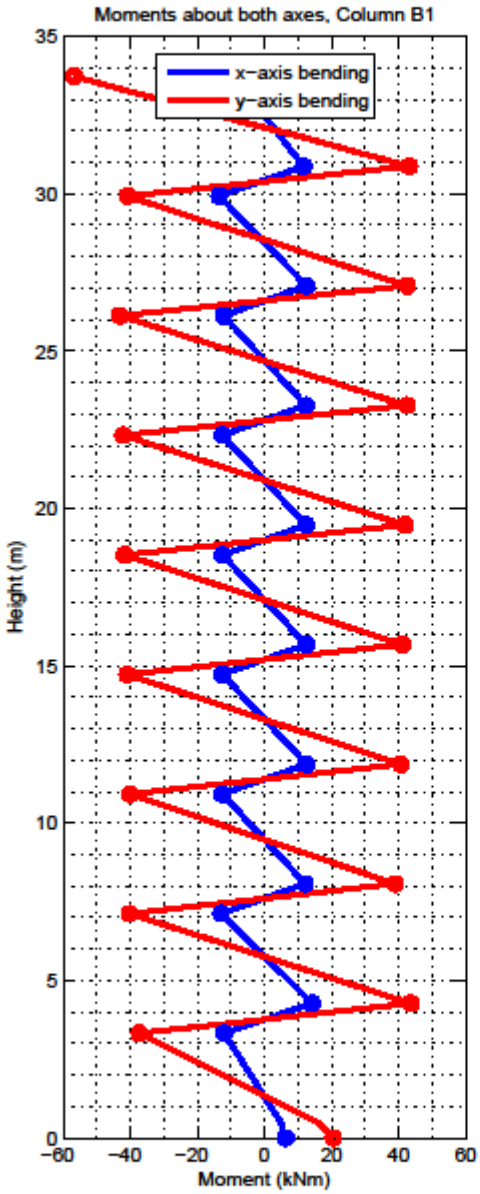
Moments about both axes, Column B1
x−axis bending
y−axis bending
Height (m)
Moment (kNm)
0
5
10
15
20
25
30
35
−60
−40
−20
0
20
40
60

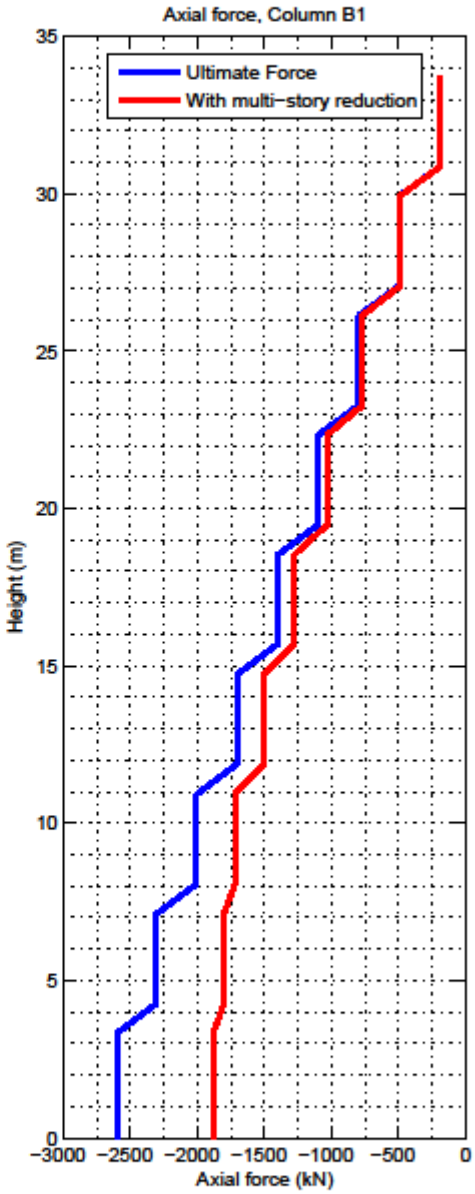
Axial force, Column B1
Ultimate Force
With multi−story reduction
Height (m)
Axial force (kN)
0
5
10
15
20
25
30
35
−3000
−2500
−2000
−1500
−1000
−500
0

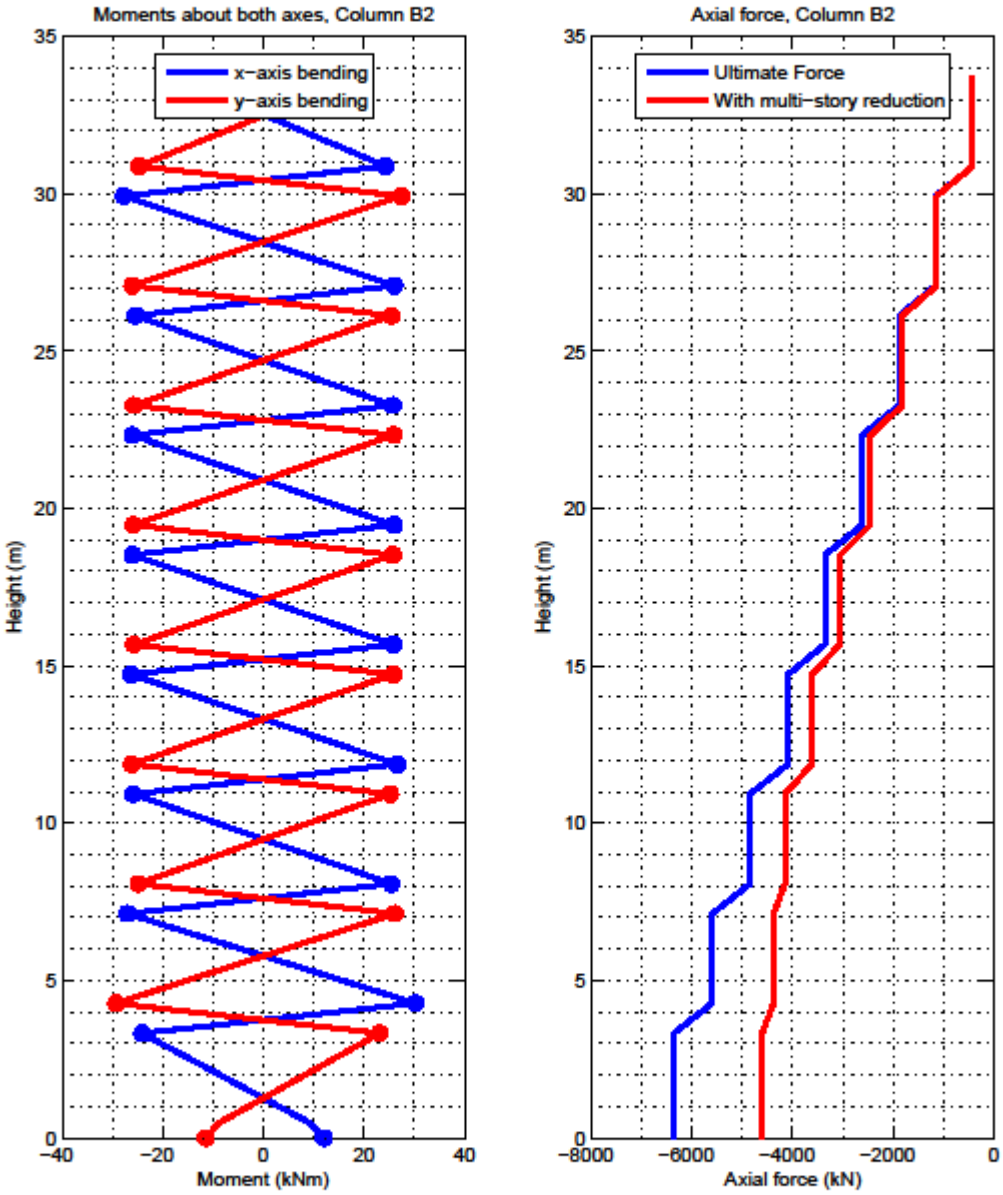
Moments about both axes, Column B2
x−axis bending
y−axis bending
Height (m)
Moment (kNm)
0
5
10
15
20
25
30
35
−40
−20
0
20
40
Axial force, Column B2
Ultimate Force
With multi−story reduction
Height (m)
Axial force (kN)
−8000
−6000
−4000
−2000
0

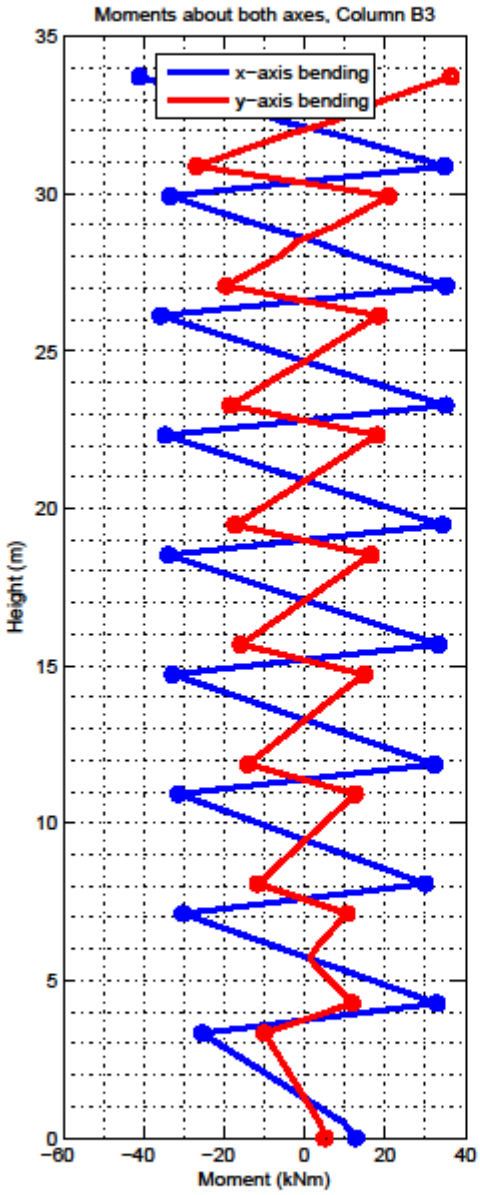
Moments about both axes, Column B3
x−axis bending
y−axis bending
Height (m)
Moment (kNm)
0
5
10
15
20
25
30
35
−60
−40
−20
0
20
40

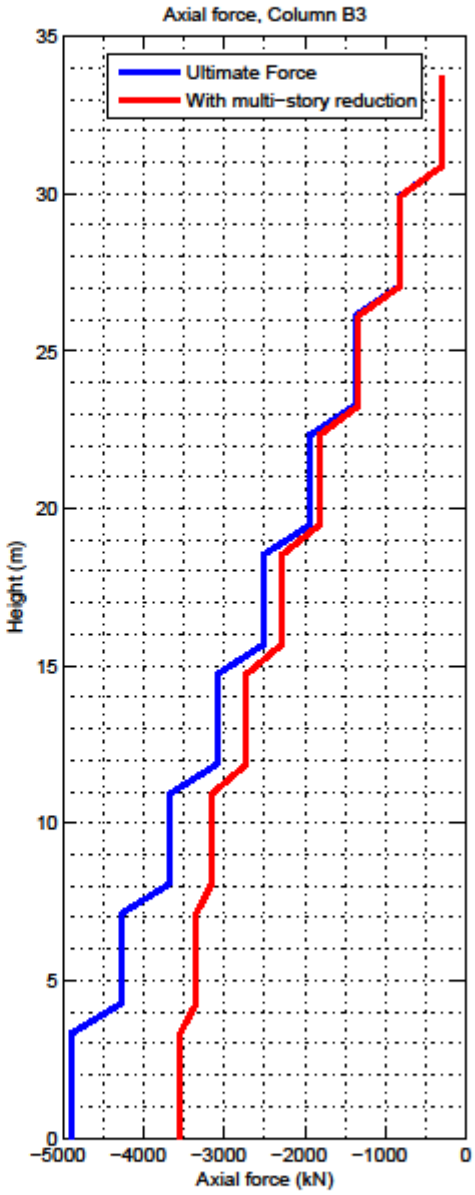
Axial force, Column B3
Ultimate Force
With multi−story reduction
Height (m)
Axial force (kN)
0
5
10
15
20
25
30
35
−5000
−4000
−3000
−2000
−1000
0

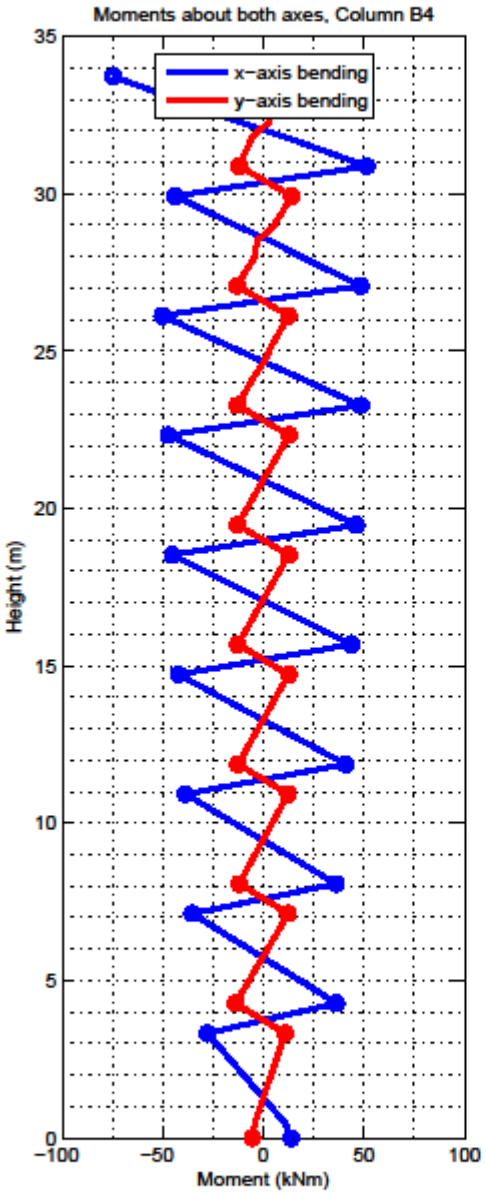
Moments about both axes, Column B4
x−axis bending
y−axis bending
Height (m)
Moment (kNm)
0
5
10
15
20
25
30
35
−100
−50
0
50
100

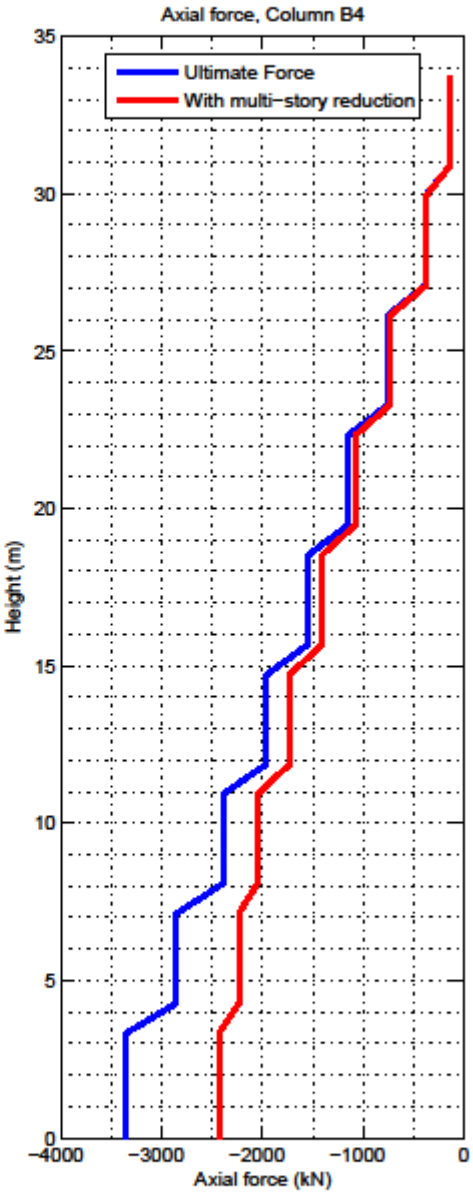
Axial force, Column B4
Ultimate Force
With multi−story reduction
Height (m)
Axial force (kN)
0
5
10
15
20
25
30
35
−4000
−3000
−2000
−1000
0

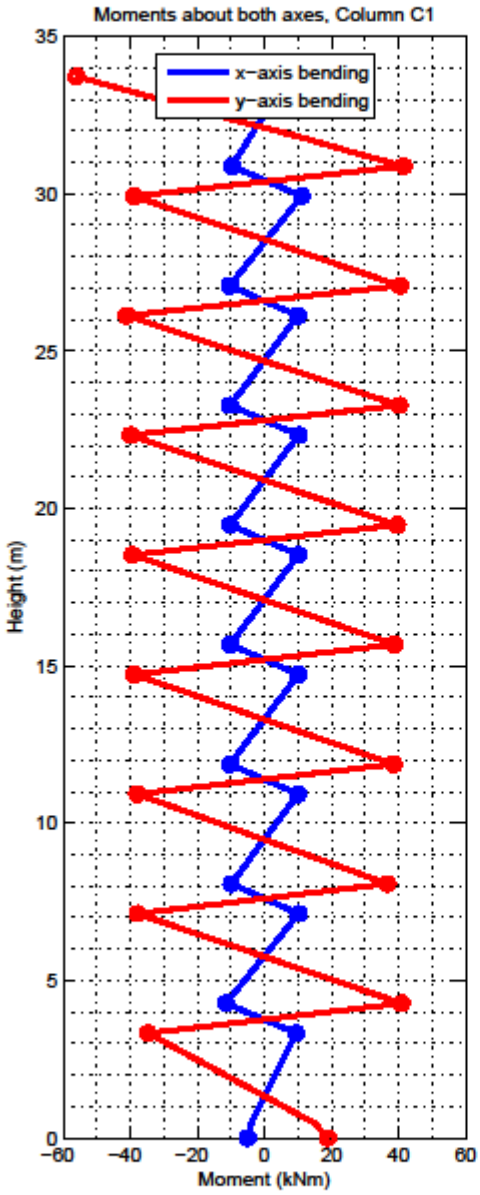
Moments about both axes, Column C1
x−axis bending
y−axis bending
Height (m)
Moment (kNm)
0
5
10
15
20
25
30
35
−60
−40
−20
0
20
40
60

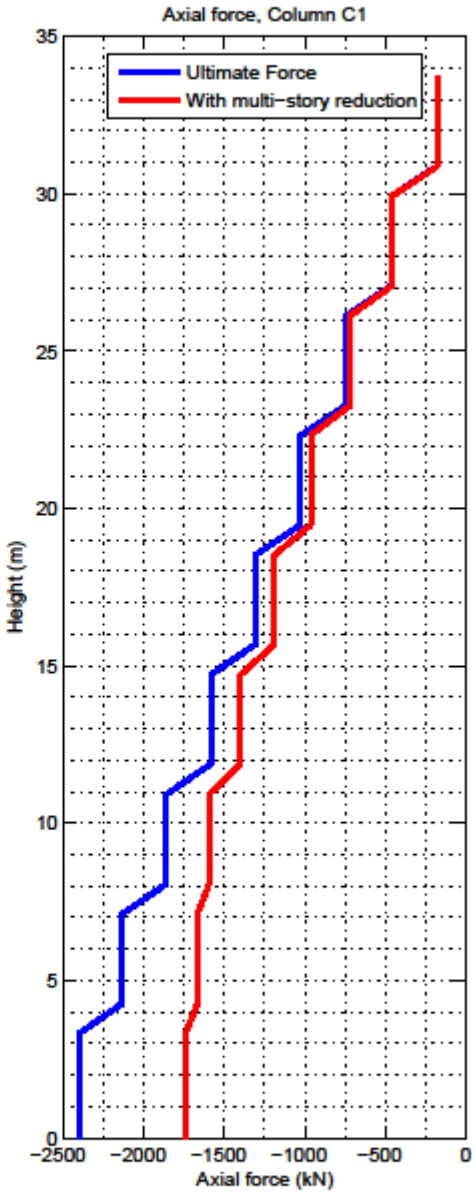
Axial force, Column C1
Ultimate Force
With multi−story reduction
Height (m)
Axial force (kN)
0
5
10
15
20
25
30
35
−2500
−2000
−1500
−1000
−500
0

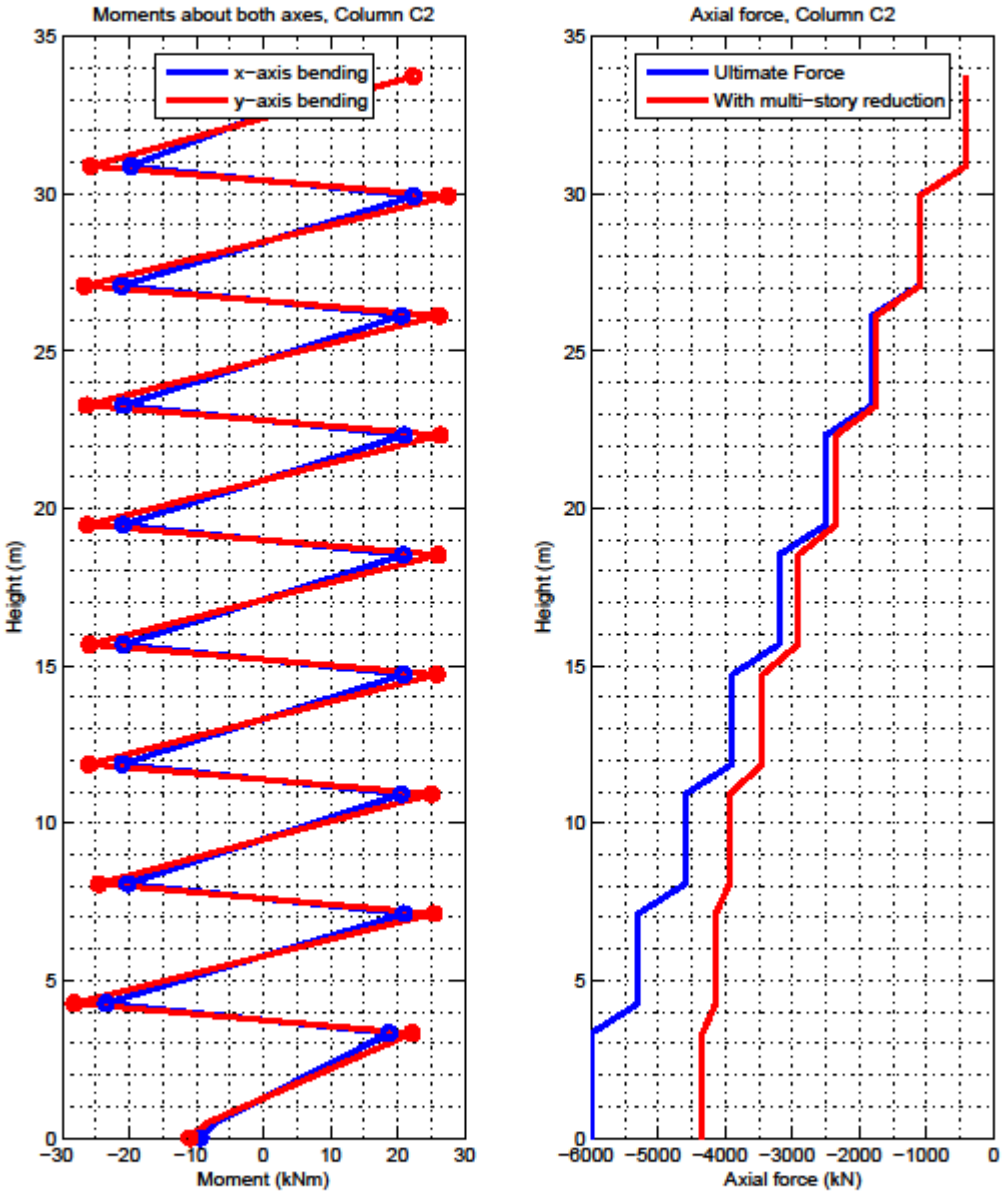
Moments about both axes, Column C2
x−axis bending
y−axis bending
Height (m)
Moment (kNm)
Axial force, Column C2
Ultimate Force
With multi−story reduction
Height (m)
Axial force (kN)

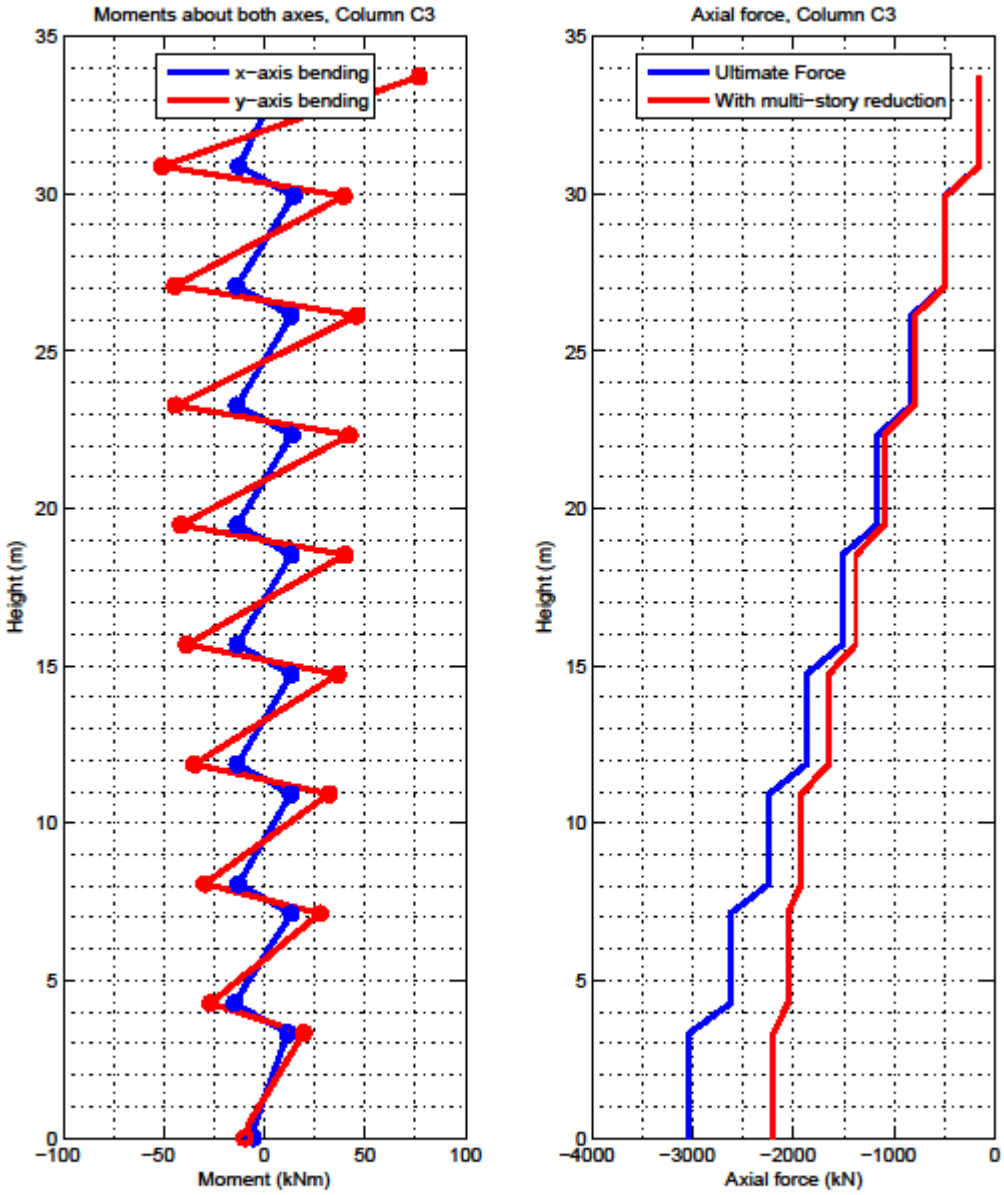
Moments about both axes, Column C3
x−axis bending
y−axis bending
Height (m)
Moment (kNm)
Axial force, Column C3
Ultimate Force
With multi−story reduction
Height (m)
Axial force (kN)

COLUMN A1:

| | 1st floor | 2nd floor | 3rd floor | 4th floor | 5th floor | 6th floor | 7th floor | 8th floor | roof |
|---|---|---|---|---|---|---|---|---|---|
| AXIAL FORCE | -767.8 | -733 | -698.2 | -610.2 | -517.2 | -416.9 | -309.4 | -194.7 | -72.96 |
| X MOMENT BASE | -9.665 | -17.57 | -16.19 | -16.65 | -16.72 | -16.89 | -17.01 | -17.08 | -16.85 |
| X MOMENT TOP | 16.13 | 16.5 | 16.5 | 16.65 | 16.81 | 16.94 | 17.12 | 16.77 | 21.73 |
| Y MOMENT BASE | 9.739 | 17.48 | 16.18 | 16.63 | 16.73 | 16.89 | 17.01 | 17.08 | 16.8 |
| Y MOMENT TOP | -16.13 | -16.47 | -16.48 | -16.65 | -16.82 | -16.94 | -17.12 | -16.8 | -21.68 |
| X ROTATION BASE | -4E-36 | 7E-05 | 5.7E-05 | 6.1E-05 | 6.1E-05 | 6.2E-05 | 6.2E-05 | 6.3E-05 | 6E-05 |
| X ROTATION TOP | 8.2E-05 | 5.5E-05 | 6.2E-05 | 6.1E-05 | 6.2E-05 | 6.2E-05 | 6.3E-05 | 6.1E-05 | 0.00013 |
| Y ROTATION BASE | -2E-36 | 7.1E-05 | 5.7E-05 | 6.1E-05 | 6.1E-05 | 6.2E-05 | 6.2E-05 | 6.3E-05 | 5.9E-05 |
| Y ROTATION TOP | 8.3E-05 | 5.5E-05 | 6.2E-05 | 6.1E-05 | 6.2E-05 | 6.2E-05 | 6.3E-05 | 5.9E-05 | 0.00013 |
| Diameter | 12 | 12 | 12 | 12 | 12 | 12 | 12 | 12 | 16 |
| Number | 4 | 4 | 4 | 4 | 4 | 4 | 4 | 4 | 4 |

COLUMN B1:

| | 1st floor | 2nd floor | 3rd floor | 4th floor | 5th floor | 6th floor | 7th floor | 8th floor | roof |
|---|---|---|---|---|---|---|---|---|---|
| AXIAL FORCE | -1884 | -1802 | -1720 | -1506 | -1279 | -1034 | -769.9 | -488.2 | -188.7 |
| X MOMENT BASE | 6.393 | 14.24 | 12.23 | 12.63 | 12.48 | 12.48 | 12.41 | 12.54 | 11.7 |
| X MOMENT TOP | -11.96 | -12.82 | -12.53 | -12.54 | -12.47 | -12.51 | -12.18 | -13.45 | -9.13 |
| Y MOMENT BASE | 20.54 | 43.7 | 39 | 40.7 | 41.27 | 41.97 | 42.53 | 42.63 | 43.28 |
| Y MOMENT TOP | -37.31 | -40.16 | -40.11 | -40.91 | -41.66 | -42.13 | -43.14 | -40.85 | -56.76 |
| X ROTATION BASE | -7E-36 | 0.00013 | 9.2E-05 | 0.0001 | 0.0001 | 0.00011 | 0.00011 | 0.00013 | 4.1E-05 |
| X ROTATION TOP | 0.00017 | 8.7E-05 | 0.00011 | 0.00011 | 0.00011 | 0.00011 | 0.00012 | 7.9E-05 | 0.00028 |
| Y ROTATION BASE | -1E-36 | -1E-05 | -1E-05 | -1E-05 | -1E-05 | -1E-05 | -1E-05 | -9E-06 | -1E-05 |
| Y ROTATION TOP | -2E-05 | -8E-06 | -1E-05 | -1E-05 | -1E-05 | -1E-05 | -9E-06 | -1E-05 | -3E-06 |
| Diameter | 12 | 12 | 12 | 12 | 12 | 12 | 12 | 12 | 16 |
| Number | 4 | 4 | 4 | 4 | 4 | 4 | 4 | 4 | 4 |

COLUMN C1:

| | 1st floor | 2nd floor | 3rd floor | 4th floor | 5th floor | 6th floor | 7th floor | 8th floor | roof |
|---|---|---|---|---|---|---|---|---|---|
| AXIAL FORCE | -1739 | -1667 | -1594 | -1398 | -1189 | -962.1 | -717.9 | -456.6 | -178.3 |
| X MOMENT BASE | -4.962 | -11.4 | -9.838 | -10.23 | -10.16 | -10.21 | -10.19 | -10.3 | -9.673 |
| X MOMENT TOP | 9.446 | 10.28 | 10.11 | 10.19 | 10.18 | 10.25 | 10.03 | 11.12 | 7.021 |
| Y MOMENT BASE | 18.97 | 40.99 | 36.8 | 38.65 | 38.98 | 39.7 | 40.39 | 40.51 | 41.56 |
| Y MOMENT TOP | -34.71 | -37.76 | -37.97 | -38.75 | -39.33 | -39.91 | -41.12 | -38.94 | -56.03 |
| X ROTATION BASE | -2E-36 | 0.00011 | 8.3E-05 | 9.5E-05 | 9.6E-05 | 0.0001 | 9.8E-05 | 0.00012 | 2.9E-05 |
| X ROTATION TOP | 0.00015 | 8E-05 | 1E-04 | 9.8E-05 | 0.0001 | 0.0001 | 0.00011 | 7E-05 | 0.00028 |
| Y ROTATION BASE | -6E-38 | 1.1E-08 | -3E-08 | -4E-08 | -3E-08 | -2E-08 | 9.4E-08 | 4E-07 | -1E-07 |
| Y ROTATION TOP | 4.9E-08 | -4E-08 | -3E-08 | -4E-08 | -4E-09 | 2.9E-08 | 3.1E-07 | 4.9E-08 | -7E-07 |
| Diameter | 12 | 12 | 12 | 12 | 12 | 12 | 12 | 12 | 16 |
| Number | 4 | 4 | 4 | 4 | 4 | 4 | 4 | 4 | 4 |

COLUMN A2:

| | 1st floor | 2nd floor | 3rd floor | 4th floor | 5th floor | 6th floor | 7th floor | 8th floor | roof |
|---|---|---|---|---|---|---|---|---|---|
| AXIAL FORCE | -1901 | -1820 | -1738 | -1523 | -1295 | -1047 | -781.4 | -497.2 | -191.9 |
| X MOMENT BASE | -20.51 | -43.95 | -39.12 | -41.06 | -41.65 | -42.36 | -42.91 | -43.02 | -43.96 |
| X MOMENT TOP | 37.4 | 40.31 | 40.24 | 41.29 | 42.04 | 42.53 | 43.49 | 41.37 | 57.12 |
| Y MOMENT BASE | -6.147 | -14.04 | -11.93 | -12.31 | -12.12 | -12.1 | -12.01 | -12.11 | -11.35 |
| Y MOMENT TOP | 11.68 | 12.56 | 12.22 | 12.2 | 12.1 | 12.12 | 11.79 | 13.02 | 8.519 |
| X ROTATION BASE | -3E-36 | -2E-05 | -9E-06 | -1E-05 | -1E-05 | -1E-05 | -9E-06 | -1E-05 | -9E-06 |
| X ROTATION TOP | -2E-05 | -7E-06 | -1E-05 | -1E-05 | -9E-06 | -9E-06 | -9E-06 | -7E-06 | 4.1E-07 |
| Y ROTATION BASE | -6E-36 | 0.00013 | 9.3E-05 | 0.00011 | 0.00011 | 0.00011 | 0.00011 | 0.00013 | 4.1E-05 |
| Y ROTATION TOP | 0.00017 | 8.8E-05 | 0.00011 | 0.00011 | 0.00011 | 0.00011 | 0.00012 | 8E-05 | 0.00028 |
| Diameter | 12 | 12 | 12 | 12 | 12 | 12 | 12 | 12 | 16 |
| Number | 4 | 4 | 4 | 4 | 4 | 4 | 4 | 4 | 4 |

COLUMN B2:

| | 1st floor | 2nd floor | 3rd floor | 4th floor | 5th floor | 6th floor | 7th floor | 8th floor | roof |
|---|---|---|---|---|---|---|---|---|---|
| AXIAL FORCE | -4606 | -4377 | -4151 | -3614 | -3053 | -2453 | -1815 | -1137 | -414.8 |
| X MOMENT BASE | 12.04 | 30.31 | 25.48 | 26.66 | 26.01 | 26.01 | 25.82 | 26.11 | 24.36 |
| X MOMENT TOP | -24.14 | -27.03 | -25.87 | -26.21 | -26 | -26.03 | -25.43 | -27.69 | -17.82 |
| Y MOMENT BASE | -11.45 | -29.3 | -24.83 | -26.19 | -25.72 | -25.86 | -25.8 | -26.08 | -24.76 |
| Y MOMENT TOP | 23.14 | 26.23 | 25.3 | 25.83 | 25.79 | 25.92 | 25.52 | 27.44 | 19.28 |
| X ROTATION BASE | 5E-37 | -3E-05 | -1E-05 | -1E-05 | -1E-05 | -9E-06 | -8E-06 | -6E-06 | -1E-05 |
| X ROTATION TOP | -3E-05 | -8E-06 | -1E-05 | -9E-06 | -8E-06 | -7E-06 | -6E-06 | -9E-06 | 1.7E-05 |
| Y ROTATION BASE | 2.1E-36 | -3E-05 | -1E-05 | -1E-05 | -1E-05 | -1E-05 | -9E-06 | -7E-06 | -1E-05 |
| Y ROTATION TOP | -3E-05 | -1E-05 | -1E-05 | -1E-05 | -9E-06 | -8E-06 | -7E-06 | -1E-05 | 9.1E-06 |
| Diameter | 20 | 16 | 12 | 12 | 12 | 12 | 12 | 12 | 12 |
| Number | 4 | 4 | 4 | 4 | 4 | 4 | 4 | 4 | 4 |

COLUMN C2:

| | 1st floor | 2nd floor | 3rd floor | 4th floor | 5th floor | 6th floor | 7th floor | 8th floor | roof |
|---|---|---|---|---|---|---|---|---|---|
| AXIAL FORCE | -4345 | -4144 | -3944 | -3445 | -2918 | -2352 | -1747 | -1103 | -418.1 |
| X MOMENT BASE | -9.385 | -23.47 | -20.23 | -21.05 | -20.81 | -20.91 | -20.87 | -21.12 | -19.78 |
| X MOMENT TOP | 18.73 | 21.01 | 20.58 | 20.88 | 20.86 | 20.97 | 20.61 | 22.43 | 14.48 |
| Y MOMENT BASE | -10.97 | -28.24 | -24.52 | -25.99 | -25.88 | -26.23 | -26.36 | -26.67 | -25.81 |
| Y MOMENT TOP | 22.19 | 25.46 | 25.11 | 25.85 | 26.06 | 26.35 | 26.24 | 27.6 | 22.38 |
| X ROTATION BASE | -5E-37 | -2E-05 | -1E-05 | -1E-05 | -1E-05 | -1E-05 | -9E-06 | -9E-06 | -7E-06 |
| X ROTATION TOP | -3E-05 | -8E-06 | -1E-05 | -9E-06 | -9E-06 | -9E-06 | -9E-06 | -8E-06 | -2E-06 |
| Y ROTATION BASE | 0 | 1.7E-08 | -2E-08 | -1E-08 | -6E-09 | 5.1E-09 | 4.1E-09 | 3E-08 | 6.5E-09 |
| Y ROTATION TOP | 7.1E-08 | -3E-08 | -8E-09 | -5E-09 | 1.8E-09 | 6.8E-09 | 2E-08 | -3E-09 | 1.4E-07 |
| Diameter | 12 | 12 | 12 | 12 | 12 | 12 | 12 | 12 | 12 |
| Number | 4 | 4 | 4 | 4 | 4 | 4 | 4 | 4 | 4 |

COLUMN A3:

| | 1st floor | 2nd floor | 3rd floor | 4th floor | 5th floor | 6th floor | 7th floor | 8th floor | roof |
|---|---|---|---|---|---|---|---|---|---|
| AXIAL FORCE | -1793 | -1717 | -1639 | -1434 | -1216 | -979.3 | -724.7 | -452.5 | -186.1 |
| X MOMENT BASE | -19.14 | -41.62 | -37.18 | -39.17 | -39.74 | -40.4 | -41.11 | -40.19 | -38.91 |
| X MOMENT TOP | 35.16 | 38.23 | 38.36 | 39.38 | 40.2 | 40.28 | 42.9 | 36.97 | 54.85 |
| Y MOMENT BASE | 5.366 | 11.53 | 10.03 | 10.34 | 10.24 | 10.25 | 10.19 | 10.33 | 9.504 |
| Y MOMENT TOP | -9.835 | -10.46 | -10.25 | -10.27 | -10.23 | -10.29 | -9.974 | -11.27 | -6.881 |
| X ROTATION BASE | -3E-36 | 1.4E-06 | 1.3E-06 | 1.8E-06 | 1.3E-06 | 2.7E-06 | -4E-06 | 2.4E-05 | -2E-05 |
| X ROTATION TOP | 8.2E-07 | 1.4E-06 | 1.6E-06 | 1.3E-06 | 1.9E-06 | -1E-06 | 1.2E-05 | -2E-05 | 2E-05 |
| Y ROTATION BASE | -6E-36 | 0.00012 | 8.6E-05 | 9.7E-05 | 9.7E-05 | 0.0001 | 9.8E-05 | 0.00012 | 3.5E-05 |
| Y ROTATION TOP | 0.00016 | 8E-05 | 0.0001 | 9.9E-05 | 0.0001 | 0.0001 | 0.00011 | 7.2E-05 | 0.00026 |
| Diameter | 12 | 12 | 12 | 12 | 12 | 12 | 12 | 12 | 16 |
| Number | 4 | 4 | 4 | 4 | 4 | 4 | 4 | 4 | 4 |

COLUMN B3:

| | 1st floor | 2nd floor | 3rd floor | 4th floor | 5th floor | 6th floor | 7th floor | 8th floor | roof |
|---|---|---|---|---|---|---|---|---|---|
| AXIAL FORCE | -3549 | -3349 | -3155 | -2728 | -2287 | -1820 | -1327 | -806.8 | -295.2 |
| X MOMENT BASE | 12.74 | 32.9 | 30.06 | 32.31 | 33.31 | 34.28 | 35.11 | 35.18 | 34.95 |
| X MOMENT TOP | -25.45 | -30.24 | -31.31 | -32.75 | -33.83 | -34.55 | -35.82 | -33.34 | -41.07 |
| Y MOMENT BASE | 4.998 | 11.85 | -11.57 | -14.08 | -15.8 | -17.3 | -18.41 | -19.54 | -26.79 |
| Y MOMENT TOP | -9.927 | 10.6 | 12.66 | 14.81 | 16.51 | 17.96 | 18.54 | 21 | 36.44 |
| X ROTATION BASE | -3E-36 | -6E-06 | -1E-05 | -2E-05 | -2E-05 | -3E-05 | -3E-05 | -4E-05 | 1.1E-05 |
| X ROTATION TOP | -1E-05 | -2E-05 | -2E-05 | -3E-05 | -3E-05 | -4E-05 | -4E-05 | -2E-05 | -0.0002 |
| Y ROTATION BASE | 6.7E-36 | -7E-05 | -6E-05 | -7E-05 | -7E-05 | -8E-05 | -7E-05 | -0.0001 | -8E-06 |
| Y ROTATION TOP | -9E-05 | -6E-05 | -8E-05 | -8E-05 | -8E-05 | -8E-05 | -1E-04 | -3E-05 | -0.0002 |
| Diameter | 12 | 12 | 12 | 12 | 12 | 12 | 12 | 12 | 12 |
| Number | 4 | 4 | 4 | 4 | 4 | 4 | 4 | 4 | 4 |

COLUMN C3:

| | 1st floor | 2nd floor | 3rd floor | 4th floor | 5th floor | 6th floor | 7th floor | 8th floor | roof |
|---|---|---|---|---|---|---|---|---|---|
| AXIAL FORCE | -2200 | -2056 | -1922 | -1653 | -1381 | -1097 | -799.6 | -487.7 | -156.6 |
| X MOMENT BASE | -5.745 | -14.84 | -12.83 | -13.42 | -13.42 | -13.52 | -13.54 | -13.73 | -12.52 |
| X MOMENT TOP | 11.67 | 13.4 | 13.21 | 13.4 | 13.46 | 13.58 | 13.41 | 14.53 | 8.714 |
| Y MOMENT BASE | -9.748 | -26.76 | -29.5 | -34.76 | -38.47 | -41.5 | -44.07 | -44.47 | -50.62 |
| Y MOMENT TOP | 19.59 | 27.5 | 32.2 | 36.55 | 40.04 | 42.43 | 46.01 | 39.55 | 77.08 |
| X ROTATION BASE | -3E-38 | -7E-05 | -7E-05 | -8E-05 | -1E-04 | -0.0001 | -0.0001 | -0.0001 | -1E-05 |
| X ROTATION TOP | -0.0001 | -8E-05 | -1E-04 | -0.0001 | -0.0001 | -0.0001 | -0.0001 | -8E-05 | -0.0004 |
| Y ROTATION BASE | 2.6E-37 | 3E-07 | 2.8E-07 | 3.2E-07 | 4.1E-07 | 5.9E-07 | 6.8E-09 | 3.1E-06 | -5E-06 |
| Y ROTATION TOP | 4.8E-07 | 3E-07 | 4E-07 | 4.8E-07 | 5.7E-07 | 3.2E-07 | 1.8E-06 | -4E-06 | 4.7E-06 |
| Diameter | 12 | 12 | 12 | 12 | 12 | 12 | 12 | 16 | 20 |
| Number | 4 | 4 | 4 | 4 | 4 | 4 | 4 | 4 | 4 |

COLUMN A4:

| | 1st floor | 2nd floor | 3rd floor | 4th floor | 5th floor | 6th floor | 7th floor | 8th floor | roof |
|---|---|---|---|---|---|---|---|---|---|
| AXIAL FORCE | -1804 | -1722 | -1637 | -1426 | -1201 | -958.6 | -698 | -419.9 | -186.8 |
| X MOMENT BASE | -19.37 | -41.86 | -37.6 | -39.47 | -39.82 | -40.23 | -40.96 | -39.06 | -36.38 |
| X MOMENT TOP | 35.42 | 38.54 | 38.79 | 39.55 | 40.24 | 39.76 | 43.89 | 33.91 | 52.45 |
| Y MOMENT BASE | -4.994 | -10.82 | -9.42 | -9.731 | -9.655 | -9.679 | -9.64 | -9.795 | -8.97 |
| Y MOMENT TOP | 9.189 | 9.81 | 9.64 | 9.682 | 9.658 | 9.73 | 9.428 | 10.72 | 6.424 |
| X ROTATION BASE | -4E-37 | -8E-10 | 6.2E-08 | -2E-08 | 4.3E-07 | -1E-06 | 7.1E-06 | -2E-05 | 3.2E-05 |
| X ROTATION TOP | 1.8E-08 | 5.4E-08 | 5.8E-08 | 2.7E-07 | -6E-07 | 3.5E-06 | -1E-05 | 2.8E-05 | -3E-05 |
| Y ROTATION BASE | -7E-36 | 0.00013 | 8.7E-05 | 9.8E-05 | 9.8E-05 | 0.0001 | 9.8E-05 | 0.00012 | 3.8E-05 |
| Y ROTATION TOP | 0.00016 | 8.1E-05 | 0.0001 | 9.9E-05 | 0.0001 | 0.0001 | 0.00011 | 7.2E-05 | 0.00025 |
| Diameter | 12 | 12 | 12 | 12 | 12 | 12 | 12 | 16 | 16 |
| Number | 4 | 4 | 4 | 4 | 4 | 4 | 4 | 4 | 4 |

COLUMN B4:

| | 1st floor | 2nd floor | 3rd floor | 4th floor | 5th floor | 6th floor | 7th floor | 8th floor | roof |
|---|---|---|---|---|---|---|---|---|---|
| AXIAL FORCE | -2431 | -2235 | -2053 | -1730 | -1407 | -1077 | -734.6 | -377.8 | -139.3 |
| X MOMENT BASE | 13.95 | 36.39 | 36.15 | 40.88 | 43.77 | 46.39 | 48.48 | 48.41 | 51.31 |
| X MOMENT TOP | -27.75 | -35.31 | -38.68 | -42.2 | -45.18 | -47.07 | -50.3 | -43.7 | -74.6 |
| Y MOMENT BASE | -5.414 | -13.76 | -11.98 | -12.6 | -12.65 | -12.8 | -12.83 | -13.11 | -12.06 |
| Y MOMENT TOP | 10.89 | 12.47 | 12.37 | 12.6 | 12.71 | 12.89 | 12.63 | 14.24 | 7.964 |
| X ROTATION BASE | 4.5E-37 | 2.9E-07 | 1.3E-07 | 2E-07 | 1E-07 | -3E-08 | 1.1E-06 | -4E-06 | 8.3E-06 |
| X ROTATION TOP | 3.6E-07 | 8.5E-08 | 1.9E-07 | 6.8E-08 | 1.1E-07 | 5.8E-07 | -2E-06 | 8.2E-06 | -4E-05 |
| Y ROTATION BASE | 2.7E-36 | -9E-05 | -8E-05 | -1E-04 | -0.0001 | -0.0001 | -0.0001 | -0.0001 | -3E-05 |
| Y ROTATION TOP | -0.0001 | -9E-05 | -0.0001 | -0.0001 | -0.0001 | -0.0001 | -0.0001 | -9E-05 | -0.0003 |
| Diameter | 12 | 12 | 12 | 12 | 12 | 12 | 12 | 12 | 16 |
| Number | 4 | 4 | 4 | 4 | 4 | 4 | 4 | 4 | 4 |

## 1.2 Sensitivity Studies

Several finite-element models of the above structure were created. The most complex was the model that was exposed to a series of fires as described in chapters five to seven. To develop this model and ensure that the conclusions drawn in the various chapters were appropriate, a series of sensitivity studies were conducted. The final results of the various sensitivity studies are presented below. Though they are presented sequentially, it should be noted that the process was an iterative one, whereby the interaction of each of the parameters was analysed.

In this sensitivity study, there were two driving motivations: firstly to ensure that the model was numerically stable; and secondly to ensure that the numerical stability did not compromise the results of the analyses. The need for stability was paramount, as the model had to be capable of running with any number of different fires, and each analysis had to be directly comparable. It was not possible, therefore, to reduce the time step, or use extra damping with only one particularly unstable model. Each of the models had to be exactly the same with the exception of the design fire.

Each of the sensitivity studies was a model of the concrete structure exposed to the "base case" 25% burn area fire. The results are reported in terms of the maximum deflection obtained and given in terms of their own variation.

### 1.2.1 Mesh Sensitivity

#### 1.2.1.1 Slab Mesh

The refinement of the shell mesh in the slab was changed to allow the overall impact if the fire to be assessed. Figure 1 shows the deflection as a function of element size. It can be seen that only very minor changes are induced by refining the shell mesh. It is also notable that only the coarsest shell refinement remains numerically stable throughout the analysis. It was, therefore, decided to use shell elements of an average size of 0.4375m; that is approximately 16 elements per span.

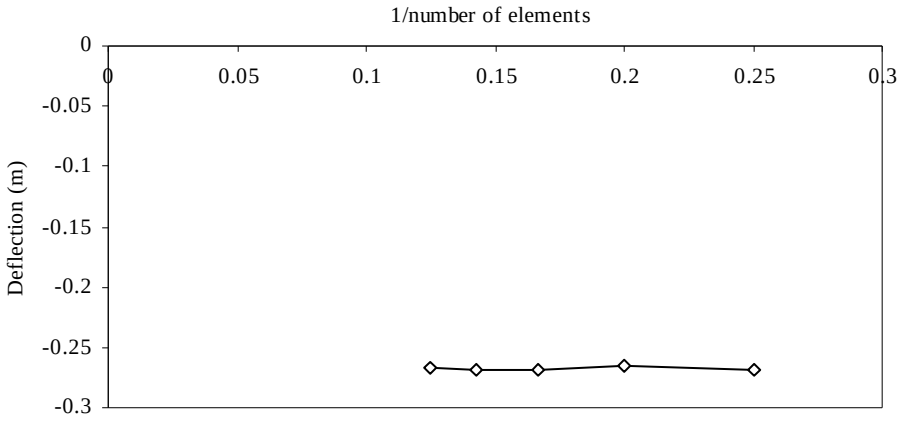


Figure 1. Shell mesh sensitivity.

#### 1.2.1.2 Vertical Column Refinement

The vertical refinement of the column mesh was changed to allow the sensitivity to be studied. The 3.8m high columns were modelled with 8, 10, 12, 14, 16, 18, 20, 22, 24, and 26 elements. Figure 2 show the variation in defection as the element size in the column mesh is changed. It can be seen that there is significant variation due to element size. There is an obvious convergence towards a single value at the intersect of the line with the *y*-axis; a best fit line shows that this intersect is at -0.3572m. It was decided to use an element size of 0.21m (or 18 elements per column height). This allowed

the simulation to take place in a non-prohibitively long time (t<48hrs on 4 processors); and allowed a relatively close match to the maximum refinement used (9.7%).

It must be acknowledged though that the total error from the predicted intersection with the *y*-axis is almost 20%. In most cases this would be unsatisfactory; however, in the case of the modelling of concrete columns at high temperature, the use of solid elements was the only viable option for the more realistic representation of differential heating across elements. Though beam elements are available within the Abaqus package, they can only be modelled with four temperature definition points and cannot be used with a material model that can adequately represent concrete.

It was decided, therefore, that though not an ideal solution, the modelling of the columns with a fairly refined mesh of solid elements was the best option available. Other authors have encountered this problem and have implemented a similar solution [15].

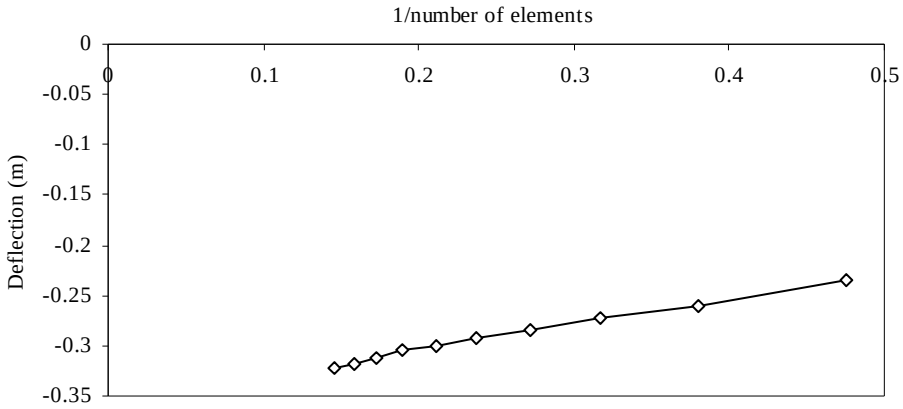


Figure 2. Sensitivity to vertical column mesh

### 1.2.1.3 Column Lateral Refinement

A similar study was conducted on the lateral refinement of the column mesh. It was found that deflections were less highly influenced by the number of elements present laterally in the column (Figure 3). However, it was also found that the model was numerically unstable when a small number of elements were used and that the simulations were very slow when a large number of elements were used. It was decided therefore to use an 8×8 element mesh. This was much more refined than the mesh used in previous studies [15].

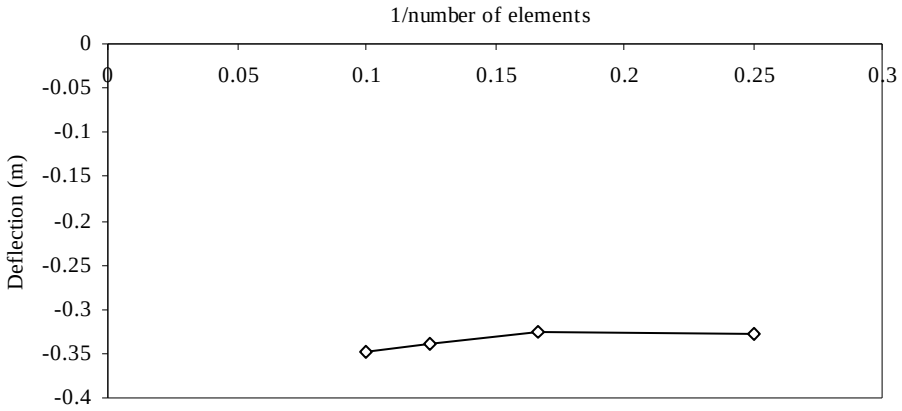


Figure 3. Sensitivity to number of element laterally across column.

### 1.2.2 Tension Sensitivity

The finite-element model was very sensitive to variations in the tension definition. It was found that minor changes in the tension material model could result in very little change in the global behaviour of the structure, but could cause numerical instabilities to arise. A number of studies were conducted to analyse the influence of tension definition on the model. The ultimate tensile strength was varied, as was the fracture energy used to model the tension softening. The fracture energy was varied through the use of tension stiffening.

#### 1.2.2.1 Ultimate tensile strength

There are a number of possible values that can be used for the ultimate tensile strength of concrete. As described in chapter two, the variation in parameters is complex and is often determined by the specific mix of concrete. Three different methods for deriving the values were used in this work: the method given by Rots [138]; the method by Shah [145]; and the

values defined in the Eurocode [54]. Though each of these parameters was studied in conjunction with fracture energy, to avoid confusion, only a single fracture energy will be presented in this section.

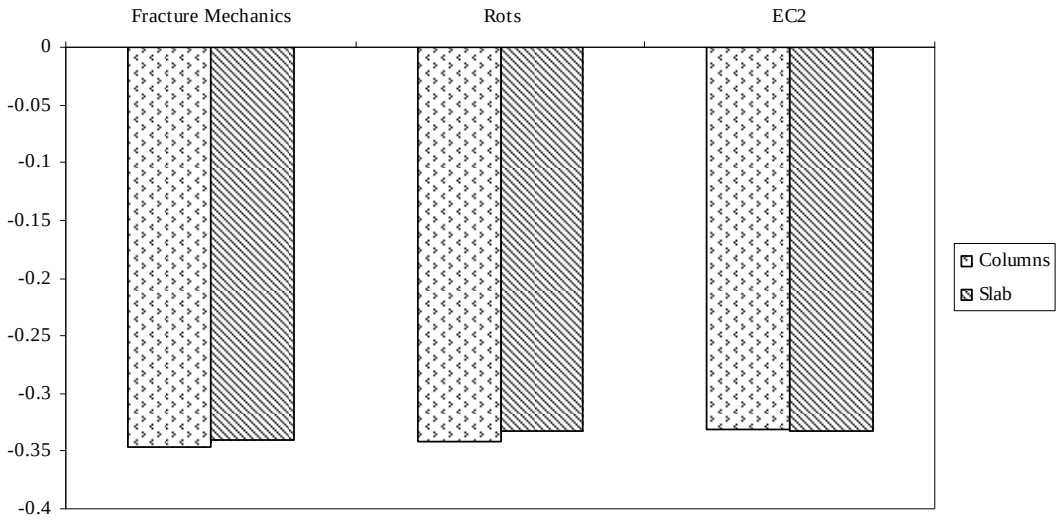


Figure 4. Sensitivity to ultimate tensile strength.

The tension properties were varied separately in the columns and in the slabs to allow the relative effects to be studied. It can be see from figure 4 that changing the value of ultimate tensile stress causes only relatively small changes in the total deflections. The differences are 4.6% by varying the properties of the columns and 1.9% by varying the properties of the slab. The aim of the modelling was to be as consistent to the Eurocode as possible while maintaining the stability of the model. It was decided therefore to use the Eurocode values of tension in the slab, but use the values given in the "Fracture Mechanics" book by Saha in the columns. It was only in using the values given by Saha that the model became sufficiently stable to be used

multiple times. Since this gave an error of only 4.6% it was decided that this was acceptable.

#### 1.2.2.2 Fracture Energy

A number of different fracture energies are available from literature [22,23,33,50]. It was found that the use of fracture energies recommended in the FIB code resulted in models that were very numerically unstable. The sensitivity study was therefore conducted to establish what degree of influence the fracture energy had over the global behaviour of the model. The fracture energies were varied in the columns and in the slabs independently to allow the relative impacts to be analysed (figure 5).

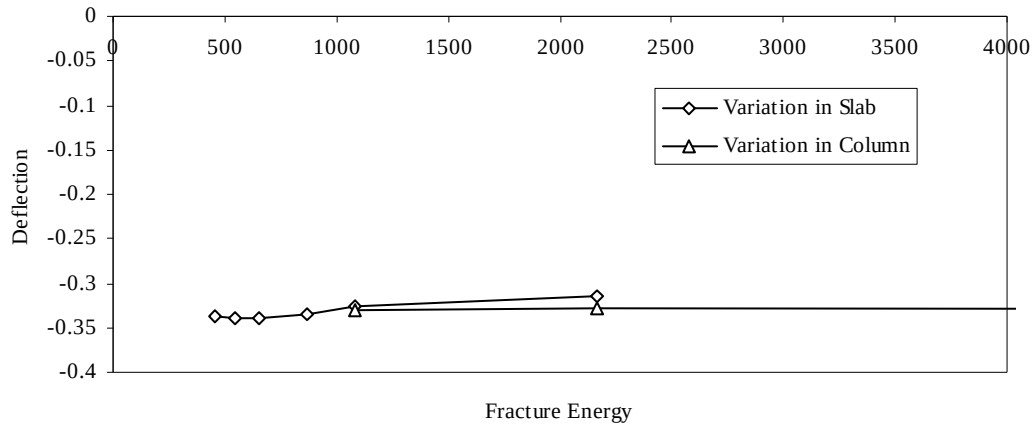


Figure 5. Variation of fracture energy in the material properties of the slab and column.

The sensitivity study showed that the solid-element columns were very numerically unstable at low fracture energies. Indeed, the only simulation which remained stable throughout was where ductile tensile properties were assumed. This gave an error of 0.3% relative to the deflection obtained at the

lowest fracture energy that produced a reliable result. It was decided that this small error was acceptable as the majority of the columns were likely to remain in compression due to the high axial loads they were carrying.

The slabs were more stable at lower fracture energies; however, when fracture energies lower than 454N/m were used, some instability remained. It was decided therefore to use the artificially high fracture energy of 1085N/m to allow repeatability of the simulation with different fires. This compromise led to an error of 3.4% when compared to the minimum value of fracture energy successfully applied. It should also be noted that unlike the mesh sensitivity studies, the fracture energy study did not clearly indicate convergence. It is difficult therefore to quantify the exact error.

# Appendix III

## Response and Capacity of Structure

## 1. Response and Capacity of Structure

In chapter five, the generic concrete structure is exposed to a number of different fires. Example plots are given to show the changes in loading and capacity which the columns in the building experience. For reference, this appendix provides the full set of plots for each building. The imposed loading, and sectional capacity at key points during the analysis are presented.

The data for three different fires are presented: the standard fire; the "short hot" fire; and the "long cool" fire. The graphs are numbered in accordance with their job number: 901 refers to the Standard Fire; 902 refers to the "short hot" fire; 903 refers to the "long cool" fire; and 905 refers to the 5% burn area base case fire.

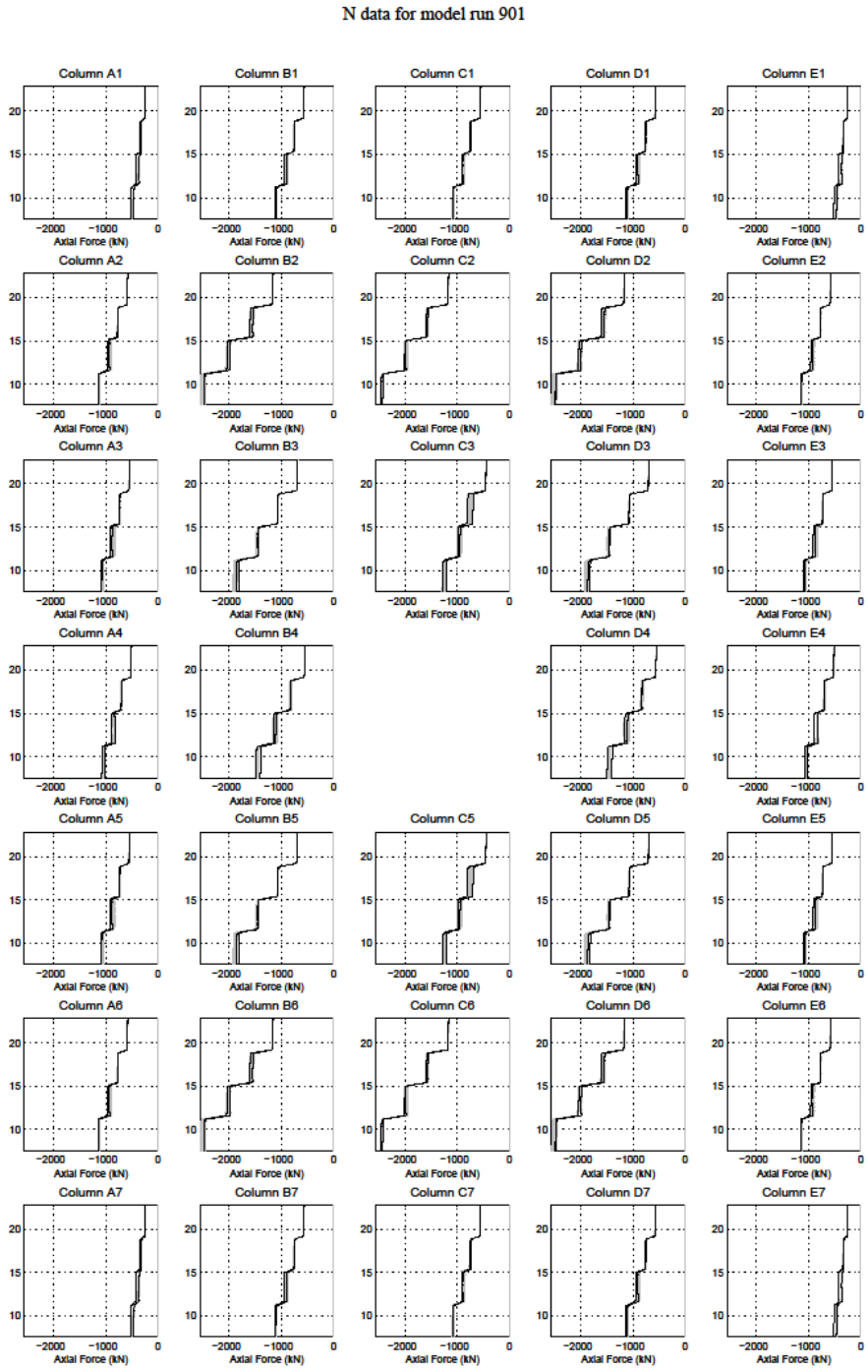
N data for model run 901
Column A1
Column B1
Column C1
Column D1
Column E1
Column A2
Column B2
Column C2
Column D2
Column E2
Column A3
Column B3
Column C3
Column D3
Column E3
Column A4
Column B4
Column D4
Column E4
Column A5
Column B5
Column C5
Column D5
Column E5
Column A6
Column B6
Column C6
Column D6
Column E6
Column A7
Column B7
Column C7
Column D7
Column E7
Axial Force (kN)

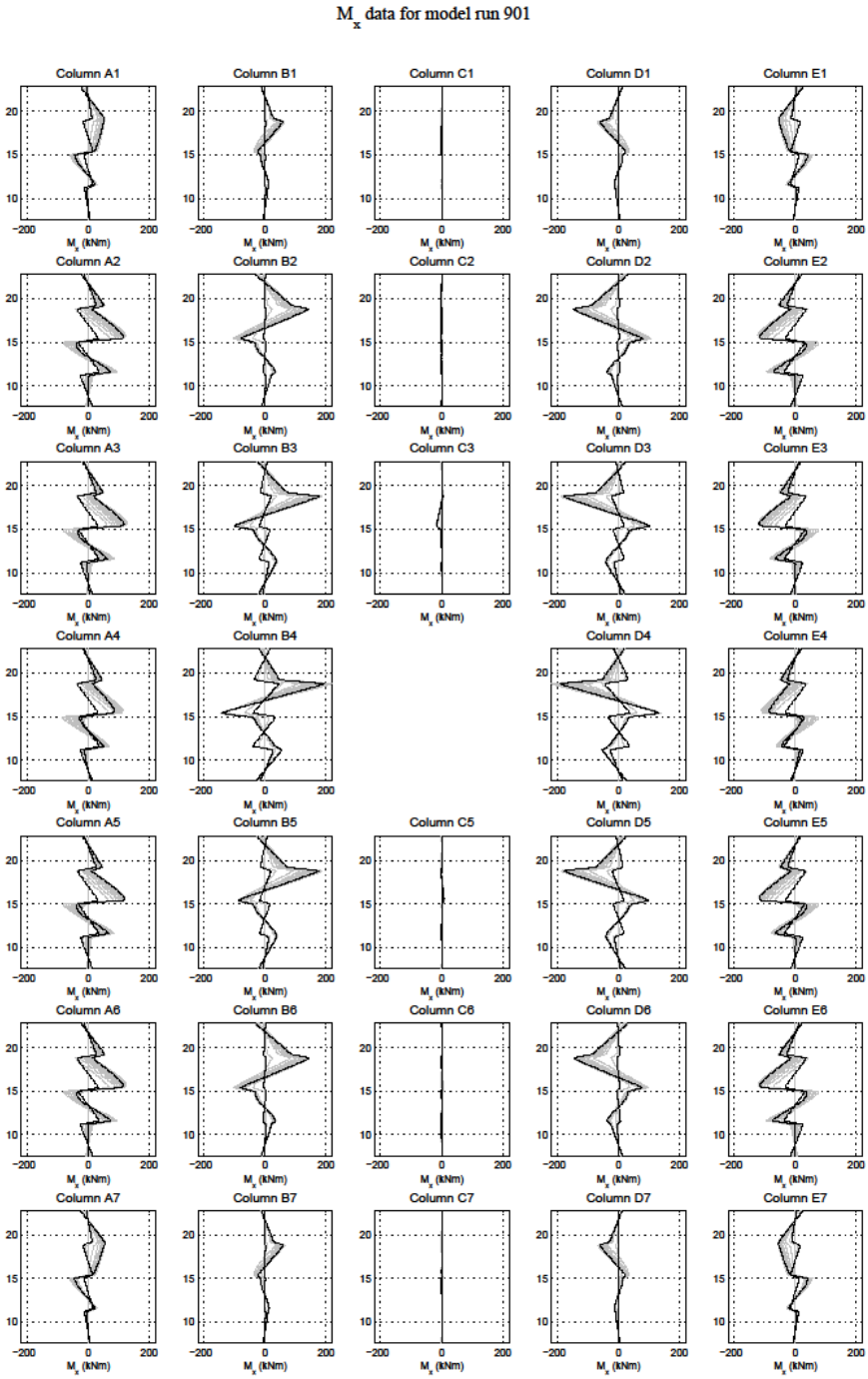
M_x data for model run 901
Column A1
Column B1
Column C1
Column D1
Column E1
Column A2
Column B2
Column C2
Column D2
Column E2
Column A3
Column B3
Column C3
Column D3
Column E3
Column A4
Column B4
Column D4
Column E4
Column A5
Column B5
Column C5
Column D5
Column E5
Column A6
Column B6
Column C6
Column D6
Column E6
Column A7
Column B7
Column C7
Column D7
Column E7
M_x (kNm)

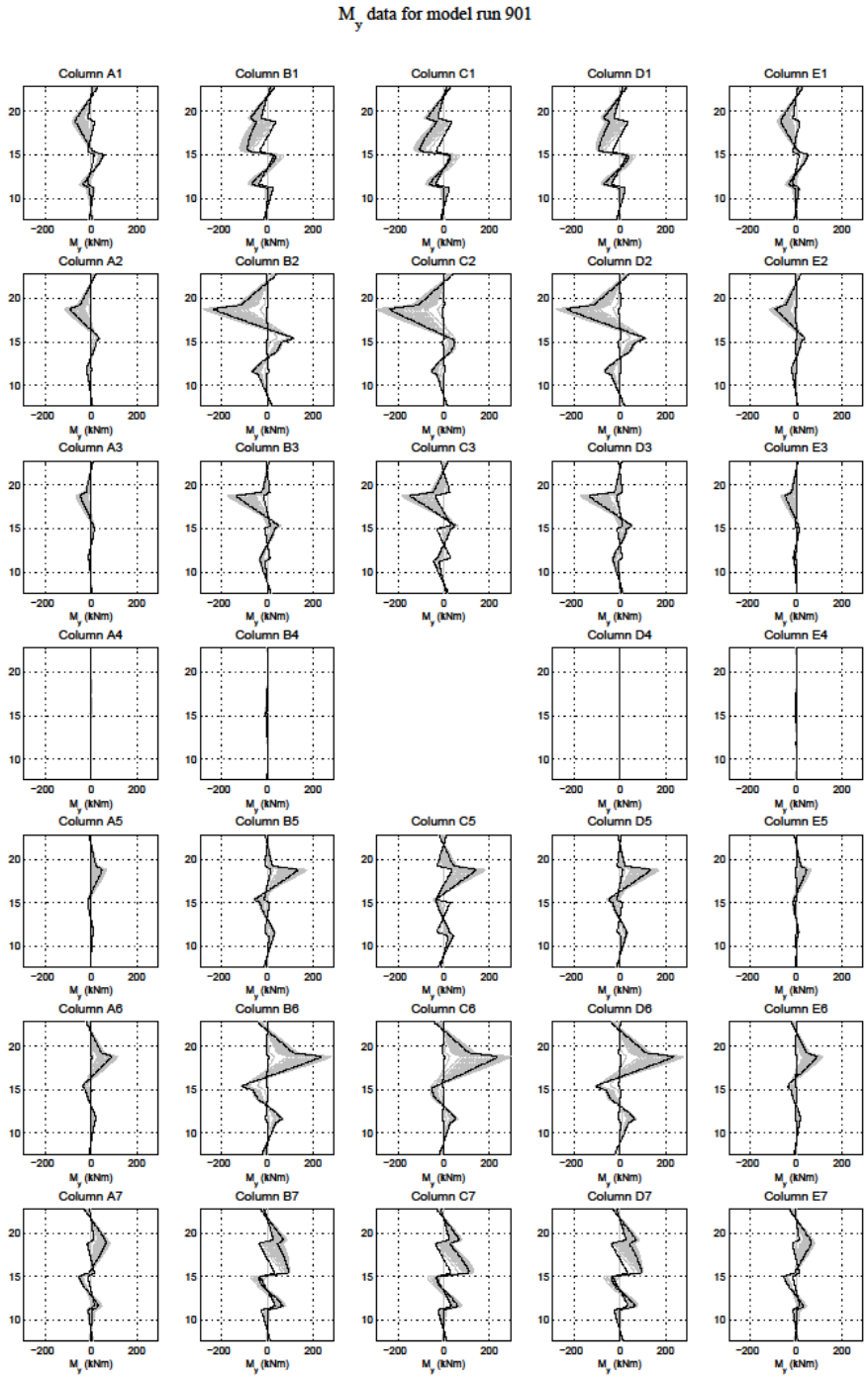
My data for model run 901
Column A1
Column B1
Column C1
Column D1
Column E1
Column A2
Column B2
Column C2
Column D2
Column E2
Column A3
Column B3
Column C3
Column D3
Column E3
Column A4
Column B4
Column D4
Column E4
Column A5
Column B5
Column C5
Column D5
Column E5
Column A6
Column B6
Column C6
Column D6
Column E6
Column A7
Column B7
Column C7
Column D7
Column E7
My (kNm)

V13 magnitude derived values 901

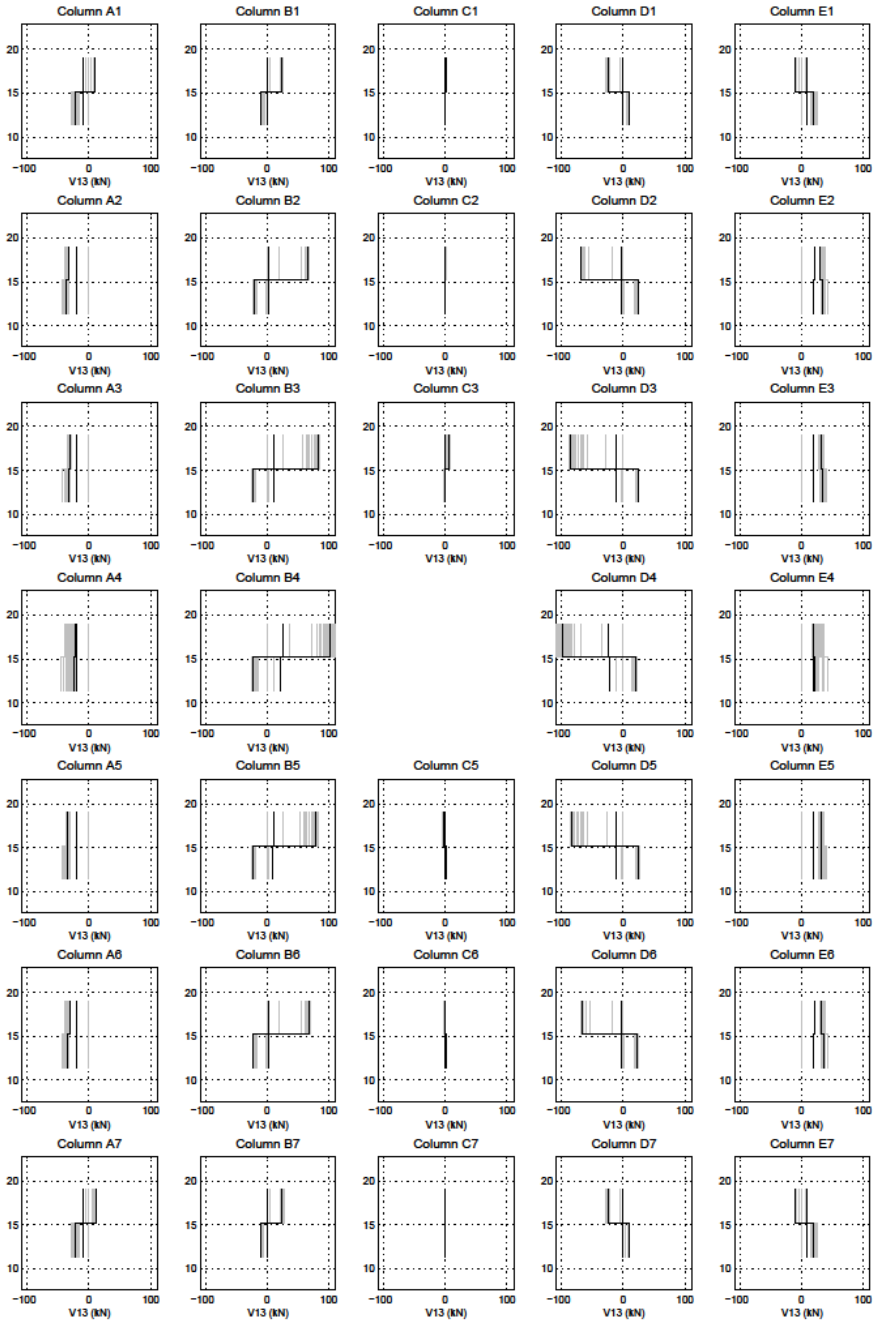

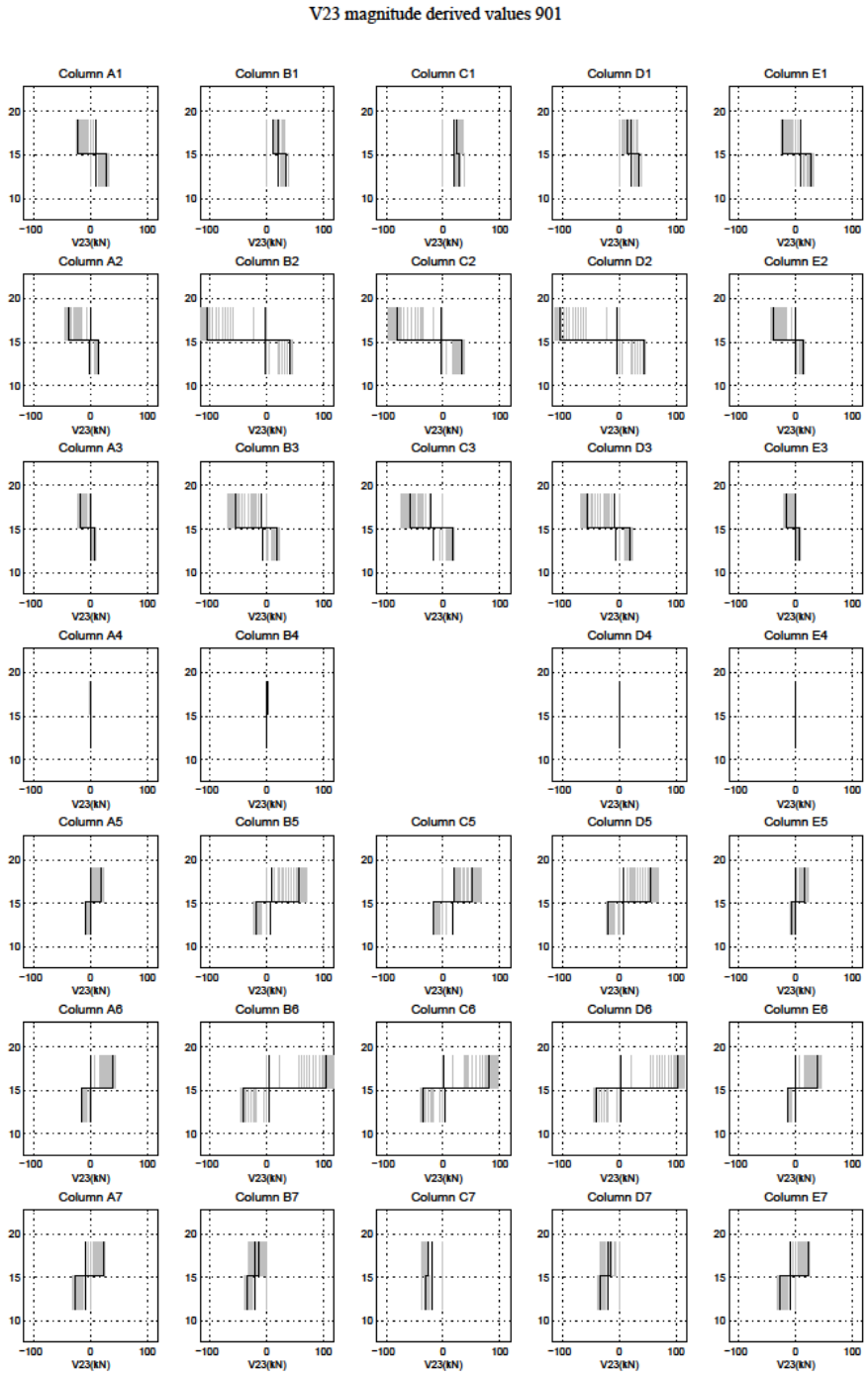
V23 magnitude derived values 901
Column A1
Column B1
Column C1
Column D1
Column E1
Column A2
Column B2
Column C2
Column D2
Column E2
Column A3
Column B3
Column C3
Column D3
Column E3
Column A4
Column B4
Column D4
Column E4
Column A5
Column B5
Column C5
Column D5
Column E5
Column A6
Column B6
Column C6
Column D6
Column E6
Column A7
Column B7
Column C7
Column D7
Column E7
V23(kN)

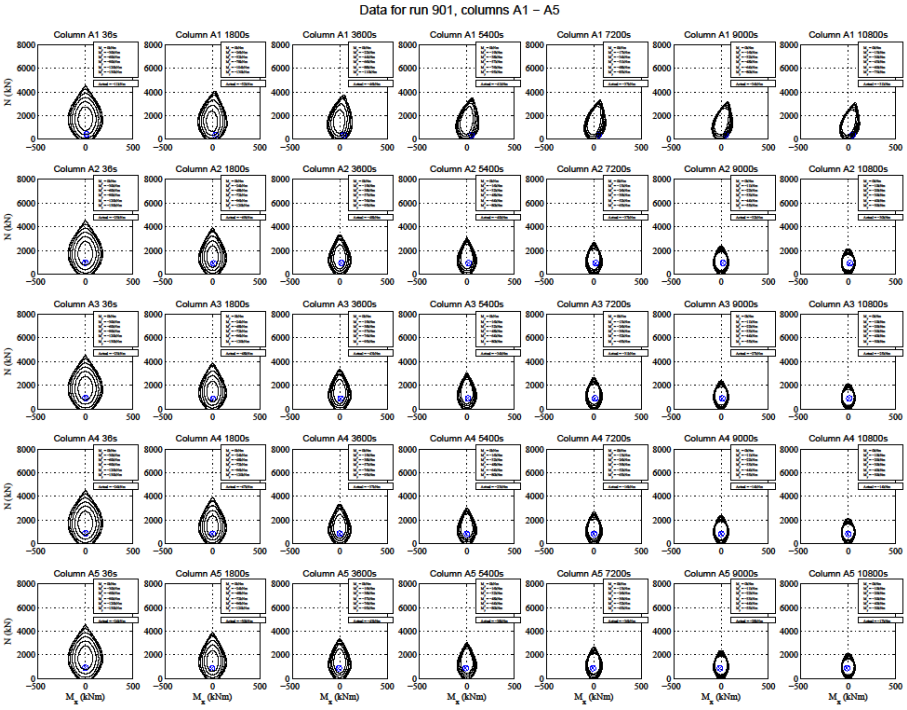
Data for run 901, columns A1 – A5
Column A1 36s
Column A1 1800s
Column A1 3600s
Column A1 5400s
Column A1 7200s
Column A1 9000s
Column A1 10800s
Column A2 36s
Column A2 1800s
Column A2 3600s
Column A2 5400s
Column A2 7200s
Column A2 9000s
Column A2 10800s
Column A3 36s
Column A3 1800s
Column A3 3600s
Column A3 5400s
Column A3 7200s
Column A3 9000s
Column A3 10800s
Column A4 36s
Column A4 1800s
Column A4 3600s
Column A4 5400s
Column A4 7200s
Column A4 9000s
Column A4 10800s
Column A5 36s
Column A5 1800s
Column A5 3600s
Column A5 5400s
Column A5 7200s
Column A5 9000s
Column A5 10800s
N (kN)
M_x (kNm)

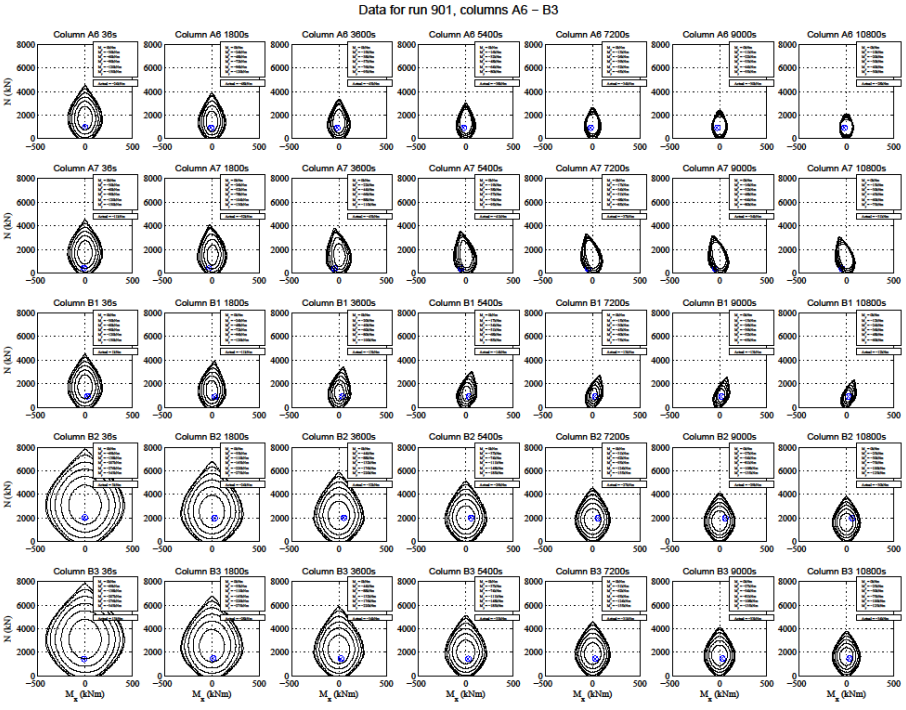
Data for run 901, columns A6 – B3
Column A6 36s
Column A6 1800s
Column A6 3600s
Column A6 5400s
Column A6 7200s
Column A6 9000s
Column A6 10800s
Column A7 36s
Column A7 1800s
Column A7 3600s
Column A7 5400s
Column A7 7200s
Column A7 9000s
Column A7 10800s
Column B1 36s
Column B1 1800s
Column B1 3600s
Column B1 5400s
Column B1 7200s
Column B1 9000s
Column B1 10800s
Column B2 36s
Column B2 1800s
Column B2 3600s
Column B2 5400s
Column B2 7200s
Column B2 9000s
Column B2 10800s
Column B3 36s
Column B3 1800s
Column B3 3600s
Column B3 5400s
Column B3 7200s
Column B3 9000s
Column B3 10800s
N (kN)
M_x (kNm)

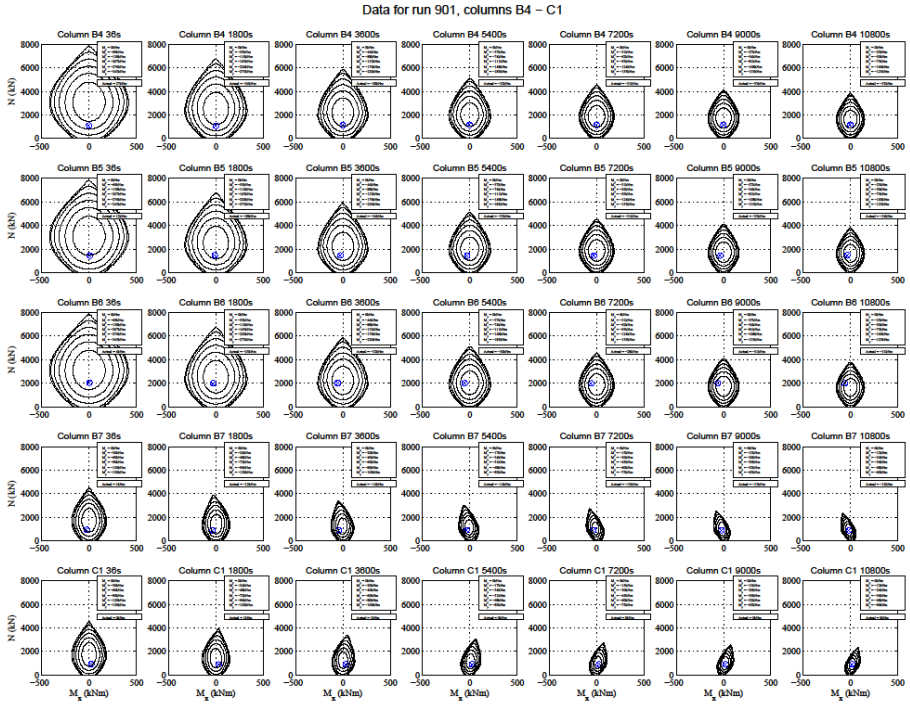
Data for run 901, columns B4 – C1
Column B4 36s
Column B4 1800s
Column B4 3600s
Column B4 5400s
Column B4 7200s
Column B4 9000s
Column B4 10800s
Column B5 36s
Column B5 1800s
Column B5 3600s
Column B5 5400s
Column B5 7200s
Column B5 9000s
Column B5 10800s
Column B6 36s
Column B6 1800s
Column B6 3600s
Column B6 5400s
Column B6 7200s
Column B6 9000s
Column B6 10800s
Column B7 36s
Column B7 1800s
Column B7 3600s
Column B7 5400s
Column B7 7200s
Column B7 9000s
Column B7 10800s
Column C1 36s
Column C1 1800s
Column C1 3600s
Column C1 5400s
Column C1 7200s
Column C1 9000s
Column C1 10800s
N (kN)
M_x (kNm)

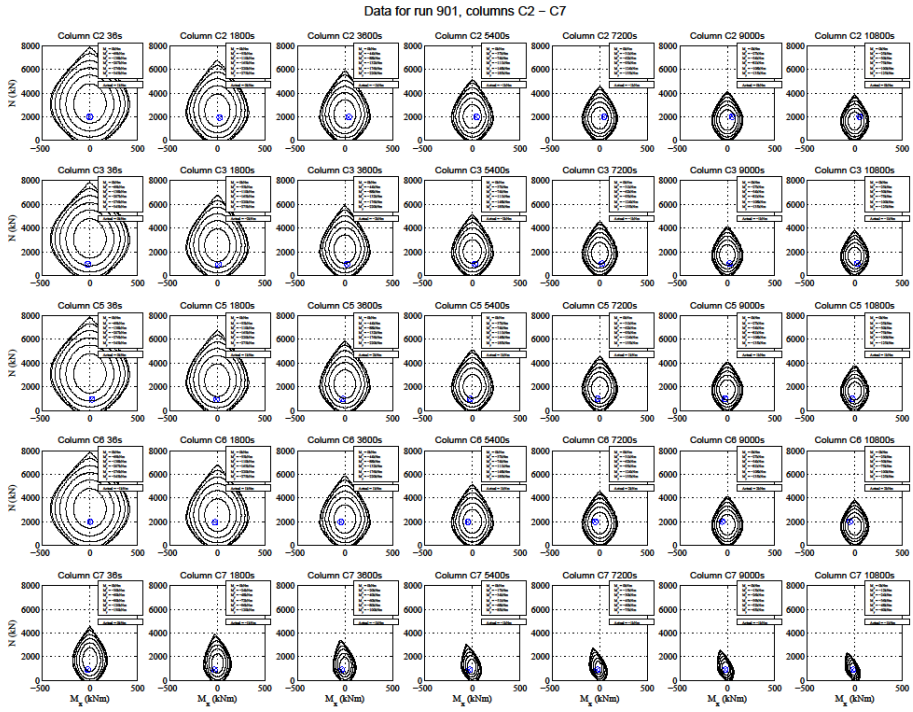
Data for run 901, columns C2 – C7
Column C2 36s
Column C2 1800s
Column C2 3600s
Column C2 5400s
Column C2 7200s
Column C2 9000s
Column C2 10800s
Column C3 36s
Column C3 1800s
Column C3 3600s
Column C3 5400s
Column C3 7200s
Column C3 9000s
Column C3 10800s
Column C5 36s
Column C5 1800s
Column C5 3600s
Column C5 5400s
Column C5 7200s
Column C5 9000s
Column C5 10800s
Column C6 36s
Column C6 1800s
Column C6 3600s
Column C6 5400s
Column C6 7200s
Column C6 9000s
Column C6 10800s
Column C7 36s
Column C7 1800s
Column C7 3600s
Column C7 5400s
Column C7 7200s
Column C7 9000s
Column C7 10800s
N (kN)
M_x (kNm)

Data for run 901, columns D1 – D5

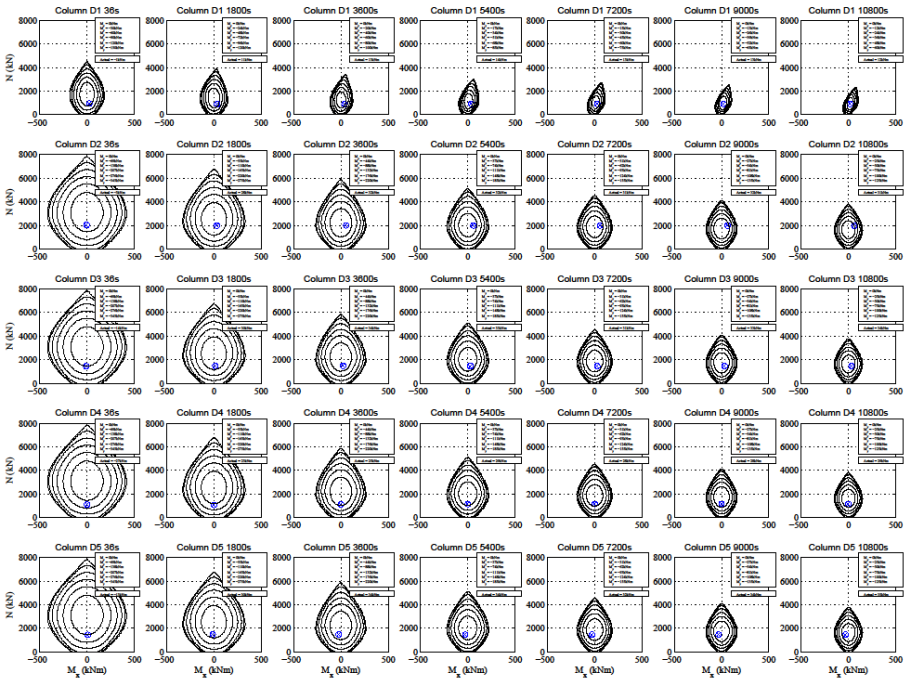


Data for run 901, columns D6 – E3

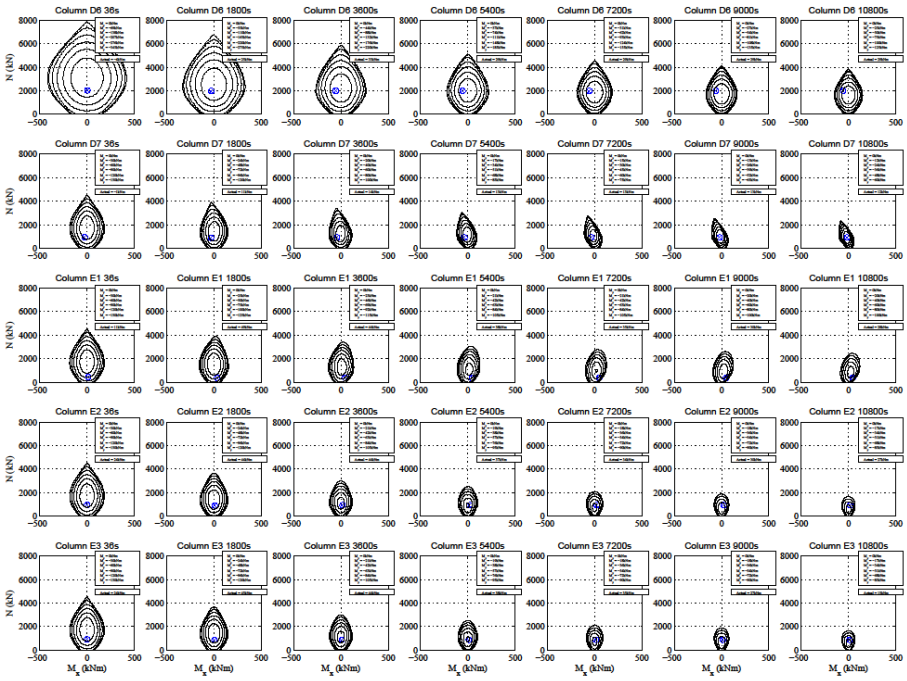

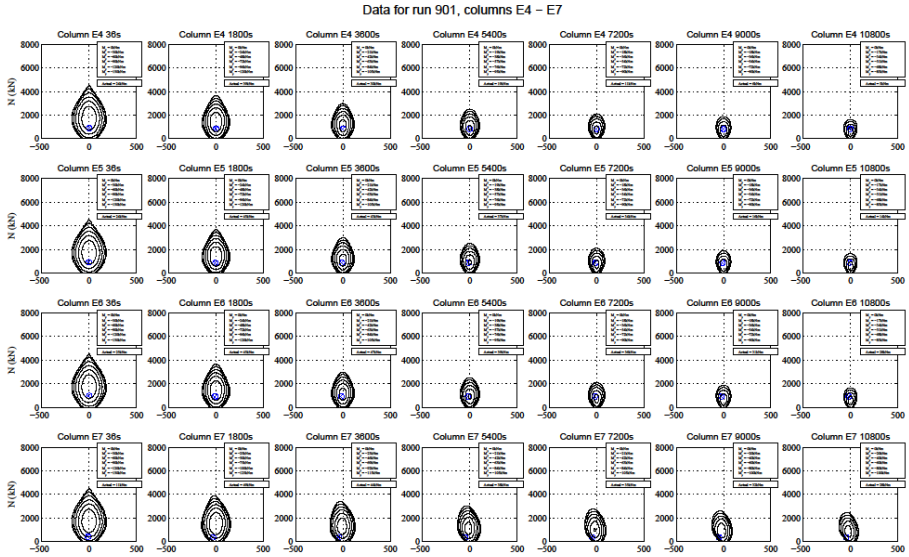
Data for run 901, columns E4 – E7
Column E4 36s
Column E4 1800s
Column E4 3600s
Column E4 5400s
Column E4 7200s
Column E4 9000s
Column E4 10800s
Column E5 36s
Column E5 1800s
Column E5 3600s
Column E5 5400s
Column E5 7200s
Column E5 9000s
Column E5 10800s
Column E6 36s
Column E6 1800s
Column E6 3600s
Column E6 5400s
Column E6 7200s
Column E6 9000s
Column E6 10800s
Column E7 36s
Column E7 1800s
Column E7 3600s
Column E7 5400s
Column E7 7200s
Column E7 9000s
Column E7 10800s
N (kN)

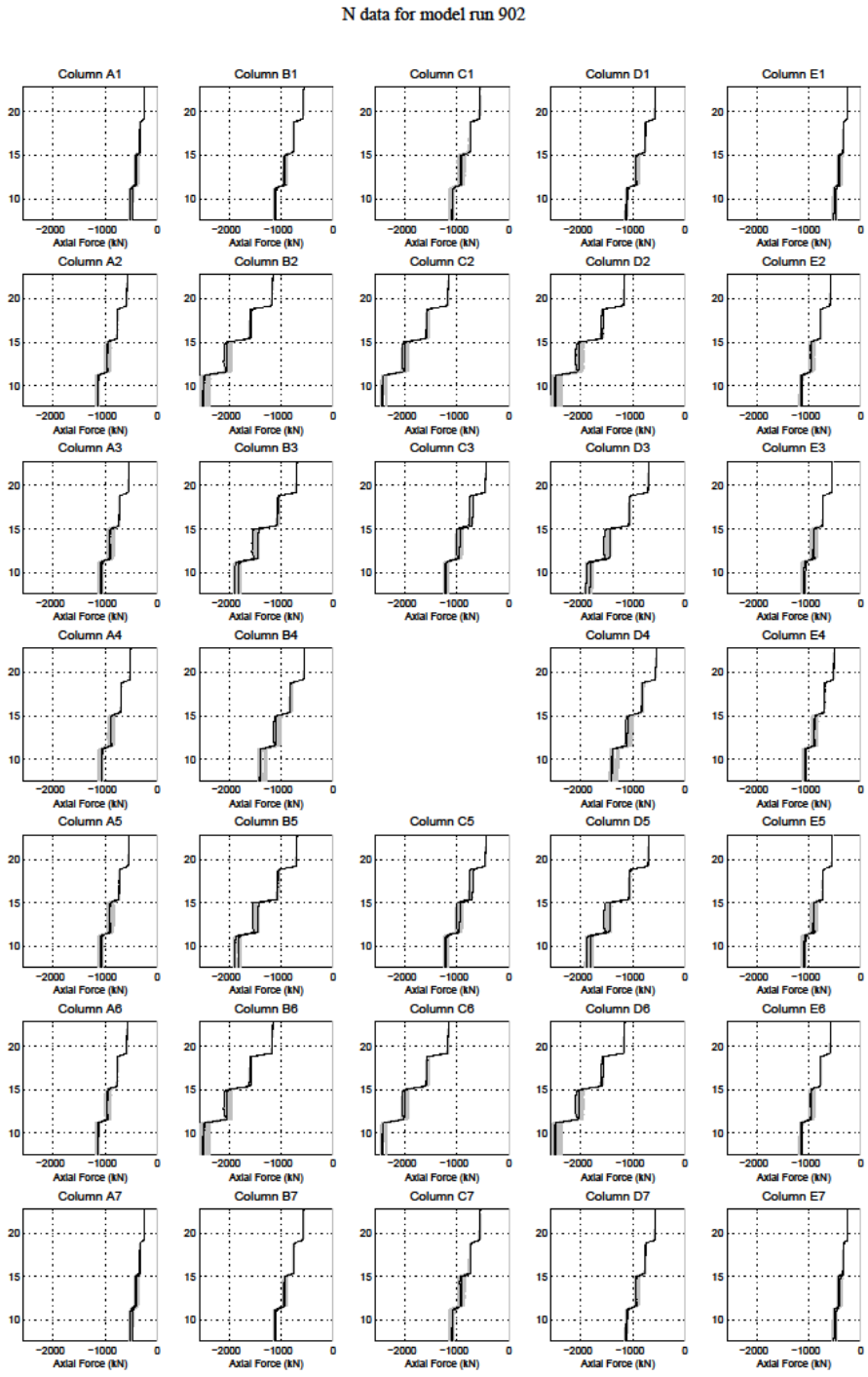
N data for model run 902
Column A1
Column B1
Column C1
Column D1
Column E1
Column A2
Column B2
Column C2
Column D2
Column E2
Column A3
Column B3
Column C3
Column D3
Column E3
Column A4
Column B4
Column D4
Column E4
Column A5
Column B5
Column C5
Column D5
Column E5
Column A6
Column B6
Column C6
Column D6
Column E6
Column A7
Column B7
Column C7
Column D7
Column E7
Axial Force (kN)

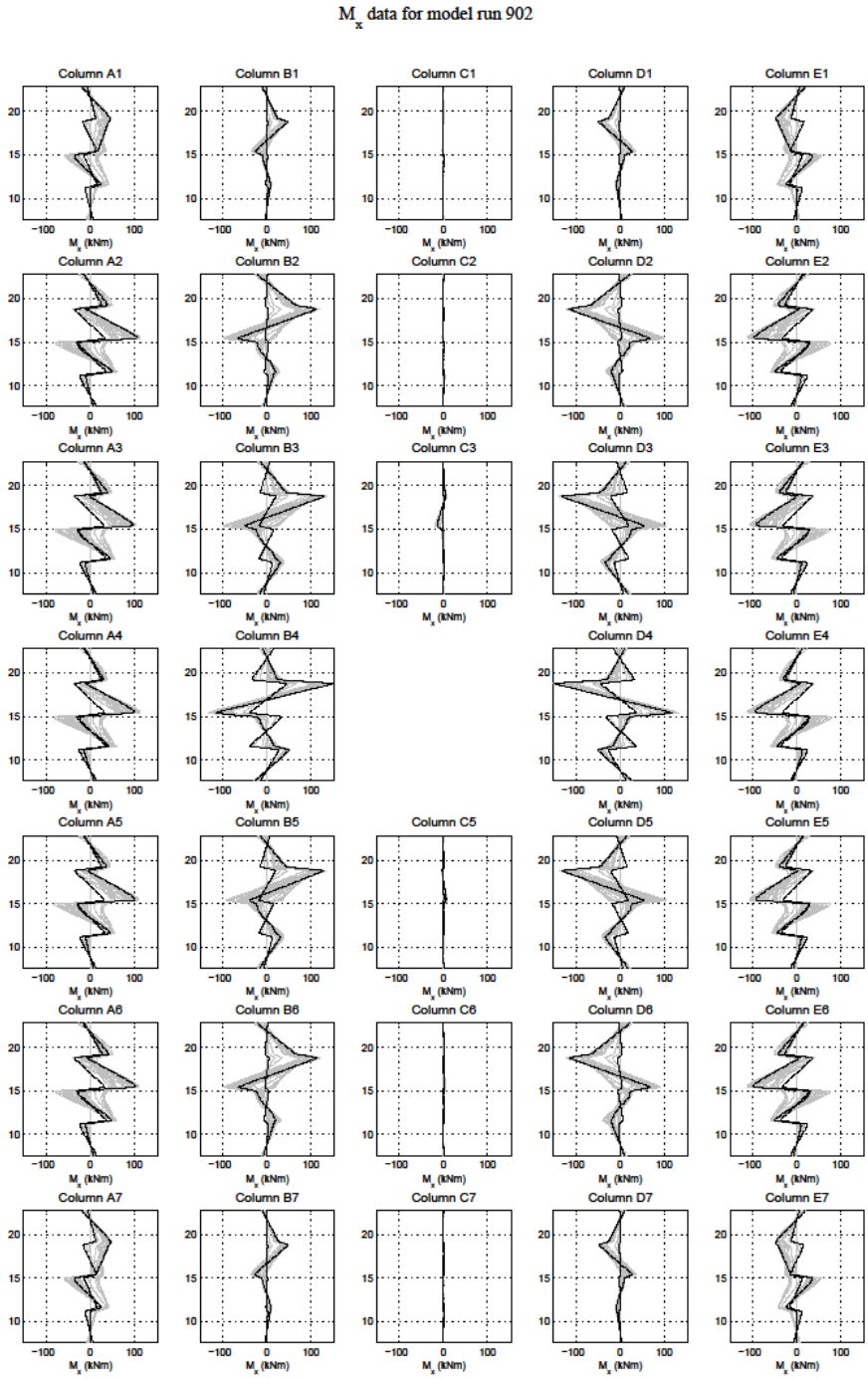
M_x data for model run 902
Column A1
Column B1
Column C1
Column D1
Column E1
Column A2
Column B2
Column C2
Column D2
Column E2
Column A3
Column B3
Column C3
Column D3
Column E3
Column A4
Column B4
Column D4
Column E4
Column A5
Column B5
Column C5
Column D5
Column E5
Column A6
Column B6
Column C6
Column D6
Column E6
Column A7
Column B7
Column C7
Column D7
Column E7
M_x (kNm)

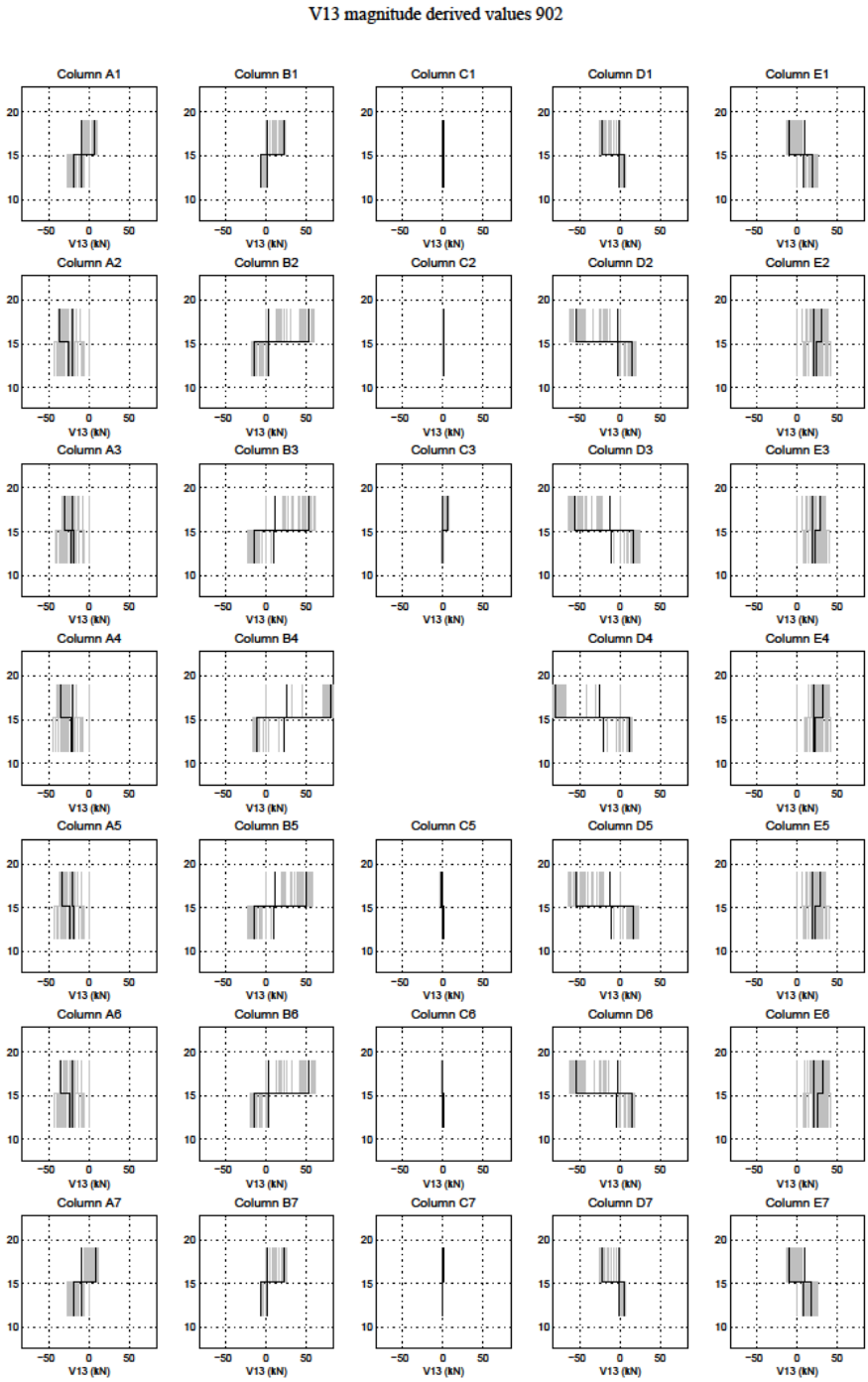
V13 magnitude derived values 902
Column A1
Column B1
Column C1
Column D1
Column E1
Column A2
Column B2
Column C2
Column D2
Column E2
Column A3
Column B3
Column C3
Column D3
Column E3
Column A4
Column B4
Column D4
Column E4
Column A5
Column B5
Column C5
Column D5
Column E5
Column A6
Column B6
Column C6
Column D6
Column E6
Column A7
Column B7
Column C7
Column D7
Column E7
V13 (kN)

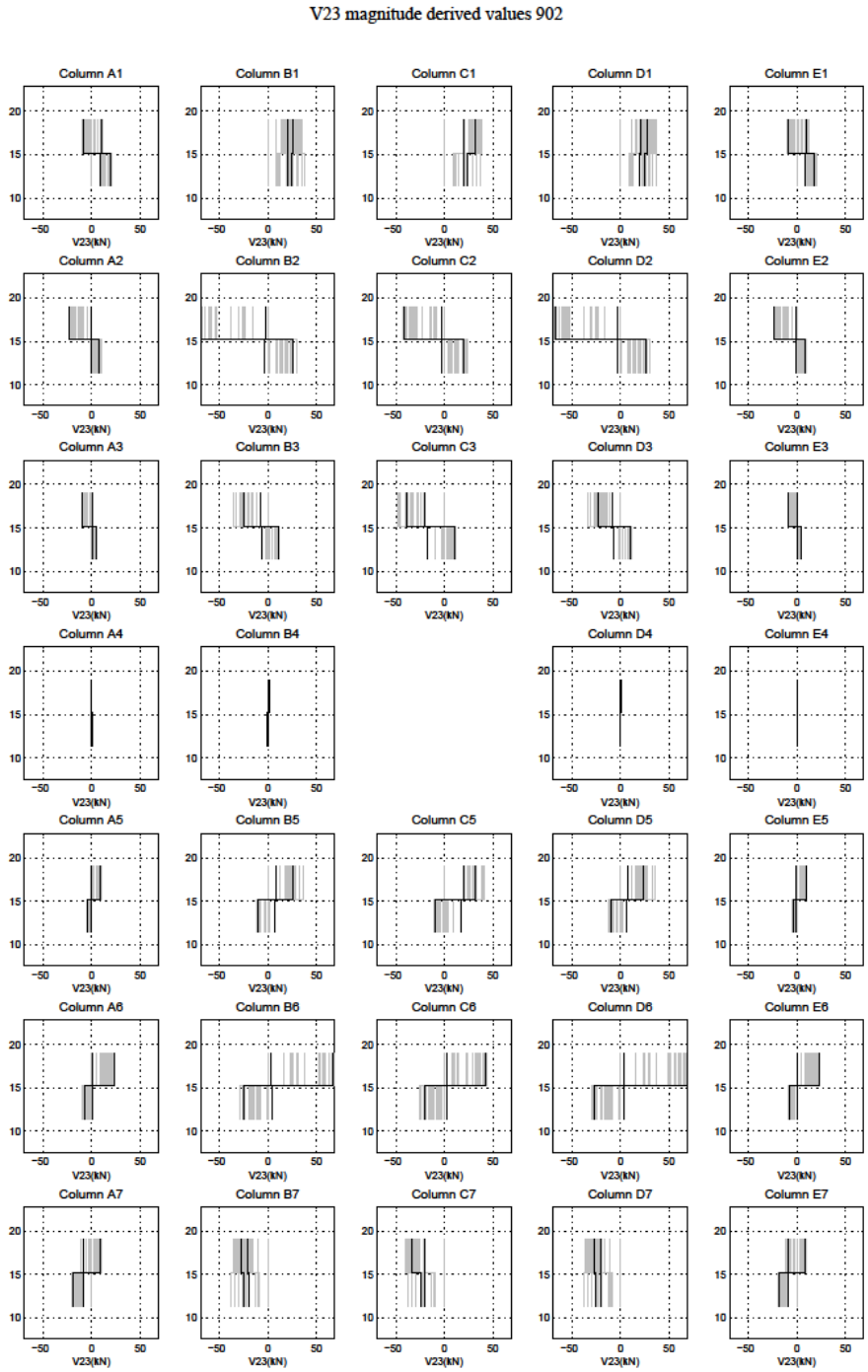
V23 magnitude derived values 902
Column A1
Column B1
Column C1
Column D1
Column E1
Column A2
Column B2
Column C2
Column D2
Column E2
Column A3
Column B3
Column C3
Column D3
Column E3
Column A4
Column B4
Column D4
Column E4
Column A5
Column B5
Column C5
Column D5
Column E5
Column A6
Column B6
Column C6
Column D6
Column E6
Column A7
Column B7
Column C7
Column D7
Column E7
V23(kN)

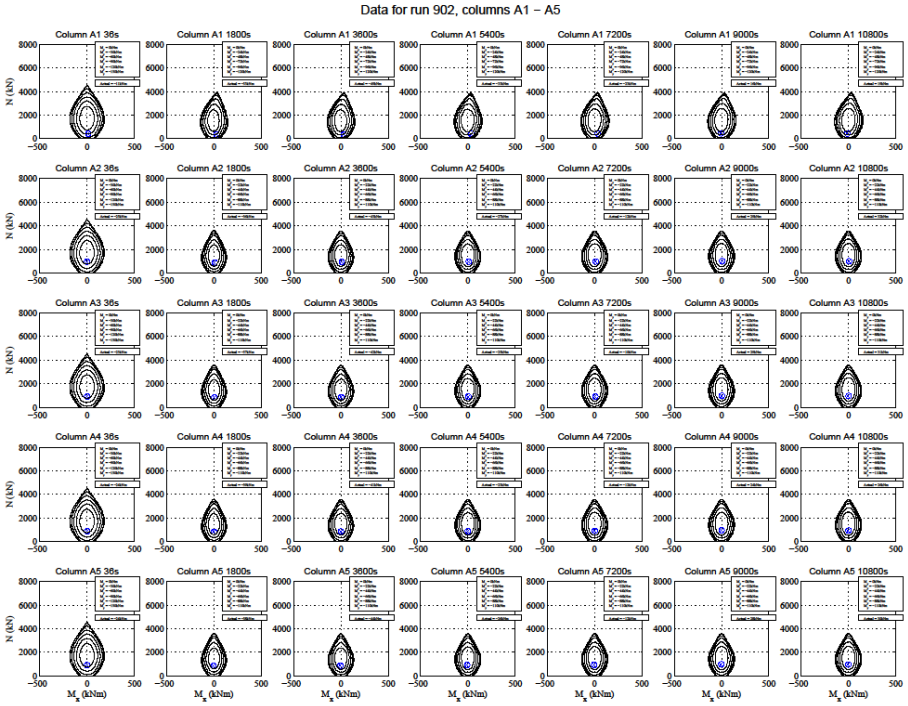
Data for run 902, columns A1 – A5
Column A1 36s
Column A1 1800s
Column A1 3600s
Column A1 5400s
Column A1 7200s
Column A1 9000s
Column A1 10800s
Column A2 36s
Column A2 1800s
Column A2 3600s
Column A2 5400s
Column A2 7200s
Column A2 9000s
Column A2 10800s
Column A3 36s
Column A3 1800s
Column A3 3600s
Column A3 5400s
Column A3 7200s
Column A3 9000s
Column A3 10800s
Column A4 36s
Column A4 1800s
Column A4 3600s
Column A4 5400s
Column A4 7200s
Column A4 9000s
Column A4 10800s
Column A5 36s
Column A5 1800s
Column A5 3600s
Column A5 5400s
Column A5 7200s
Column A5 9000s
Column A5 10800s
N (kN)
M_x (kNm)

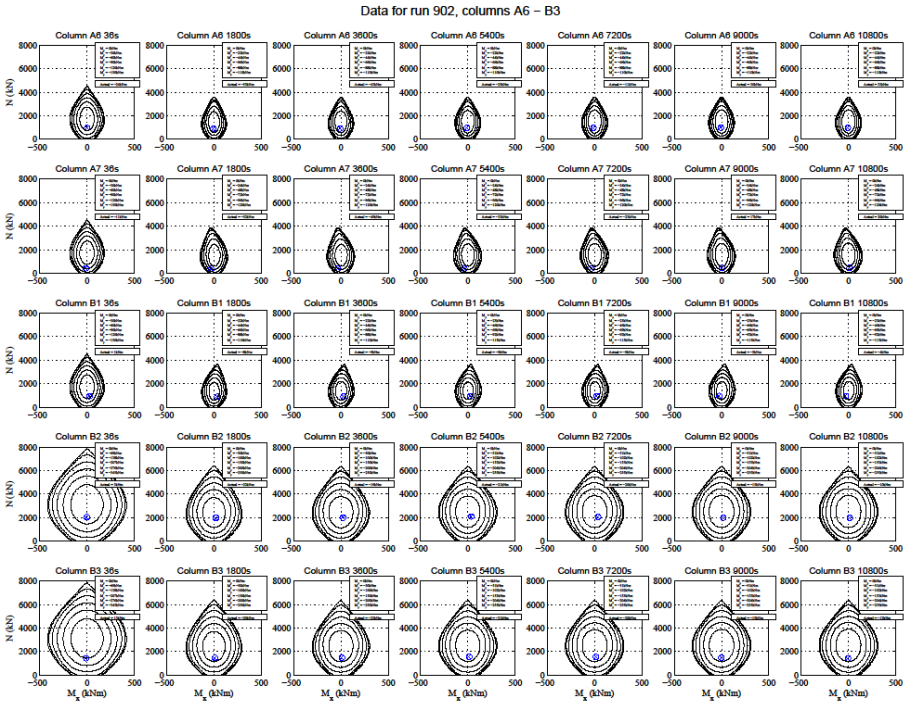
Data for run 902, columns A6 – B3
Column A6 36s
Column A6 1800s
Column A6 3600s
Column A6 5400s
Column A6 7200s
Column A6 9000s
Column A6 10800s
Column A7 36s
Column A7 1800s
Column A7 3600s
Column A7 5400s
Column A7 7200s
Column A7 9000s
Column A7 10800s
Column B1 36s
Column B1 1800s
Column B1 3600s
Column B1 5400s
Column B1 7200s
Column B1 9000s
Column B1 10800s
Column B2 36s
Column B2 1800s
Column B2 3600s
Column B2 5400s
Column B2 7200s
Column B2 9000s
Column B2 10800s
Column B3 36s
Column B3 1800s
Column B3 3600s
Column B3 5400s
Column B3 7200s
Column B3 9000s
Column B3 10800s
N (kN)
M_x (kNm)

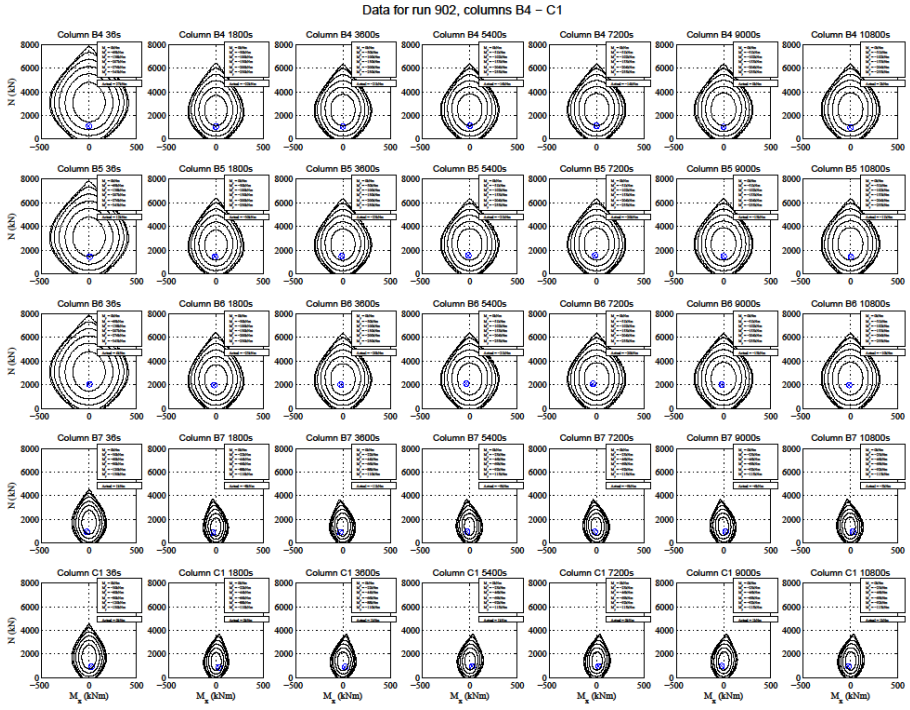
Data for run 902, columns B4 – C1
Column B4 36s
Column B4 1800s
Column B4 3600s
Column B4 5400s
Column B4 7200s
Column B4 9000s
Column B4 10800s
Column B5 36s
Column B5 1800s
Column B5 3600s
Column B5 5400s
Column B5 7200s
Column B5 9000s
Column B5 10800s
Column B6 36s
Column B6 1800s
Column B6 3600s
Column B6 5400s
Column B6 7200s
Column B6 9000s
Column B6 10800s
Column B7 36s
Column B7 1800s
Column B7 3600s
Column B7 5400s
Column B7 7200s
Column B7 9000s
Column B7 10800s
Column C1 36s
Column C1 1800s
Column C1 3600s
Column C1 5400s
Column C1 7200s
Column C1 9000s
Column C1 10800s
N (kN)
M_x (kNm)

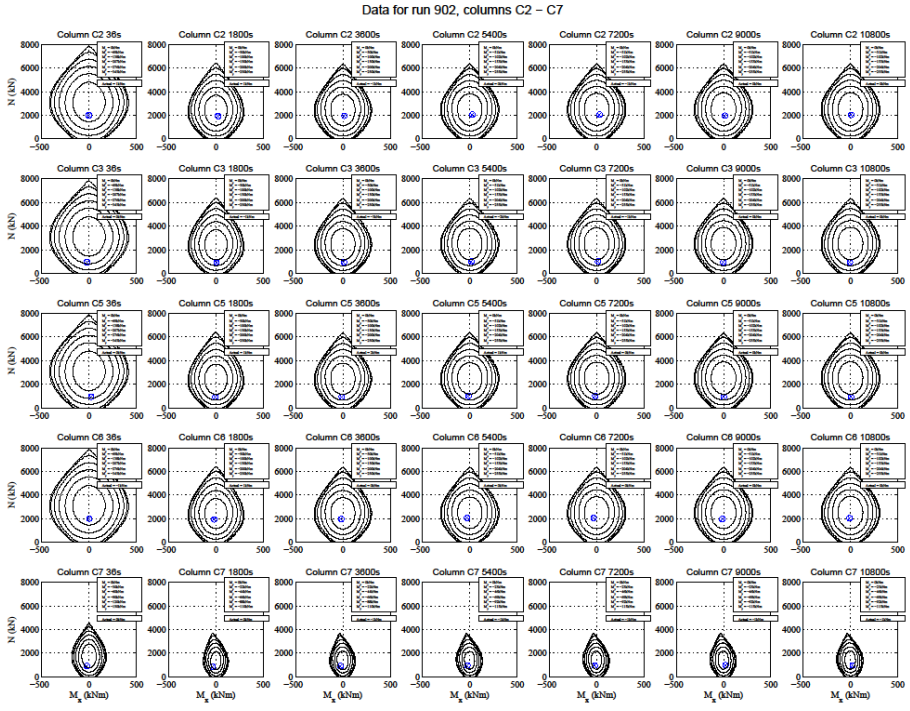
Data for run 902, columns C2 – C7
Column C2 36s
Column C2 1800s
Column C2 3600s
Column C2 5400s
Column C2 7200s
Column C2 9000s
Column C2 10800s
Column C3 36s
Column C3 1800s
Column C3 3600s
Column C3 5400s
Column C3 7200s
Column C3 9000s
Column C3 10800s
Column C5 36s
Column C5 1800s
Column C5 3600s
Column C5 5400s
Column C5 7200s
Column C5 9000s
Column C5 10800s
Column C6 36s
Column C6 1800s
Column C6 3600s
Column C6 5400s
Column C6 7200s
Column C6 9000s
Column C6 10800s
Column C7 36s
Column C7 1800s
Column C7 3600s
Column C7 5400s
Column C7 7200s
Column C7 9000s
Column C7 10800s
N (kN)
M_x (kNm)

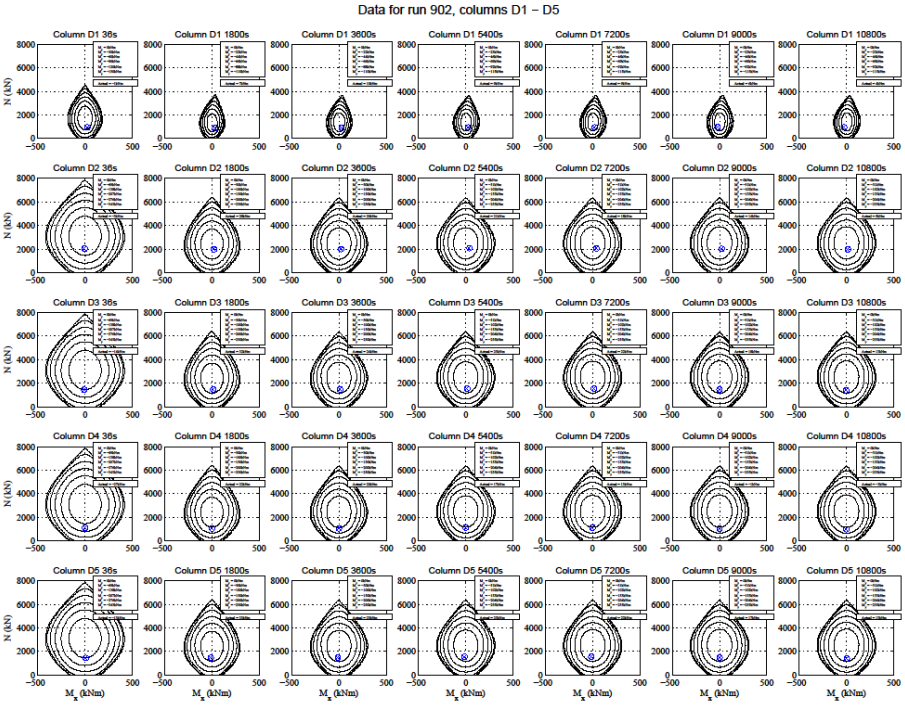
Data for run 902, columns D1 – D5
Column D1 36s
Column D1 1800s
Column D1 3600s
Column D1 5400s
Column D1 7200s
Column D1 9000s
Column D1 10800s
Column D2 36s
Column D2 1800s
Column D2 3600s
Column D2 5400s
Column D2 7200s
Column D2 9000s
Column D2 10800s
Column D3 36s
Column D3 1800s
Column D3 3600s
Column D3 5400s
Column D3 7200s
Column D3 9000s
Column D3 10800s
Column D4 36s
Column D4 1800s
Column D4 3600s
Column D4 5400s
Column D4 7200s
Column D4 9000s
Column D4 10800s
Column D5 36s
Column D5 1800s
Column D5 3600s
Column D5 5400s
Column D5 7200s
Column D5 9000s
Column D5 10800s
N (kN)
M_x (kNm)

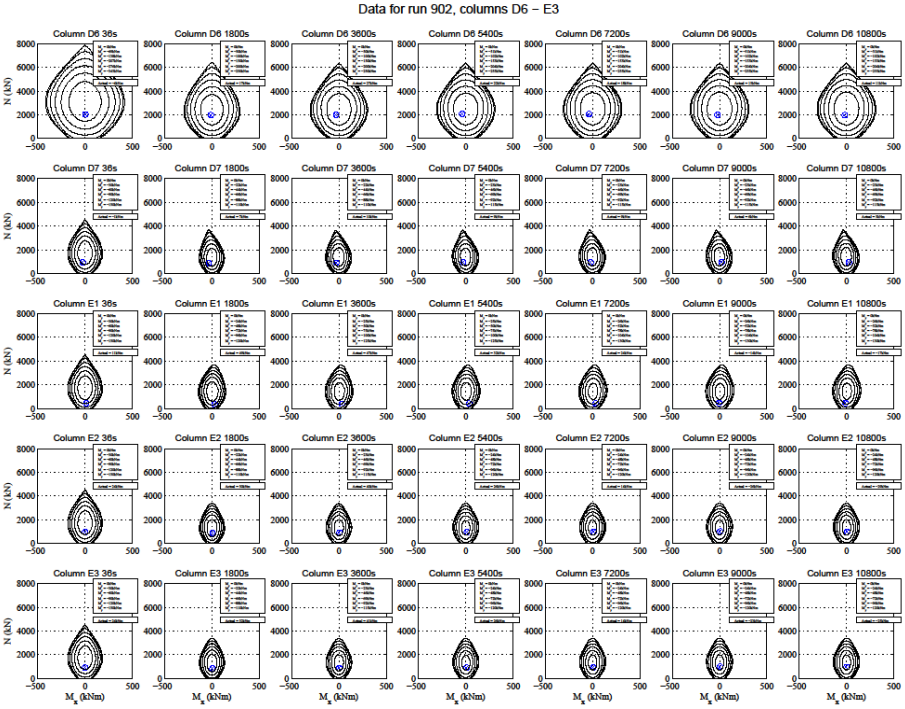
Data for run 902, columns D6 – E3
Column D6 36s
Column D6 1800s
Column D6 3600s
Column D6 5400s
Column D6 7200s
Column D6 9000s
Column D6 10800s
Column D7 36s
Column D7 1800s
Column D7 3600s
Column D7 5400s
Column D7 7200s
Column D7 9000s
Column D7 10800s
Column E1 36s
Column E1 1800s
Column E1 3600s
Column E1 5400s
Column E1 7200s
Column E1 9000s
Column E1 10800s
Column E2 36s
Column E2 1800s
Column E2 3600s
Column E2 5400s
Column E2 7200s
Column E2 9000s
Column E2 10800s
Column E3 36s
Column E3 1800s
Column E3 3600s
Column E3 5400s
Column E3 7200s
Column E3 9000s
Column E3 10800s
N (kN)
M_x (kNm)

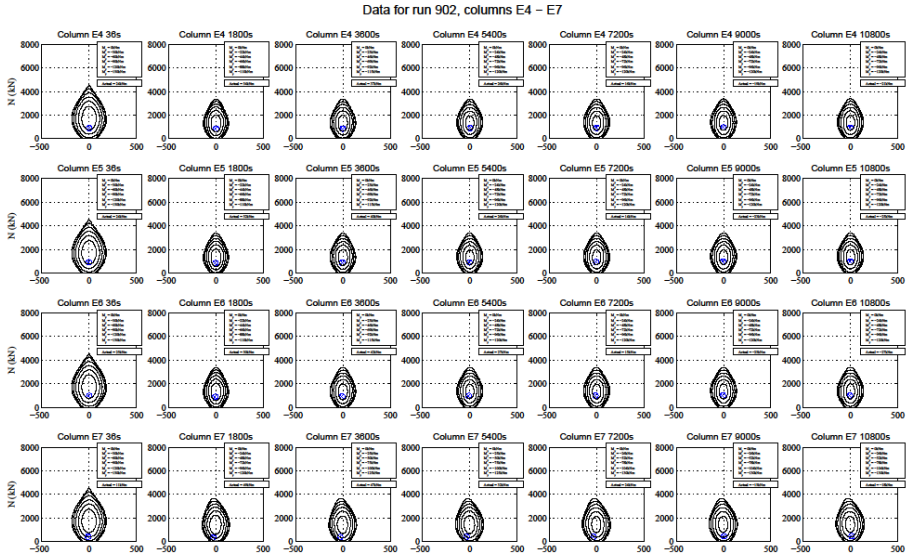
Data for run 902, columns E4 – E7
Column E4 36s
Column E4 1800s
Column E4 3600s
Column E4 5400s
Column E4 7200s
Column E4 9000s
Column E4 10800s
Column E5 36s
Column E5 1800s
Column E5 3600s
Column E5 5400s
Column E5 7200s
Column E5 9000s
Column E5 10800s
Column E6 36s
Column E6 1800s
Column E6 3600s
Column E6 5400s
Column E6 7200s
Column E6 9000s
Column E6 10800s
Column E7 36s
Column E7 1800s
Column E7 3600s
Column E7 5400s
Column E7 7200s
Column E7 9000s
Column E7 10800s
N (kN)

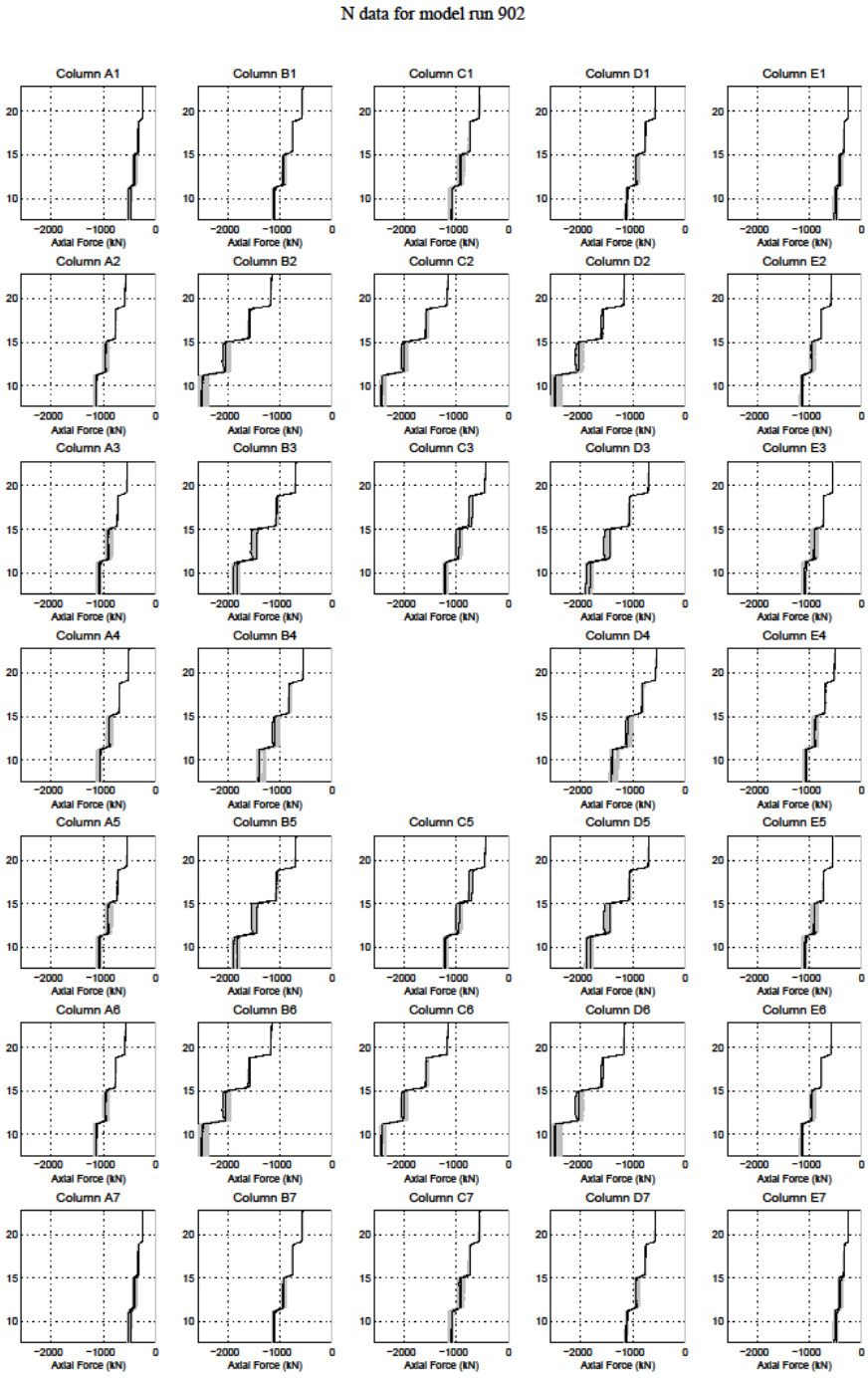
N data for model run 902
Column A1
Column B1
Column C1
Column D1
Column E1
Column A2
Column B2
Column C2
Column D2
Column E2
Column A3
Column B3
Column C3
Column D3
Column E3
Column A4
Column B4
Column D4
Column E4
Column A5
Column B5
Column C5
Column D5
Column E5
Column A6
Column B6
Column C6
Column D6
Column E6
Column A7
Column B7
Column C7
Column D7
Column E7
Axial Force (kN)

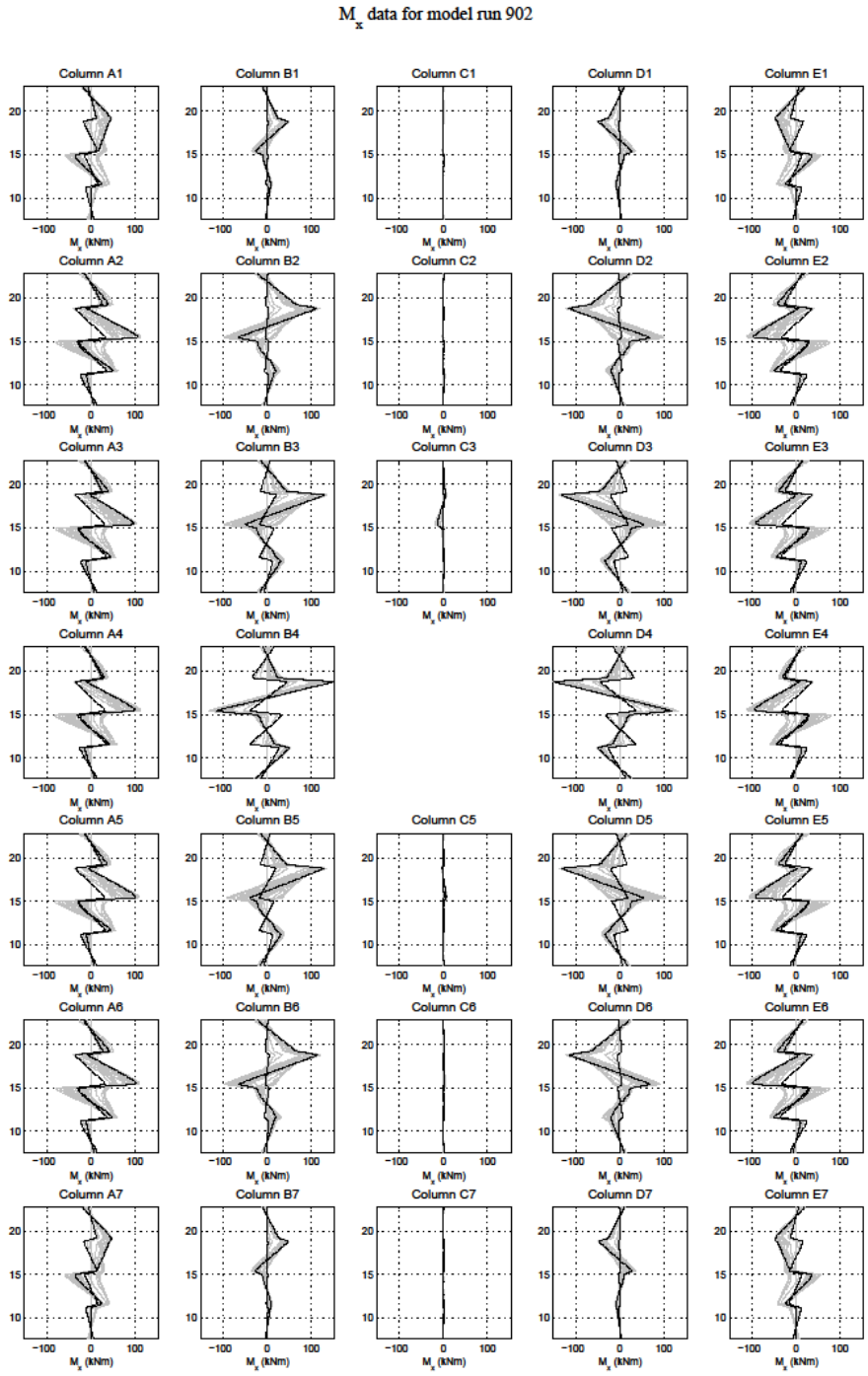
M_x data for model run 902
Column A1
Column B1
Column C1
Column D1
Column E1
Column A2
Column B2
Column C2
Column D2
Column E2
Column A3
Column B3
Column C3
Column D3
Column E3
Column A4
Column B4
Column D4
Column E4
Column A5
Column B5
Column C5
Column D5
Column E5
Column A6
Column B6
Column C6
Column D6
Column E6
Column A7
Column B7
Column C7
Column D7
Column E7
M_x (kNm)

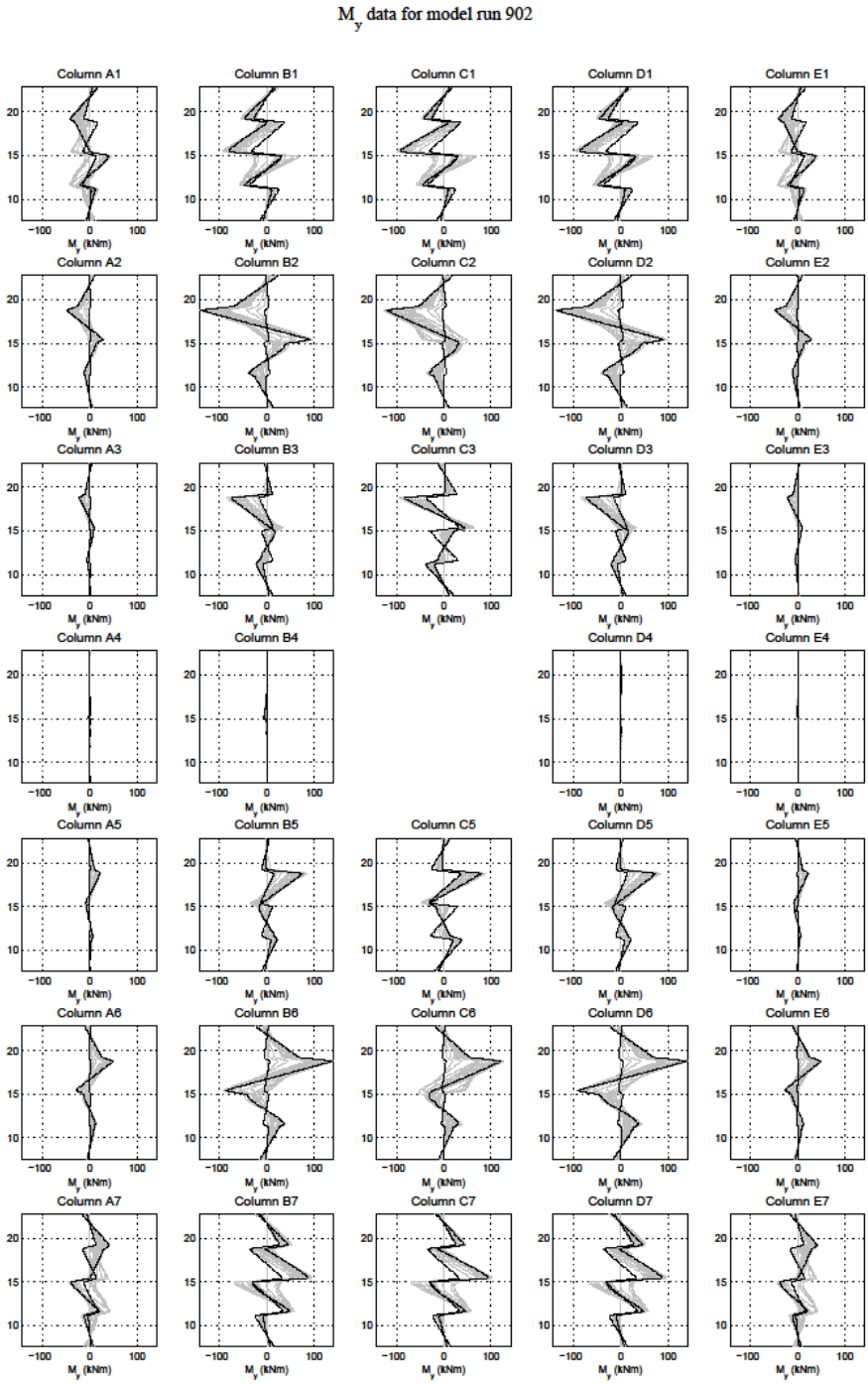
My data for model run 902
Column A1
Column B1
Column C1
Column D1
Column E1
Column A2
Column B2
Column C2
Column D2
Column E2
Column A3
Column B3
Column C3
Column D3
Column E3
Column A4
Column B4
Column D4
Column E4
Column A5
Column B5
Column C5
Column D5
Column E5
Column A6
Column B6
Column C6
Column D6
Column E6
Column A7
Column B7
Column C7
Column D7
Column E7
My (kNm)

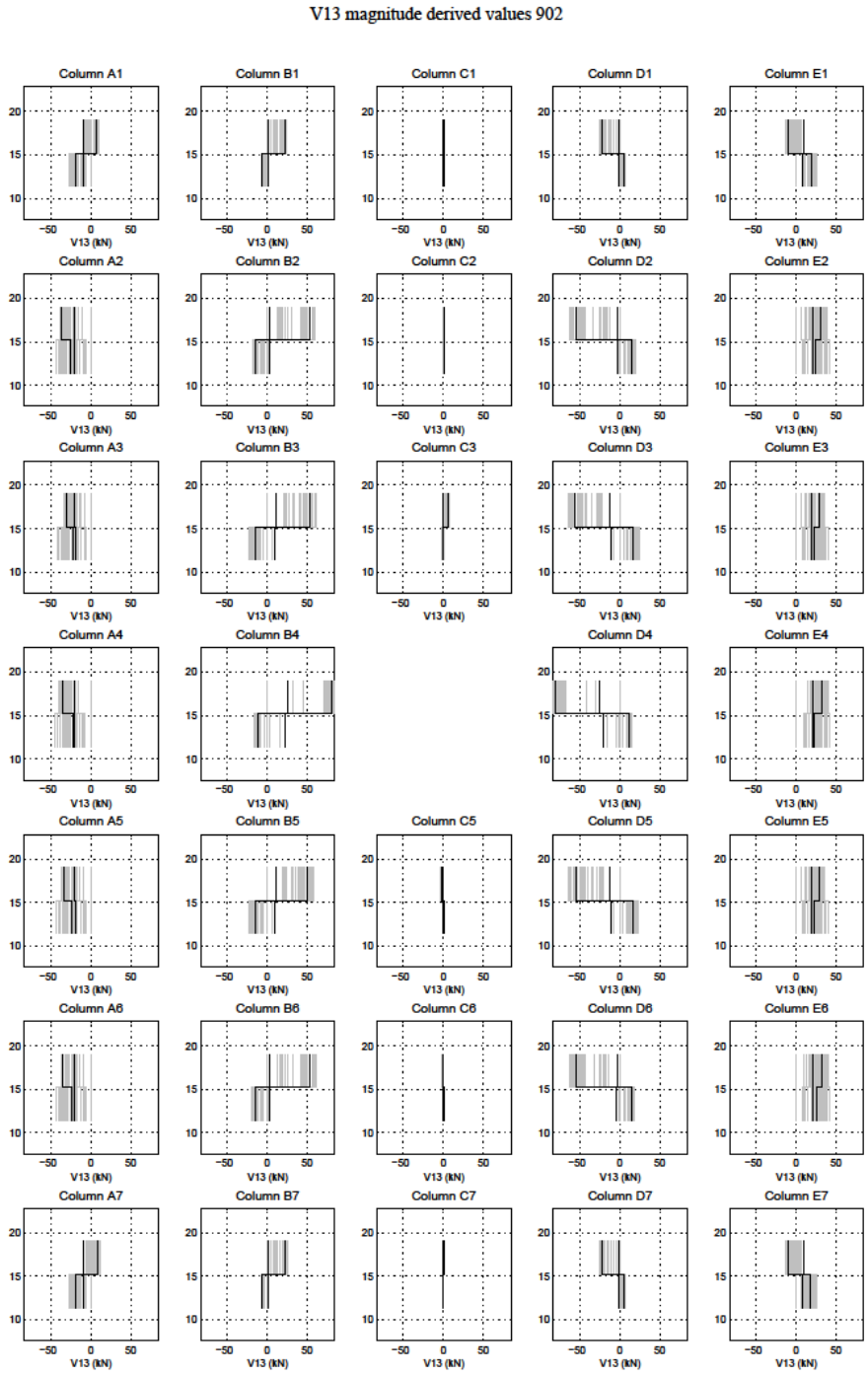
V13 magnitude derived values 902
Column A1
Column B1
Column C1
Column D1
Column E1
Column A2
Column B2
Column C2
Column D2
Column E2
Column A3
Column B3
Column C3
Column D3
Column E3
Column A4
Column B4
Column D4
Column E4
Column A5
Column B5
Column C5
Column D5
Column E5
Column A6
Column B6
Column C6
Column D6
Column E6
Column A7
Column B7
Column C7
Column D7
Column E7
V13 (kN)

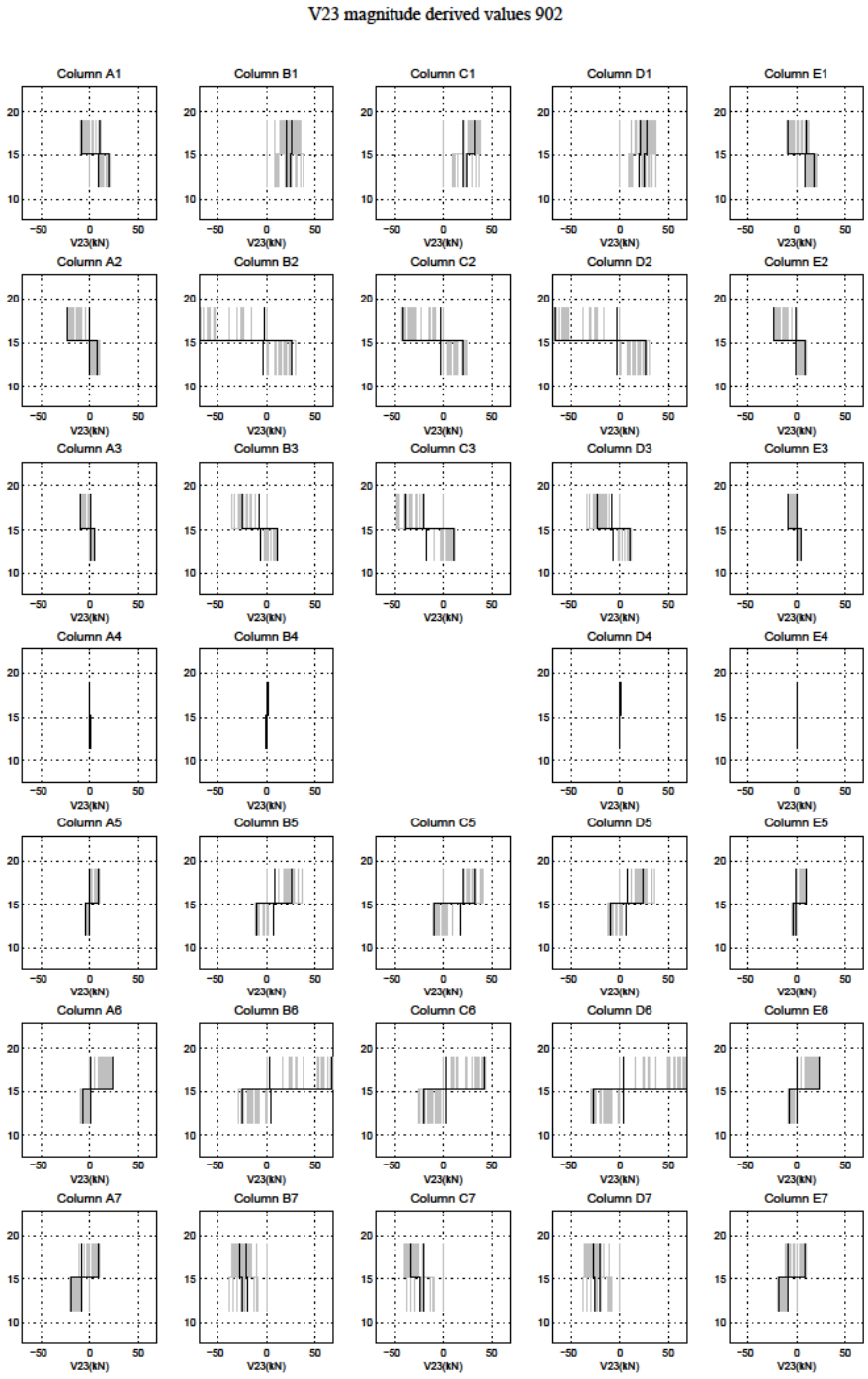
V23 magnitude derived values 902
Column A1
Column B1
Column C1
Column D1
Column E1
Column A2
Column B2
Column C2
Column D2
Column E2
Column A3
Column B3
Column C3
Column D3
Column E3
Column A4
Column B4
Column D4
Column E4
Column A5
Column B5
Column C5
Column D5
Column E5
Column A6
Column B6
Column C6
Column D6
Column E6
Column A7
Column B7
Column C7
Column D7
Column E7
V23(kN)

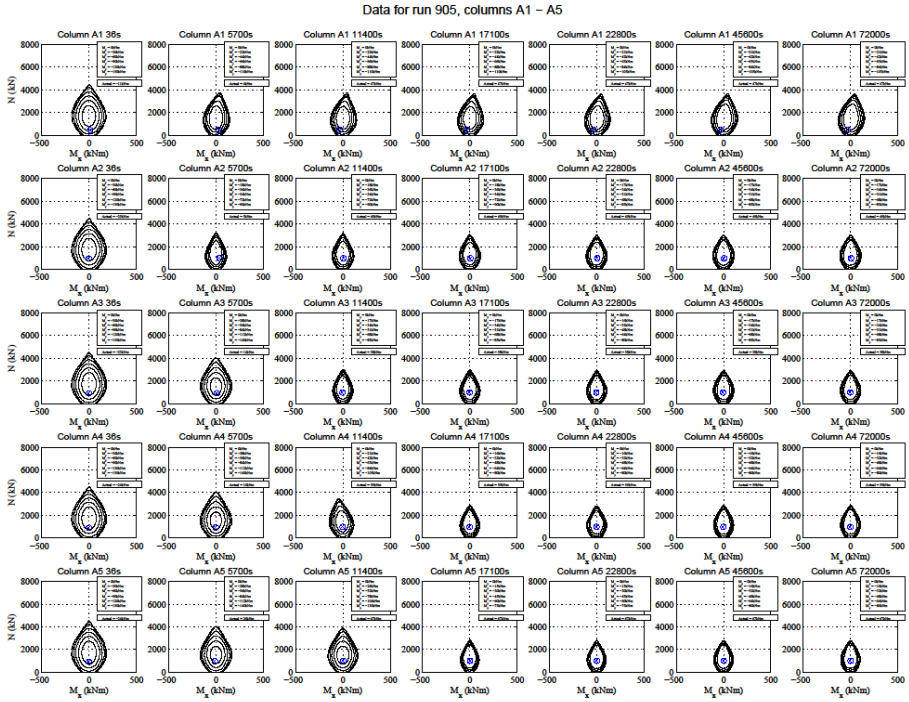
Data for run 905, columns A1 – A5
Column A1 36s
Column A1 5700s
Column A1 11400s
Column A1 17100s
Column A1 22800s
Column A1 45600s
Column A1 72000s
Column A2 36s
Column A2 5700s
Column A2 11400s
Column A2 17100s
Column A2 22800s
Column A2 45600s
Column A2 72000s
Column A3 36s
Column A3 5700s
Column A3 11400s
Column A3 17100s
Column A3 22800s
Column A3 45600s
Column A3 72000s
Column A4 36s
Column A4 5700s
Column A4 11400s
Column A4 17100s
Column A4 22800s
Column A4 45600s
Column A4 72000s
Column A5 36s
Column A5 5700s
Column A5 11400s
Column A5 17100s
Column A5 22800s
Column A5 45600s
Column A5 72000s
N (kN)
M_x (kNm)

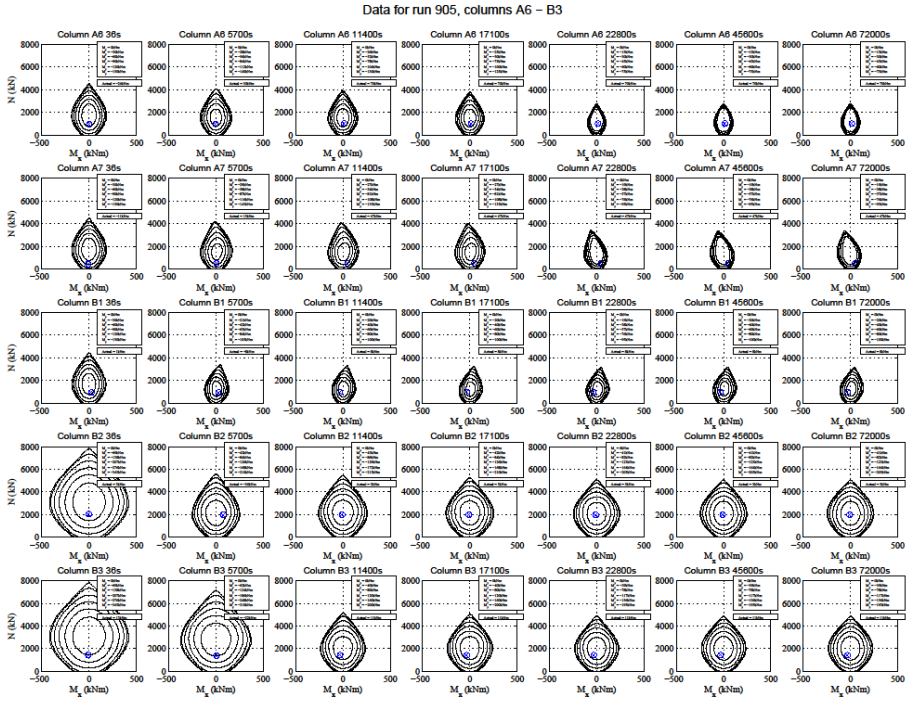
Data for run 905, columns A6 – B3
Column A6 36s
Column A6 5700s
Column A6 11400s
Column A6 17100s
Column A6 22800s
Column A6 45600s
Column A6 72000s
Column A7 36s
Column A7 5700s
Column A7 11400s
Column A7 17100s
Column A7 22800s
Column A7 45600s
Column A7 72000s
Column B1 36s
Column B1 5700s
Column B1 11400s
Column B1 17100s
Column B1 22800s
Column B1 45600s
Column B1 72000s
Column B2 36s
Column B2 5700s
Column B2 11400s
Column B2 17100s
Column B2 22800s
Column B2 45600s
Column B2 72000s
Column B3 36s
Column B3 5700s
Column B3 11400s
Column B3 17100s
Column B3 22800s
Column B3 45600s
Column B3 72000s
N (kN)
M_x (kNm)

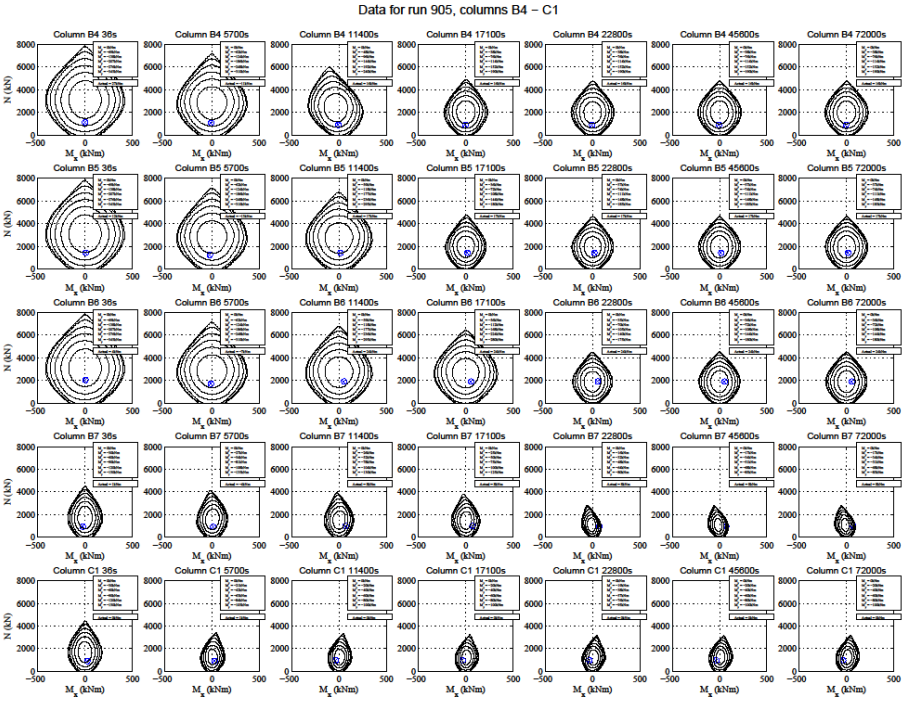
Data for run 905, columns B4 – C1
Column B4 36s
Column B4 5700s
Column B4 11400s
Column B4 17100s
Column B4 22800s
Column B4 45600s
Column B4 72000s
Column B5 36s
Column B5 5700s
Column B5 11400s
Column B5 17100s
Column B5 22800s
Column B5 45600s
Column B5 72000s
Column B6 36s
Column B6 5700s
Column B6 11400s
Column B6 17100s
Column B6 22800s
Column B6 45600s
Column B6 72000s
Column B7 36s
Column B7 5700s
Column B7 11400s
Column B7 17100s
Column B7 22800s
Column B7 45600s
Column B7 72000s
Column C1 36s
Column C1 5700s
Column C1 11400s
Column C1 17100s
Column C1 22800s
Column C1 45600s
Column C1 72000s
N (kN)
M_x (kNm)

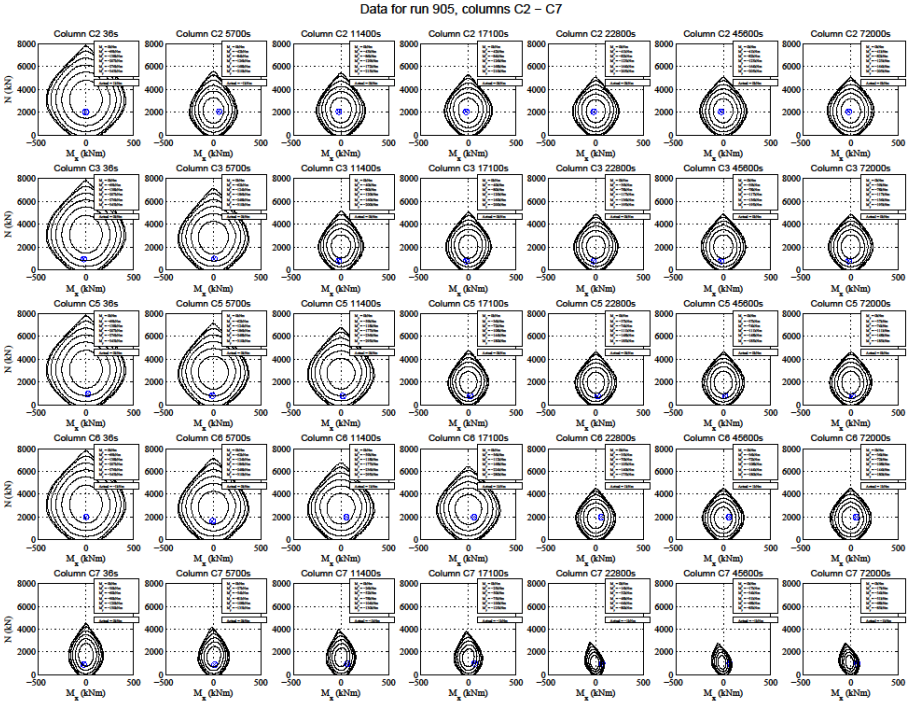
Data for run 905, columns C2 – C7
Column C2 36s
Column C2 5700s
Column C2 11400s
Column C2 17100s
Column C2 22800s
Column C2 45600s
Column C2 72000s
Column C3 36s
Column C3 5700s
Column C3 11400s
Column C3 17100s
Column C3 22800s
Column C3 45600s
Column C3 72000s
Column C5 36s
Column C5 5700s
Column C5 11400s
Column C5 17100s
Column C5 22800s
Column C5 45600s
Column C5 72000s
Column C6 36s
Column C6 5700s
Column C6 11400s
Column C6 17100s
Column C6 22800s
Column C6 45600s
Column C6 72000s
Column C7 36s
Column C7 5700s
Column C7 11400s
Column C7 17100s
Column C7 22800s
Column C7 45600s
Column C7 72000s
N (kN)
M_x (kNm)

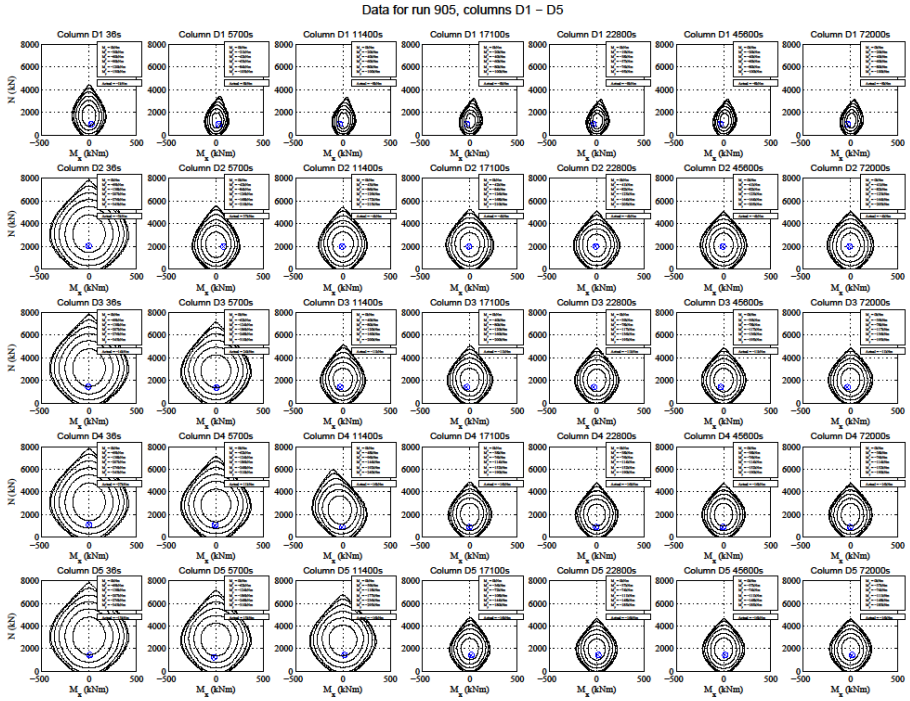
Data for run 905, columns D1 – D5
Column D1 36s
Column D1 5700s
Column D1 11400s
Column D1 17100s
Column D1 22800s
Column D1 45600s
Column D1 72000s
Column D2 36s
Column D2 5700s
Column D2 11400s
Column D2 17100s
Column D2 22800s
Column D2 45600s
Column D2 72000s
Column D3 36s
Column D3 5700s
Column D3 11400s
Column D3 17100s
Column D3 22800s
Column D3 45600s
Column D3 72000s
Column D4 36s
Column D4 5700s
Column D4 11400s
Column D4 17100s
Column D4 22800s
Column D4 45600s
Column D4 72000s
Column D5 36s
Column D5 5700s
Column D5 11400s
Column D5 17100s
Column D5 22800s
Column D5 45600s
Column D5 72000s
N (kN)
M_x (kNm)

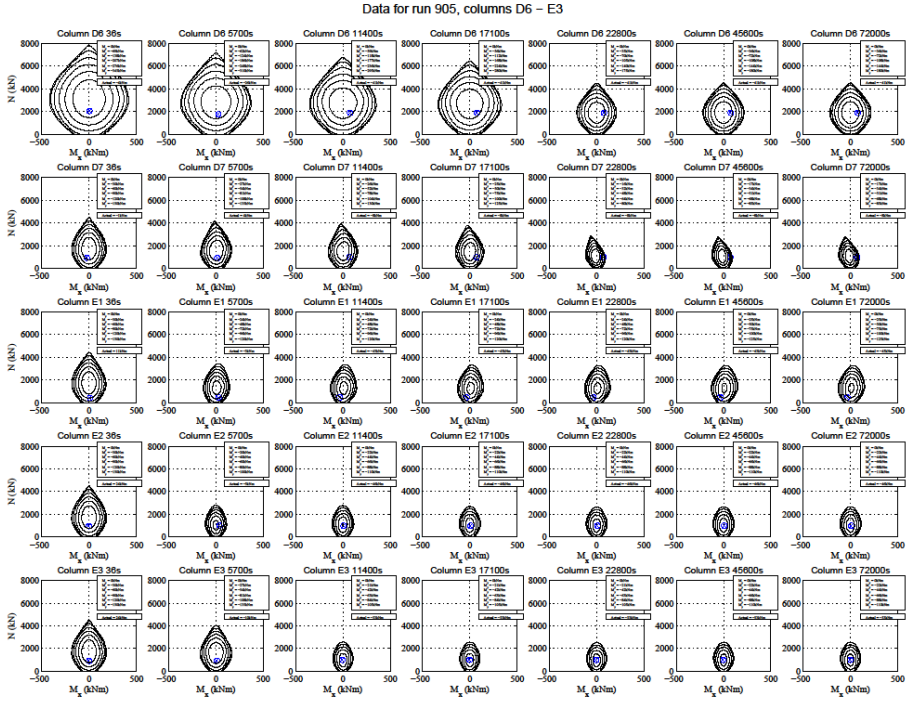
Data for run 905, columns D6 – E3
Column D6 36s
Column D6 5700s
Column D6 11400s
Column D6 17100s
Column D6 22800s
Column D6 45600s
Column D6 72000s
Column D7 36s
Column D7 5700s
Column D7 11400s
Column D7 17100s
Column D7 22800s
Column D7 45600s
Column D7 72000s
Column E1 36s
Column E1 5700s
Column E1 11400s
Column E1 17100s
Column E1 22800s
Column E1 45600s
Column E1 72000s
Column E2 36s
Column E2 5700s
Column E2 11400s
Column E2 17100s
Column E2 22800s
Column E2 45600s
Column E2 72000s
Column E3 36s
Column E3 5700s
Column E3 11400s
Column E3 17100s
Column E3 22800s
Column E3 45600s
Column E3 72000s
N (kN)
M_x (kNm)

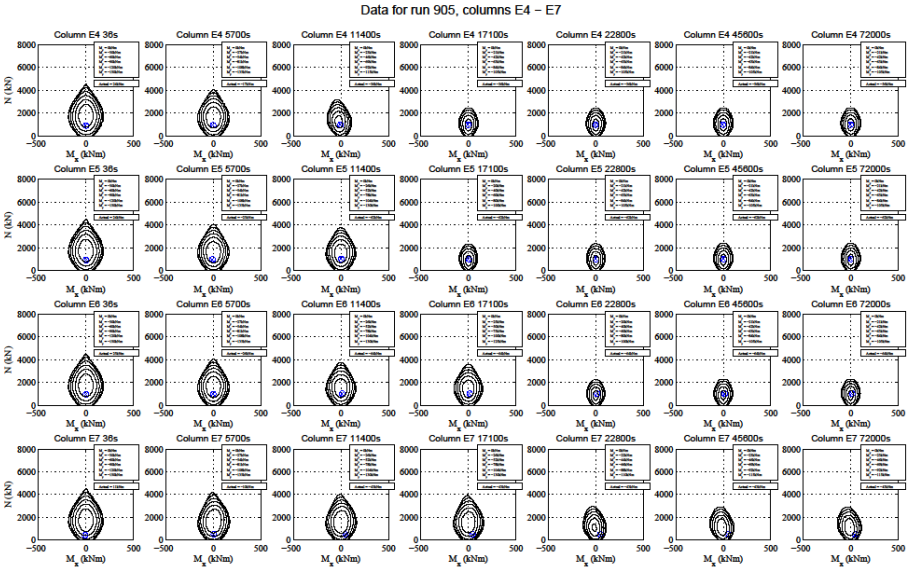
Data for run 905, columns E4 – E7
Column E4 36s
Column E4 5700s
Column E4 11400s
Column E4 17100s
Column E4 22800s
Column E4 45600s
Column E4 72000s
Column E5 36s
Column E5 5700s
Column E5 11400s
Column E5 17100s
Column E5 22800s
Column E5 45600s
Column E5 72000s
Column E6 36s
Column E6 5700s
Column E6 11400s
Column E6 17100s
Column E6 22800s
Column E6 45600s
Column E6 72000s
Column E7 36s
Column E7 5700s
Column E7 11400s
Column E7 17100s
Column E7 22800s
Column E7 45600s
Column E7 72000s
N (kN)
M_x (kNm)

# Appendix IV

## Selected Publications

## 1. Selected Publications

This Appendix contains four papers which have resulted from the work contained within the main body of the thesis. For a full list of publications, see page vii in the prologue of the thesis. In order of appearance, the publications presented below are:

A. Law, M. Gillie; Interaction Diagrams for Ambient and Heated Concrete Sections; Engineering Structures; Volume 32, Issue 6, June 2010, Pages 1641-1649

A. Law, M. Gillie; Interaction Diagrams for Heated Concrete Sections using the Tangent Stiffness Matrix; Structural Engineering Mechanics and Computation, September 2010; Cape Town.

J. Stern-Gottfried, A. Law, G. Rein, M. Gillie, J. L. Torero; A Performance Based Methodology Using Travelling Fires for Structural Analysis; Eighth International Conference on Performance-Based Codes and Fire Safety Design Methods, Lund, June 2010

A. Law, M. Gillie, P. Pankaj; Incorporation of Load Induced Thermal Strain in Finite Element Models; Applications of Structural Fire Engineering, Prague, February 2009

# Interaction Diagrams for Ambient and Heated Concrete Sections

Angus Law[1], Martin Gillie[2]

## *ABSTRACT*

Bending moment axial force interaction diagrams are a commonly used tool in any design office. When designing for fire conditions, the large axial forces which develop place an additional importance on the consideration of the interplay between axial forces and moments. This paper presents a new method for calculating the biaxial bending moment/axial force capacity for a general section through the use of the sectional tangent stiffness. A beam-column section subject to fire is assessed, and comparisons made with simplified design tools. It is concluded that derivation of the interaction surface from the tangent stiffness matrix is possible, and that current simplified methods for fire design cannot be assumed conservative.

**Keywords**

Interaction Diagrams, High Temperatures, Concrete, Tangent Stiffness, Fire, Biaxial Bending

## 1 INTRODUCTION

The design of reinforced concrete sections requires the specification of a number of parameters such as the section breadth and depth; the area of steel; and the strengths of the concrete and steel. Where a section is subject to both an axial force and bending moments about one or both axes, interaction diagrams are commonly used to determine the area of steel required to resist the moments and forces to which the section is subjected. Structural design codes (e.g. Eurocode 2 [1]) often provide interaction diagrams for use with typical concrete sections at ambient temperature that allow the user to circumvent the cumbersome calculations necessary to determine suitable section parameters directly. However, there are many situations, such as fire loading, where structural engineers may need interaction diagrams for sections which are not covered by the standard cases. In these circumstances it is necessary to produce interaction diagrams from first principles.

This paper considers the creation, use and reliability of interaction diagrams for concrete sections; in particular those subject to fire loading. One of the problems frequently encountered in structural fire engineering is that of the definition of failure. The motivation for creating interaction diagrams for sections at high temperature lies in the difficulty of defining failure for a single element. Often failure

[1] Address: BRE Centre for Fire Safety Engineering, The School of Engineering and Electronics, The University of Edinburgh, The King's Buildings, Mayfield Road, Edinburgh, EH9 3JL, Scotland. Email: A.Law@ed.ac.uk Tel: +44 (0)131 650 7241, Fax: +44 (0)131 650 6781
[2] Address: BRE Centre for Fire Safety Engineering, The School of Engineering and Electronics, The University of Edinburgh, The King's Buildings, Mayfield Road, Edinburgh, EH9 3JL, Scotland. Email: M.Gillie@ed.ac.uk Tel: +44 (0)131 650 7204, Fax: +44 (0)131 650 6781

of heated sections is loosely defined as the beginning of run-away deflections, or the time at which steel reinforcement reaches a pre-determined temperature, but such definitions are too vague to lead to efficient design. The use of carefully prepared interaction diagrams allows for a much tighter definition of section failure. Although a full understanding of the failure *process* requires global structural modelling, the use of an interaction diagram in conjunction with knowledge of the loading state of a section allows an engineer to determine how close a single member is to failure.

The first section of the paper reviews the available methods for constructing interaction diagrams for use in the design and also the assessment of concrete sections. It highlights the difficulties associated with obtaining interaction diagrams for determining ultimate capacity using existing methods. A new method of creating two- or three-dimensional interaction diagrams of sections under any temperature field based the tangent stiffness matrix of a section is then presented. It is anticipated that this technique will allow design engineers to make rapid assessments of the capacity of any concrete section when subject to arbitrary fire loading. The method can be implemented easily in any of the programming languages or mathematical analysis packages commonly available in design offices. . Finally the paper makes comparisons between using interaction diagrams constructed using this method to design heated concrete sections, and existing Eurocode design methods. It is concluded that current methods are not conservative.

## 2 CREATING INTERACTION DIAGRAMS – EXISTING METHODS

### 2.1 Interaction Diagrams for Ambient Temperature Design

Interaction diagrams used for design are based on the assumption that there is a maximum allowable concrete compressive strain which prevents concrete crushing (Fig. 1). It is also frequently assumed that plane sections remain plane, that the tensile strength of concrete is negligible [2-4] and that the concrete stress distribution can be represented by a rectangular stress-block [5, 6]. From these assumptions, the derivation of an interaction diagram is relatively simple. By holding extreme fibre strains at the maximum permissible value while curvature is varied, moment and axial force (M-N) pairs that lie on the interaction diagram for the section can be obtained by appropriate integrations of the resulting stresses over the section.

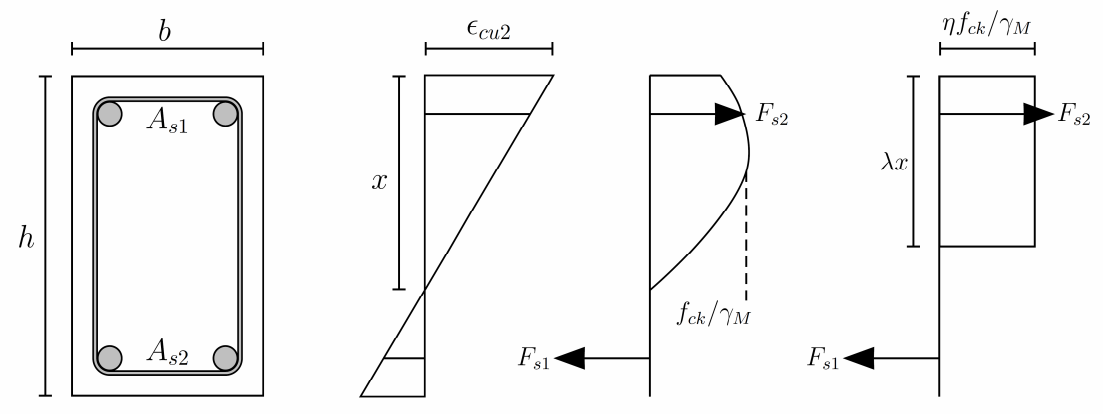


*Figure 1. The development of a stress block from first principles.*

This method enables the creation of interaction curves in uniaxial bending, and also interaction surfaces when biaxial bending is considered. The method is efficient because each M-N pair calculated is know to lie on the design interaction curve due to the assumption of a maximum permissible concrete strain. Diagrams produced this way can either be used directly or be normalised appropriately to allow the engineer to specify the section properties. However, because the assumptions made regarding maximum strain and the size of the associated stress block are design assumptions (which may include safety factors), the interaction diagrams obtained are not indications of failure strength, but rather show an appropriate conservative design capacity.

**2.2 Interaction Diagrams for Assessment**

Assessment of the ultimate, rather than design, capacity of a section may be required in a number of situations, including that of assessing the strength of a section under fire loading. Assessing ultimate capacity requires a different approach to that used for assessing design capacity. The assumption of a maximum fixed permissible concrete strain cannot be made because, for heated sections, the ultimate strain is temperature dependent and, consequently, the maximum moment capacity may occur at curvature that induces a strain greater than, or less than, the strain required to crush the concrete in different parts of the section. Similarly, a realistic concrete stress-strain relationship should be used, rather than a simplified stress block. Since the maximum compressive strain is not limited, it is no longer straightforward to find strain-curvature pairs that lie on the interaction curve for a section.

Several methods for obtaining interaction diagrams when maximum compressive strains are not specified have been presented. The simplest rely on variations of a "brute force" approach in which a section is analysed for many combinations of $\varepsilon_a$ and $\kappa$; appropriate integrations of the section stresses are then used to plot a point in M-N space for each combination. Assembly of all these points gives a "cloud" of points which are all inside or on the interaction curve [7-9]. By connecting the outer-most points in this cloud, the interaction curve can be drawn. Figure 2c demonstrates the generation of a number points which would contribute to the cloud of data. A significant problem with this method is that there is no clear way of determining which points lie on the interaction curve and which points lie just inside it, so determining the interaction curve from a cloud of points is awkward. These problems are magnified if biaxial bending is considered and an interaction surface required. The method is also computationally expensive as many integrations of the stresses over the section are required.

An alternative approach to integrating stresses over an entire section is to use the "rapid exact" inelastic biaxial bending analysis technique [10, 11] which allows very efficient analytical integration of the stresses. This method relies on Green's Theorem [12] to convert the costly double integration of stresses over a section to a highly efficient line integral around the section boundary. Implementation of the method requires the stress-strain relationships of the materials be analytically integrable but can be applied to any cross-section. Although computationally much more efficient than simple brute-force methods, the problem of identifying points that lie on the interaction diagram remains.

**2.3 Section Analysis at High Temperatures**

Exposure of a concrete section to a fire, and the resulting temperature increase cause the capacity to reduce and the shape of the failure surface to change. In design, several methods are available for assessment of a heated member's capacity [13]. The most commonly used and simplest is the 500ºC

isotherm method [14, 15]. This method allows the design bending capacity of a heated section to be calculated based on the assumption that concrete retains its full strength below 500ºC and has negligible strength above 500ºC. Reinforcement material properties are calculated based on centre-line temperatures. The design capacity is assessed using the stress block method based on accidental limit-state (fire) partial safety factors. This approach avoids the need to calculate an interaction diagram altogether but is very crude can be unconservative, as will be demonstrated later in this study.

Several authors have created M-N interaction diagrams for sections at high temperatures [7, 16, 17], and others have created moment-curvature relationships based on similar assumptions [3, 18, 19]. These studies have predominantly focussed on uniaxial bending. In order to create interaction diagrams for heated sections, it is necessary to correctly represent the degradation of material properties caused by temperature and also to represent the strains due to thermal expansion. The effects of concrete spalling on section capacity can be included by the adjustment of the geometry of the section. Once these effects have been taken into account, it is then in principle possible to create an interaction diagram using any of the (non-design) methods outlined above. However, in practice each method has practical difficulties when used at high temperature.

"Brute-force" methods are relatively simple to implement for heated sections but the problems associated with these for ambient temperature analyses are amplified for high temperature analyses as a new diagram must be generated for every cross-sectional temperature distribution. The rapid exact method becomes unwieldy at high temperatures for two reasons. First, the stress-strain relationship of concrete becomes more complex and this makes it difficult to integrate with respect to strain. Second, as the integration is over a region of both non-uniform strain and temperature, the stress-strain curve must be integrated with respect to the both change in strain and change in temperature over the region.

## 3 AN ALTERNATIVE - THE TANGENT MODULUS METHOD

In this section an alternative method is proposed to create interaction diagrams for sections both at ambient temperature and when heated by exploiting tangent stiffness matrices. The method has the key benefit of bypassing the difficulties in determining M-N pairs that lie exactly on an interaction curve or surface.

### 3.1 Theory

Although typically used in structural stability calculations as part of Shandley's tangent modulus equation [8], tangent stiffness matrices can also be used to locate failure surfaces. A section's tangent stiffness matrix relates small changes in generalized strains (typically an axial strain and two curvatures are needed for the analysis of biaxial bending of concrete sections) to small changes in the corresponding stress-resultants (an axial force and two bending moments). When a section's response is non-linear, the tangent stiffness matrix is distinct from the elastic stiffness matrix. For the set of stress-resultants mentioned, the relationship between incremental stress-resultants, tangent stiffness matrix, and incremental generalized strains of a section can be written in the standard form:

$$\begin{bmatrix} \delta P \\ \delta M_x \\ \delta M_y \end{bmatrix} = \begin{bmatrix} K_{11} & K_{12} & K_{13} \\ K_{21} & K_{22} & K_{23} \\ K_{31} & K_{32} & K_{33} \end{bmatrix} \begin{bmatrix} \delta \varepsilon_a \\ \delta \kappa_x \\ \delta \kappa_y \end{bmatrix} \quad (1)$$

or,

$$\delta \mathbf{F} = \mathbf{K} \delta \boldsymbol{\varepsilon}, \quad (2)$$

where Rotter [10] gives:

$$\begin{aligned} K_{11} &= \int\int E_T dA \\ K_{12} &= K_{21} = \int\int E_T y dA \\ K_{13} &= K_{31} = \int\int E_T x dA \\ K_{22} &= \int\int E_T y^2 dA \\ K_{23} &= K_{32} = \int\int E_T xy dA \\ K_{33} &= \int\int E_T x^2 dA \end{aligned} \quad (3)$$

The set of stress-resultants that lie on the failure surface of a section are those that arise when an incremental change in the generalized strain vector result in $\delta\mathbf{F}$=0. That is, stress-resultants on the failure surface are those that occur when **K** is singular, or

$$\det(\mathbf{K}) = 0 \quad (4)$$

This fact can be used to determine stress-resultant vectors, **F,** for a section that are located on the interaction surface if incremental strain vectors which correspond to above condition can be determined.

**3.2 Implementation**

The following calculations were all completed using the commercially available software, Matlab [20].

*Ambient Temperature*

Implementation of the tangent stiffness method for constructing interaction diagrams will be discussed with reference to a simple section at ambient temperature. The section dimensions and properties are shown in Fig. 2a. Assumptions made in this implementation are: plane sections remain plane; the

concrete compressive stress-strain behaviour is as given in Eurocode 2 [21]; the tensile strength of concrete is zero; the stress-strain relationship of steel is elasto-plastic; and there is no bond slip between steel and concrete. Each of these assumptions has been made in various combinations by other authors [2, 9, 22]. They result in a marginally conservative estimate of strength (with the exception of bond slip).

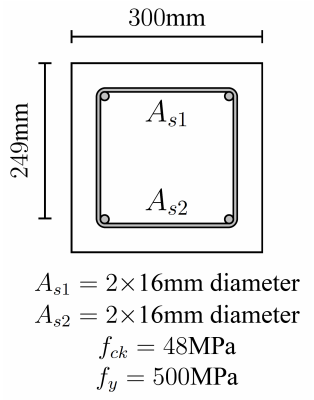


a)

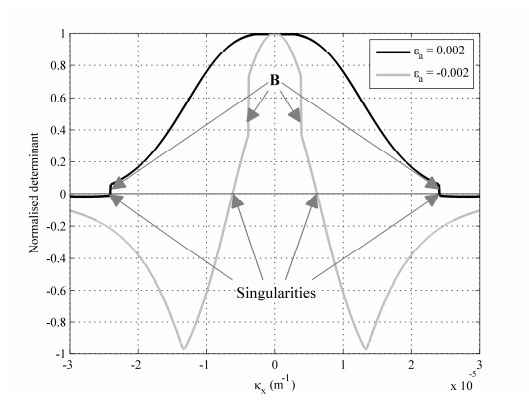


b)

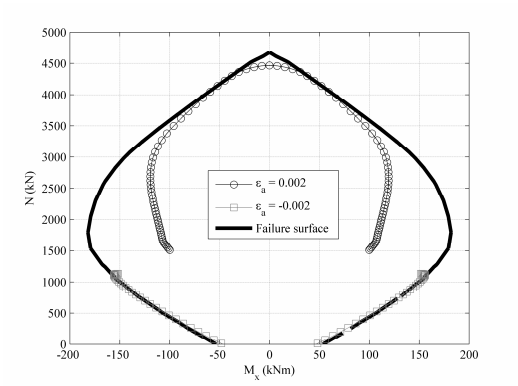


c)

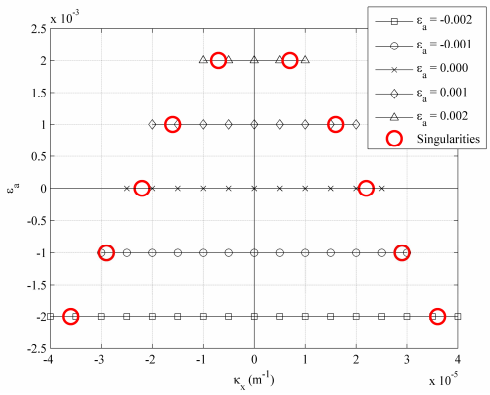


d)

*Figure 2. a) Arrangement of the section, and material properties; b) Change of the determinant of the stiffness matrix with respect to curvature for two values of axial strain; c) Interaction plot for two different values of axial strain with varying curvature; d) Conceptual illustration of the search algorithm used for identifying strain-curvature points on the interaction diagram. Points where the stiffness matrix determinant is singular (circles) lie between curvatures that cause the determinant to change sign. The precise location of singularities between such curvatures is found using the secant method.*

To produce the interaction curve for the section subject to uniaxial bending ($\kappa_y$=0), values of curvature for which $\det(\mathbf{K})=0$ were found for discrete values of axial strain. These curvatures were identified using the Secant method, in conjunction with a simple search function to identify the neighbourhoods where $\det(\mathbf{K})$ approached zero. For example, variation of $\det(\mathbf{K})$ against curvature for axial strain values of $\varepsilon_a$ = -0.002 and 0.002 is shown in Fig. 2b. Points where $\det(\mathbf{K})=0$ are marked as singularities on the figure; each of these represents a point on the interaction curve in terms of strain and curvature. Step changes in the value of $\det(\mathbf{K})$, caused by yielding of the reinforcement in either compression or tension, are marked by B on the figure. The corresponding curves in terms of moment and axial force are plotted in Fig. 2c. Fig. 2d illustrates conceptually an effective search algorithm for finding points where $\det(\mathbf{K})=0$. For incremental values of axial strain the determinant is evaluated at a number of curvatures. A change in the sign of the determinant between curvature values indicates

that a region where a singularity occurs has been reached. Once the singularity region is located, the secant method can be invoked to locate the precise location of the highlighted singularities.

Once strain vectors that lay on the interaction surface had been determined, numerical integration was used to compute **K** and the corresponding **F**. The final interaction curve in terms of force and moment is shown in Fig. 3b.

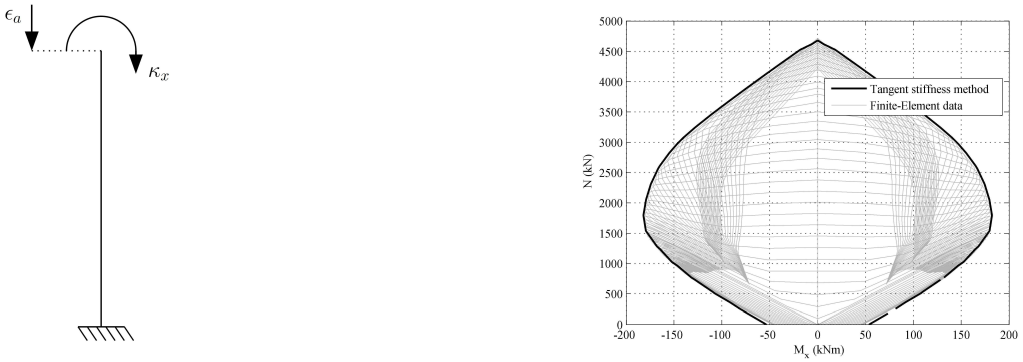


a) b)

*Figure 3. a) Geometry, boundary conditions, and loading of the finite element model; b) Interaction diagram from tangent modulus method (bold) and the full field of data generated by the finite-element model.*

The procedure was easily extended to produce interaction surfaces corresponding to biaxial bending by introducing variations to $\kappa_y$. This was achieved by the use of a parameter which defined $\kappa_y$ as a ratio of $\kappa_x$. Variation of this parameter from a large negative ratio to a large positive number ratio (e.g. -100.0 to 100.0) gave the full range of the biaxial failure surface, where a value of zero gave uniaxial bending about the *x*-axis. This full surface is shown in Fig. 4a and discussed in more detail below.

Presentation of interaction curves for uniaxial bending is well established and straightforward (e.g. Fig 2b). Presentation of interaction surfaces for biaxial bending in a form readily accessible to the design engineer is less easy. The presentation of a surface plot (Fig 4a) is not terribly useful in this respect. Visualisation choices are often dependent on the purpose for which the plot to be used. For generality, the plots in this study are presented as $M_x$, $N$ interaction diagrams with multiple curves representing different values of $M_y$ (Figs 4b and 4c). Thus, a large amount of information can be summarised on one diagram (Fig. 4d). The process employed to create these diagrams is shown sequentially in Fig 4. A single plot is sufficient for a member with a minimum of one axis of symmetry. However, where a section is entirely asymmetric, two diagrams may be required to encompass all of the information. In design, the tensile capacity of concrete sections is not normally considered. As such, just the compressive capacities are presented in this paper.

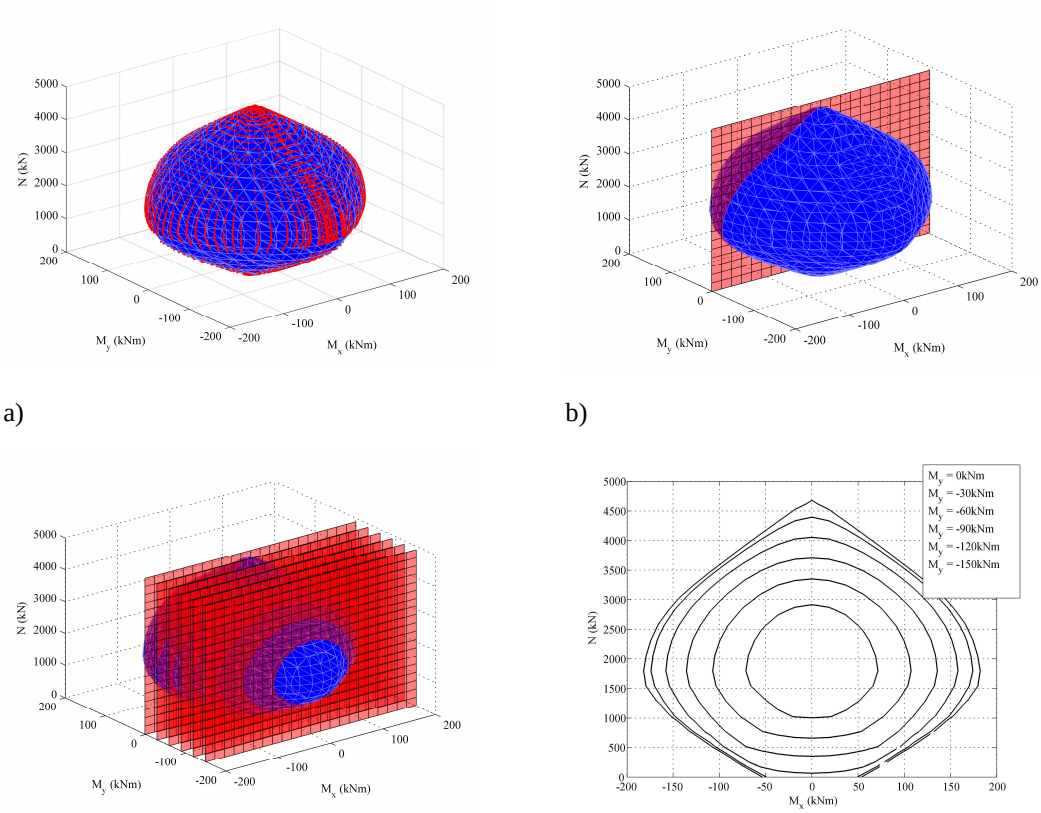


a) b)

c) d)

*Figure 4. a) Surface plotted through all points; b) Slice taken through uniaxial bending plane; c) Multiple slices taken at different values of $M_y$; d) Surface removed, plot rotated and viewed from one side, and the different values of $M_x$ and N displaced for each value of $M_y$.*

*Verification*

Verification of the above implementation was undertaken by comparing the results with finite element analyses of the same problem. A stocky cross-section of the section was subject to a series of strain/curvature analyses using the finite-element program Abaqus [23] (effectively a brute-force type of analysis). The analyses were conducted on a single beam element, and the effects of non-linear geometry were neglected (to ensure a purely sectional analysis). The arrangement of the model is shown in Fig. 3a. The full "cloud" of data resulting from the finite element analyses and the failure curve resulting from employing the tangent modulus method are shown in Fig. 3b. The outer points in the data from the finite element analyses are in good agreement with the interaction curve predicted by the tangent stiffness method so the implementation is considered verified.

*Thermal strains*

Applying a tangent stiffness analysis to a heated section is very similar to applying it to a section at ambient temperature. However, the assumption of plane sections remaining plane must be examined more closely.

In unloaded axially and flexurally restrained members, the mechanical strain in any fibre is equal to the thermal strain. Thermal strains, therefore, directly induce stresses within the member. In unrestrained members, this is not the case; thermal strains induce changes in curvature and length, but no net moment or force [24]. Instead, they produce a deflection and internal self equilibrating internal stresses. The forces in the section balance as some regions are in compression, and some are in tension. In an unrestrained member, this leads to an initial mechanical strain state which is not zero. Thus, it has been recognised that to obtain valid load-axial strain or moment-curvature relationships, adjustments must be made to the initial state of the strain field to compensate for the thermal strain. In symmetrically heated sections, this can be done by the application of an axial strain to cancel out the axial force. The axial strain is calculated iteratively, such that the forces due to the combination of axial strain and thermal strain are in equilibrium [3].

Where a section is non-symmetrically heated, and thermal curvature is induced, the procedure is more complicated, but similar. Instead of the application of axial strain to equilibrate the axial force, a curvature and an axial strain must be applied until both the internal moment and axial force are in equilibrium. Where biaxial moments are introduced, equilibrium must be obtained by the adjustment of biaxial curvatures and axial strains.

Application of the initial strain state and subsequent calculation of the sectional yield surface allows the surface to be drawn for a cross section without reference to the member boundary conditions. In the case where an axial member remains un-restrained, no axial force will develop, and the loading state can be plotted from the applied bending moments. On the other hand, where a member is fully restrained the axial loading the member undergoes can be derived from simple calculations, or a finite element model. In this situation, the axial load would be equal and opposite to the axial load due to the initial strain state [25]. Likewise, in a flexurally unrestrained member no net bending moment would be induced by the thermal curvature. In the case where a member is at least partially restrained in rotation at both ends, bending moments would develop due to the thermal strains.

*Heating*

The section described and analysed above was now assumed to be uniformly exposed to a gas temperature of 600ºC for one hour. A heat-transfer analysis was conducted using material properties from Eurocode 2 for calcareous concrete as inputs to the finite-element program Abaqus. The temperature distribution in the column at one hour is shown in Fig. 5a. Subsequently, mechanical analysis using the tangent stiffness method was undertaken to determine the interaction curve after one hour of heating. The steel stiffness and strength degradation rates given in Eurocode 2 were approximated to those of a perfectly elasto-plastic material and used in this analysis. A direct comparison between the uniaixal capacities of the ambient and heated sections can be made; Fig. 5b shows the progressive change in the extent of the failure surface for the value of $M_y = 0$ and demonstrates the use of the tangent-stiffness method for determining interaction curves of heated sections.

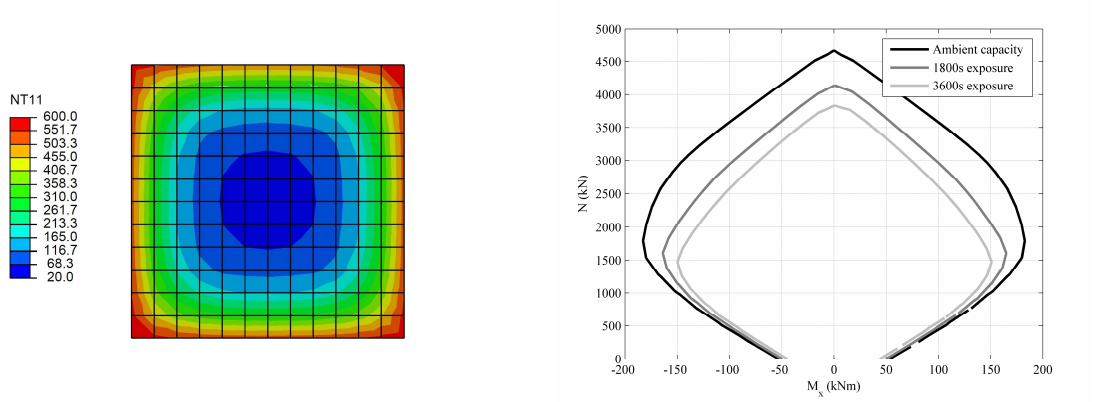


a) b)

*Figure 5. a) Temperature distribution in the column at one hour (°C); b) Uniaxial interaction diagram at ambient, t = 1800s and t = 3600s.*

## 4 APPLICATION OF THE METHOD

### 4.1Analysis of a Heated Section

To show the versatility of the tangent modulus method and to compare its predictions with existing methods, a beam similar to that of Dwaikat [18] was analysed (Fig. 6a). The section was assumed to be subject to a standard fire [13] from three sides for a duration of two hours, and a heat transfer analysis of the section was conducted using Abaqus in the same manner as described above. The beam cross-section was then analysed using the tangent stiffness method for the predicted temperature fields at several intervals during the heating for a range of biaxial bending conditions. A bending capacity analysis of the beam was also conducted using the Eurocode 500ºC isotherm method. The same heat transfer data was used for this analysis, and values of $\eta$ = 1.0, $\gamma_{M,fi}$ = 1.0 and $\lambda$ = 0.8 (Fig. 1) were used in accordance with EC2. The results of all these analyses are also shown in Fig. 6 and a direct comparison between failure surfaces at different temperatures with $M_y$ = 0 is shown in Fig. 7. Unlike a uniformly heated section [17, 26], an asymmetrically heated section's interaction surface distorts as well shrinking during heating [16]. The asymmetry in the failure diagram results from the reference axis remaining at a constant location while the plastic neutral axis moves through the section.

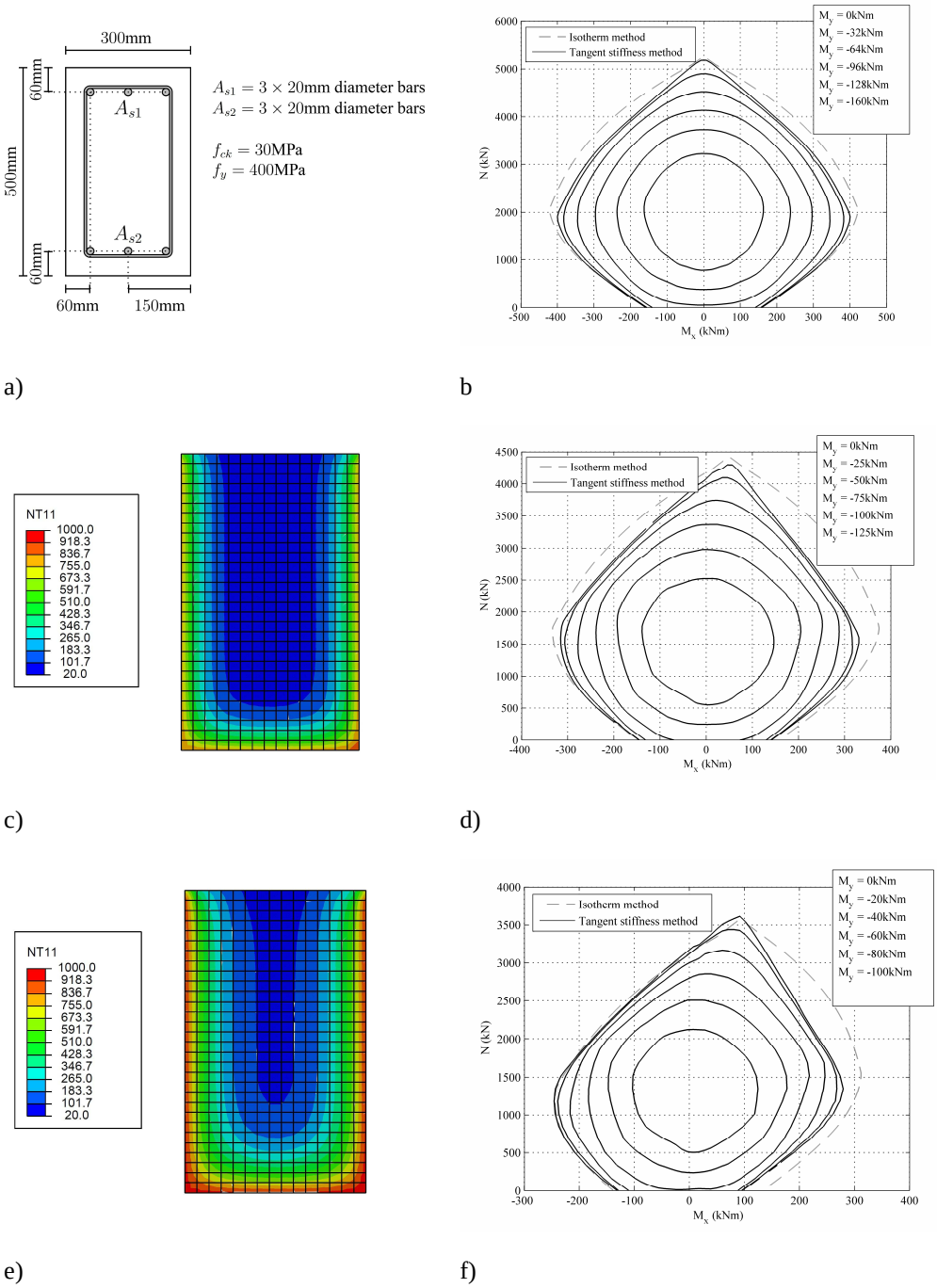


*Figure 6. a) Arrangement of the section; b) Ambient interaction diagram for the section using both tangent method and isotherm method; c) Section temperature profile after one hour (°C); d) Interaction diagram for the section at one hour using both tangent method and isotherm method; e) Section temperature profile after two hours (°C); f) Interaction diagram for the section at two hours using both tangent method and isotherm method.*

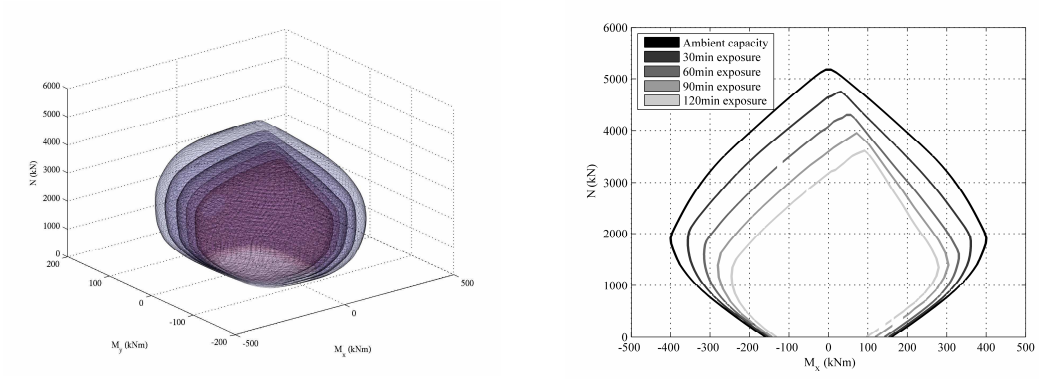


a) b)

*Figure 7. a) Multiple failure surfaces; b) Comparison of uniaxial interaction diagram*

**4.2 DISCUSSION**

Comparison of the results highlights significant differences between the predictions of the two methods. For uniaxial bending, Fig. 6 shows:

- The methods predict maximum axial capacity to within 2% of each other at all temperatures.
- At ambient temperature (Fig. 2b), the pure bending capacities given by the two methods are negligibly different. There is less than 1% difference between the calculations.
- At ambient temperature (Fig. 2b), the isotherm method overestimates the capacity of the beam under combinations of moment and axial force by a maximum of 5%.
- As the temperature of the section increases, the pure bending capacities given by the isotherm method are significantly above those given by the tangent stiffness method. This is particularly the case in sagging, where up to a 35% overestimation is obtained. Pure hogging produces a moment overestimation of 5%.
- The isotherm method almost universally over-estimates the capacity of the section under combinations of sagging moment and axial force. In the high axial load region, this overestimation grows from 5% to 15% as the section is heated.
- In contrast, overestimation of the hogging moment decreases as the section is heated. In fact, when the section is at its hottest, the agreement between the two results is very good with an error of less than 3% throughout.

These observations of the uniaxial bending results for both methods show that the 500ºC isotherm method cannot be assumed to be a conservative design approach. It consistently overestimates the capacity of the section, particularly in sagging. Other researchers have found the isotherm method to be unconservative in pure uniaxial bending [27]. This study shows that the unconservatism extends to bending with different levels of axial force.

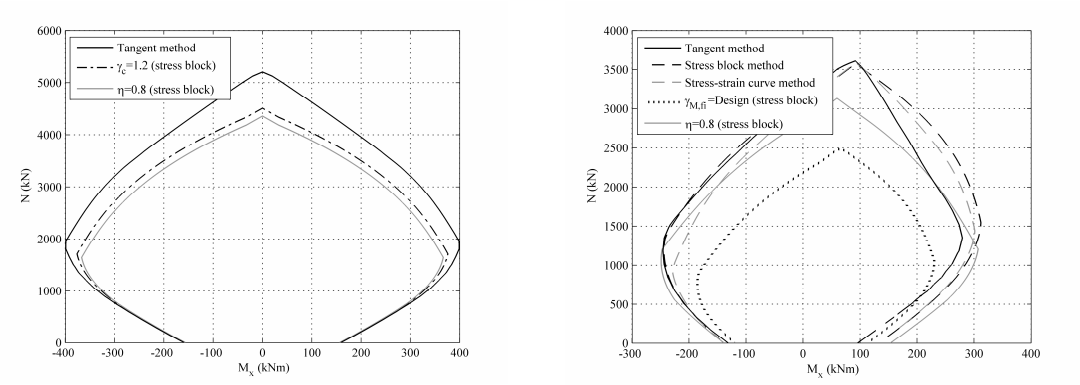


a) b)

*Figure 8. a) Different individual safety factors; b) Equivalent capacities for the tangent method, stress block method, full stress-strain curve method, design safety factors, and with a reduced stress block.*

Although it is unsurprising that a crude assessment such as the isotherm method does not give accurate results, it is of concern that the results are unconservative. The causes of this unconservatism are twofold: the specific differences between the prediction of sagging and hogging capacity at higher temperatures are largely attributable to the assumptions inherent in the isotherm method. However, it is possible to attribute some of the error directly to the use of a stress block technique.

Heated concrete reaches its maximum compressive strength at a higher strain than cold concrete. Thus, in order for a section to develop a given axial load when subject to sagging bending, the neutral axis will be lower in a heated section than a cold section. Consequently, the internal lever arm and hence the moment capacity will be reduced. These effects are fully captured the tangent stiffness method but ignored in the isotherm method, which is unconservative as a result. In hogging, however, the effect described is largely cancelled out by the fact that the heated section soffit has been effectively removed in the isotherm method due to its high temperature. The removal of this area and its corresponding contribution to the total bending moment largely cancels out the overestimation caused by the inappropriate maximum strain assumptions. The above considerations highlight how the isotherm method has certain assumptions that inevitably will lead to unconservative predictions for some strain-curvature combinations, as demonstrated above. However, there are aspects of the underlying stress-block method that produce further inaccuracies.

The dimensions of the stress block used in this method are determined by the parameters $\lambda$ and $\eta$ as shown in Fig. 1. These in turn are specified to ensure that under pure bending at ambient temperature the stress-block applies a force of the same magnitude and with the same lever-arm about the neutral axis as would occur if a full material stress-strain curve were used in an analysis. For a concrete strength of 50MPa or less, values of $\lambda$ and $\eta$ are given as 0.8, and 1.0 respectively in Eurocode 2. Under accidental loading (fire) conditions, the value of $\gamma_M$ for concrete in Eurocode 2 is modified from 1.5 to 1.0 thus meaning any section analysis undertaken using the isotherm method has effectively no material safety factor and relies only on the values of $\lambda$ and $\eta$. These simplified terms cannot accurately represent both the correct stresses and the appropriate lever arms which result from the true concrete stress-strain curve under any but the simplest load cases. This is particularly the case when the neutral axis is not in the section, and the stress block acts over the whole section. Although an accurate prediction of the pure axial capacity can be obtained (because $\eta$ = 1, and the value of $\lambda$ is irrelevant) this study shows that this method produces inaccurate and unconservative results when bending moments are present.

Given the interdependence of these safety factors for obtaining a conservative design at high temperature, it is of interest to examine the effect of arbitrary modifications of the stress-block. Modification of either $\eta$ to 0.8, or $\gamma_c$ to 1.2, allow a conservative result to be obtained for the ambient case (Figure 8a). However, this is an inefficient approach as in both of these cases the maximum axial capacity is significantly underestimated. Furthermore, neither of these modifications is sufficient to ensure that the entire interaction envelope of the isotherm method was within the failure surface given by the tangent stiffness method for the heated (120min) case. Further modification of the material partial safety factors to the ambient temperature design values (1.15 and 1.5 for steel and concrete respectively) in the heated case reveals that the predictions of moment capacity remain unconservative (Figure 8b). The overestimation caused by the stress block technique can be further analysed by applying the isotherm technique with a full concrete stress-strain relationship Fig. 8b. This modification, however, is not sufficient to allow for a fully conservative capacity assessment.

The variation of parameters and techniques in the manner described above allows the source of the unconservatism in the heated sections to be more closely analysed. It is possible to obtain a more conservative result by modification of the stress block. However, despite modification of the partial safety factors, the permissible sagging moment in the heated section (as predicted by the isotherm method) remained significantly unconservative. The sagging overestimation is specifically caused by the difference in the location of the neutral axis between the two methods. The lower neutral axis in the heated section causes a lower moment to be generated than in the ambient, reduced area, section. The adoption of a more realistic stress-strain curve for the ambient concrete, does not give a conservative result. It is therefore concluded that the unconservatism in the predicted capacities is caused more by the assumption of ambient concrete behaviour inherent in the isotherm method, rather than because of the use of the stress block technique. Another cut-off value such as 400ºC or 300ºC would, inevitably, give a more conservative answer. However, this would not solve the underlying problem with the cool concrete assumption.

## 5) CONCLUSIONS

Several conclusions can be drawn from this study:

- The failure surfaces of ambient and heated reinforced concrete sections can be found rapidly and accurately by locating singularities in the sectional tangent modulus matrix.
- The 500ºC isotherm method is unconservative in predicting the failure surface of a heated section due to the stress block method (see above) and the assumption of uniform temperature in the concrete.
- Biaxial failure surfaces for ambient and heated reinforced concrete sections can be clearly represented on a single diagram.
- When all the partial safety factors are removed, the stress block method is unconservative in predicting the failure surface of a section at ambient temperature.

## ACKNOWLEDGEMENTS

The authors of this paper would like to acknowledge BRE Trust for their financial support of this project. The authors would also like to thank Professor J. Michael Rotter and Dr Antonis Giannopoulos for their help in developing this work.

**REFERENCES**

[1] EN1992-1-1. Eurocode 2: Design of Concrete Structures - Part 1-1: General rules and rules for buildings, 1999.

[2] Yen JYR. Quasi-Newton Method for Reinforced-Concrete Column Analysis and Design. Journal of Structural Engineering 1991;117:657.

[3] El-Fitiany SF, Youssef MA. Assessing the flexural and axial behaviour of reinforced concrete members at elevated temperatures using sectional analysis. Fire Safety Journal 2009;44:691.

[4] Rocca S, Galati N, Nanni A. Interaction diagram methodology for design of FRP-confined reinforced concrete columns. Construction and Building Materials 2009;23:1508.

[5] Mosley B, Bungey J, Hulse R. Reinforced Concrete Design to Eurocode 2. New York: Palgrave MacMillan, 2007.

[6] Nawy EG. Reinforced Concrete; a Fundamental Approach. London: Pearson, 2009.

[7] Gillie M, Usmani A, Rotter M. Bending and Membrane Action in Concrete Slabs. Fire and Materials 2004;28:139.

[8] Bazant ZP, Cedolin L. Stability of Structures: Elastic, Inelastic, Fracture, and Damage Theories. New York: Oxford University Press, 1991.

[9] Rodriguez JA, Aristizabal-Ochoa JD. Biaxial Interaction Diagrams for Short RC Columns of Any Cross Section. Journal of Structural Engineering 1999;125:672.

[10] Rotter M. Rapid Exact Inelastic Biaxial Bending Analysis. Journal of Structural Engineering 1985;111:2659.

[11] Fafitis A. Interaction Surfaces of Reinforced-Concrete Sections in Biaxial Bending. Journal of Structural Engineering 2001;127:840.

[12] Kreyszig E. Advance Engineering Mathematics. New York: Wiley, 1999.

[13] EN1991-1-2. Eurocode 1: Actions of Structures - Part 1-2: General Actions - Actions on Structures Exposed to Fire, 1999.

[14] EN1992-1-2. Design of Concrete Structures - Part1-2: General rules- Structural fire design, 1992.

[15] Lennon T, Rupasinghe R, Canisius G, Waleed N, Matthews S. Concrete Structures in Fire: Performance, design and analysis. Watford: BRE press, 2007.

[16] Garlock MEM, Quiel SE. Plastic Axial Load and Moment Interaction Curves for Fire-Exposed Steel Sections with Thermal Gradients. Journal of Structural Engineering 2008;134:874.

[17] Bamonte P. On the Role of Second-Order Effects in HSC Columns Exposed to Fire. In: Tan KH, Kodur VKR, Tan TH, editors. Fifth International Conference of Structures in Fire. Singapore, 2008.

[18] Dwaikat MB, Kodur VKR. A numerical approach for modeling the fire induced restraint effects in reinforced concrete beams. Fire Safety Journal 2008;43:291.

[19] Rodriguez-Gutierrez JA, Aristizabal-Ochoa JD. Reinforced, Partially, and Fully Prestressed Slender Concrete Columns under Biaxial Bending and Axial Load. Journal of Structural Engineering 2001;127:774.

[20] MATLAB. Natick: The MathWorks Inc, 2008.

[21] EN1992-1-2. Design of Concrete Structures - Part1-2: General rules- Structural fire design, , 1992.

[22] Bonet JL, Miguel PF, Fernandez MA, Romero ML. Analytical Approach to Failure Surfaces in Reinforced Concrete Sections Subjected to Axial Loads and Biaxial Bending. Journal of Structural Engineering 2004;130:2006.

[23] Abaqus. Abaqus Analysis User's Manual. Providence: Dassault Systemes Simulia Corp, 2008.

[24] Tassios TP, Chronopoulos MP. Structural Response of RC Elements Under Fire. The Structural Engineer 1991;69:227.

[25] Usmani AS, Rotter JM, Lamont A, Sanad AM, Gillie M. Fundamental Principles of Structural Behaviour under Thermal Effects. 36 2001:721.

[26] Taerwe L. From Member Design to Global Structural Behaviour. In: Rodrigues JPC, Khoury GA, Hoj NP, editors. International Workshop of Fire Design of Concrete Structures. Coimbra, Portugal, 2007. p.253.

[27] Goncalves MC, Rodrigues JPC. Ultimate Bending Moment Capacity of Reinforced Concrete Beam Sections at High Temperatures. In: Rodrigues JPC, Khoury GA, Hoj NP, editors. International Workshop of Fire Design of Concrete Structures. Coimbra, Portugal, 2007. p.281.

# Interaction Diagrams for Heated Concrete Sections using the Tangent Stiffness Matrix

A. H. Law & M. Gillie
*The University of Edinburgh, Edinburgh, UK*

ABSTRACT: Bending moment axial force interaction diagrams are a commonly used tool in any design office. When designing for fire conditions, the large axial forces which develop place an additional importance on the consideration of the interplay between axial forces and moments. This paper presents a new method for calculating the biaxial bending moment/axial force capacity for a general section through the use of the sectional tangent stiffness. A beam-column section subject to fire is assessed, and comparisons made with simplified design tools. It is concluded that derivation of the interaction surface from the tangent stiffness matrix is possible, and that current simplified methods for fire design cannot be assumed conservative.

## 1 INTRODUCTION

The design of reinforced concrete sections requires the specification of a number of parameters such as the section breadth and depth; the area of steel; and the strengths of the concrete and steel. Where a section is subject to both an axial force and bending moments about one or both axes, interaction diagrams are commonly used to determine the area of steel required to resist the moments and forces to which the section is subjected. Structural design codes (e.g. (EN1992-1-1 1999)) often provide interaction diagrams for use with typical concrete sections at ambient temperature that allow the user to circumvent the cumbersome calculations necessary to determine suitable section parameters directly. However, there are many situations, such as fire loading, where structural engineers may need interaction diagrams for sections which are not covered by the standard cases. In these circumstances it is necessary to produce interaction diagrams from first principles, or to rely on very crude approaches such as the "isotherm" method (EN1992-1-2, 2004). This paper presents a method based on the tangent stiffness matrix of a section by which interaction diagrams can be produced accurately and rapidly for arbitrary heated sections.

## 2 CURRENT APPROACH

### 2.1 *Interaction Diagrams for Design*

Interaction diagrams used for design are based on the assumption that there is a maximum allowable concrete compressive strain which prevents concrete crushing. It is also frequently assumed that plane sections remain plane, that the tensile strength of concrete is negligible (El-Fitiany 2009; Rocca 2009; Yen 1991) and that the concrete stress distribution can be represented by a rectangular stress-block (Mosley 2007; Nawy 2009). From these assumptions, the derivation of an interaction diagram is relatively simple. By holding extreme fibre strains at the maximum permissible value while curvature is varied, moment and axial force (M-N) pairs that lie on the interaction diagram for the section can be obtained by appropriate integrations of the resulting stresses over the section.

This method enables the creation of interaction curves in uniaxial bending, and also interaction surfaces when biaxial bending is considered. The method is efficient because each M-N pair calculated is known to lie on the design interaction curve due to the assumption of a maximum permissible concrete strain. Diagrams produced this way can either be used directly or be normalised appropriately to allow the engineer to specify the section properties. However, because the assumptions made regarding maximum strain and the size of the associated stress block are design assumptions (which may include safety factors), the interaction diagrams obtained are not indications of failure strength, but rather show an appropriate, conservative design capacity.

### 2.2 *Interaction Diagrams for Assessment*

Obtaining an interaction diagram when a maximum compressive strain is not specified is a more

difficult problem. The simplest methods of creating these diagrams rely on a "brute force" approach in which a section is analysed for many combinations of $\kappa_x$, $\kappa_y$ and $\varepsilon_a$; appropriate integrations of the section stresses are then used to plot a point in $M_x$-$M_y$-N space for each combination. Assembly of all these points gives a "cloud" of points which are all inside or on the interaction curve (Bazant 1991; Gillie 2004; Rodriguez 1999). By connecting the outermost points in this cloud, the interaction curve can be drawn. Figure 2c demonstrates the generation of a number points which would contribute to the cloud of data. A significant problem with this method is that there is no clear way of determining which points lie on the interaction curve and which points lie just inside it, so determining the interaction curve from a cloud of points is awkward. These problems are magnified if biaxial bending is considered and an interaction surface required. The method is also computationally expensive as many integrations of the stresses over the section are required.

Several authors have used analytical integration to allow the more rapid calculation of stresses over a cross section (Rodriguez 1999; Rotter 1985). However, these methods loose their rapidity in the case of concrete at high temperature; in this case, several different integrations must be made for areas of different temperature or, the integration itself must be temperature dependent.

## 3 THE TANGENT STIFFNESS METHOD

### 3.1 *Background*

Although typically used in structural stability calculations as part of Shandley's tangent modulus equation (Bazant 1991), tangent stiffness matrices can also be used to locate failure surfaces. A section's tangent stiffness matrix relates small changes in generalized strains (typically an axial strain and two curvatures are needed for the analysis of biaxial bending of concrete sections) to small changes in the corresponding stress-resultants (an axial force and two bending moments). When a section's response is non-linear, the tangent stiffness matrix is distinct from the elastic stiffness matrix. For the set of stress-resultants mentioned, the relationship between incremental stress-resultants, tangent stiffness matrix, and incremental generalized strains of a section can be written in the standard form:

$$\begin{bmatrix} \delta P \\ \delta M_x \\ \delta M_y \end{bmatrix} = \begin{bmatrix} K_{11} & K_{12} & K_{13} \\ K_{21} & K_{22} & K_{23} \\ K_{31} & K_{32} & K_{33} \end{bmatrix} \begin{bmatrix} \delta \varepsilon_a \\ \delta \kappa_x \\ \delta \kappa_y \end{bmatrix} \quad (1)$$

or,

$$\delta \mathbf{F} = \mathbf{K} \delta \boldsymbol{\varepsilon} \quad (2)$$

The set of stress-resultants that lie on the failure surface of a section are those that arise when an incremental change in the generalized strain vector results in $\delta\mathbf{F}$=0. That is, stress-resultants on the failure surface are those that occur when **K** is singular, or:

$$\det(\mathbf{K}) = 0 \quad (3)$$

### 3.2 *Implementation*

Implementation of the tangent stiffness method for constructing interaction diagrams will be discussed with reference to a simple section at ambient temperature that is shown in Figure 1. Assumptions made in this implementation are: plane sections remain plane; the concrete compressive stress-strain behaviour is as given in Eurocode 2 (EN1992-1-2 1992); the tensile strength of concrete is zero; the stress-strain relationship of steel is elasto-plastic; and there is no bond slip between steel and concrete. Each of these assumptions has been made in various combinations by other authors (Bonet 2004; Rodriguez 1999; Yen 1991). They result in a marginally conservative estimate of strength (with the exception of bond slip).

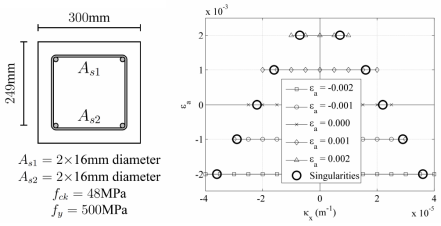


Figure 1. Section diagram and the location of the singularity points with in terms of strain and curvature

The section was divided into a 20x20 grid of elements; each moment and axial force was calculated by making the appropriate stress calculation and integrating it with respect to the element area, and summing the forces and moments for all the elements.

To produce the interaction curve for the section subject to uniaxial bending ($\kappa_y$=0), discrete values of axial strain were considered. A simple search algorithm was then initiated to trial different values of curvature for each value of axial strain. Once the region of singularity was located, a more refined search could be conducted to locate the precise location of the singularity. The procedure for the search algorithm is illustrated in Figure 1. A change in the sign of the determinant between curvature values indicated that a region of singularity had been reached.

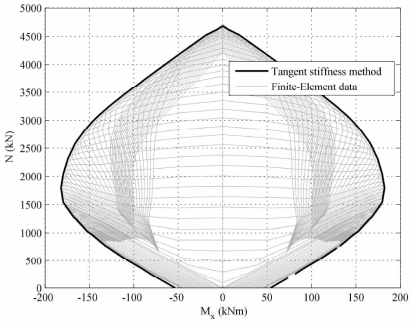


Figure 2. Uniaxial interaction diagram and finite element verification data

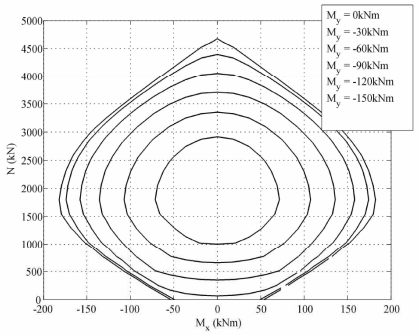


Figure 3. Interaction surface presented in two dimensions.

Using this method, a uniaxial interaction diagram can quickly be derived for a section of any cross section. The method can be verified against "brute force" results from established finite element software. Figure 2 shows the final uniaxial diagram in conjunction with the results from an Abaqus analysis of an equivalent beam element.

### 3.3 *Presentation*

The presentation of interaction curves for uniaxial bending is well established and straightforward. Presentation of interaction surfaces for biaxial bending in a form readily accessible to the design engineer is less easy. The method described above can easily be used to create biaxial interaction surfaces as well as uniaxial interaction curves. However, the presentation of a surface plot is not terribly useful in this respect. Visualisation choices are often dependent on the purpose for which the plot to be used. For generality, the plots in this study are presented as $M_x$, N interaction diagrams with multiple curves representing different values of $M_y$. Thus, a large amount of information can be summarised on one diagram (Fig. 3). A single plot is sufficient for a member with a minimum of one axis of symmetry. However, where a section is entirely asymmetric, two diagrams may be required to encompass all of the information. In design, the tensile capacity of concrete sections is not normally considered. As such, just the compressive capacities are presented in this paper.

Also of some interest is the representation of the failure surface in terms of $\varepsilon_a$, $\kappa_x$ and $\kappa_y$ shown in Figure 4. This failure surface bares a striking resemblance to a conventional yield surface such as Drucker-Prager or Mohr-Coulomb, particularly in the tensile axial strain region. It should be noted that if rebar rupture were included in the material model, then the surface would be capped at the higher tensile strains.

Despite its similarity to conventional yield surfaces, the variation in the determinant as the values of strain and curvature change is quite irregular. It does not, therefore, lend itself to solution via the backward Euler method.

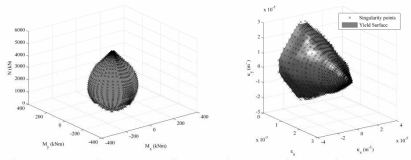

Figure 4. The M-N interaction surface; the corresponding strain-curvature failure surface.

## 4 HEATED SECTION EXAMPLE

### 4.1 *Application of Tangent Stiffness Method*

The section described and analysed in the previous section was assumed to be exposed from three sides to a 3 hour Standard Fire. A heat-transfer analysis was conducted using the finite-element program, Abaqus. The material properties for calcareous concrete from Eurocode 2 were used as inputs for the model. The temperature distribution in the column at one hour, two hours and three hours is shown in Figure 5. Subsequently, a mechanical analysis using the tangent stiffness method was undertaken to determine the interaction curves at half hour intervals throughout the heating process. The steel stiffness and strength degradation rates given in Eurocode 2 were approximated to those of a perfectly elasto-plastic material and used in this analysis.

A direct comparison between the uniaxial capacities of the ambient and heated sections can be made; Figure 6 shows the progressive change in the extent of the failure surface for the value of $M_y - 0$ and demonstrates the use of the tangent-stiffness method for determining interaction curves of heated sections.

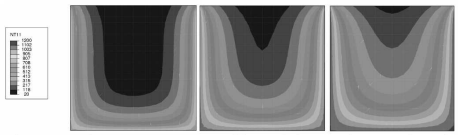

Figure 5. The temperature profiles of the section at 1hr, 2hrs, and 3hrs.

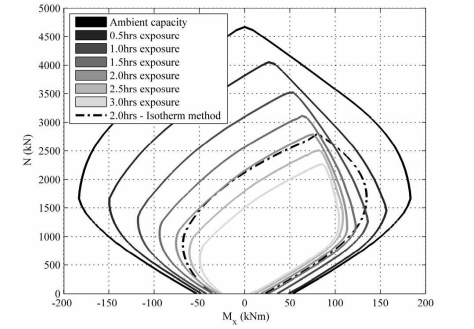


Figure 6. Comparison of interaction envelope at after different durations of exposure.

### 4.2 *Comparison with Isotherm method*

The 500C isotherm method was also used to assess the section for the 1hr exposure temperature profile. The corresponding interaction curve is displayed on Figure 6. It can be clearly seen that the isotherm method gives an unconservative answer particularly in sagging, high compression region.

This result is of concern as it demonstrates that the isotherm method cannot be assumed to be conservative. Heated concrete reaches its maximum compressive strength at a higher strain than cold concrete. Thus, in order for a section to develop a given axial load when subject to sagging bending, the neutral axis must be lower in a heated section than a cold section. Consequently, the internal lever arm and hence the moment capacity is reduced. These effects are fully captured the tangent stiffness method but ignored in the isotherm method, which is unconservative as a result.

## 5 CONCLUSIONS

There are several conclusions which can be drawn from this study:

- The failure surfaces of ambient and heated reinforced concrete sections can be found rapidly and accurately by locating singularities in the sectional tangent modulus matrix.
- Biaxial failure surfaces for ambient and heated reinforced concrete sections can be clearly represented on a single diagram.
- The 500ºC isotherm method is unconservative in predicting the failure surface of a heated section primarily due to the assumption of uniform temperature in the concrete.

## 6 ACKNOWLEDGEMENTS

The authors would like to acknowledge and thank BRE Trust for funding this project.

## 7 REFERENCES

Bazant, Z. P., & Cedolin, L. 1991. *Stability of Structures: Elastic, Inelastic, Fracture, and Damage Theories*, Oxford University Press, New York.

Bonet, J. L., Miguel, P. F., Fernandez, M. A., & Romero, M. L. 2004. "Analytical Approach to Failure Surfaces in Reinforced Concrete Sections Subjected to Axial Loads and Biaxial Bending." *Journal of Structural Engineering*, 130(12): 2006-2015.

El-Fitiany, S. F., & Youssef, M. A. 2009. "Assessing the flexural and axial behaviour of reinforced concrete members at elevated temperatures using sectional analysis." *Fire Safety Journal*, 44(5): 691-703.

EN1992-1-1. 1999. *Eurocode 2: Design of Concrete Structures - Part 1-1: General rules and rules for buildings*.

EN1992-1-2. 1992. *Design of Concrete Structures - Part1-2: General rules- Structural fire design*.

Gillie, M., Usmani, A., & Rotter, M. 2004. "Bending and Membrane Action in Concrete Slabs." *Fire and Materials*, 28: 139-157.

Mosley, B., Bungey, J., & Hulse, R. 2007. *Reinforced Concrete Design to Eurocode 2*, Palgrave MacMillan, New York.

Nawy, E. G. 2009. *Reinforced Concrete; a Fundamental Approach*, Pearson, London.

Rocca, S., Galati, N., & Nanni, A. 2009. "Interaction diagram methodology for design of FRP-confined reinforced concrete columns." *Construction and Building Materials*, 23(4): 1508-1520.

Rodriguez, J. A., & Aristizabal-Ochoa, J. D. 1999. "Biaxial Interaction Diagrams for Short RC Columns of Any Cross Section." *Journal of Structural Engineering*, 125(6): 672-683.

Rotter, M. 1985. "Rapid Exact Inelastic Biaxial Bending Analysis." *Journal of Structural Engineering*, 111(12): 2659-2674.

Yen, J. Y. R. 1991. "Quasi-Newton Method for Reinforced-Concrete Column Analysis and Design." *Journal of Structural Engineering*, 117(3): 657-666.

# A Performance Based Methodology Using Travelling Fires for Structural Analysis

Jamie Stern-Gottfried[1,2], Angus Law[1], Guillermo Rein[1], Martin Gillie[1], and Jose L. Torero[1]

1) BRE Centre for Fire Safety Engineering
The University of Edinburgh
The King's Buildings
Edinburgh, EH9 3JL, UK

2) Arup Fire
13 Fitzroy St
London W1T 4BQ, UK

## INTRODUCTION

Close inspection of real fires in large, open compartments reveals that they do not burn simultaneously throughout the whole compartment. Instead, these fires tend to move as flames spread, partitions or false ceilings break, and ventilation changes through glazing failure. These fires have been labelled 'travelling fires.'

Despite these observations, fire scenarios currently used for the structural fire design of modern buildings are based on one of two traditional methods for specifying the fire environment; the standard temperature-time curve (which has its origins in the late 19th century [1]) or parametric temperature-time curves, such as that specified in Eurocode 1 [2]. These methods are based on the extrapolation of existing fire test data, which stems from tests performed in small compartments that are almost cubic in nature. This test geometry allows for good mixing of the fire gases and thus for a uniform temperature distribution throughout the compartment.

While both of these methods have great merits and represented breakthroughs in the discipline at their times of adoption, they have inherent limitations with regards to their range of applicability [3, 4, 5]. For example, Eurocode 1 states that the design equations are only valid for compartments with floor areas up to 500m$^2$ and heights up to 4m, the enclosure must have no openings through the ceiling, and the compartment linings are also restricted to a thermal inertia between 1000 and 2200 J/m$^2$s$^{½}$K, which means that highly conductive linings such as glass facades and highly insulating materials cannot be taken into account. As a result, common features in modern construction like large enclosures, high ceilings, atria, large open spaces, multiple floors connected by voids, and glass façades are excluded from the range of applicability of the current methodologies. These limitations, which are largely associated with the physical size and geometric features of the experimental compartments on which the methods are based, ought to be carefully considered when the methods are applied to an engineering design. This is particularly relevant given the large floor plates and complicated architecture of modern buildings.

A recent survey of buildings in Edinburgh, UK [6] underlines the narrow design fire specifications in the Eurocodes. For buildings built over a long period of time starting in the early 20th century, 66% of their total volume falls within the limitations. However, in a newly constructed, modern building that has open spaces and glass facades, only 8% of the total volume is within the limitations. This suggests that modern building trends are moving out of the limits of current design practices.

The limitations of the existing methods arise from the assumption of uniform temperature conditions throughout the whole floor of a compartment. A fire that would cause these uniform conditions burns uniformly within the enclosure and generates high temperatures for

SFPE – Lund, Sweden

a relatively short duration. This is opposed to a travelling fire that burns locally but spreads through the enclosure with time, generating lower temperatures for longer times. Buchanan [7] notes that post-flashover fires in open plan offices are unlikely to burn throughout the whole space at once. Real, large fires that have lead to structural failure, such as those in the World Trade Center towers 1, 2 [8] and 7 [9] in September 2001, the Windsor Tower in Madrid, Spain in February 2005 [10] and the Faculty of Architecture building at TU Delft in the Netherlands in May 2008 [11] were all observed to travel across floor plates, and vertically between floors, rather than burn uniformly for their duration. Travelling fires have also been observed experimentally in compartments with non-uniform ventilation [12, 13, 14].

While the traditional methods have inherent assumptions of fire behaviour different from that observed in real fires, they have generally been deemed to be conservative, and therefore appropriate, tools for structural fire design in the absence of better and more relevant data. Although these methods might be considered acceptable for most design cases, the need for better optimisation of structural behaviour in fire will eventually require a more performance-based definition of the fire. This is particularly relevant given that computational methods for determining structural behaviour have matured over the last decade and have enabled analysis of more complex structural systems. This has led to an understanding that many modern structures do not behave in the same manner as simpler, more traditional frame based systems. Thus, in order to address these differences, and continue to enable innovation in structural design, a more sophisticated characterisation of fire scenarios is required.

Therefore a methodology is being developed that allows for a wide range of possible fires, including both uniform burning and travelling fires, by considering the fire dynamics within a given building [3, 4, 5]. This methodology also facilitates the collaboration between fire safety engineers and structural fire engineers, which is an identified need within the structural fire community [15], to jointly determine the most challenging fire scenarios for a structure.

This paper presents the framework of the methodology and applies it to calculate the thermal environment and corresponding structural response for a case study in a generic concrete structure.

**TRAVELLING FIRES**

The key aspect of the new methodology is to characterise the thermal environment for structural analysis accounting for the fire dynamics specific to the building, including a wide range of possible fires. In order to achieve this, a simple fire model is selected that enables capturing the spatial and temporal changes of the fire-induced thermal field. This model is then applied to a particular floor of the building accounting for a family of fires that range between one that burns in a small area and travels across the floor plate for a long duration and one that is well distributed across the whole floor plate but burns for a short duration.

**Temperature Field**

The methodology divides the effect of a fire on structural elements into the near field and the far field. The near field is when a structural element is exposed directly to the flames of the fire and the far field is when it is exposed to the hot gases, i.e. the smoke layer away from the flames, as shown in Figure 1. This division of the thermal field allows the methodology to avoid the well-known inaccuracies of flame temperature prediction of most fire models

In previous work, a CFD fire model [3] was selected to study the temperature field as a function of distance from the fire. In other work [4], as in this paper, a ceiling jet correlation was used. The ceiling jet correlation developed by Alpert [16] and given below in Eq. (1) was selected in this case as the simple fire model to study the temperature field as a function of distance from the fire. The use of such a correlation is deemed appropriate if the floor area is large and the smoke layer is thin relative to the floor to ceiling height.

$$T_{\max} - T_{\infty} = \frac{5.38\left(\dot{Q}/r\right)^{2/3}}{H} \qquad (1)$$

where $T_{\max}$ is the maximum ceiling jet temperature (K)
$T_{\infty}$ is the ambient temperature (K)
$\dot{Q}$ is the total heat release rate (kW)
$r$ is the distance from the centre of the fire (m)
$H$ is the floor to ceiling height (m)

Note that while Alpert gives a piecewise equation for maximum ceiling jet temperatures to describe the near field ($r/H \leq 0.18$) and far field ($r/H > 0.18$) temperatures, only the far field equation is utilised in the present case study as the near field temperature is assumed to be the flame temperature.

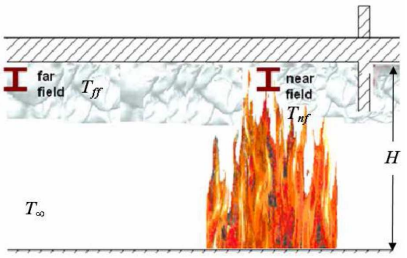


*Figure 1: Illustration of near and far fields*

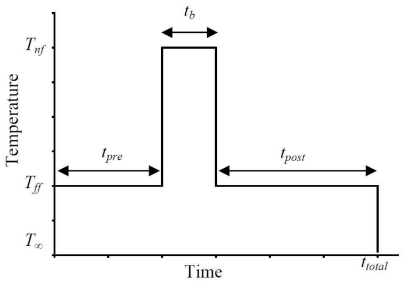


*Figure 2: Temperature-time curve at one ceiling location for a travelling fire*

The ceiling jet correlation characterises the spatial variation of the temperature field only as a function of the distance from the fire. This simple correlation was chosen to provide a straightforward description of the temperature field that is qualitatively sufficient to progress the development of the methodology. Alternative fire models, including computational fluid dynamics, can be utilised instead.

**Family of Fires**

A family, or set, of fires that covers the range of possible fires, both travelling and uniformly burning, needs to be selected as an input for the temperature field. To do this it was assumed that each fire in the family would burn over a surface, $A_b$, which is a percentage of the total floor area, $A_f$, of the building, ranging from 1% to 100%. The burning area of the fire that is

equal to 100% of the floor area is a well distributed fire. All other burning areas represent travelling fires of different sizes.

It is assumed that there is a uniform fuel load across the fire path and the fire will burn at a constant heat release per unit area typical of the building load under study. Thus the burning time can be calculated by Eq. (2).

$$t_b = \frac{q_f}{\dot{Q}''} \tag{2}$$

where $t_b$ is the burning time (s)
$q_f$ is the fuel load density (MJ/m$^2$)
$\dot{Q}''$ is the heat release rate per unit area (MW/m$^2$)

For the case study presented below, the fuel load density, $q_f$, is assumed to be 570 MJ/m$^2$, as per the 80$^{th}$ percentile design value [17] for office buildings. The heat release rate per unit area, $\dot{Q}''$, is taken as 500 kW/m$^2$ which is deemed to be a typical value for densely furnished spaces, as design guidance [18] gives this value for retail spaces. Based on these two values, the characteristic burning time, $t_b$, is calculated by Eq. (2) to be 19min.

Note that the burning time is independent of the burning area. Thus the 100% burning area and the 1% burning area will both consume all of the fuel over the specified area in the same time, $t_b$. However, a travelling fire moves from one burning area to the next so that the total burning duration, $t_{total}$, across the floor plate is extended. This time is given in Eq. (3).

$$t_{total} = \frac{t_b}{A_b / A_t} \tag{3}$$

This means that there is a longer total burning duration for smaller burning areas. For example, the 100% burning area has a total burning duration of 19min and the 1% burning area a total burning duration of 1900min.

**Near Field vs. Far Field**

In the case of the 100% burning area, all of the structure will experience near field (flame) conditions for the total burning duration (which is equal to the burning time, $t_b$). However, for the travelling fire cases, any one structural element will feel far field (smoke) conditions for the majority of the total burning duration and near field conditions for the burning time as the fire burns locally to the element. The time one element experiences far field conditions prior to the arrival of the flame is defined as $t_{pre}$ and the time the element experiences far field conditions after the departure of the flame is defined as $t_{post}$. Figure 1 illustrates the difference between the near field and far field.

The near field temperature, $T_{nf}$, is taken here as the flame temperature, which for the accuracy levels required in structural fire analysis, is more or less constant and approximately 1200°C to 1300°C for a typical office fire [19]. The far field conditions vary as a function of distance away from the fire. However, it is desirable to express the results in simple terms but without loss of generality in order to be of valuable engineering use. Thus, the far field is reduced to a

single characteristic temperature, $T_{ff}$, which keeps the amount of information passed to the structural analysis manageable. To do this, the far field temperature is taken as the fourth-power average of $T_{max}$ (to favour high temperatures in a bias towards radiation heat transfer and worst case conditions) over the distance between the end of the near field, $r_{nf}$, and the end of the far field, $r_{ff}$. This average is calculated by Eq. (4).

$$T_{ff} = \frac{\left[\int_{r_{nf}}^{r_{ff}} (T_{\max})^4 \, dr\right]^{1/4}}{(r_{ff} - r_{nf})^{1/4}} \tag{4}$$

Once the far field temperature is determined for a given fire size, the temperature time history of a point can be described, as shown in Figure 2. Determining both $t_{pre}$ and $t_{post}$ is dependent on the path of the fire and the exact position being examined. However, it is not possible to establish a fire's path of travel a priori, as there are many potential paths in principle; therefore assumptions must be made for worst case conditions.

The growth and decay phases of the gas temperatures for the travelling fires detailed in this paper are assumed to be very fast. This is because the larger an enclosure is, the lower the importance of the thermal inertial of its linings are, thus the faster the growth and decay phases will be. In other words, the transport of the hot gases in the smoke layer is faster than the heat transfer to the surfaces. Note that the cooling is not neglected in the structural analysis, only the decay phase is eliminated from the fire environment.

**CASE STUDY: A GENERIC MULTI-STOREY CONCRETE STRUCTURE**

The methodology described above has been applied to a generic multi-storey concrete structure. Travelling fires are applied to one storey of this generic structure for comparison to the traditional methods. The structure was designed in accordance with Eurocode 2 [20, 21]. The plan and elevation for the structure is shown in Figure 3. The total floor plate is 6 structural bays by 4 bays (total dimensions of 42m x 28m) with a central core. The bays along the length of the structure are numbered for reference in the figures below. Every floor is of flat slab construction and each floor slab is 200mm thick; the interior columns are 400mm x 400mm; and the exterior columns are 300mm x 300mm. The design strength of the concrete in the columns is 48MPa, and the design strength of the concrete in the slabs is 40MPa. As the intended fires were to take place on the mid-floors of the structure, the foundations were not designed, and the columns were assumed to be rigidly fixed at the base. To allow the study of the different fires and their effects, a finite element model for heat transfer and structural response was created.

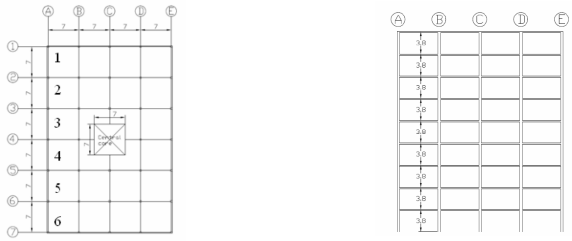


***Figure 3: Plan and elevation of the generic concrete structure (distances in m)***

In addition to the application of the method as given in this paper, a parametric study has been conducted to determine the influence of various assumptions of the methodology on the ultimate structural response. The base case assumes that a uniform line fire begins at one end of the structure and travels across the floor plate, as illustrated in Figure 4 (the white arrow indicates direction of travel). In the base case, the fire moves in discrete units, based on the size of the fire, staying in each location for the burning duration.

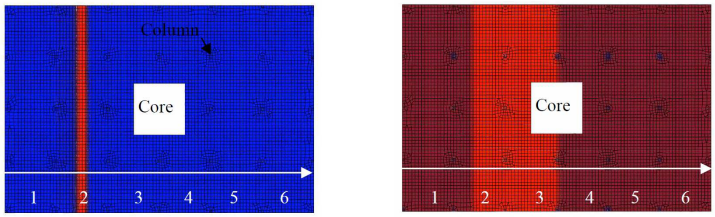


a) 2.5% fire b) 25% fire

***Figure 4: Progression of both a small and large fire across floor plates***

**Fire Environment Results – Base Case**

The Base Case results in a range of far field temperatures and total burning durations, as shown in Table 1. These results illustrate the concept that hotter far field temperatures will occur for larger fires, but for shorter durations.

The family of results for the far field temperatures vs. total burning duration are plotted in Figure 5. Note that Figure 5 provides the far field values that need to be combined with the near field to produce curves of the type shown in Figure 2. For travelling fires, every point on the floor plate will at some point experience the near field temperature for the burning time (19 min) and the far field temperature for the rest of the total burning duration. Figure 5 also contains the temperature-time curves of traditional design methods; the standard fire and two applications of the Eurocode 1 parametric temperature-time curve. The parametric curves include a short, hot fire due to a large amount of ventilation (100% façade glass breakage) and a long, cooler fire due to less ventilation (25% façade glass breakage).

| **Fire Size (% of Floor Area)** | **Burning Area $A_b$ ($m^2$)** | **Total Heat Release Rate $\dot{Q}$ (MW)** | **Total Burning Duration $t_b$ (min)** | **Far Field Temperature $T_{ff}$ (°C)** |
|---|---|---|---|---|
| 1% | 11 | 6 | 1900 | 204 |
| 2.5% | 28 | 14 | 760 | 325 |
| 5% | 56 | 28 | 380 | 432 |
| 10% | 113 | 56 | 190 | 566 |
| 25% | 282 | 141 | 76 | 805 |
| 50% | 564 | 282 | 38 | 1037 |
| 100% | 1127 | 564 | 19 | *1200 (near field)* |

***Table 1: Results for the family of travelling fires of different sizes***

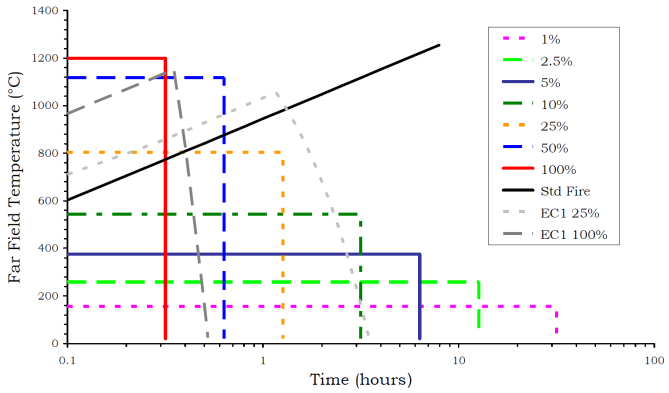


***Figure 5: Far field temperatures travelling fires compared with traditional design curves***

The results show that hotter far field temperatures last for less time. The standard fire and parametric fire curves fall close to travelling fires for sizes between 25% and 50% , but after one hour of burning time, the standard fire curve results cannot be explained in terms of the possible fire dynamics in large buildings.

**Structural Response – Base Case**

A series of heat transfer analyses were conducted using the commercially available finite-element software Abaqus. The temperature-time curves generated from the methodology and traditional design methods were applied to the generic concrete structure in an Abaqus model. The slab was 200mm thick with a concrete cover of 30mm. modelled using a shell element. Gas phase temperatures defined for each of the fires were applied via radiation and convection to the surface of each element as described in Eurocode 2 [20, 21]. An emissivity of 0.7 and a convective coefficient of 25W/m$^2$K was used. The temperature on the top side of the slab was assumed to be ambient. The thermal properties were in accordance with the Eurocode 2 definition of a 1.5% moisture content in concrete. The average temperature of the two lower rebar layers was calculated by interpolating between the two nearest integration points in the model. Further details of the heat transfer analysis are presented elsewhere [22].

The resultant temperature of the rebar nearest the ceiling was spatially averaged for each structural bay. The averaging of the rebar temperatures was done within a bay, over the full extent of the bay, to smooth out the effect of localised high temperatures. For example, if a fire were to heat the mid-span of one of the bays, very high temperatures would be recorded in the rebar locally, despite a negligible overall effect on the rest of the structure. The results shown here are for the bay that reached the highest average temperature, as it represents the worst case scenario for the structure. In all cases, except where stated, this corresponds with the final bay to be heated (Bay 6).

Figure 6 shows the average rebar temperature profiles for Bay 6 for each of the base case fire curves. Also displayed are the temperature profiles for the standard fire, the short Eurocode curve (100% glass breakage), and the long Eurocode curve (25% glass breakage). Figure 6

and Table 2 show that the travelling fires between 10% and 25% induce higher average rebar temperatures than both of the Eurocode parametric fires. This is because the smoke in the far field pre-heats the structure before the flames of the near field arrive, causing higher final temperatures

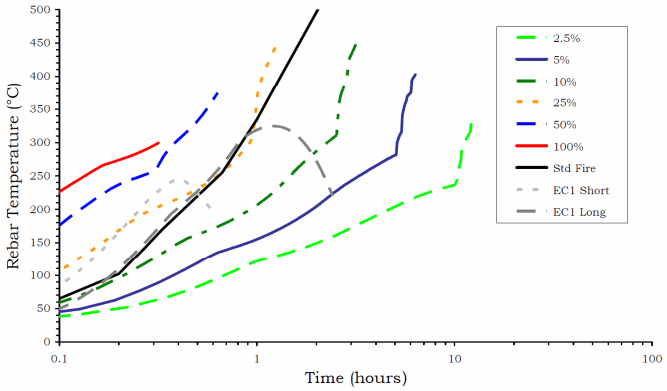


***Figure 6: Rebar temperatures for the base case fire and traditional design curves***

The maximum temperature reached for a travelling fire (450°C by the 25% case) would be reached with a standard fire that lasted for approximately 100min. That is, the 25% travelling fire in this case study is equivalent to a 100min exposure of the standard fire. However, note that the standard fire behaviour is non-physical in nature as highlighted earlier.

| Fire Scenario | Far Field Temperature (°C) | Maximum Rebar Temperature (°C) |
|---|---|---|
| 2.5% | 325 | 333 |
| 5% | 432 | 403 |
| 10% | 566 | 448 |
| 25% | 805 | 450 |
| 50% | 1037 | 374 |
| 100% | *1200 (near field)* | 299 |
| Standard Fire | *N/A* | 450 (after 100min) |
| EC1 Short | *N/A* | 246 |
| EC1 Long | *N/A* | 325 |

***Table 2: Maximum rebar temperatures for the base case fire and traditional design curves***

**PARAMETRIC STUDY**

As the results from the base case highlight, the 10% and 25% floor area fires prove to be the most onerous cases for the structure, as they result in highest rebar temperatures. Therefore the sensitivity of various input parameters on the rebar temperatures are examined in this parametric study, keeping the fire size constant at 25% of the floor area. Parameters examined include discretisation of the far field temperature, progression of the fire through

the space (gradual or sudden), and the fire path. The changes in these parameters and the subsequent results are explored.

**Far Field Temperature Discretisation**

The base case assumed a single temperature for the whole far field over the floor plate not directly exposed to the flames. In real fires, gas temperatures decrease with distance from the fire. Thus, two further spatial temperature decays from the near field are investigated; two far field temperatures and a monotonic far field. The two far field temperture includes one far field temperature ahead of the linear travelling fire and a different one behind. Both are calculated using Eq. (4) and different distances. The continuous far field is a monotonic decay and decreasing with distance from the near field, as defined in Eq. (4). A representative spatial temperature distribution for one fire location is given in Figure 7.

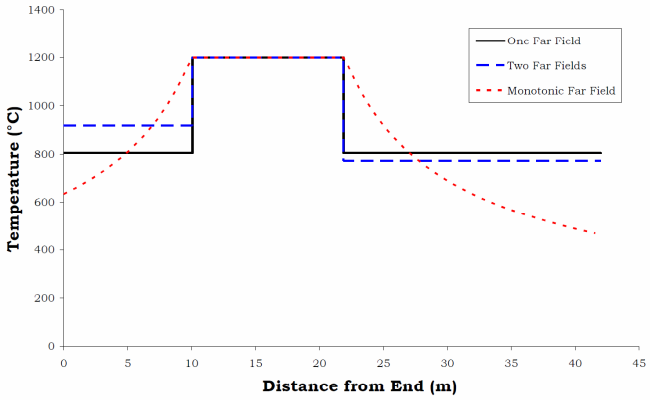


*Figure 7: Representative curve for three different far field temperature discretisations*

Figure 8 shows the resulting rebar temperature from the different far field descriptions. It can be seen that there is little difference between the maximum temperatures calculated for the one and two far field temperature cases. This is due to the similar temperatures of both cases and the damping effect of the concrete structure. The monotonically decreasing far field temperature causes a different pattern of heating to emerge; however, the difference in the maximum rebar temperature is small (below 4%). The rebar temperatures obtained using the one far field temperature description are marginally higher than the other cases and, therefore, represent a more conservative design case. They are also much simpler to implement.

**Fire Progression**

The fires in the base case scenarios are assumed to move linearly across the floor plate in a sudden manner, i.e. the fire is assumed to remain in one place for the local burning time, then jump to adjacent burning area. An alternate to this assumption is allowing the fire to move gradually across the floor plate. This comparison of the two fire progressions was made with the monotonic far field.

The results for the two types of fire progression (gentle and sudden) each are shown in Figure 7 for the monotonic far field case. It is noted that the total burning duration had to be artificially extended to account for the full movement of the travelling fire in the gentle progression case. The results show that the sudden progression induces marginally higher (6%) rebar temperatures than the gentle progression, despite a shorter total burning duration. It is noted, that for the sudden progression fire, the highest average bay temperatures were in Bay 5 rather than in Bay 6. This is due to the fact that the discretisation of the fire meant that Bay 5 had portions of the near field temperatures for twice the duration of Bay 6, resulting in hotter rebar temperatures.

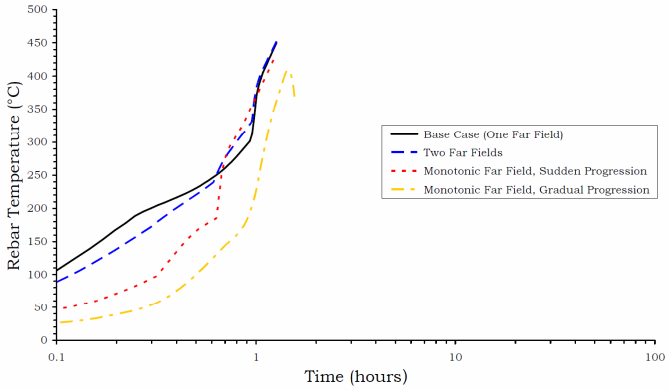


***Figure 8: Rebar temperatures for different far field temperature characterisations***

**Fire Path**

A real fire could take on differing shapes and travel in numerous paths. However, the path of the fire cannot be determined *a priori*. Thus, the effect of differing shapes and paths is examined here. Three types are examined: linear (base case), corner, and ring travelling fires. Figure 9 illustrates these fire shapes for a 25% floor area fire. The base case assumes linear fires uniform over the width of the structure and travelling along its length. The corner fire is assumed to travel around the core. Two paths of the ring fire have been assumed; from façade to core and from core to façade.

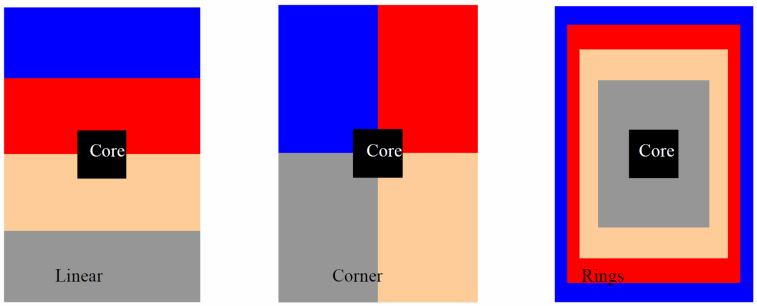


***Figure 9: Rebar temperatures for different far field temperature characterisations***

SFPE – Lund, Sweden

The results show that there is little difference between the different paths and the rebar temperatures, as given in Figure 10. This is due to the fact that the duration and temperature of the exposure to the bays producing the hottest rebar temperature in each scenario were the same. The exception was the ring fire with travel from the core to the façade; in this case, part of the bay was heated by one near field until it burned out, and then the rest of the bay was heated by the next near field as it progressed towards the edge of the structure.

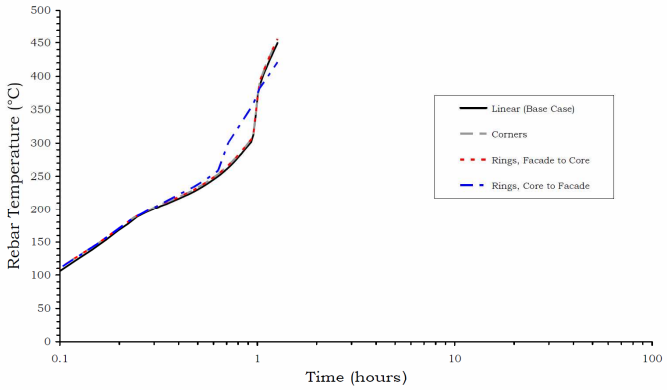


***Figure 10: Rebar temperatures for various fire paths***

**CONCLUSIONS**

This paper has presented a performance based methodology for specifying design fires for structural analysis using travelling fires. The method allows for inclusion of a family of fires, to cover a wide range of possible fire dynamics in a building, ultimately leading to quantification of a range of possible structural responses. This range includes potentially more challenging cases than are included in the traditional design methods. This travelling fires methodology has been applied to a generic concrete structure for a base case scenario, and a further parametric study. Specific observations from this analysis are listed below:

Travelling fires between 10% and 25% of the floor area induced the highest rebar temperatures. These temperatures are higher than the maximum temperatures induced by the equivalent parametric fires and similar to those induced by a 100min standard fire. This finding is important because it demonstrates that considering only uniform fires in structural design may not always be as conservative as previously assumed.

The parametric study shows that the secondary details about the implementation of the travelling fires methodology do not have a large impact on the structural performance. The resultant rebar temperatures are shown to be relatively insensitive to the far field temperature description, fire progression, and fire path. Specification of a linear fire with a single temperature far field, progressing in discrete steps is sufficient to capture the range of structural responses. Higher levels of complexity are not justified with the current level of accuracy required for the thermal inputs for structural fire design.

SFPE – Lund, Sweden

**REFERENCES**


1 Babrauskas, V. and Williamson R.B., "The historical basis of fire resistance testing – Part II." Fire Technology, 14(4) 1978, pp. 304-316.
2 Eurocode 1: Actions on structures – Part 1-2: General actions – Actions on structures exposed to fire, European standard EN 1991-1-2, 2002. CEN, Brussels.
3 Rein, G. et al, "Multi-story Fire Analysis for High-Rise Buildings," *11th International Interflam Conference*, London, 2007. http://www.era.lib.ed.ac.uk/handle/1842/1980
4 Stern-Gottfried, J., Rein, G., Lane, B., and Torero, J. L., "An innovative approach to design fires for structural analysis of non-conventional buildings: A case study," *Application of Structural Fire Engineering*, Prague, Czech Republic, 2009, http://eurofiredesign.fsv.cvut.cz/Proceedings/1st_session.pdf
5 Stern-Gottfried, J., Rein, G., and Torero, J. L, "Travel Guide", *Fire Risk Management*, Nov 2009, pp. 12-16. http://www.era.lib.ed.ac.uk/handle/1842/3184
6 Jonsdottir, A. and Rein, G. "Out of Range", *Fire Risk Management*, Dec 2009, pp. 14-17. http://www.era.lib.ed.ac.uk/handle/1842/3204
7 Buchanan, A., *Structural Design for Fire Safety*, John Wiley & Sons, 2001
8 Gann, R.G. et al, "Reconstruction of the Fires in the World Trade Center Towers", *NIST NCSTAR 1-5*, September 2005.
9 McAllister, T.P. et al, "Structural Fire Response and Probably Collapse Sequence of the World Trade Center Building 7", *NIST NCSTAR 1-9*, November 2008.
10 Fletcher, I. et al, "Model-Based Analysis of a Concrete Building Subjected to Fire," *Advanced Research Workshop on Fire Computer Modelling*, Santander, Spain, 2007.
11 Zannoni, M. et al, "Brand bij Bouwkunde", *COT Instituut voor Veilingheids – en Crisismanagement*, December 2008.
12 Thomas, I.R. and Bennets, I.D., "Fires in Enclosures with Single Ventilation Openings – Comparison of Long and Wide Enclosures," *The 6th International Symposium on Fire Safety Science*, Poitiers, France, 1999.
13 Kirby, B.R. et al, "Natural Fires in Large Scale Compartments", *British Steel*, 1994
14 The Dalmarnock Fire Tests: Experiments and Modelling, *University of Edinburgh*, Eds Rein, Empis, and Carvel, University of Edinburgh, 2007.
15 Buchanan, A., "The Challenges of Predicting Structural Performance in Fires." *The 9th International Symposium on Fire Safety Science*, Karlsruhe, Germany, 2008.
16 Alpert, R.L., "Calculation of Response Time of Ceiling-Mounted Fire Detectors," *Fire Technology*, Vol. 8, 1972, pp. 181–195.
17 PD 6688-1-2:2007, Background Paper to the UK National Annex to BS EN 1991-1-2.
18 TM19, "Relationships for Smoke Control", *CIBSE*, 1995
19 Drysdale, D., *An Introduction to Fire Dynamics*, 2nd Edition, John Wiley & Sons, 1999.
20 EN1992-1-2. Eurocode 2: Design of Concrete Structures - Part1-2: General rules-Structural fire design, 1992.
21 EN1991-1-2. Eurocode 1: Actions of Structures - Part 1-2: General Actions - Actions on Structures Exposed to Fire, 1999.
22 Law, A., Gillie, M., Stern-Gottfried, J., and Rein, G., "The Influence of Travelling Fires on the Response of a Concrete Frame", *6th International Conference on Structures in Fire*, East Lancing, MI, USA 2010.

Application of Structural Fire Engineering, 19-20 February 2009, Prague, Czech Republic

# INCORPORATION OF LOAD INDUCED THERMAL STRAIN IN FINITE ELEMENT MODELS

Angus Law[a], Martin Gillie[a], Pankaj Pankaj[a]

[a] The University of Edinburgh, BRE Centre for Fire Safety Engineering, Edinburgh, UK

## INTRODUCTION

Load induced thermal strain (LITS) is an integral part of the behaviour of concrete in fire. The existence of LITS has been well documented and modelled by different researchers. It is vital that this strain development is correctly represented in structural models, as the locked in strains due to LITS constituents are significant. Current methods of modelling LITS involve incorporating the strains into constitutive curves. This approach allows the total strains developed due to LITS to be simply included in a finite element analysis. More thorough representation is needed to accurately represent the plastic components in loading directions, and the total strains in non-loading directions. This paper presents a technique to allow the evolution of LITS in accordance with the rules developed in several academic material models [1-3]. The technique is implemented with a simple Drucker-Prager yield surface and the results assessed.

## 1 CURRENT METHODS

Inclusion of LITS in a concrete constitutive curve is a convenient way of representing LITS in finite element analyses. It allows the modeller to make the LITS constituents temperature dependent and stress dependent – through the use of multiple curves and by giving strains for different stresses respectively. A number of models are available from different sources and for different concretes [1-4]. Failure to represent LITS will result in the modeller not modelling the strains developed in the material accurately, thereby giving an excessively stiff structure. In fact, it could be argued that since LITS is an integral part of concrete behaviour, a modeller failing to include it will not be modelling concrete but some other, non-physical, material.

Once the total strains caused by LITS have been represented, one can then think about the division between elastic and plastic strains. It has been observed that the largest LITS constituents are irrecoverable [5], i.e. they are plastic strains. Therefore, to accurately model these plastic strains it is necessary to determine the elastic modulus of the material as a function of temperature. If the modulus is too stiff, the plastic strains will be overestimated; too soft, and they will be underestimated. The correct modelling of plastic strain constituents becomes increasingly important as a structure cools as the plastic strains will induce greater tension on strain reversal.

Some authors have presented their material models in parts, allowing the user to build the strain constituents into the full curve. The elastic modulus is, therefore, a precisely identifiable constituent of the material model and can be included in a structural model as such; henceforth, this will be termed the “actual” modulus. Other material data such as that presented in the Eurocode do not specify the value of the elastic modulus. In this case, extra care must be taken to represent the strain components accurately. Where the elastic modulus is the initial gradient of the constitutive curve, this will be termed the “apparent” modulus.

## 2 MULTIPLE DIMENSIONS

The primary focus for research has been on total and plastic strains in the direction of loading. However, attention must also be paid to the non-loading directions. Depending on the model in use, failure to carefully consider the elastic modulus of the material will result in unrepresentative plastic strains, unexpected strains in the non-loading directions, or a mixture of both. The potential for these effects to manifest themselves can be demonstrated by simple example.

### 2.1 Simple Example

Consider a small cube of concrete, subject to a displacement controlled loading in principle direction 2, but free to move in the transverse directions with a Drucker-Prager yield surface and a perfectly plastic material behaviour, as shown in Figure 1. The associative isotropic flow rule (used here for simplicity) dictates that once the yield surface is reached, plastic strain must occur in a direction orthogonal to the yield surface in stress space. This means that plastic strains are induced in directions other than the one in which the load is applied.

Since the location of trial stress is a function of the elastic modulus, the implications of this for the implementation of LITS via a constitutive curve are significant. The inclusion of LITS whether implicitly (with an "apparent" elastic modulus) or explicitly (with an "actual" elastic modulus) will result in a proportion of that LITS becoming active in the transverse directions. The magnitude of the extra strain would depend on the stress state of the material, and on the degree of plasticity developed in the principle direction. For example: should the element described above be at a stress state at point A, no plastic strains would be induced in the 1-direction.

In the case of the apparent modulus, a large proportion of the extra transverse strain may be elastic; while in the case of the actual modulus, the major constituent of the incremental strain would be plastic.

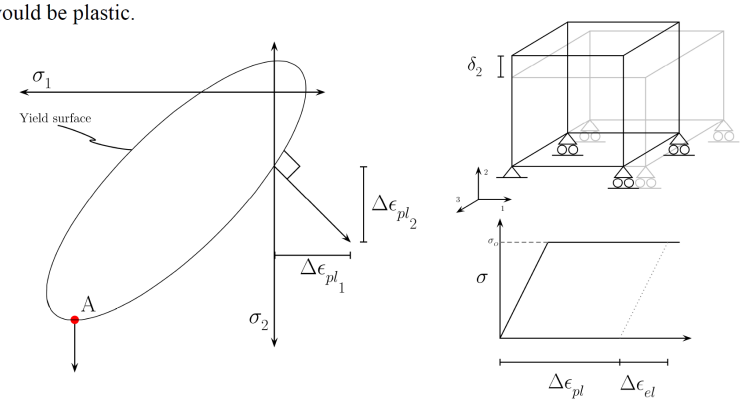


*Fig. 1.* Plastic flow, and model setup.

The impact of this difference is demonstrated below using the Drucker-Prager yield criterion with a constitutive curve corresponding to that of the 200ºC Terro [2] LITS curve. This temperature was used as there is a significant difference between the actual and apparent

moduli, but the temperature is not too extreme. Two different models were created each with a different elastic modulus – apparent or actual – but with the same constitutive curve (Figure 2(a)). The numerical models consisted of a single cubic finite element, restrained at the base in the 2-direction (but free to displace in the 1 and 3-directions) and were strained in the 2-direction. The corresponding deformations and plastic strains were recorded.

Figure 2(b) shows the total strains in the lateral deformation direction. The strains in the 2-direction (i.e. the direction of strain control) are the same for both of the models. In the unrestricted directions, however, there are significant differences in the total strains, particularly in the inelastic phase of the constitutive model. The origin of these differences can be clearly seen from Fig. 2(c). In the "apparent" model the plastic strains do not develop until much later in the deformation process. The "actual" model on the other hand – because of the difference between the elastic modulus and the shape of the constitutive curve – activates the plastic strain constituents immediately. This difference in plastic strain is entirely due to the activation of the flow rule at a much lower stress. Consequently, though the plastic strain in the loading direction is what would be expected from using the "actual" modulus in the constitutive curve, the impact of this approach can be clearly seen in the non-loading directions.

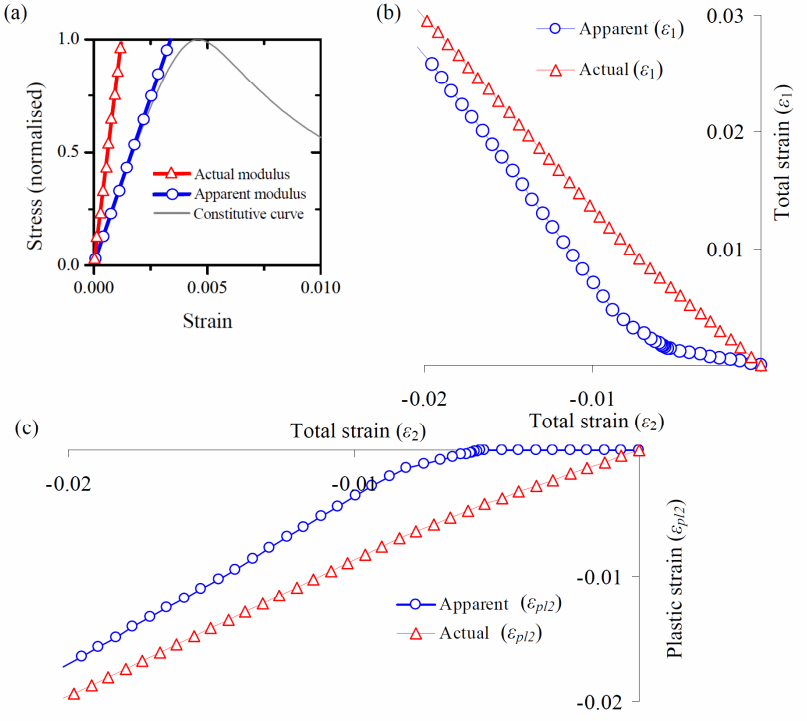


*Fig. 2.* The same constitutive curve with different elastic moduli gives different lateral deformations and direct plastic strains.

Since equations to represent LITS are all functions of temperature and direct stress, the use of either the apparent or the actual modulus is inadequate if one wants to model the plastic strains accurately, whilst limiting the lateral deformations.

## 3 THE EMBEDDED MODULUS

To allow the modelling of LITS to be more representative, a new method for the inclusion of LITS in the constitutive model while avoiding the transverse strain issue outlined above is proposed. The Drucker-Prager yield criterion and plasticity equations are solved in a two step method: first, the elastic strains and corresponding plastic strains are calculated using the apparent modulus and the normal solution methods (Figure 3); secondly, the elastic ($\varepsilon_{el1}$) and plastic ($\varepsilon_{pl1}$) strains are recalculated using the actual modulus (Fig. 4). As such, the actual modulus is *embedded* within the solution procedure. This second stage can expressed simply as:

$$\varepsilon_{el1} = \frac{\sigma}{E_{em}} \tag{1}$$

where $E_{em}$ is the embedded actual modulus and $\sigma$ is the stress calculated from the previous solution. Since:

$$\varepsilon_{el0} + \varepsilon_{pl0} = \varepsilon_{total} \tag{2}$$

where $\varepsilon_{el0}$ and $\varepsilon_{pl0}$ are the original elastic and plastic strains, and $\varepsilon_{total}$ is the total strain. The new plastic strain can be directly calculated from:

$$\varepsilon_{pl1} = \varepsilon_{total} - \varepsilon_{el1} \tag{3}$$

The new plastic and elastic strains are then used in the subsequent analysis. The equivalent plastic strain is not, however, changed. Consequently, the strains developed in the transverse directions are in line with those that would occur when using an apparent modulus, but the plastic strains developed in the principle direction are as would be expected from using the actual modulus. It should also be noted that where plastic strain has occurred, but the yield function is found to be negative (i.e. the total strain is reduced), the corresponding elastic stresses must be recalculated using the embedded modulus. Otherwise, the redistributed strains would be reabsorbed into the elastic region on return to zero stress.

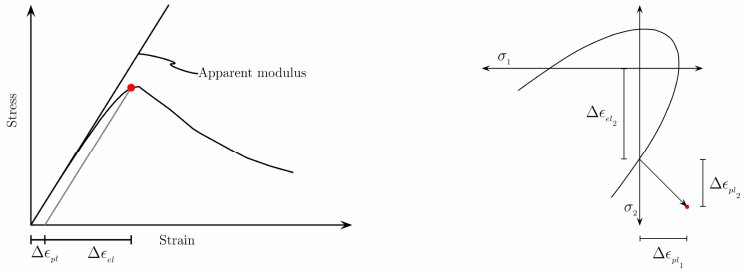


(a) Hardening with apparent modulus (b) Corresponding strains

*Fig. 3.* Calculation of plastic and elastic strains.

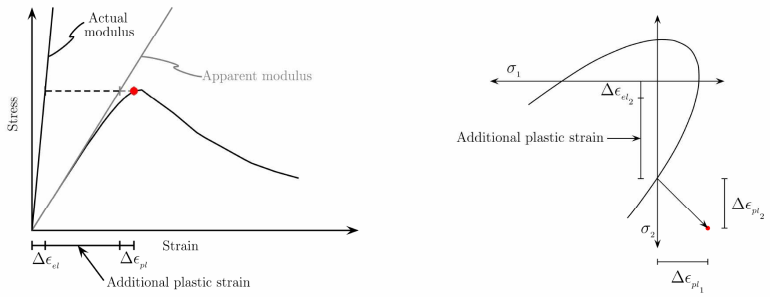


(a) Redistribution found using actual modulus (b) Corresponding strains

*Fig. 4.* Redistribution of strains due to the difference between actual modulus and apparent modulus.

A Drucker-Prager model was created [6-12] which incorporated this method of modification by the embedded modulus. A model with an apparent elastic modulus and an embedded actual modulus was subjected to the previously described test. The results were compared with the previous models (Figure 5).

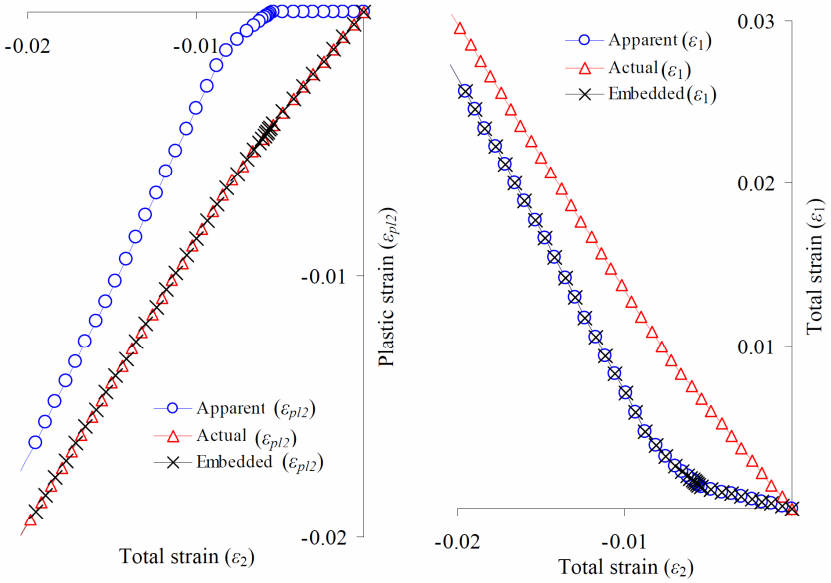


*Fig.5.* Comparison of two stage approach with results from original models.

The total lateral strains experienced by the "embedded" material are the same as those experienced by the "apparent" material. Equally, the total plastic strain experienced in the loading direction is the same as those experienced by the "actual" material. Thus, a fully

plastic, transient strain constituent has been included in the model without affecting the deformations in the non-loading directions. This allows the plastic LITS effect to be successfully modelled uni-axially and in proportion to the applied stress in the way stated in the governing LITS equations.

## 4 CONCLUSION

There are several conclusions to be drawn from this study:

- There are significant differences between a constitutive curve which includes LITS, and a full constitutive model which accurately represents LITS components.
- Inclusion of the plastic strains by means of an "apparent" modulus is useful in one dimension; however, plastic flow rules cause unwanted strains to develop laterally when more than one dimension is considered
- Use of a two step model with an "apparent" modulus, and an embedded "actual" modulus within the material model is one approach which can be used to correctly model the plastic strain due to the LITS equations, while allowing the strain in the lateral directions to be modelled correctly. This model has been demonstrated in the case of an element deformed uniaxially.

The authors of this work would like to gratefully thank the project sponsors; BRE Trust, and the EPSRC.

## 5 REFERENCES

[1] Anderberg Y, Thelandersson S: Stress and Deformation Characteristics of Concrete, 2 - Experimental Investigation and Material Behaviour Model. Sweden, University of Lund, 1976

[2] Terro MJ: Numerical Modeling of the Behaviour of Concrete Structures in Fire. *ACI Structural Journal 95:183-193*, 1998

[3] Nielsen CV, Pearce CJ, Bicanic N: Theoretical Model of High Temperature Effects on Uniaxial Concrete Member under Elastic Restraint. *Magazine of Concrete Research 54:239-249*, 2002

[4] EN1992-1-2: Design of Concrete Structures - Part1-2: General Rules- Structural Fire Design, 1992

[5] Khoury GA, Grainger BN, Sullivan PJE: Transient Thermal Strain of Concrete: Literature Review, Conditions within Specimen and Behaviour of Individual Constituents. *Magazine of Concrete Research 37:131-144*, 1985

[6] Calladine CR: Plasticity for Engineers: Theory and Applications. Chichester, Horwood Publishing, 2000

[7] Crisfield MA: Non-Linear Finite Element Analysis of Solids and Structures. Chichester, Wiley, 1991

[8] Crisfield MA: Non-Linear Finite Element Analysis of Solids and Structures: Advanced Topics. Chichester, Wiley, 1997

[9] Cook RD, Malkus DS, Plesha ME, *et al.*: Concepts and Λpplications of Finite Element Analysis. Chichester, Wiley, 2002

[10] Hill R: The Mathematical Theory of Plasticity. Oxford, Oxford University Press, 1950

[11] Pankaj: Finite Element Analysis in Strain Softening and Localisation Problems, in Department of Civil Engineering. Swansea, University College of Swansea, 1990

[12] Zienkiewicz OC: The Finite Element Method (ed 3). London, McGraw-Hill, 1977

# Appendix V

## Selected Code

## 1. Selected Extracts of Code

Over the course of the research completed, a large amount of code was written. The code was primarily written in FORTRAN, MATLab, and Python and several examples are given in this appendix.

Abaqus Subroutine: USDFLD

This subroutine links the 1st field variable to the maximum temperature which has previously occurred at that integration point. It can only be used in Abaqus Standard

```
      SUBROUTINE USDFLD(FIELD,STATEV,PNEWDT,DIRECT,T,CELENT,
     1 TIME,DTIME,CMNAME,ORNAME,NFIELD,NSTATV,NOEL,NPT,LAYER,
     2 KSPT,KSTEP,KINC,NDI,NSHR,COORD,JMAC,JMATYP,MATLAYO,
     3 LACCFLA)
C
      INCLUDE 'ABA_PARAM.INC'
C
      CHARACTER*80 CMNAME,ORNAME
      CHARACTER*3  FLGRAY(15)
      DIMENSION FIELD(NFIELD),STATEV(NSTATV),DIRECT(3,3),
     1 T(3,3),TIME(2)
      DIMENSION ARRAY(15),JARRAY(15),JMAC(*),JMATYP(*),
     1 COORD(*)
C
      CALL GETVRM('TEMP',ARRAY,JARRAY,FLGRAY,JRCD,JMAC,JMATYP,
     1 MATLAYO,LACCFLA)
      TEMP = ABS( ARRAY(1) )
      print*,ARRAY
      CALL GETVRM('SDV',ARRAY,JARRAY,FLGRAY,JRCD,JMAC,JMATYP,
     1 MATLAYO,LACCFLA)
      TEMPMAX = ARRAY(1)
      FIELD(1) = MAX( TEMP , TEMPMAX )
      STATEV(1) = FIELD(1)
      IF(JRCD.NE.0)THEN
       WRITE(6,*) 'REQUEST ERROR IN USDFLD FOR ELEMENT NUMBER ',
     1      NOEL,'INTEGRATION POINT NUMBER ',NPT
      ENDIF
C
      RETURN
      END
```

Abaqus Subroutine: VUSDFLD

This subroutine links the 1st field variable to the maximum temperature which has previously occurred at that integration point. It can only be used in Abaqus Explicit

```
      subroutine vusdfld(
     *   nblock, nstatev, nfieldv, nprops, ndir, nshr,
     *   jElem, kIntPt, kLayer, kSecPt,
     *   stepTime, totalTime, dt, cmname,
     *   coordMp, direct, T, charLength, props,
     *   stateOld,
     *   stateNew, field )
C
      include 'vaba_param.inc'
C
      dimension jElem(nblock), coordMp(nblock,*),
     *          direct(nblock,3,3), T(nblock,3,3),
     *          charLength(nblock), props(nprops),
     *          stateOld(nblock,nstatev),
     *          stateNew(nblock,nstatev),
     *          field(nblock,nfieldv)
      character*80 cmname
      parameter( nrData=6 )
      character*3 cData(maxblk*nrData)
      dimension rData(maxblk*nrData), jData(maxblk*nrData)
C
      jStatus = 1
      call vgetvrm( 'TEMP', rData, jData, cData, jStatus )
C
      if( jStatus .ne. 0 ) then
         call xplb_abqerr(-2,'Utility routine VGETVRM failed '//
     *        'to get variable.',0,zero,' ')
         call xplb_exit
      end if
C
      call setField( nblock, nstatev, nfieldv, nrData,
     *   rData, stateOld, stateNew, field)
C
      return
      end
      subroutine setField( nblock, nstatev, nfieldv, nrData,
     *   strain, stateOld, stateNew, field )
C
      include 'vaba_param.inc'
C
      dimension stateOld(nblock,nstatev), stateNew(nblock,nstatev),
     *   field(nblock,nfieldv), strain(nblock,nrData)
C
      do k = 1, nblock
         temp = abs( strain(k,1) )
         tempmax = stateOld(k,1)
         field(k,1) = max( temp, tempmax )
         stateNew(k,1) = field(k,1)
C
      end do
C
      return
      end
```

Sectional Analysis Tool: Primary routine

Simplified routine to initiate the various subroutines required for the full sectional analysis program described in chapter 4.

```
function sectional_analysis=sectional_analysis
% This funciton initiates a series of subroutines which calcuate the
% ultimate capacity of a concrete section in terms of axial force, and
% biaxial moment.
%
% The alorithm is based on "Interaction Diagrams for ambient and heated
% concrete sections" by Law and Gillie (Engineering Structures, Volume 32,
% issue 6, June 2010, pp. 1641-1649). It this program is used, a full
% reference should be provided to the above paper.
%
% It should be noted that this verson of the routine does not correct for
% thermal expansion in the concrete. The original routine did make this
% correction, however it was taylor made for a particular section and
% therefore is not general. This section can be reinstated at the end of
% the "temperature_data_mluti_use_updated" subroutine.
%
% This routine has been adapted for use with the excel speadsheet
% "Pro-forma.xls". If the sheets in this file are completed correctly, then
% a the program will generate and print a biaxial interaction diagram.
%
% It should be noted that the subroutines in this program are provided
% as-is, and have many redundent sections of code within them. Users are
% welcome to modify the code, but may find it easier to create there own.
%
% It should also be noted that thought the algorithm should work well with
% any arrangement of steel/concrete, the interpolation function may leave
% gaps for heavily reinforced sections
%
% This interface subroutine is annotated to allow the users to interperate
% their results
%
%%%%%%%%%%%%%%%%%%%%%%%%%%%%%%%%%%%%%%%%%%%%%%%%%%%%%%%%%%%%%%%%%%%%%%%%%%%
% The first section of this program extracts the required information     %
% from the pro-forma spreadsheet                                         %
%%%%%%%%%%%%%%%%%%%%%%%%%%%%%%%%%%%%%%%%%%%%%%%%%%%%%%%%%%%%%%%%%%%%%%%%%%%
filename='Pro-forma.xls'                % Identifies spreadsheet
[sheet1, txt]=xlsread(filename, 1)     % Reads sheet one as both text and real numbers
sheet2=xlsread(filename, 2);            % Reads sheet two as real numbers
fc_amb=sheet1(3,3);                     % Defines concrete compressive strength at↙
ambient
ft_amb=sheet1(4,3);                     % Defines concrete tensile strength at ambient
fy_amb=sheet1(5,3);                     % Defines steel ultimate strength at ambient
bredth=sheet1(9,3);                     % Defines the bredth of the section
depth=sheet1(10,3);                     % Defines the total depth of the section
steel_x=sheet1(:,1);                    % Defines the x-coordinates for the rebar
steel_y=sheet1(:,2);                    % Defines the y-coordinates for the rebar
diameter=sheet1(:,3);                   % Defines the rebar diameter
output_name=txt{25,2}                   % Defines the base name for the output data
a=isnan(steel_x);                       % Identifies the NaNs in the rebar definitions
steel_x(a)=[]                          % Leaves only the useful data by setting the↙
NaNs = []
steel_y(a)=[]                          % Leaves only the useful data by setting the↙
NaNs = []
diameter(a)=[]                         % Leaves only the useful data by setting the↙
NaNs = []
if length(sheet2)==4                    % If only four temperature points are provided,↙
```

```
...
    x_coord=[sheet2(:,1);0];            % an additional mean point will be created to↙
allow ...
    y_coord=[sheet2(:,2);0];            % the interpolation alorithms to function↙
correclty.
    temp=[sheet2(:,3);mean(sheet2(:,3))];
else
x_coord=[sheet2(:,1)];                  % If more than 4 points are specified, they↙
will just ...
y_coord=[sheet2(:,2)];                  % be used direclty.
temp=[sheet2(:,3)];
end
steel_A=0.25*pi*diameter.^2               % Works out the area of each rebar
%%%%%%%%%%%%%%%%%%%%%%%%%%%%%%%%%%%%%%%%%%%%%%%%%%%%%%%%%%%%%%%%%%%%%%%%%%%%%%%
% The second part of the program invokes the main subroutines. The first  %
% routine runs the alorithm descibed in the above paper and locates a     %
% number of points on the interaction surface. It does this for different %
% ratios of phix to phiy, and its progress can be monitored in the        %
% command prompt.                                                         %
%                                                                         %
% The second subroutine, interperates these points and allows them to be  %
% displayed in a flexible format. The output from the second program is   %
% four large cubic arrays. They represent a 3D space where each point has %
% a value. This value, is a proportion relative to the location of the    %
% interaction surface. The interaction surface is located where the value %
% of the space is 100.                                                    %
%%%%%%%%%%%%%%%%%%%%%%%%%%%%%%%%%%%%%%%%%%%%%%%%%%%%%%%%%%%%%%%%%%%%%%%%%%%%%%%
reattempt_locate_points_again_tension_play(output_name,steel_x,steel_y,steel_A,bredth,↙
depth,temp,temp,x_coord,y_coord,fy_amb,steel_A,fc_amb,ft_amb);
datainput_multi_use(output_name);
%%%%%%%%%%%%%%%%%%%%%%%%%%%%%%%%%%%%%%%%%%%%%%%%%%%%%%%%%%%%%%%%%%%%%%%%%%%%%%%
% The final part of the program creates two figures showing the           %
% interaction surface and an interaction diagram.                         %
% The figure is printed as a pdf.                                         %
%%%%%%%%%%%%%%%%%%%%%%%%%%%%%%%%%%%%%%%%%%%%%%%%%%%%%%%%%%%%%%%%%%%%%%%%%%%%%%%
load([output_name '_processed']);       % Loads the data for the required display
myfigure=figure↙
('papertype','A4','color','w','PaperPositionMode','manual','PaperPosition',[0 0 21↙
29.5],'paperorientation','portrait'); % sets up an A4 sheet of paper
xi1=xi1/1000000;                        % Transfers the data into the correct units
yi1=yi1/1000000;                        % Transfers the data into the correct units
zi1=zi1/1000000;                        % Transfers the data into the correct units
subplot(2,1,1);                         % Sets up the first subplot
p = patch(isosurface(xi1,yi1,zi1,w1,100)); % creates a surface at the 100 point in the↙
data
set(p,'FaceColor','blue','EdgeColor','k'); % Defines the surface properties
set(gca,'fontname','times')
daspect([1 1 1]);                       % Aspect ratio
view(3);                                % 3D viewpoint
camlight;                               % Sepcifies the light source
lighting gouraud;                       % Specifies the lighting type
xlabel('M_x (kNm)');                    % x-axis label
ylabel('M_y (kNm)');                    % y-axis label
zlabel('N (kN)');                       % z-axis label
set(gca,'fontname','times')
grid on;                                % Turns on the gridlines
```

```
subplot(2,1,2);                          % Sets up the second subplot
b=contourslice(xi1,yi1,zi1,w1,[],[0],[],[100 100]); % Creates a slice of the data along
the My=0 plane
set(b, 'edgecolor','k','linewidth',2);  % Specifies the line properties
set(gca,'fontname','times')
view(0,0);                               % Specifies the 2D viewpoint
xlabel('M_x (kNm)');                     % x-axis label
zlabel('N (kN)');                        % y-axis label
set(gca,'fontname','times')
grid on;                                 % Turns the grid lines on
box on;                                  % Turns the box around the plot on
g=find(output_name=='_')                 % Locates any underscores in the title of the
file
if g>=1                                  % If there are any underscores, will enter this
if statement
    output_name1=output_name             % Creates new name
    output_name1(g)=' '                  % replaces underscores with a space to provent
inadvertent subscripts
end
string1=(['Interaction diagrams for "' output_name1 '"']); % Secifies the title of the
page
    annotation('textbox',[0.46 0.88 0.1 0.1],...
        'FitBoxToText','on',...
        'HorizontalAlignment','center',...
        'String',string1,...
        'fontsize',14,...
        'fontname','times',...
        'backgroundcolor','none',...
        'edgecolor','none') % Places and formats the title on the page
print('-dpdf','-painters',output_name)  % Prints the surface as a vectored pdf
set(p,'FaceColor','blue','EdgeColor','none'); % Removes the black lines to allow easy
inspection in the figure
```

Parametric study of column.

The verification of the sectional analysis method conducted in chapter four was conductued using a parametric study.

```
column_paper = ParStudy(par='ea', name='shell')
column_paper.define(CONTINUOUS, par='ea', domain=(0.000, 0.0025))
##thick.sample(VALUES,par='ea',values=(0,100,200,300,400,500,600,700,800,900,1000))
column_paper.sample(NUMBER, par='ea', number=25)
column_paper.combine(MESH)
column_paper.generate(template='column_paper')
column_paper.execute(ALL)
column_paper.output(file=ODB, step=1)
column_paper.gather(results='RF2,1', request='HISTORY', frameValue=0.05, variable='RF2')
column_paper.gather(results='RF2,2', request='HISTORY', frameValue=0.1, variable='RF2')
column_paper.gather(results='RF2,3', request='HISTORY', frameValue=0.15, variable='RF2')
column_paper.gather(results='RF2,4', request='HISTORY', frameValue=0.2, variable='RF2')
column_paper.gather(results='RF2,5', request='HISTORY', frameValue=0.25, variable='RF2')
column_paper.gather(results='RF2,6', request='HISTORY', frameValue=0.3, variable='RF2')
column_paper.gather(results='RF2,7', request='HISTORY', frameValue=0.35, variable='RF2')
column_paper.gather(results='RF2,8', request='HISTORY', frameValue=0.4, variable='RF2')
column_paper.gather(results='RF2,9', request='HISTORY', frameValue=0.45, variable='RF2')
column_paper.gather(results='RF2,10', request='HISTORY', frameValue=0.5, variable='RF2')
column_paper.gather(results='RF2,11', request='HISTORY', frameValue=0.55, variable='RF2')
column_paper.gather(results='RF2,12', request='HISTORY', frameValue=0.60, variable='RF2')
column_paper.gather(results='RF2,13', request='HISTORY', frameValue=0.65, variable='RF2')
column_paper.gather(results='RF2,14', request='HISTORY', frameValue=0.7, variable='RF2')
column_paper.gather(results='RF2,15', request='HISTORY', frameValue=0.75, variable='RF2')
column_paper.gather(results='RF2,16', request='HISTORY', frameValue=0.8, variable='RF2')
column_paper.gather(results='RF2,17', request='HISTORY', frameValue=0.85, variable='RF2')
column_paper.gather(results='RF2,18', request='HISTORY', frameValue=0.9, variable='RF2')
column_paper.gather(results='RF2,19', request='HISTORY', frameValue=0.95, variable='RF2')
column_paper.gather(results='RF2,20', request='HISTORY', frameValue=1.00, variable='RF2')
##
column_paper.output(file=ODB, step=2)
column_paper.gather(results='RF2,21', request='HISTORY', frameValue=.05, variable='RF2')
column_paper.gather(results='RF2,22', request='HISTORY', frameValue=.1, variable='RF2')
column_paper.gather(results='RF2,23', request='HISTORY', frameValue=.15, variable='RF2')
column_paper.gather(results='RF2,24', request='HISTORY', frameValue=.2, variable='RF2')
column_paper.gather(results='RF2,25', request='HISTORY', frameValue=.25, variable='RF2')
column_paper.gather(results='RF2,26', request='HISTORY', frameValue=.3, variable='RF2')
column_paper.gather(results='RF2,27', request='HISTORY', frameValue=.35, variable='RF2')
column_paper.gather(results='RF2,28', request='HISTORY', frameValue=.4, variable='RF2')
column_paper.gather(results='RF2,29', request='HISTORY', frameValue=.45, variable='RF2')
column_paper.gather(results='RF2,30', request='HISTORY', frameValue=.5, variable='RF2')
column_paper.gather(results='RF2,31', request='HISTORY', frameValue=.55, variable='RF2')
column_paper.gather(results='RF2,32', request='HISTORY', frameValue=.60, variable='RF2')
column_paper.gather(results='RF2,33', request='HISTORY', frameValue=.65, variable='RF2')
column_paper.gather(results='RF2,34', request='HISTORY', frameValue=.7, variable='RF2')
column_paper.gather(results='RF2,35', request='HISTORY', frameValue=.75, variable='RF2')
column_paper.gather(results='RF2,36', request='HISTORY', frameValue=.8, variable='RF2')
column_paper.gather(results='RF2,37', request='HISTORY', frameValue=.85, variable='RF2')
column_paper.gather(results='RF2,38', request='HISTORY', frameValue=.9, variable='RF2')
column_paper.gather(results='RF2,39', request='HISTORY', frameValue=.95, variable='RF2')
column_paper.gather(results='RF2,40', request='HISTORY', frameValue=1.00, variable='RF2')
##
##
column_paper.output(file=ODB, step=1)
column_paper.gather(results='RM3,1', request='HISTORY', frameValue=0.05, variable='RM3')
column_paper.gather(results='RM3,2', request='HISTORY', frameValue=0.1, variable='RM3')
column_paper.gather(results='RM3,3', request='HISTORY', frameValue=0.15, variable='RM3')
column_paper.gather(results='RM3,4', request='HISTORY', frameValue=0.2, variable='RM3')
column_paper.gather(results='RM3,5', request='HISTORY', frameValue=0.25, variable='RM3')
column_paper.gather(results='RM3,6', request='HISTORY', frameValue=0.3, variable='RM3')
column_paper.gather(results='RM3,7', request='HISTORY', frameValue=0.35, variable='RM3')
column_paper.gather(results='RM3,8', request='HISTORY', frameValue=0.4, variable='RM3')
column_paper.gather(results='RM3,9', request='HISTORY', frameValue=0.45, variable='RM3')
column_paper.gather(results='RM3,10', request='HISTORY', frameValue=0.5, variable='RM3')
column_paper.gather(results='RM3,11', request='HISTORY', frameValue=0.55, variable='RM3')
column_paper.gather(results='RM3,12', request='HISTORY', frameValue=0.60, variable='RM3')
column_paper.gather(results='RM3,13', request='HISTORY', frameValue=0.65, variable='RM3')
column_paper.gather(results='RM3,14', request='HISTORY', frameValue=0.7, variable='RM3')
column_paper.gather(results='RM3,15', request='HISTORY', frameValue=0.75, variable='RM3')
column_paper.gather(results='RM3,16', request='HISTORY', frameValue=0.8, variable='RM3')
column_paper.gather(results='RM3,17', request='HISTORY', frameValue=0.85, variable='RM3')
```

```
column_paper.gather(results='RM3,18', request='HISTORY', frameValue=0.9, variable='RM3')
column_paper.gather(results='RM3,19', request='HISTORY', frameValue=0.95, variable='RM3')
column_paper.gather(results='RM3,20', request='HISTORY', frameValue=1.00, variable='RM3')
##
column_paper.output(file=ODB, step=2)
column_paper.gather(results='RM3,21', request='HISTORY', frameValue=.05, variable='RM3')
column_paper.gather(results='RM3,22', request='HISTORY', frameValue=.1, variable='RM3')
column_paper.gather(results='RM3,23', request='HISTORY', frameValue=.15, variable='RM3')
column_paper.gather(results='RM3,24', request='HISTORY', frameValue=.2, variable='RM3')
column_paper.gather(results='RM3,25', request='HISTORY', frameValue=.25, variable='RM3')
column_paper.gather(results='RM3,26', request='HISTORY', frameValue=.3, variable='RM3')
column_paper.gather(results='RM3,27', request='HISTORY', frameValue=.35, variable='RM3')
column_paper.gather(results='RM3,28', request='HISTORY', frameValue=.4, variable='RM3')
column_paper.gather(results='RM3,29', request='HISTORY', frameValue=.45, variable='RM3')
column_paper.gather(results='RM3,30', request='HISTORY', frameValue=.5, variable='RM3')
column_paper.gather(results='RM3,31', request='HISTORY', frameValue=.55, variable='RM3')
column_paper.gather(results='RM3,32', request='HISTORY', frameValue=.60, variable='RM3')
column_paper.gather(results='RM3,33', request='HISTORY', frameValue=.65, variable='RM3')
column_paper.gather(results='RM3,34', request='HISTORY', frameValue=.7, variable='RM3')
column_paper.gather(results='RM3,35', request='HISTORY', frameValue=.75, variable='RM3')
column_paper.gather(results='RM3,36', request='HISTORY', frameValue=.8, variable='RM3')
column_paper.gather(results='RM3,37', request='HISTORY', frameValue=.85, variable='RM3')
column_paper.gather(results='RM3,38', request='HISTORY', frameValue=.9, variable='RM3')
column_paper.gather(results='RM3,39', request='HISTORY', frameValue=.95, variable='RM3')
column_paper.gather(results='RM3,40', request='HISTORY', frameValue=1.00, variable='RM3')
##
#column_paper.gather(results='RM1', request='HISTORY', frameValue='10', variable='RM1')
#column_paper.gather(results='RM3', request='HISTORY', frameValue='10', variable='RM3')
#column_paper.report(FILE, truncation='OFF', file='parametric_study_RF.rpt', par='ea',
results=('RF2,1', 'RF2,3', 'RF2,5', 'RF2,7', 'RF2,9', 'RF2,11', 'RF2,13', 'RF2,15', 'RF2,17',
'RF2,19', 'RF2,21', 'RF2,23', 'RF2,25', 'RF2,27', 'RF2,28', 'RF2,29', 'RF2,30', 'RF2,31',
'RF2,32', 'RF2,33', 'RF2,34', 'RF2,35', 'RF2,36', 'RF2,37', 'RF2,38', 'RF2,39', 'RF2,40'))#,
'RM1', 'RM3'))
column_paper.report(FILE, truncation='OFF', file='parametric_study_RF.rpt', par='ea',
results=('RF2,1', 'RF2,2', 'RF2,3', 'RF2,4', 'RF2,5', 'RF2,6', 'RF2,7', 'RF2,8', 'RF2,9',
'RF2,10', 'RF2,11', 'RF2,12', 'RF2,13', 'RF2,14', 'RF2,15', 'RF2,16', 'RF2,17', 'RF2,18',
'RF2,19', 'RF2,20','RF2,21', 'RF2,22', 'RF2,23', 'RF2,24', 'RF2,25', 'RF2,26', 'RF2,27',
'RF2,28', 'RF2,29', 'RF2,30', 'RF2,31', 'RF2,32', 'RF2,33', 'RF2,34', 'RF2,35', 'RF2,36',
'RF2,37', 'RF2,38', 'RF2,39', 'RF2,40'))#, 'RM1', 'RM3'))
##column_paper.report(FILE, file='parametric_study_RM1.rpt', par='ea', results=('RM1,1', 'RM1,2',
'RM1,3', 'RM1,4', 'RM1,5', 'RM1,6', 'RM1,7', 'RM1,8', 'RM1,9', 'RM1,10', 'RM1,11', 'RM1,12',
'RM1,13', 'RM1,14', 'RM1,15', 'RM1,16', 'RM1,17', 'RM1,18', 'RM1,19', 'RM1,20','RM1,21',
'RM1,22', 'RM1,23', 'RM1,24', 'RM1,25', 'RM1,26', 'RM1,27', 'RM1,28', 'RM1,29', 'RM1,30',
'RM1,31', 'RM1,32', 'RM1,33', 'RM1,34', 'RM1,35', 'RM1,36', 'RM1,37', 'RM1,38', 'RM1,39',
'RM1,40'))#, 'RM1', 'RM3'))
column_paper.report(FILE, truncation='OFF', file='parametric_study_RM3.rpt', par='ea',
results=('RM3,1', 'RM3,2', 'RM3,3', 'RM3,4', 'RM3,5', 'RM3,6', 'RM3,7', 'RM3,8', 'RM3,9',
'RM3,10', 'RM3,11', 'RM3,12', 'RM3,13', 'RM3,14', 'RM3,15', 'RM3,16', 'RM3,17', 'RM3,18',
'RM3,19', 'RM3,20','RM3,21', 'RM3,22', 'RM3,23', 'RM3,24', 'RM3,25', 'RM3,26', 'RM3,27',
'RM3,28', 'RM3,29', 'RM3,30', 'RM3,31', 'RM3,32', 'RM3,33', 'RM3,34', 'RM3,35', 'RM3,36',
'RM3,37', 'RM3,38', 'RM3,39', 'RM3,40'))#, 'RM3', 'RM3'))
```

Column data collection.

The macro that was used to extract all of the nodal data from the columns in chapters five and six.

```
def column_data_collection():
    import section
    import regionToolset
    import displayGroupMdbToolset as dgm
    import part
    import material
    import assembly
    import step
    import interaction
    import load
    import mesh
    import job
    import sketch
    import visualization
    import xyPlot
    import displayGroupOdbToolset as dgo
    import connectorBehavior
    outputs=['A1', 'A2', 'A3', 'A4', 'A5', 'A6', 'A7', 'B1', 'B2', 'B3',
        'B4', 'B5', 'B6', 'B7', 'C1', 'C2', 'C3', 'C5', 'C6', 'C7',
        'D1', 'D2', 'D3', 'D4', 'D5', 'D6', 'D7', 'E1', 'E2', 'E3',
        'E4', 'E5', 'E6', 'E7']
    odb = session.odbs['E:/Simulations/Temp/solid_column_273.odb']
    for names in outputs:
        data_name=names
        session.xyDataListFromField(odb=odb, outputPosition=NODAL, variable=(('COORD',
            NODAL, ((COMPONENT, 'COOR1'), (COMPONENT, 'COOR2'), (COMPONENT,
            'COOR3'), )), ('S', INTEGRATION_POINT, ((COMPONENT, 'S33'), )), ),
            nodeSets=(names, ))
        xyData=session.xyDataObjects.keys()
        data=[]
        for xy in xyData:
            a=xy.replace(',','-')
            session.xyDataObjects.changeKey(fromName=xy, toName=a)
            b = session.xyDataObjects[a]
            data.append(b)
        session.writeXYReport(fileName= names+'.rpt',appendMode=OFF, xyData=data)
        del data
        for xy in xyData:
            a=xy.replace(',','-')
            del session.xyDataObjects[a]
        print 'Completed data collection for column '+names+'...'
```